Spring 2015

On the design and analysis of compliant mechanisms using the pseudo-rigid-body model concept

Sushrut Gangadhar Bapat

Department: Mechanical and Aerospace Engineering

ON THE DESIGN AND ANALYSIS OF COMPLIANT MECHANISMS USING THE PSEUDO-RIGID-BODY MODEL CONCEPT

by

SUSHRUT GANGADHAR BAPAT

A DISSERTATION

Presented to the Faculty of the Graduate School of the

MISSOURI UNIVERSITY OF SCIENCE AND TECHNOLOGY

In Partial Fulfillment of the Requirements for the Degree

DOCTOR OF PHILOSOPHY

in

MECHANICAL ENGINEERING

2015

Approved by:

Ashok Midha, Advisor
Xiaoping Du
Edward Kinzel
Gearoid MacSithigh
Shun Takai

ABSTRACT

The pseudo-rigid-body model (PRBM) concept, developed for the analysis and design of large-deflection flexible members, has proved over time to be a simple, efficient and accurate tool for the synthesis, analysis and design of compliant mechanisms. This dissertation investigates a variety of compliant mechanism analysis and design problems using the PRBM concept and assists in further advancement of the implementation of the PRBMs. The dissertation begins with the development of a PRBM for a fixed-guided compliant beam with one inflection point in the deformed state. This research investigation advances the concept of characteristic deflection domain to a new synthesis framework for the design of fully-compliant mechanisms containing fixed-guided segments with an inflection point. The dissertation then formalizes a new approach for the evaluation of mechanical advantage of compliant mechanisms. In order to extend the approach towards synthesis and design of compliant mechanisms with higher mechanical advantage, the dissertation revisits the *synthesis with compliance* method of compliant mechanism design and provides an implementation strategy. A new method to determine an appropriate PRBM is presented. The method also allows determination of the expected static mode shape(s) of a given compliant mechanism structural configuration. Finally, the dissertation provides experimental results to validate the simplicity, accuracy, efficiency and applicability of the PRBM concept towards the synthesis, analysis and design of compliant segments and compliant mechanisms. The test setup design utilized for the experimental investigations may be found in the addendum to this dissertation.

ACKNOWLEDGMENTS

The author would like to express his appreciation and thank his advisor, Professor Ashok Midha, for being a constant source of guidance and encouragement. The author recognizes the invaluable exposure provided by him, not only in the area of compliant mechanism design, but generally in mechanical engineering design education. The author is grateful and would like to express his sincere thanks to Professor Midha for being selfless in his teachings and generously providing his time and support throughout the research effort.

Thanks are also due to Professors Xiaoping Du, Edward Kinzel, Gearoid MacSithigh, and Shun Takai for their invaluable time and service as members of the Advisory Committee.

The author would like to thank the Department of Mechanical and Aerospace Engineering at the Missouri University of Science and Technology for the financial support provided through the teaching assistantships, and for use of the computational facilities. The support of the Product Innovation and Creativity Center (PICC) at the Missouri University of Science and Technology, through the PICC Fellow appointments, is gratefully acknowledged.

The author extends his thanks to his parents, Gangadhar P. Bapat and Bhagyashree G. Bapat, and his sister, Samhita G. Bapat, for their constant support and faith in him. The author would like to thank his friends Rohan M. Raje and Swapnil Dhake for their encouragements and support.

Last but not least, the author would like to thank his research group colleagues: Raghvendra S. Kuber, Ashish B. Koli, Vivekananda Chinta, Pratheek B. Prasanna, Vamsi Lodagala, Krutika Karthik, Andrew Christian, Andrew Willis and Ethan Winberg, for their endless support and many an enlightening conversation throughout this research effort.

TABLE OF CONTENTS

LIST OF ILLUSTRATIONS

Page

LIST OF TABLES

Page

NOMENCLATURE

Symbol	Description
a	Beam end point location w.r.t. the fixed-end measured along the undeformed beam configuration
b	Beam end point location measured transverse to the undeformed beam configuration
θ_0	Beam end slope measured w.r.t. the undeformed configuration of the compliant segment
n	Load factor
P	Transverse force applied at the beam end
M	Moment applied at the beam end
κ	Nondimensional moment index
α	Nondimensional load index
γ	Characteristic radius factor
γ_l	Characteristic radius factor for lower bound of characteristic deflection domain
γ_u	Characteristic radius factor for upper bound of characteristic deflection domain
$\bar{Z}_n$	Vector notation of link n
R_n	Magnitude of $\bar{Z}_n$
Θ_n	Angle of $\bar{Z}_n$ measured ccw from right horizontal
P_j	j^{th} precision position (coupler point location)
γ_j	Rotation of coupler link from the first to the j^{th} precision position
$\bar{\delta_j}$	Vector from the first to the j^{th} precision position
Θ	Pseudo-rigid-body angle
K_Θ	Characteristic stiffness coefficient
U_j	Energy of the mechanism in the j^{th} precision position
ϕ_j	Rotation of input link from the first to the j^{th} precision position
ψ_j	Rotation of output link from the first to the j^{th} precision position

k_i	Spring constant of the i^{th} torsional spring
β_{ij}	j^{th} angular position of the i^{th} torsional spring
T_j	Input torque to the mechanism at the j^{th} precision position
T_c	Compliance torque
F_c	Compliance force
F_o	Force generated at the output port
F_i	Force applied at the input port
d_i	Location of input force w.r.t instant center
d_o	Location of output force w.r.t. instant center

1. INTRODUCTION

1.1 COMPLIANT MECHANISMS

Complaint mechanisms are mechanical devices that gain some or all of their mobility through the deflection of their flexible members, while transferring or transforming motion, force and/or energy [1, 2]. Figure 1.1 shows an ergonomic modular compliant chair designed by Mettlach et al. [3] using a partially-compliant mechanism. The schematic representation of the partially-compliant mechanism involved in the ergonomic modular compliant chair is shown in Figure 1.2. The reclining feature provided by this chair is made possible due to the flexibility in the front legs.

Compliant mechanisms integrate form with function, and therefore, exhibit the following inherent advantages:

1. Reduced number of parts or monolithic designs
2. Reduced assembly time and cost
3. Less wear, lash, shock and noise
4. Reduced or no need for lubrication
5. Improved mechanical precision, and reliability
6. Improved ergonomics and manufacturability
7. Miniaturization of components

Compliant mechanisms typically involve large deflections. The highly nonlinear nature of these deflections complicates the analysis and design approaches. In addition, the devices manufactured with polymers often exhibit lower creep life, and fatigue life.

Figure 1.1. An Ergonomic Modular Compliant Chair in its Undeformed State

Figure 1.2. Schematic Representation of the Partially-Compliant Mechanism Synthesized for the Ergonomic Modular Compliant Chair

1.2 NOMENCLATURE AND CLASSIFICATION

Compliant mechanisms form a relatively newer area of research in mechanism synthesis, analysis and design. For facilitating better understanding of the research effort presented in this dissertation, a brief overview of important terminologies associated with compliant mechanisms is provided below. Foundational work related to the nomenclature and classification of compliant segments and compliant mechanisms may be found in Midha et al. [1, 2].

Link: A mechanism link is defined as the continuum connecting the mating surfaces of one or more joints.

Fully-compliant mechanism: A compliant mechanism that contains no links is called as a fully-compliant mechanism. In such a mechanism, all of the mobility is achieved through the deflection of its flexible members.

Partially-compliant mechanism: A compliant mechanism in which some of the mobility is obtained through the rigid-body body joints is called a partially-compliant mechanism.

Figure 1.3 shows a one-link compliant mechanism; Figure 1.4 shows a fully-compliant mechanism, also referred to as a structurally zero-link mechanism; and Figure 1.5 shows a partially-compliant mechanism.

Links may be classified into two broad categories: rigid and compliant, as shown in Figure 1.6. A compliant link may be composed of only one segment or a combination of segments, which may include rigid segments. A compliant segment that is initially-straight, has homogenous material properties, and has a constant in-plane and out-of-plane thickness is called as a simple compliant segment. All other compliant segment types come under the category of compound compliant segments. Depending upon the material properties of the constituent segments, a compound compliant segment can be classified as homogenous compound compliant segment and nonhomogeneous compound compliant segment. Schematic representations of the commonly used simple and compound compliant segments are shown in Figure 1.7, Figure 1.8 and Figure 1.9.

Figure 1.3. One-Link Compliant Mechanism

Figure 1.4. A Fully-Compliant Mechanism

Figure 1.5. A Partially-Compliant Mechanism

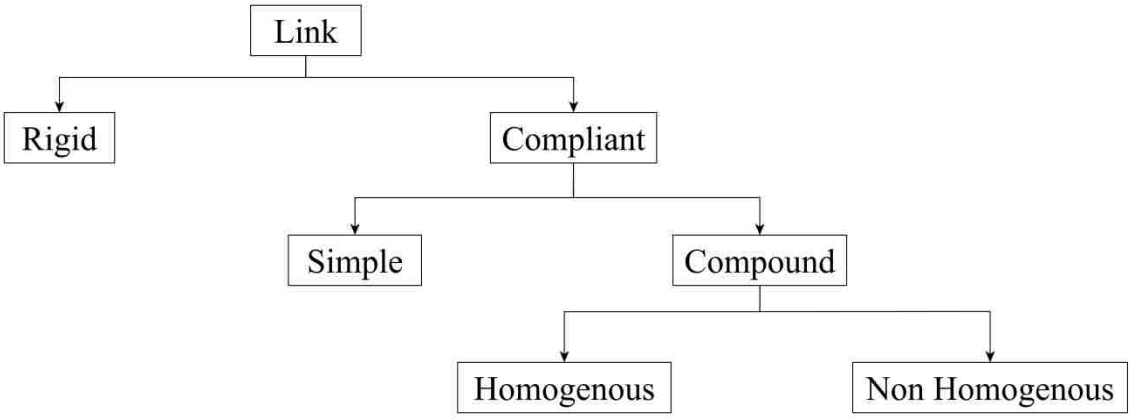

Figure 1.6. Classification of Links and Segments

Figure 1.7. Schematic Representation of an Initially-Straight and Initially-Curved Fixed-Pinned Compliant Segment

Figure 1.8. Schematic Representation of a Fixed-Free Compliant Segment with an Initially-Straight and Initially-Curved Small-Length Flexural Pivot

Figure 1.9. Schematic Representation of an Initially-Straight Fixed-Fixed (Fixed-Guided) Compliant Segment

1.3 COMPLIANT MECHANISM EXAMPLES

Compliant mechanisms, in only the last two or three decades, have provided an excellent forum and fresh impetus for revitalizing the area of mechanism design with abundant opportunities for creativity and innovation. In just this short a time period, compliant mechanisms have found their way into multiple disciplines: biotechnology, micro-electromechanical system (MEMS), mechanical devices, aerospace and origami applications, to name a few, and have been identified and acknowledged as one of the three "research trends that we can expect to persist into the future [4]." Presented below are some examples that utilize compliant mechanisms for their functioning.

Figure 1.10 shows a CAD rendering of Compliers®, a fish hook remover. It constitutes of three small-length flexural pivots (SLFPs) and one rolling point of contact. Figure 1.11 shows an image of the Michelin Tweel™ Airless Tire [5]. It constitutes of fixed-guided compliant segments that allow for energy storage while providing structural integrity to the airless tire.

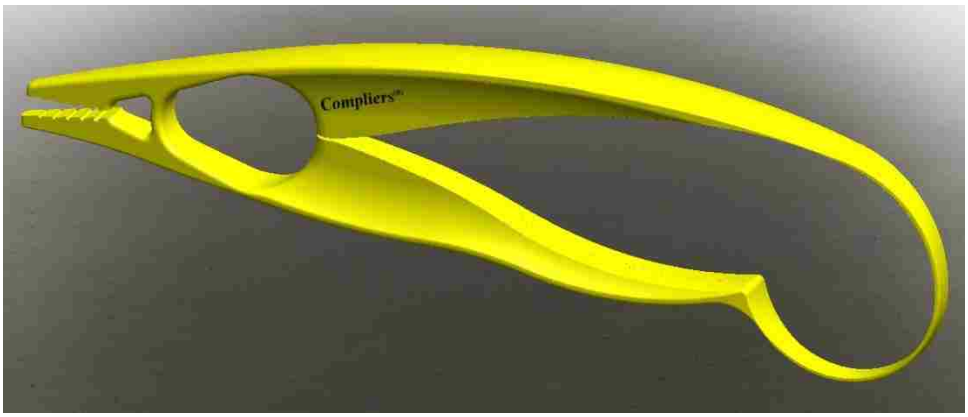

Figure 1.10. CAD Rendering of Compliers®: A Fish Hook Remover

Figure 1.11. Michelin Tweel™ Airless Tire [5]

Figure 1.12 shows CAD renderings of two versions of fully-compliant crimping mechanisms designed by AMP, Inc. The crimping mechanism contains two fixed-guided compliant segments. One of the segments is fixed to the ground and the other to the slider, and guided at the rigid-coupler. Figure 1.13 shows an image of a shoe design by Adidas® [6]. The shoe consists of fixed-free compliant segments for energy storage. Figure 1.14 shows an image of the compliant module designed by researchers at Brigham Young University (BYU) [7]. The module is designed to be a replacement for spinal column discs. Figure 1.15 shows a CAD rendering of a sense-clamp design [8]. It constitutes of a fully-compliant mechanism with fixed-guided segments. Figure 1.16 shows images of a fully-compliant gripper designed by Byers and Midha [9, 10]. It constitutes of two initially-curved SLFPs and one fixed-guided compliant segment to provide a near parallel grasping feature. Figure 1.17 shows an image of an out-of-plane compliant restrainer [11], consisting of four fully compliant mechanisms, each of them containing two fixed-guided compliant segments.

In addition to the examples presented here, many more intriguing and exciting application may be found, recently compiled in [12].

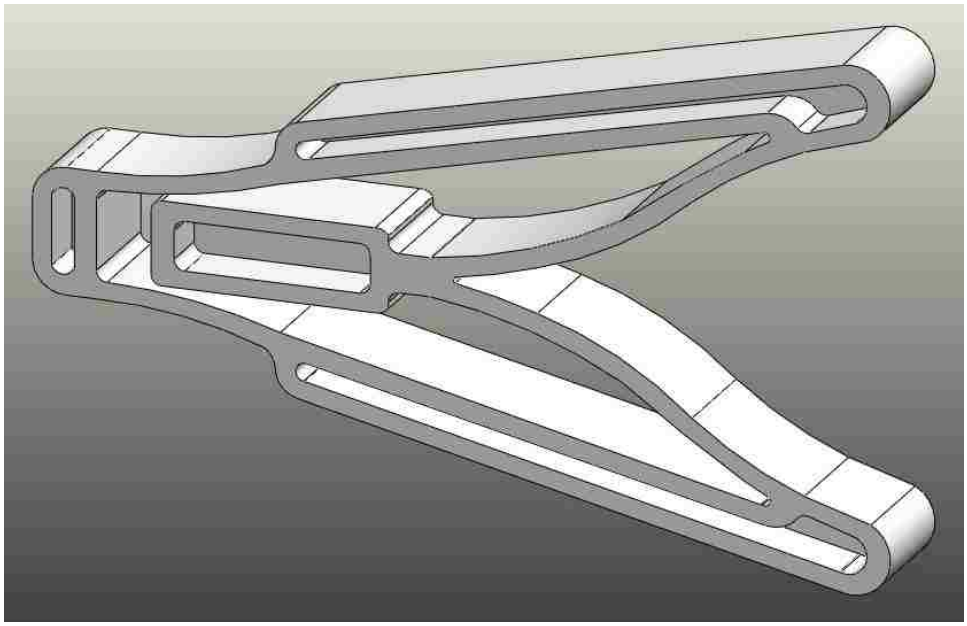

(a)

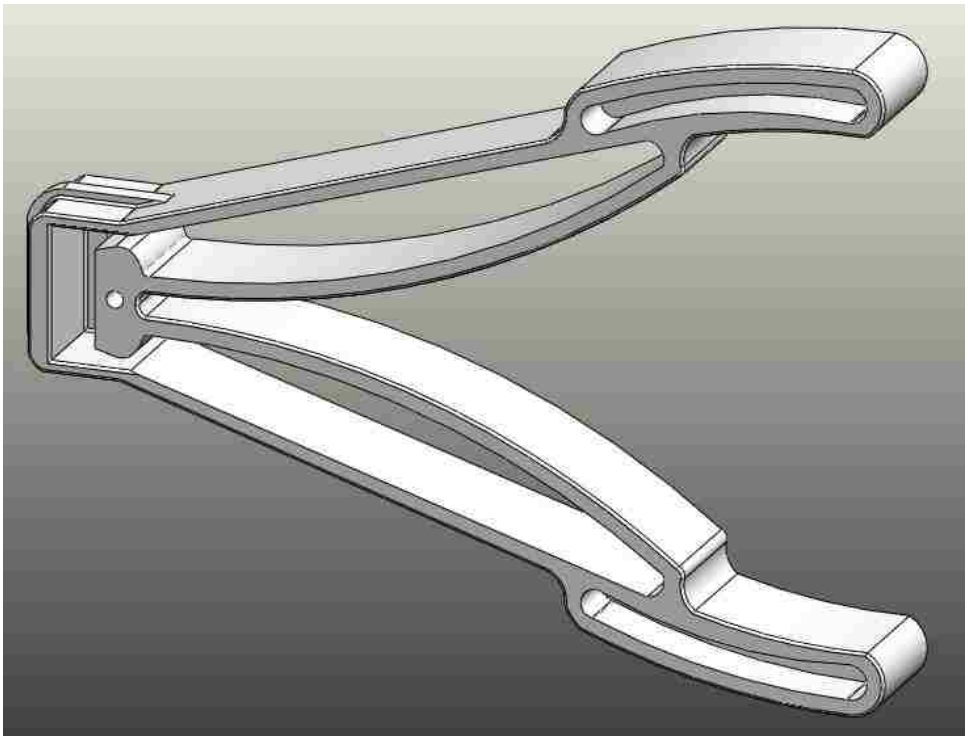

(b)

Figure 1.12. CAD Rendering of the Crimping Mechanisms Designed by AMP, Inc.

Figure 1.13. adidas® Springblade Shoe [6]

Figure 1.14. Spine Disc Replacement Compliant Module [7]

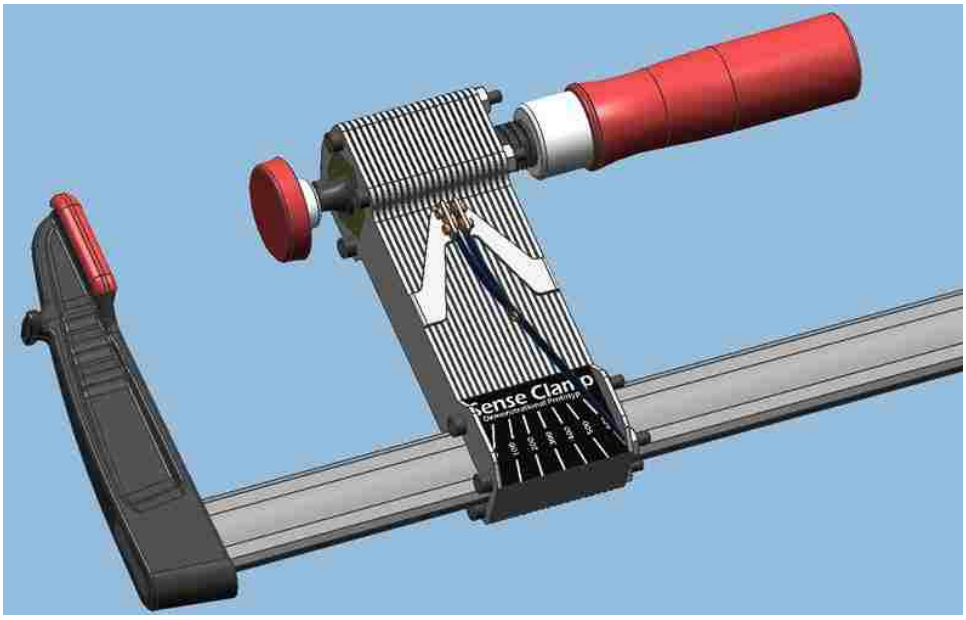

Figure 1.15. CAD Rendering of Sense-Clamp [8]

Figure 1.16. A Photograph of a Compliant Gripper Mechanism [9, 10]

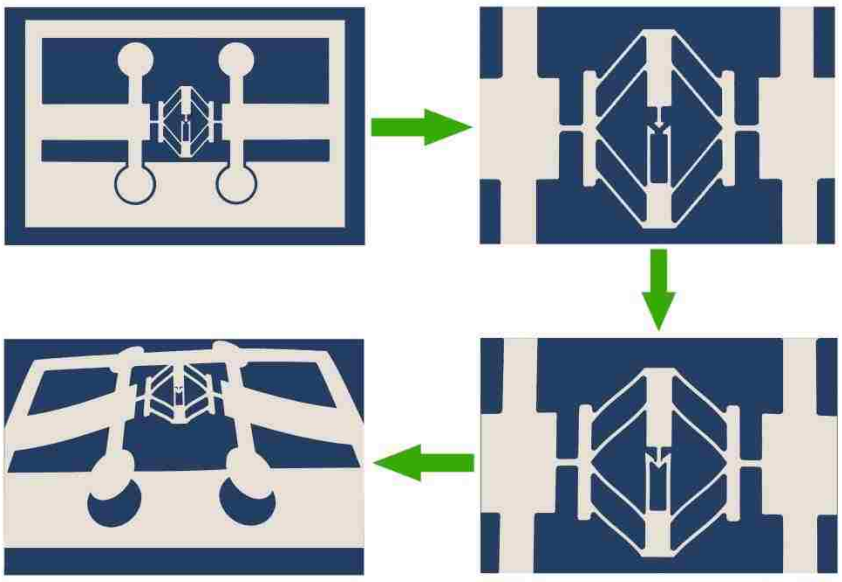

Figure 1.17. A Photograph of an Out-of-Plane Compliant Restrainer

1.4 BACKGROUND AND LITERATURE REVIEW

The first application of compliant mechanism can be dated back to the medieval times, wherein the Romans utilized compliant segments for energy storage in catapults and crossbows. The same property of compliant mechanisms is utilized even today, however, for providing comfort, e.g. the NASA mars rover wheel design [13].

Research in the area of compliant mechanism design that involves transfer of motion, force and energy storage initiated about five decades ago. The first publication in the area of synthesis of flexible link mechanisms was presented by Burns and Crossley [14, 15]. Burns and Crossley provided a graphical technique called as kinetostatic synthesis for synthesis of flexible link mechanisms. The authors considered mechanisms with flexible coupler attached to two fixed-pinned segments. The approach allows performing dimensional synthesis for function generation with specified output torque values at various precision-positions. Sevak and McLarnan [16] presented a finite element analysis based approach for synthesis of flexible link mechanisms for function generation. The authors utilize an optimization formulation in conjunction with the finite

element analysis methods for the design of flexible link mechanisms. The approach considers a nonlinear finite element formulation to determine the response of a candidate compliant mechanism solution. The optimization routine compares the results with the desired response to determine the next step for synthesis. Once the error between the finite element analysis results and the desired response is within an acceptable small value, the solution is finalized. The optimization is performed using the variable metric method by Fletcher and Powell.

Bisshopp and Drucker [17, 18] provided the first known mathematical closed-form solution for the large-deflection cantilevered beam using elliptic integrals. The complex nature of the solution approach allowed it to be applied towards model boundary conditions and is typically used for analysis purposes. Shoup [19] provided closed-form solutions using elliptic integrals for flexible segments subjected to a variety of beam end load and displacement boundary conditions. The results obtained from analysis were later applied towards synthesis of flexible segments and flexible mechanisms. These formulations could, however, handle only a limited number and type of design specifications.

After a long hiatus, Midha [20, 21] revived the interest in flexible mechanism design and analysis and began the process of its formalization, naming it as the field of compliant mechanisms [22]. Midha et al. [23, 24] and Her [25] began the initial investigations in the area of compliant mechanism design. They provided a large-deflection analysis technique called as the Chain Algorithm, and utilized it for compliant mechanism design and analysis. The Chain Algorithm could successfully analyze and design fully-compliant mechanisms. The newly developed shooting method decreased the numerical computations by about an order, when compared to the finite element analysis formulation. Her and Midha [26] investigated the mobility characteristics of compliant mechanisms and presented a methodology to estimate the maximum possible degrees of freedom of a compliant mechanism. Her and Midha [26] introduced the concept of compliance number and utilized it towards the qualitative assessment of the compliance content within a given compliant mechanism. A systematic approach is also presented to perform type synthesis of compliant mechanisms.

Salamon and Midha [27, 28] performed introductory work towards understanding the mechanical advantage aspects of compliant mechanisms. They categorized mechanical advantage of compliant mechanisms into three types, depending upon the independent variable. The authors utilized the Chain Algorithm to derive the conclusions, and presented a methodology for designing compliant mechanisms with higher mechanical advantage. The thesis develops many important terminologies related to mechanical advantage of compliant mechanisms.

Nahvi [29] developed numerical procedures for static and dynamic analysis of compliant mechanisms. Analysis and synthesis is accomplished using the Chain Algorithm in conjunction with the shooting method based on Newton-Raphson iteration scheme, to meet the specified displacement boundary conditions. The work modifies the Chain Algorithm and formulates a flexibility matrix for a beam element taking into account the effect of shear deformation for beams with larger cross-sections. A three-dimensional version of the Chain Algorithm is also developed. Nahvi [29] implemented the iterative-incremental finite element procedure for static and dynamic analysis of compliant mechanisms. The technique is also implemented to analyze compliant mechanisms near its mobility limits. Hill and Midha [30, 31] developed the graphical user driven interface for the Chain Algorithm and implemented it towards the analysis and synthesis of compliant mechanisms.

During these early investigations, Midha and Her [32] and Midha et al. [23, 24 and 27, 28] embarked on the preliminary discussions on the feasibility of a simple yet robust methodology that may use rigid-body equivalent models and discrete springs for compliant mechanism analysis, synthesis and design; and called it as the pseudo-rigid-body model (PRBM) concept.

In order to facilitate the application of the PRBM concept towards compliant mechanism design, Midha et al. [1, 2] presented formal nomenclature and classification for compliant segments and compliant mechanisms. Later, Howell and Midha [33-36] and Howell et al. [37] systematically developed the PRBM concept for analysis and design of a fixed-free compliant segment subjected to beam end forces. The methodology utilized elliptic integral results to determine the parametric values such that beam end point location is within a small acceptable error, of say 0.5%. Recently, Pauly

and Midha [38, 39] provided improved parametric expressions for the PRBM of a fixed-free compliant segment subjected to beam end forces.

Howell [36, 40] advanced the approach and developed PRBMs for initially-curved fixed-pinned segment, and initially-straight fixed-guided segment wherein the beam end angle in the deformed state is the same as in the undeformed state. Mettlach and Midha [41, 42] presented a PRBM for a fixed-free compliant beam with multiple characteristic pivots, in order to increase the prediction range of the PRBM. They investigated the mobility characteristics of various compliant segment types. The concept of 'domain of attraction' and the concept of 'characteristic deflection domain' was introduced in this work. Characteristic deflection domains for simple compliant segment types were derived using the available PRBM parametric equations. The characteristic deflection domain for complex shaped compliant segments was determined using the iterative-incremental finite element analysis procedure developed by Nahvi [29].

Edwards et al. [43, 44] developed PRBM for initially-curved pinned-pinned compliant segments. Saxena and Kramer [45] provided a PRBM for a fixed-free compliant segment subjected to beam end force and moment. Moment loading is considered in the same sense as the vertical component of the force. The PRBM presented consist of a slider link, as well. Lyon [46] and Lyon et al. [47] provided PRBM for a fixed-guided compliant segment with one inflection point in its deformed state, wherein the beam end angle can take any value w.r.t. its undeformed configuration. The model is valid for certain special loading conditions. Lyon and Howell [48] provided a simplified PRBM for fixed-guided compliant segment with one inflection point in its deformed state. The model decouples the load and deflections for a fixed-guided compliant segment with one inflection point. This assumption introduces significant errors in the PRBM, and therefore, is recommended for visualization purposes only.

Kimball and Tsai [49] provided PRBM for a compliant segment subjected to arbitrary beam end loads. The authors develop the closed-form solution for such a problem type using elliptic integrals. Elliptic integral formulations provided can be used to analyze compliant segments that display an inflection point in its deformed state or display a monotonically increasing curvature in its deformed state. Authors identify that

obtaining solutions to the closed-form formulation becomes cumbersome when all three beam end loads are specified. In order to assist a designer with the solution process a differential geometry based approach is presented to determine the best possible initial estimates. Authors convert the three degrees of freedom problem into a one degree of freedom problem by generating relationships between associated variables. PRBM parametric expressions are developed using an optimization routine.

Mavanthoor and Midha [50, 51] investigated the stability of compliant mechanisms using the iterative-incremental finite element analysis developed by Nahvi [29]. Su [52] presented a PRBM with three characteristic pivots to predict the beam end point locations for a wide range of load specifications. The properties of the PRBM are calculated by an optimization routine. The PRBM predicts beam end locations fairly well when the loading conditions do not result in an inflection point in the beam continuum. The errors increase in the estimation of beam end coordinates for configurations with one inflection point in the deformed state. Midha and Kuber [53, 54] provided elliptic integral formulations for analysis of a fixed-free compliant beam with an initially-straight SLFP or with an initially-curved SLFP, subjected to beam end forces. This work validates the assumptions made in the PRBM analysis of such segment types. Zhang and Chen [55] presented elliptic integral formulations for a cantilever beam subjected to a variety of boundary conditions. The formulation can handle loadings that result in multiple inflection points in the beam continuum. The formulation needs specification of the number of inflection points, and other specific variables to obtain a solution.

Howell and Midha [56] and Midha et al. [57] extended the PRBM concept for the analysis and synthesis of compliant mechanisms and developed a systematic methodology called as ‘synthesis with compliance.’ The method utilizes the state of the art rigid-body synthesis techniques, along with energy and torque equations to generate a set of weakly coupled and strongly coupled equations. Mettlach [42] applied synthesis with compliance towards synthesis of compliant mechanisms using Burmester Theory. Mettlach [42] also applied the rigid-body graphical synthesis techniques towards compliant mechanism design. Murphy [58] and Murphy et al. [59, 60] applied the matrix element method for performing the type synthesis of compliant mechanisms. Murphy et al. [61] reinvestigated the mobility of compliant mechanisms. Authors presented an

equation for the evaluation of maximum possible degrees of freedom, which is a function of the number and type of the constituent compliant segments. The analysis procedure, in conjunction with compliant element matrix, is utilized to determine compliant mechanism topologies that can provide requisite degrees of freedom. Howell and Midha [62] investigated the type 3 mechanical advantage of a toggle mechanism, wherein the work piece stiffness is considered as the independent variable. Midha et al. [63] applied the PRBM concept towards the evaluation of mobility limits of compliant mechanisms.

Midha et al. [64] and Annamalai [65] provided design tables for synthesis of compliant mechanisms for conventional tasks of function generation, path and motion generation, and path generation with prescribed timing, with energy/torque values specified at the precision positions. The design tables provide the type of the coupling between kinematic and compliance equations and the number of equations, unknowns, and free-choices required for a given problem specification. Midha et al. [66] and Kolachalam [67] extended the synthesis with compliance method for single-strip mechanisms, and presented a design methodology for synthesis of single-strip compliant mechanisms for path and motion generation with specified energy, torque or force values at the precision position. Midha et al. [68] provided some insights into the challenges associated with the implementation of the synthesis with compliance method.

Su and McCarthy [69, 70] presented an approach for designing bistable compliant mechanisms using the polynomial homotopy technique. The approach assumes the first precision position as the energy free state of the compliant mechanism. The approach transforms the energy and torque equations provided by Howell and Midha [56] into approximate polynomials. The polynomial equations are then solved using homotopy solvers to obtain all possible solutions. Unrealistic solutions are filtered out to determine the set of acceptable solutions. The transformation of energy and torque equations into polynomials introduce errors in the solutions, thus allowing them to be used only as initial estimates while solving the energy and torque equations specified by Howell and Midha [56]. The approach is demonstrated for a compliant mechanism having a PRBM of a four-bar mechanism containing two fixed-pinned compliant segments that are fixed at the coupler. Tari and Su [71] modified this approach with a vectorial representation of

links for the design of compliant mechanisms. This approach tends to be computationally intensive.

Ananthasuresh [72] provided the foundational work towards the design of compliant mechanisms with structural optimization approach. The well-established structural optimization routines are adapted towards the synthesis and design of compliant mechanisms. The synthesis approach is divided into three steps, starting with topology optimization and then followed by shape and size optimization. This work concentrates greatly on topology optimization and just touches upon the size optimization. The structural optimization techniques that have been in use to design structures for minimizing weight and maximizing stiffness, or in other words limiting maximum deflection are utilized. Various objective functions are generated that allow adapting these structural optimization techniques. Due to the inherent limitations in these techniques, compliant mechanisms may be designed for only minimizing compliance (maximizing stiffness) and not for a fixed displacement at output port. The method is built upon the small displacement Euler-Bernoulli equation. The method utilizing an existing homogenization method for topology optimization. Often the results obtained need further improvement, that is, designer's intuition to convert them into realistic solutions. The method generates a multi-degree of freedom mechanism and therefore has to analyze the mechanism for every possible scenario. Also, only fully-compliant planar mechanisms are considered in this work. Based on the formulations, it is unlikely that partially compliant mechanisms may be possible.

Frecker et al. [73] provided a multi-criteria optimization formulation to design compliant mechanisms with the homogenization method. This formulation considers the ratio of the strain energy, i.e. the energy stored in the compliant mechanism while approaching the work piece to the energy stored while performing useful work. One of the criteria in the objective function is to maximize compliance and the other is to maximize stiffness. The two objectives are required during the two phases of operation. In the first phase, the mechanism should demonstrate maximum compliance during its approach towards the work piece, while in the second phase the mechanism should provide maximum stiffness in order to transmit forces at the output port. Mutual strain energy is used in developing the objective function. The method needs an initial design

and uses truss elements to generate a compliant mechanism. Saggere and Kota [74] provided an approach for synthesis of compliant mechanism for compliant-segment motion generation. This approach is applicable to partially-compliant mechanisms with flexible coupler segment that is attached to two fixed-pinned segments. The method requires specifications of the initial and final shape of the coupler segment, and considers small deflection to facilitate the application of linearized beam theory. It utilizes equilibrium equations, along with a structural optimization routine with the path vector of the side links as its objective function to design a partially-compliant mechanism for compliant-segment motion generation.

Parkinson et al. [75] provided an optimization-based approach for designing fully-compliant mechanisms. This method considers a compliant mechanism as a spline with various control points. The approach parameterizes the design solution obtained from the optimization routine, and creates a finite element model in ANSYS® to analyze the response of a candidate compliant mechanism solution. The response is compared to the desired outcome to determine the next step of the optimization process. Rai et al. [76] presented a structural optimization-based approach for synthesis of fully-compliant mechanisms for path generation using initially-curved frame elements. This method designs a compliant mechanism for tracing the path with the actuating forces serving as design variables.

It is evident that the research in the area of compliant mechanism synthesis, analysis and design has come a long way since the initial push given by Midha [20, 21]. It can be said that there have been three drivers for the advancements in compliant mechanisms: i) PRBM concept, ii) structural optimization using homogenization method, and iii) finite element analysis techniques.

Experiences in the recent decades have shown that PRBMs can be potentially simple, efficient, and accurate tools for modeling compliant mechanisms. The PRBM approach is versatile in handling problems of analysis and synthesis, with displacement and force boundary conditions, lending itself well to visualization of the kinematics of deformation of compliant segment types. The concept of characteristic deflection domain graphically reveals an intrinsic limitation of compliant segments, and provides a pathway to feasible analysis and synthesis with clear understanding. The other methods simply

lack this capability, and efforts to employ them in such contexts frequently fail to converge, or converge to a realistic solution, leaving the designer guessing as to the reasons. The largest benefit in the use of the PRBM approach comes from considering compliant mechanisms as equivalent pseudo-rigid-body mechanisms with characteristic compliance (discrete springs), thus making available a wealth of existing rigid-body mechanism analysis and synthesis knowledge to the treatment of compliant mechanisms.

1.5 SCOPE OF INVESTIGATION

The objective of this work is to develop synthesis and analysis techniques for compliant segments and compliant mechanisms. This work strives to systematically develop a fundamental understanding of various aspects of compliant mechanism design. Focus is placed on five areas to further advance the application of the PRBM concept towards compliant mechanism design and analysis. The design and analysis methodologies provided herein build on the rigid-body synthesis and analysis techniques for compliant mechanism design.

This work provides an efficient method for the analysis of a fixed-guided compliant beam with one inflection point in its deformed state using the PRBM concept. The formulation is also implemented towards the two-position synthesis of a fixed-guided compliant segment with an inflection point. The formulation is then extended to the synthesis of fully-compliant mechanisms containing fixed-guided segments.

To assist a designer in the specification of realistic beam end point characteristics, the concept of characteristic deflection domain is developed. Characteristic deflection domains for various compliant segment types are presented. Pseudo-rigid-body representation of the lower and upper bounding curves of the characteristic deflection domain is evaluated, which are helpful in analysis and synthesis of compliant mechanisms.

The synthesis with compliance approach is revisited to reduce or eliminate the limitations associated with it. The approach presented in this work considers the kinematics and compliance equations as a weakly coupled set of equations to design compliant mechanisms for conventional tasks, such as, function generation, path and motion generation, and path generation with prescribed timing with energy, torque or

force values specified at the precision positions. The proposed strategy allows the application of the synthesis with compliance method towards a wide range of user specifications.

A simple and straight-forward approach is presented to evaluate the mechanical advantage of a given compliant mechanism. The formulation utilizes the PRBM approach to derive the mechanical advantage expression for a compliant mechanism. Significant factors affecting the mechanical advantage are studied. Important inferences are derived from the results obtained. The analysis procedure is coupled with the aforementioned improved implementation of synthesis with compliance to design compliant mechanisms with higher mechanical advantage.

The PRBM concept is used in conjunction with the Grubler's criterion and the principle of total minimum potential energy to determine the expected model shape of a given compliant mechanism. The approach is also utilized to identify appropriate PRBM transformations of a compliant mechanism design.

Finally, experimental investigations are performed to validate the PRBM concept for compliant mechanism design and analysis. Tests are performed on compliant segments, partially-compliant mechanisms and fully-compliant mechanisms.

1.6 ORGANIZATION OF THE DISSERTATION

The dissertation is organized in ten sections. Section 1 provided an introduction to compliant mechanisms. A brief discussion on the background, literature review, and scope of the investigation is also presented in section 1. Section 2 reviews commonly used large-deflection analysis techniques. The PRBM concept is introduced in section 2.

In section 3, an efficient method for the analysis of a fixed-guided compliant segment with an inflection point is presented. The method is also applied towards a two-position synthesis of a fixed-guided compliant beam.

In section 4, the concept of characteristic deflection domain is developed. Characteristic deflection domains are provided for various compliant segment types. Pseudo-rigid-body representation of the lower and upper boundary curves of the characteristic deflection domain is calculated. The pseudo-rigid-body representation is utilized to determine the characteristic deflection domain for complaint mechanisms. The

resulting formulation is applied towards analysis and synthesis of compliant segments and compliant mechanisms.

In section 5 a new synthesis framework is presented to develop a methodology for synthesis of fully-compliant mechanisms with fixed-guided compliant segments.

In section 6, a generalized approach for the design of compliant mechanisms is presented. The approach provides a newer implementation strategy for the synthesis with compliance framework. The approach utilizes a conventional, simple yet efficient optimization formulation to reduce/eliminate the limitations associated with the synthesis with compliance framework.

In section 7, a simple and straight-forward approach is presented for the evaluation of mechanical advantage of a compliant mechanism. The PRBM approach is utilized to determine the expression for the mechanical advantage of the compliant mechanism. Significant factors affecting the mechanical advantage are identified and important inferences are made from the results obtained.

In section 8, a new method is presented to determine the suitable PRBM for a given compliant mechanism. The approach utilizes the PRBM concept in conjunction with the Grubler's criterion and the principle of total minimum potential energy. The approach is utilized in determining the expected mode shape of the compliant mechanism.

In section 9, experimental investigations are performed to validate the PRBM approach for the design and analysis of compliant mechanisms.

The summary of the dissertation, remarks on the proposed methodologies and future work possibilities are presented in section 10.

2. LARGE-DEFLECTION ANALYSIS

The Bernoulli-Euler equation states that the bending moment at any point is proportional to the curvature of the beam [35, 36], given by

$$M = EI\frac{d\theta}{ds} \tag{1}$$

where, M is the bending moment, E the modulus of elasticity, I the area moment of inertia, and $\frac{d\theta}{ds}$ the change of curvature along the beam, that is curvature, given by

$$\frac{d\theta}{ds} = \frac{d^2y/dx^2}{[1 + (dy/dx)^2]^{3/2}} \tag{2}$$

For small deflections the slope (dy/dx) is small, and therefore, the denominator of equation (2) can be assumed to be unity. This assumption leads to the classical moment-curvature equation for beams, given by

$$M = EI\frac{d^2y}{dx^2} \tag{3}$$

Advancements in material technology and the ease of availability of resilient materials have assisted in the explosive nature of the development of compliant mechanisms. However, with the use of resilient materials compliant segments and compliant mechanisms often undergo large-deflections. For the deflections involved in compliant mechanisms, the assumptions for small-deflection do not hold true, leading to errors in the calculation of beam end point locations. The highly nonlinear nature of the large-deflections with compliant segments complicates the analysis and design approaches, limiting the use of compliant mechanisms to much simpler applications. This section reviews the large-deflection analysis techniques like closed-form elliptic integral formulation, the Chain Algorithm, and the pseudo-rigid-body model (PRBM) concept for the design and analysis of compliant segments and compliant mechanisms.

The development of the latter has provided a much needed impetus for nurturing the innovation and creativity involved in compliant mechanism design.

2.1 CLOSED-FORM ELLIPTIC INTEGRAL FORMULATIONS

2.1.1 An Initially-Straight Fixed-Pinned Compliant Segment Subjected to a Transverse Force at the Beam End.

Bisshopp and Drucker [17] provided the closed-form elliptic integral formulation for the large-deflection analysis of cantilevered beam subjected to a transverse force, P, at the beam end point, as shown in Figure 2.1.

Figure 2.1. An Initially-Straight Large-Deflection Cantilevered Beam Subjected to Transverse Force at the Beam End Point

The closed-form solutions derived using elliptic integrals for such a segment type is given by the following relationships:

$$\frac{b}{l} = \frac{1}{\alpha}[F(t) - F(\gamma, t) + 2(E(\gamma, t) - E(t))] \tag{4}$$

$$\frac{a}{l} = 1 - \frac{\sqrt{2}}{\alpha}\sqrt{2t^2 - 1} \tag{5}$$

where,

$$\alpha = \sqrt{\frac{Pl^2}{EI}}$$

$$t = \sqrt{\frac{1 + \sin\theta_0}{2}}$$

$$\gamma = \operatorname{asin}\left(\frac{1}{t\sqrt{2}}\right)$$

$F(t)$ and $F(\gamma, t)$ are the complete and incomplete elliptic integrals of first kind, respectively; and $E(t)$ and $E(\gamma, t)$ are the complete and incomplete elliptic integrals of second kind, respectively, given by the following relations.

$$F(\gamma, t) = \int_0^{\gamma} \frac{d\theta}{\sqrt{1 - t^2\sin^2\theta}};\ F(t) = \int_0^{\pi/2} \frac{d\theta}{\sqrt{1 - t^2}}$$

$$E(\gamma, t) = \int_0^{\gamma} \sqrt{1 - t^2\sin^2\theta}\ d\theta;\ E(t) = \int_0^{\pi/2} \sqrt{1 - t^2}\ d\theta$$

2.1.2 An Initially-Straight Fixed-Pinned Compliant Segment Subjected to Beam End Transverse and Axial Forces.

Howell [35] provided the closed-form elliptic integral formulation for a large-deflection cantilever beam subjected to a combination of beam end forces P and nP, as shown in Figure 2.2.

Figure 2.2. An Initially-Straight Large-Deflection Cantilever Beam Subjected to Beam End Forces P and nP

The beam end point location can be calculated using the following equations:

$$\frac{b}{l} = \frac{1}{\alpha\eta^{5/2}}\left\{\eta\left[F(t) - F(\gamma, t) + 2[E(\gamma, t) - E(t)]\right] + n\sqrt{2\eta(\eta + \lambda)}\cos(\gamma)\right\} \quad (6)$$

$$\frac{a}{l} = \frac{1}{\alpha\eta^{5/2}}\left\{-n\eta\left[F(t) - F(\gamma, t) + 2[E(\gamma, t) - E(t)]\right] + \sqrt{2\eta(\eta + \lambda)}\cos(\gamma)\right\} \quad (7)$$

where,

$$\alpha = \sqrt{\frac{Pl^2}{EI}} = \frac{1}{\sqrt{\eta}}[F(t) - F(\gamma, t)], \text{for } \theta_0 < \phi$$

$$\phi = \operatorname{atan}\left(\frac{1}{-n}\right)$$

$$\lambda = \sin(\theta_0) - n\cos(\theta_0)$$

$$\eta = \sqrt{1 + n^2}$$

$$\gamma = \text{asin}\sqrt{\frac{\eta + n}{\eta + \lambda}};\ t = \sqrt{\frac{\eta + \lambda}{2\eta}}$$

2.1.3 An Initially-Curved Fixed-Pinned Compliant Segment Subjected to Beam End Transverse and Axial Forces. Howell [36] provided the closed-form elliptic integral formulation for an initially-curved large-deflection cantilever beam subjected to a combination of beam end forces P and nP, as shown in Figure 2.3.

Figure 2.3. An Initially-Curved Large-Deflection Cantilever Beam Subjected to Beam End Forces P and nP

For $0 < |\lambda| < \eta;\ \phi' - \text{acos}\left(\frac{-\lambda}{\eta}\right) \leq -\theta_0 < \phi';$ and $\alpha \neq 0$

$$\frac{b}{l} = \frac{1}{\alpha\eta^{5/2}}\{\eta[F(\gamma_2, t) - F(\gamma_1, t) + 2[E(\gamma_1, t) - E(\gamma_2, t)]] + n\sqrt{2\eta(\eta+\lambda)}\,[\cos(\gamma_1) - \cos(\gamma_2)]\} \tag{8}$$

$$\frac{a}{l} = \frac{1}{\alpha\eta^{\frac{5}{2}}}\Big\{-n\eta[F(\gamma_2, t) - F(\gamma_1, t) + 2[E(\gamma_1, t) - E(\gamma_2, t)]] + \sqrt{2\eta(\eta+\lambda)}\,[\cos(\gamma_1) - \cos(\gamma_2)]\Big\} \tag{9}$$

where,

$$\alpha = \sqrt{\frac{Pl^2}{EI}} = \frac{1}{\sqrt{\eta}}[F(\gamma_2, t) - F(\gamma_1, t)]$$

For $\lambda > \eta > 0;\ \phi' - \pi \leq -\theta_0 < \phi';$ and $\alpha \neq 0$

$$\frac{b}{l} = \frac{\sqrt{2(\eta+\lambda)}}{\alpha\eta^2}\left\{\frac{\lambda}{\eta+\lambda}[F(\psi_2, r) - F(\psi_1, r)] + [E(\psi_1, r) - E(\psi_2, r)] + n\left[\sqrt{1 - \frac{\eta - n}{\eta+\lambda}} - \sqrt{1 - \frac{\eta + \sin(\theta_0) - n\cos(\theta_0)}{\eta+\lambda}}\right]\right\} \tag{10}$$

$$\frac{a}{l} = \frac{\sqrt{2(\eta+\lambda)}}{\alpha\eta^2}\left\{-n\left[\frac{\lambda}{\eta+\lambda}[F(\psi_2, r) - F(\psi_1, r)] + [E(\psi_1, r) - E(\psi_2, r)]\right] + \left[\sqrt{1 - \frac{\eta - n}{\eta+\lambda}} - \sqrt{1 - \frac{\eta + \sin(\theta_0) - n\cos(\theta_0)}{\eta+\lambda}}\right]\right\} \tag{11}$$

where,

$$\alpha = \sqrt{\frac{Pl^2}{EI}} = \sqrt{\frac{2}{\lambda+\eta}}\,[F(\psi_2, r) - F(\psi_1, r)]$$

$$\lambda = \kappa + \sin(\theta_0) - n\cos(\theta_0)$$

$$\kappa = \frac{\kappa_0^2}{2\alpha^2}$$

$$\kappa_0 = \frac{l}{R_i}$$

where, R_i is the initial radius of the fixed-pinned compliant segment,

$$\kappa = \frac{M^2}{2PEI}$$

$$\eta = \sqrt{1 + n^2};\ \phi = \operatorname{atan}\left(\frac{1}{-n}\right)$$

$$\phi' = \operatorname{atan}\left(\frac{1}{n}\right)$$

$$\gamma_1 = \operatorname{asin}\left(\sqrt{\frac{\eta - n}{\eta + \lambda}}\right);\ \gamma_2 = \operatorname{asin}\left(\sqrt{\frac{\eta + \sin(\theta_0) - n\cos(\theta_0)}{\eta + \lambda}}\right)$$

$$\psi_1 = \operatorname{asin}\left(\sqrt{\frac{\eta - n}{2\eta}}\right);\ \psi_2 = \operatorname{asin}\left(\sqrt{\frac{\eta + \sin(\theta_0) - n\cos(\theta_0)}{2\eta}}\right)$$

$$t = \sqrt{\frac{\eta + \lambda}{2\eta}};\ r = \sqrt{\frac{2\eta}{\eta + \lambda}}$$

Su [52] provided relationships to determine the maximum allowable beam end angle w.r.t the nondimensional moment index κ, given as:

$$\theta_{0max} = \phi + \operatorname{acos}(1 - \kappa)\text{, for } \kappa \leq 2$$

$$\theta_{0max} = \infty\text{, for } \kappa > 2$$

2.1.4 An Initially-Straight Fixed-Fixed Compliant Segment. Figure 2.4 shows an initially-straight fixed-fixed compliant segment. The reaction loads at the beam end point may result in one of the two possible configurations in the deformed state of an initially-straight fixed-fixed segment, as shown in Figure 2.5 and Figure 2.6. A deformation configuration will be a result of the type and magnitude of the reaction load at the beam end point. The necessary and sufficient conditions for the occurrence of a deformed state with an inflection point are provided in Table 2.1 and Equation (12), respectively.

Figure 2.4. An Initially-Straight Fixed-Fixed Compliant Segment

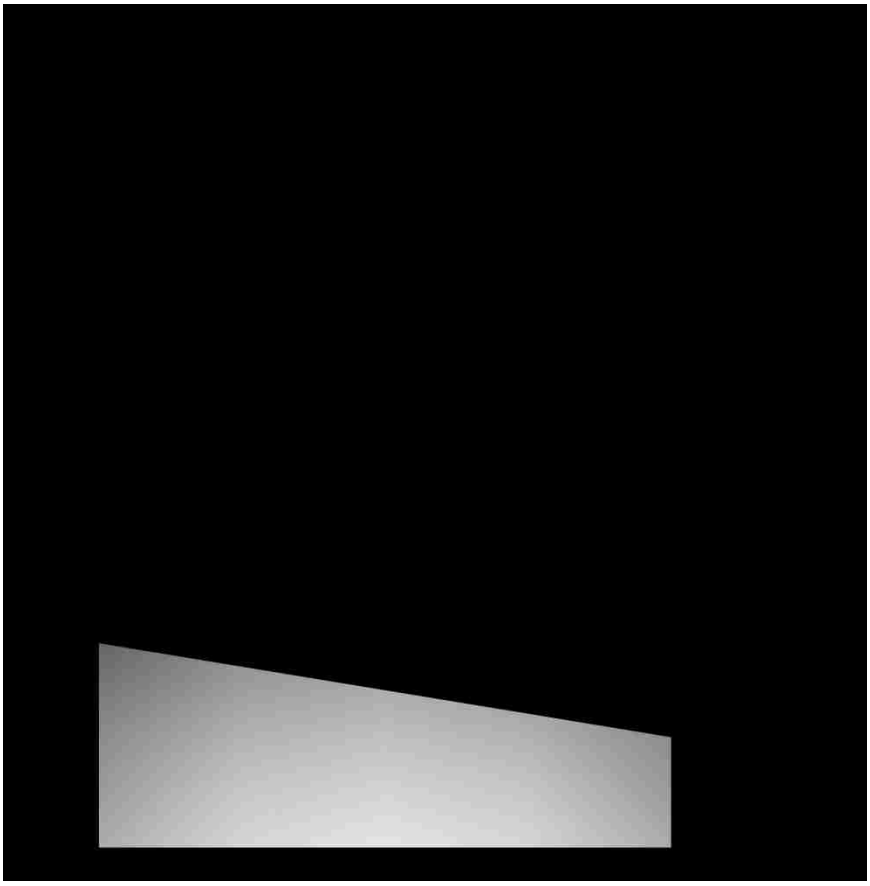

Figure 2.5. An Initially-Straight Fixed-Fixed Compliant Segment with a Monotonically Increasing Curvature in its Deformed Configuration

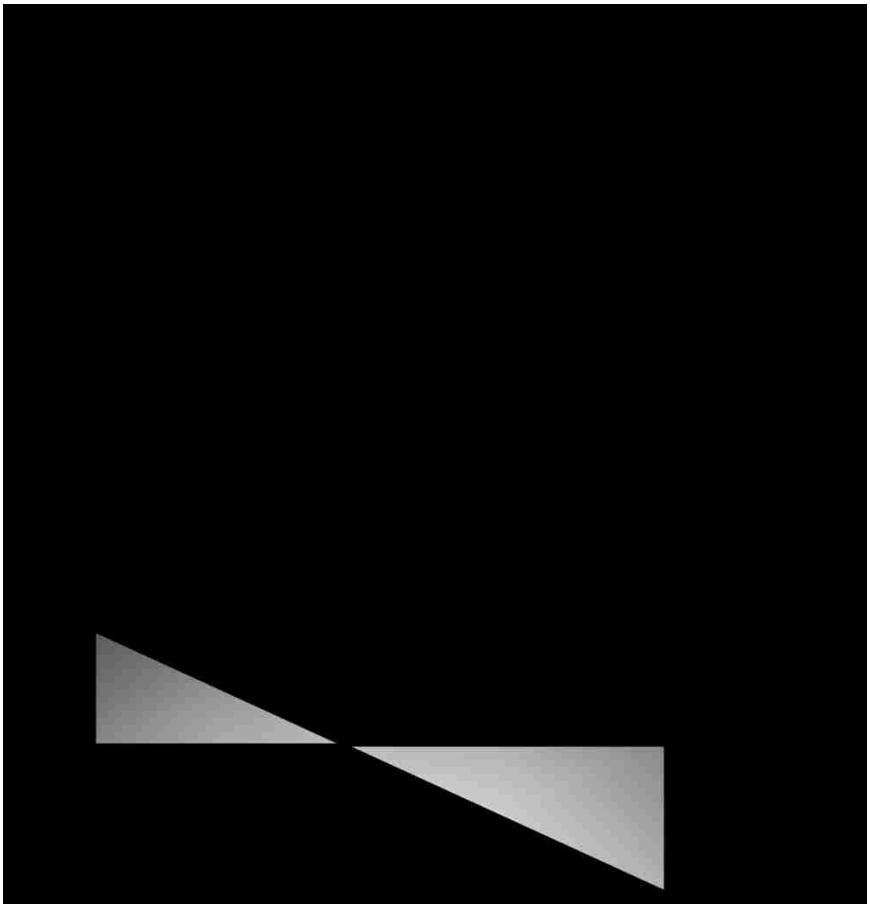

Figure 2.6 An Initially-Straight Fixed-Guided Compliant Segment with an Inflection Point in its Deformed Configuration

Table 2.1. Necessary Condition for the Occurrence of an Inflection Point in a Fixed-Guided Compliant Segment

P	M	Point of Inflection (P_i)
+	+	Not Possible
+	−	Possible
−	+	Possible
−	−	Not Possible

$$\cos(\theta_0 - \phi) - \cos(\theta_i - \phi) + \kappa \geq 0 \tag{12}$$

where, θ_i is the slope at the inflection point, and

$$\kappa = \frac{M^2}{2PEI} \tag{13}$$

Section 8 provides a new method to estimate the deformed configuration of an initially-straight fixed-guided compliant segment.

The elliptic integral formulation for the large-deflection analysis of an initially-curved fixed-pinned compliant segment can be applied to the large-deflection analysis of an initially-straight fixed-guided segment with a monotonically increasing curvature in its deformed state, shown in Figure 2.5, such that

$$\kappa_0 = \frac{Ml}{EI} \tag{14}$$

Kimball and Tsai [49] provided the closed-form elliptic integral formulation for the large-deflection analysis of an initially-straight fixed-guided segment with an inflection point in its deformed state, shown in Figure 2.6, such that

$$\begin{aligned} \frac{b}{l} = \frac{1}{\alpha\eta^{5/2}} \Bigg\{ & \eta[F(\gamma_1, k) + F(\gamma_2, k)] - 2\eta[E(\gamma_1, k) + E(\gamma_2, k)] \\ & + \sqrt{2\eta}\left[\sqrt{\lambda + \eta}\left(\sqrt{\frac{\eta - n}{\eta + n}} - n\right)\right. \\ & \left. + \sqrt{\kappa}\left(\sqrt{\frac{\eta + \sin(\theta_0) - n\cos(\theta_0)}{\eta - \sin(\theta_0) + n\cos(\theta_0)}} - n\right)\right]\Bigg\} \end{aligned} \tag{15}$$

$$\frac{a}{l} = \frac{1}{\alpha\eta^{5/2}}\Bigg\{-n\eta[F(\gamma_1,k) + F(\gamma_2,k)] + 2n\eta[E(\gamma_1,k) + E(\gamma_2,k)] + \sqrt{2\eta}\Bigg[-\sqrt{\lambda+\eta}\left(n\sqrt{\frac{\eta-n}{\eta+n}} - 1\right) - \sqrt{\kappa}\left(n\sqrt{\frac{\eta+\sin(\theta_0)-n\cos(\theta_0)}{\eta-\sin(\theta_0)+n\cos(\theta_0)}} - 1\right)\Bigg]\Bigg\} \quad (16)$$

where,

$$\alpha = \sqrt{\frac{Pl^2}{EI}} = \sqrt{\frac{2}{\eta}}\,[F(\gamma_1,k) + F(\gamma_2,k)]$$

$$\lambda = \kappa + \sin(\theta_0) - n\cos(\theta_0)$$

$$\kappa = \frac{M^2}{2PEI}$$

$$\eta = \sqrt{1+n^2};\ \phi = \operatorname{atan}\left(\frac{1}{-n}\right)$$

$$\gamma_1 = \operatorname{asin}\left(\sqrt{\frac{2\eta}{\lambda+\eta}\left(\frac{\lambda+\eta}{\eta+n}\right)}\right);\ \gamma_2 = \operatorname{asin}\left(\sqrt{\frac{2\eta}{\lambda+\eta}\left(\frac{\kappa}{\eta-\sin(\theta_0)+n\cos(\theta_0)}\right)}\right)$$

$$k = \sqrt{\frac{\eta+\lambda}{2\eta}}$$

2.1.5 An Initially-Curved Fixed-Fixed Compliant Segment. The closed-form elliptic integral formulation for an initially-straight fixed-fixed compliant segment can be utilized for the large-deflection analysis of an initially-curved fixed-fixed compliant segment, such that

$$\kappa_0 = \frac{Ml}{EI} + \frac{l}{R_i} \quad (17)$$

2.1.6 Fixed-Free Compliant Segment with an Initially-Straight Small-Length Flexural Pivot (SLFP).

Midha and Kuber [53] and Kuber [54] provided the closed-form elliptic integral formulation for a fixed-free compliant segment with an initially-straight SLFP subjected to beam end forces, as shown in Figure 2.7, such that

Figure 2.7 A Fixed-Free Compliant Segment with an Initially-Straight SLFP

For $0 < |\lambda| < \eta;\ \phi' - \operatorname{acos}\left(\frac{-\lambda}{\eta}\right) \leq -\theta_0 < \phi';$ and $\alpha \neq 0$

$$\mathrm{b} = \frac{l}{\alpha\eta^{5/2}}\Big\{\eta\big[\mathrm{F}(\gamma_2,\mathrm{t}) - \mathrm{F}(\gamma_1,\mathrm{t}) + 2[\mathrm{E}(\gamma_1,\mathrm{t}) - \mathrm{E}(\gamma_2,\mathrm{t})]\big] + \mathrm{n}\sqrt{2\eta(\eta+\lambda)}\,[\cos(\gamma_1) - \cos(\gamma_2)]\Big\} + \mathrm{L}\sin(\theta_0) \tag{18}$$

$$\mathrm{a} = \frac{l}{\alpha\eta^{5/2}}\Big\{-\mathrm{n}\eta\big[\mathrm{F}(\gamma_2,\mathrm{t}) - \mathrm{F}(\gamma_1,\mathrm{t}) + 2[\mathrm{E}(\gamma_1,\mathrm{t}) - \mathrm{E}(\gamma_2,\mathrm{t})]\big] + \sqrt{2\eta(\eta+\lambda)}\,[\cos(\gamma_1) - \cos(\gamma_2)]\Big\} + \mathrm{L}\cos(\theta_0) \tag{19}$$

where,

$$\alpha = \sqrt{\frac{Pl^2}{EI}} = \frac{1}{\sqrt{\eta}}[F(\gamma_2, t) - F(\gamma_1, t)]$$

For $\lambda > \eta > 0;\ \phi' - \pi \leq -\theta_0 < \phi';$ and $\alpha \neq 0$

$$b = \frac{l\sqrt{2(\eta+\lambda)}}{\alpha\eta^2}\left\{\frac{\lambda}{\eta+\lambda}[F(\psi_2, r) - F(\psi_1, r)] + [E(\psi_1, r) - E(\psi_2, r)] + n\left[\sqrt{1 - \frac{\eta - n}{\eta+\lambda}} - \sqrt{1 - \frac{\eta + \sin(\theta_0) - n\cos(\theta_0)}{\eta+\lambda}}\right]\right\} + L\sin(\theta_0) \quad (20)$$

$$a = \frac{l\sqrt{2(\eta+\lambda)}}{\alpha\eta^2}\left\{-n\left[\frac{\lambda}{\eta+\lambda}[F(\psi_2, r) - F(\psi_1, r)] + [E(\psi_1, r) - E(\psi_2, r)]\right] + \left[\sqrt{1 - \frac{\eta - n}{\eta+\lambda}} - \sqrt{1 - \frac{\eta + \sin(\theta_0) - n\cos(\theta_0)}{\eta+\lambda}}\right]\right\} + L\cos(\theta_0) \quad (21)$$

where,

$$\alpha = \sqrt{\frac{Pl^2}{EI}} = \sqrt{\frac{2}{\lambda+\eta}}\ [F(\psi_2, r) - F(\psi_1, r)]$$

$$\lambda = \kappa + \sin(\theta_0) - n\cos(\theta_0)$$

$$\kappa = \frac{M^2}{2PEI}$$

$$\kappa = \frac{\kappa_0^2}{2\alpha^2}$$

$$\kappa_0 = \frac{Ml}{EI}$$

$$M = FL\sin(\phi - \theta_0); F = \eta P$$

$$\eta = \sqrt{1 + n^2};\ \phi = \operatorname{atan}\left(\frac{1}{-n}\right)$$

$$\phi' = \operatorname{atan}\left(\frac{1}{n}\right)$$

$$\gamma_1 = \operatorname{asin}\left(\sqrt{\frac{\eta - n}{\eta + \lambda}}\right);\ \gamma_2 = \operatorname{asin}\left(\sqrt{\frac{\eta + \sin(\theta_0) - n\cos(\theta_0)}{\eta + \lambda}}\right)$$

$$\psi_1 = \operatorname{asin}\left(\sqrt{\frac{\eta - n}{2\eta}}\right);\ \psi_2 = \operatorname{asin}\left(\sqrt{\frac{\eta + \sin(\theta_0) - n\cos(\theta_0)}{2\eta}}\right)$$

$$t = \sqrt{\frac{\eta + \lambda}{2\eta}};\ r = \sqrt{\frac{2\eta}{\eta + \lambda}}$$

2.1.7 Fixed-Free Compliant Segment with an Initially-Curved Small-Length Flexural Pivot (SLFP). Midha and Kuber [53] and Kuber [54] provided the closed-form elliptic integral formulation for a fixed-free compliant segment with an initially-straight SLFP subjected to beam end forces, as shown in Figure 2.8, such that

Figure 2.8 A Fixed-Free Compliant Segment with an Initially-Curved SLFP

For $0 < |\lambda| < \eta;\ \phi' - \operatorname{acos}\left(\frac{-\lambda}{\eta}\right) \leq -\theta_0 < \phi';$ and $\alpha \neq 0$

$$\begin{aligned} b = \frac{l}{\alpha\eta^{5/2}}\{&\eta\left[F(\gamma_2, t) - F(\gamma_1, t) + 2[E(\gamma_1, t) - E(\gamma_2, t)]\right] \\ &+ n\sqrt{2\eta(\eta+\lambda)}\,[\cos(\gamma_1) - \cos(\gamma_2)]\} + L\sin(\theta_0) \end{aligned} \tag{22}$$

$$\begin{aligned} a = \frac{l}{\alpha\eta^{5/2}}\Big\{&-n\eta\left[F(\gamma_2, t) - F(\gamma_1, t) + 2[E(\gamma_1, t) - E(\gamma_2, t)]\right] \\ &+ \sqrt{2\eta(\eta+\lambda)}\,[\cos(\gamma_1) - \cos(\gamma_2)]\Big\} + L\cos(\theta_0) \end{aligned} \tag{23}$$

where,

$$\alpha = \sqrt{\frac{Pl^2}{EI}} = \frac{1}{\sqrt{\eta}}[F(\gamma_2, t) - F(\gamma_1, t)]$$

For $\lambda > \eta > 0;\ \phi' - \pi \leq -\theta_0 < \phi';$ and $\alpha \neq 0$

$$\begin{aligned} b = \frac{l\sqrt{2(\eta+\lambda)}}{\alpha\eta^2}\Bigg\{&\frac{\lambda}{\eta+\lambda}[F(\psi_2, r) - F(\psi_1, r)] + [E(\psi_1, r) - E(\psi_2, r)] \\ &+ n\left[\sqrt{1 - \frac{\eta - n}{\eta+\lambda}} - \sqrt{1 - \frac{\eta + \sin(\theta_0) - n\cos(\theta_0)}{\eta+\lambda}}\right]\Bigg\} \\ &+ L\sin(\theta_0) \end{aligned} \tag{24}$$

$$\begin{aligned} a = \frac{l\sqrt{2(\eta+\lambda)}}{\alpha\eta^2}\Bigg\{&-n\left[\frac{\lambda}{\eta+\lambda}[F(\psi_2, r) - F(\psi_1, r)] + [E(\psi_1, r) - E(\psi_2, r)]\right] \\ &+ \left[\sqrt{1 - \frac{\eta - n}{\eta+\lambda}} - \sqrt{1 - \frac{\eta + \sin(\theta_0) - n\cos(\theta_0)}{\eta+\lambda}}\right]\Bigg\} + L\cos(\theta_0) \end{aligned} \tag{25}$$

where,

$$\alpha = \sqrt{\frac{Pl^2}{EI}} = \sqrt{\frac{2}{\lambda+\eta}}\,[F(\psi_2, r) - F(\psi_1, r)]$$

$$\lambda = \kappa + \sin(\theta_0) - n\cos(\theta_0)$$

$$\kappa = \frac{M^2}{2PEI}$$

$$\kappa = \frac{\kappa_0^2}{2\alpha^2}$$

$$\kappa_0 = \frac{Ml}{EI} + \frac{l}{R_i}$$

$$M = FL\sin(\phi - \theta_0);\ F = \eta P$$

$$\eta = \sqrt{1 + n^2};\ \phi = \operatorname{atan}\left(\frac{1}{-n}\right)$$

$$\phi' = \operatorname{atan}\left(\frac{1}{n}\right)$$

$$\gamma_1 = \operatorname{asin}\left(\sqrt{\frac{\eta - n}{\eta + \lambda}}\right);\ \gamma_2 = \operatorname{asin}\left(\sqrt{\frac{\eta + \sin(\theta_0) - n\cos(\theta_0)}{\eta + \lambda}}\right)$$

$$\psi_1 = \operatorname{asin}\left(\sqrt{\frac{\eta - n}{2\eta}}\right);\ \psi_2 = \operatorname{asin}\left(\sqrt{\frac{\eta + \sin(\theta_0) - n\cos(\theta_0)}{2\eta}}\right)$$

$$t = \sqrt{\frac{\eta + \lambda}{2\eta}};\ r = \sqrt{\frac{2\eta}{\eta + \lambda}}$$

2.2 CHAIN ALGORITHM

The Chain Algorithm is a numerical technique for the large-deflection analysis of cantilevered compliant segments. The Chain Algorithm can be extended for the analysis of compliant mechanisms wherein at least one of its constituent segments is clamped to the ground. Harrison [77] utilized the Chain Algorithm to analyze non-uniform elastic columns. Miller [78] and Coutler and Miller [79] utilized the Chain Algorithm to solve nonlinear problems. Midha [20], Midha et al. [23], Her et al. [24], and Her [25] improved the Chain Algorithm for the large-deflection analysis of compliant segments.

The Chain Algorithm discretizes a compliant beam into multiple segments, as shown in Figure 2.9. Each element i is composed of two nodes i and $i-1$. The large-

deflection analysis begins from the cantilevered end of the compliant beam. The algorithm utilizes small-deflection analysis to calculate the deflection of node i of element i, in its isolation. The procedure then provides a rigid-body rotation to all subsequent elements of the compliant beam and cantilevers it at the deflected node i. Typically, each element is considered inextensible, and therefore δ_{ax} is assumed to be negligible. Consequently, a large number of elements are required for accurate results. The mathematical formulation of the large-deflection analysis using the Chain Algorithm constitutes of equations (26) through (40).

Figure 2.9 A Cantilevered Compliant Segment and its Discretization for Chain Algorithm

Beam end loads are transferred to each node i using the following equations:

$$(P_{ax})_i = \left[\sum_{j=1}^{n}(f_x)_j\right]\cos(\psi_i) + \left[\sum_{j=1}^{n}(f_y)_j\right]\sin(\psi_i) \tag{26}$$

$$(P_{tr})_i = -\left[\sum_{j=1}^{n}(f_x)_j\right]\sin(\psi_i) + \left[\sum_{j=1}^{n}(f_y)_j\right]\cos(\psi_i) \tag{27}$$

$$M_i = \sum_{j=1}^{n} m_j + \sum_{j=1}^{n}\left[(f_y)_j\Delta\tilde{x}_{ji} - (f_x)_j\Delta\tilde{y}_{ji}\right] \tag{28}$$

where, $(P_{ax})_i$, $(P_{tr})_i$, and M_i are the internal axial, transverse, and moment loads at node i, respectively, and $(f_x)_j$, $(f_y)_j$, and m_j are the external applied loads at node j, respectively, relative to the global coordinate system O-X-Y.

$$\psi_j = \theta_i + \Delta\Theta_{i-1} \tag{29}$$

where, $\Delta\Theta_{i-1}$is the total angular displacement of the previous element, and θ_i the orientation of the segment in its undeformed configuration.

In order to incorporate the effects of axial stiffening, the transverse load is modified, such that

$$(P_{tr})_{i,eq} = \frac{(P_{tr})_i}{1-\alpha_i} \tag{30}$$

$$\alpha_i = \frac{4(P_{ax})_i {L_i}^2}{E_i I_i \pi^2} \tag{31}$$

The deflection of each element can be calculated using the following equations:

$$(\delta_{tr})_i = \frac{1}{E_i I_i}\left[\frac{(P_{tr})_i {L_i}^3}{3} + \frac{M_i {L_i}^2}{2}\right] \tag{32}$$

$$\Delta\theta_i = \frac{1}{E_i I_i}\left[\frac{(P_{tr})_i {L_i}^2}{2} + M_i L_i\right] \quad (33)$$

Figure 2.10 Deflection of Element i as Calculated by the Chain Algorithm

Total displacement of the i^{th} node is given by equations (34) thru (40), as shown in Figure 2.10.

$$\Delta X_i = \Delta X_{i-1} + {\Delta x_i}^r + {\Delta x_i}^e \quad (34)$$

$$\Delta Y_i = \Delta Y_{i-1} + {\Delta y_i}^r + {\Delta y_i}^e \quad (35)$$

$$\Delta\Theta_i = \Delta\Theta_{i-1} + \Delta\theta_i \quad (36)$$

where, $\Delta x_i{}^r$ and $\Delta y_i{}^r$ represent the change in the location of node i due its rigid-body rotation caused by the displacement of the $i-1^{th}$ element in the global coordinate system O-X-Y, and $\Delta x_i{}^e$ and $\Delta y_i{}^e$ represent the change in the coordinate of the node i due the deflection caused by the applied loading, given by:

$$\Delta x_i{}^r = L_i(\cos(\psi_i) - \cos(\theta_i)) \quad (37)$$

$$\Delta y_i{}^r = L_i(\sin(\psi_i) - \sin(\theta_i)) \quad (38)$$

$$\Delta x_i{}^e = -(\delta_{tr})_i \sin(\psi_i) + (\delta_{ax})_i \cos(\psi_i) \quad (39)$$

$$\Delta y_i{}^e = (\delta_{tr})_i \cos(\psi_i) + (\delta_{ax})_i \sin(\psi_i) \quad (40)$$

The solution procedure utilizes the conventional matrix theory, in line with the finite element analysis approach. However, the element equations developed above reduces the order of the final matrix to the number of unknowns, thus significantly reducing the matrix operations. Therefore, the Chain Algorithm has proved to be an efficient approach for large-deflection analysis of compliant segments and compliant segments. The shooting method proposed by Her et al. [24] allows the Chain Algorithm to be applied towards the large-deflection analysis of compliant segments and compliant mechanisms subjected to load or displacement boundary conditions, or a combination thereof.

Even though the approach is efficient and provides accurate results, recent experiences have demonstrated that the convergence becomes challenging with the increase of displacement boundary condition specifications [80]. In addition, the design approach requires specification of an initial configuration. Considering these challenges, Midha and Her [32] embarked on preliminary discussions on the feasibility of the use of rigid-body equivalent models and discrete springs to simulate compliant mechanisms, later to be known as the pseudo-rigid-body model (PRBM) concept. Inspired by this notion, Salamon and Midha [27, 28] undertook the first studies in evaluating the mechanical advantage in compliant mechanisms, using the PRBM concept.

2.3 PSEUDO-RIGID-BODY MODEL (PRBM) CONCEPT

The pseudo-rigid-body model (PRBM) concept assists in an accurate and efficient modeling of large-deflection compliant members. A flexible member, compliant segment, is represented as an equivalent rigid-body kinematic chain. The number of rigid-links required in the PRBM representation depends on the segment type and the applied boundary conditions. The rigid-links in a PRBM are connected using pin joints called as the characteristic pivot. The beam's resistance to bending is simulated using a torsional spring, placed at the characteristic pivot. PRBM concept allows the development of parametric relationships that can replace the complicated elliptic integral formulations, thus simplifying compliant mechanism synthesis, analysis and design. PRBM parameters are evaluated such that the beam end point location can be estimated within a small error tolerance, of say 0.5%, w.r.t. the closed-form elliptic integral solutions.

Experiences in the recent decades have shown that PRBMs can be potentially simple, efficient, and accurate tools for modeling compliant segment types. The largest benefit in the use of the PRBM approach comes from considering compliant mechanisms as equivalent rigid-body mechanisms with characteristic compliance (discrete springs), thus making available a wealth of existing rigid-body mechanism analysis and synthesis knowledge to the treatment of compliant mechanisms. The PRBMs developed for various compliant segment types are discussed in this section.

2.3.1 PRBM for an Initially-Straight Fixed-Pinned Compliant Segment.

Figure 2.11 shows an initially-straight fixed-pinned compliant segment of length *l*, area moment of inertia I, and made from a material of modulus of elasticity E; subjected to beam end force F at an angle ϕ, measured from the undeformed beam orientation.

The PRBM for this segment type was proposed by Howell and Midha [33], and consists of two rigid-body links with one torsional spring placed at the characteristic pivot, as shown in Figure 2.12. The length of the rigid-body links is calculated using the characteristic radius factor γ, which is a function of load factor n. Load factor n is the ratio of the axial force, denoted by nP, to the transverse force, denoted by P. The spring stiffness of the torsional spring k is a function of characteristic radius factor γ and the

beam stiffness coefficient K_Θ. The beam end angle is represented by θ_0, and pseudo-rigid-body angle by Θ. The beam end angle and pseudo-rigid-body angle are related with the parametric angle coefficient c_θ. The location of the beam end point along the undeformed beam orientation is defined by 'a,' and the location of the beam end point transverse to the undeformed beam orientation is defined by 'b.'

Howell and Midha [33] provided the parametric expressions for the characteristic radius factor and parametric angle coefficient and Howell et al. [37] provided the parametric expressions for the beam stiffness coefficient. Later, Pauly and Midha [38] provided improved expressions for these PRBM variables, which constitute the following set of equations.

Figure 2.11. An Initially-Straight Fixed-Pinned Compliant Segment

Figure 2.12. PRBM of an Initially-Straight Fixed-Pinned Compliant Segment

The characteristic radius factor γ is given by:

$$\gamma = 0.855651 - 0.016438n \quad \text{for } -4 < n \leq -1.5$$

$$\gamma = 0.852138 - 0.018615n \quad \text{for } -1.5 < n \leq -0.5 \tag{41}$$

$$\gamma = 0.851892 - 0.020805n + 0.005867n^2 - 0.000895n^3 + 0.000069n^4 - 0.000002n^5 \quad \text{for } -0.5 < n \leq 10$$

The parametric angle coefficient c_θ is given by:

$$c_\theta = 1.238945 + 0.012035n + 0.00454n^2 \quad \text{for } -4 < n \leq -0.5$$

$$c_\theta = 1.238845 + 0.009113n - 0.001929n^2 + 0.000191n^3 - 0.000007n^4 \quad \text{for } -0.5 < n \leq 10 \tag{42}$$

The beam stiffness coefficient K_Θ is given by:

$$K_\Theta = 2.66041 - 0.069005n - 0.002268n^2 \quad \text{for } -4 < n \leq -0.5$$

$$K_\Theta = 2.648834 - 0.074727n + 0.026328n^2 - 0.004609n^3 + 0.000390n^4 - 0.000013n^5 \quad \text{for } -0.5 < n \leq 10 \tag{43}$$

where,

$$n = \frac{-1}{\tan(\phi)} = \frac{F_x}{F_y} = \frac{nP}{P}$$

The beam end angle θ_0 can be related to the pseudo-rigid-body angle Θ through the parametric angle coefficient c_θ [33], such that:

$$\theta_0 = c_\theta \Theta \tag{44}$$

The spring constant of the torsional spring can be determined using the following relation [36]

$$k = \gamma K_\Theta \frac{EI}{l} \tag{45}$$

The nondimensional transverse load factor [37] is given as

$$\alpha_t^2 = \frac{F_t l^2}{EI} \tag{46}$$

where,

$$F_t = F\sin(\phi - \Theta); \text{and } F = P\sqrt{1 + n^2}$$

Also,

$$\alpha_t^2 = K_\Theta \Theta \tag{47}$$

Using equations (41) through (47) the beam end point coordinates can be readily calculated, given as

$$a = l - \gamma l[1 - \cos(\Theta)] \tag{48}$$

$$b = \gamma l \sin(\Theta) \tag{49}$$

$$\Theta = \operatorname{atan} \frac{b}{a - (1-\gamma)l} \tag{50}$$

Recently Midha et al. [81] presented a method for more accurate calculation of the beam stiffness coefficient K_Θ. The newer expressions, considered as functions of load factor n and the pseudo-rigid-body angle Θ, significantly reduce the relative error of beam end point estimation. These expressions are given as:

$$\begin{aligned} K_\Theta = \frac{1}{\Theta}(&0.004233 - 0.012972n + 2.567095\Theta + 0.003993n^2 - 0.037173\Theta^2 \\ &- 0.000297n^3 + 0.117997\Theta^3 - 0.034678n\Theta + 0.003467n^2\Theta \\ &- 0.009474n\Theta^2 \end{aligned} \tag{51}$$

$$\text{for } 0 \le n \le 10, 0 < \Theta \le 65^0$$

$$\begin{aligned} K_\Theta = \frac{1}{\Theta}(&0.000651 - 0.008244n + 2.544577\Theta - 0.004764n^2 + 0.071215\Theta^2 \\ &- 0.000104n^3 + 0.079696\Theta^3 + 0.069274n\Theta + 0.061507n^2\Theta \\ &- 0.347588n\Theta^2 \end{aligned} \tag{52}$$

$$\text{for } 0 \le n \le 10, 0 < \Theta \le 65^0$$

2.3.2 PRBM for an Initially-Curved Fixed-Pinned Compliant Segment.

Figure 2.13 shows an initially-curved fixed-pinned compliant segment of length $\boldsymbol{l}$, subjected to beam end forces P and nP. The PRBM for this segment type was proposed by Howell [37], and consists of two rigid-body links with one torsional spring placed at the characteristic pivot, as shown in Figure 2.14.

Figure 2.13. An Initially-Curved Fixed-Pinned Compliant Segment

Figure 2.14. PRBM of an Initially-Curved Fixed-Pinned Compliant Segment

The initial curvature of the beam can be represented as

$$\kappa_0 = \frac{l}{R_i} \tag{53}$$

The initially-curved compliant beam is transformed into an initially-straight compliant beam using the following relations. Such a transformation allows the application of the parametric expressions of an initially-straight compliant segment for the large-deflection analysis of an initially-curved compliant segment.

$$\Theta_i = \operatorname{atan}\frac{b_i}{a_i - l(1-\gamma)} \tag{54}$$

$$a_i = \frac{l}{\kappa_0}\sin(\kappa_0) \tag{55}$$

$$b_i = \frac{l}{\kappa_0}(1-\cos(\kappa_0)) \tag{56}$$

$$\rho = \left\{\left[\frac{a_i}{l} - (1-\gamma)\right]^2 + \left[\frac{b_i}{l}\right]^2\right\}^{1/2} \tag{57}$$

$$k = \rho K_\Theta \frac{EI}{l} \tag{58}$$

where, a_i and b_i are the initial beam end coordinates, respectively, γ the characteristic radius factor for the initially-straight compliant segment, and ρl the equivalent length of the pseudo-rigid-body link, as shown in Figure 2.14.

The beam end point coordinates are calculated using the following equations:

$$a = l - \gamma l + \rho l\cos(\Theta) \tag{59}$$

$$b = \rho l\sin(\Theta) \tag{60}$$

$$\Theta = \operatorname{atan}\frac{b}{a - (1-\gamma)l} \tag{61}$$

2.3.3 PRBM for an Initially-Straight Fixed-Fixed Segment with a Monotonically Increasing Curvature.

Figure 2.15 shows an initially-straight fixed-fixed compliant segment in its deformed and undeformed state. The deformed state of the beam has a monotonically increasing curvature.

Howell [36] showed that the PRBM for an initially-curved fixed-pinned compliant segment can be utilized for the large-deflection analysis of an initially-straight fixed-fixed compliant segment that has a monotonically increasing curvature in its deformed state, such that

$$\kappa_0 = \frac{\mathrm{M}l}{\mathrm{EI}} \tag{62}$$

where, M is the reaction moment at the guided end.

Figure 2.15 An Initially-Straight Fixed-Fixed Compliant Segment with a Monotonically Increasing Curvature

Saxena and Kramer [45] also presented a PRBM for an initially-straight fixed-fixed compliant segment that has a monotonically increasing curvature in its deformed state. This PRBM includes a slider at the characteristic pivot that is attached to a linear spring.

2.3.4 PRBM for an Initially-Straight Fixed-Fixed Segment with an Inflection Point in its Deformed State. Figure 2.16 shows an initially-straight fixed-fixed compliant segment in its deformed and undeformed state. The deformed state of the beam has an inflection point in its continuum, and a zero beam end angle.

Howell [36] provided the PRBM for a fixed-guided compliant beam with one inflection point in its deformed state, with a constant beam end angle, i.e. $\theta_0 = 0$ deg., as shown in Figure 2.17.

Figure 2.16. An Initially-Straight Fixed-Guided Compliant Beam with an Inflection Point in its Deformed Configuration and a Zero Beam End Angle

Figure 2.17. PRBM of an Initially-Straight Fixed-Guided Compliant Beam with an Inflection Point in its Deformed Configuration and a Zero Beam End Angle

The characteristic radius factor γ and beam stiffness coefficient K_Θ are evaluated using the expressions generated for an initially-straight fixed-pinned compliant segment. The spring constant of the torsional springs are given by:

$$k = 2\gamma K_\Theta \frac{EI}{l} \tag{63}$$

Figure 2.18 shows an initially-straight fixed-guided compliant beam with an inflection point in its deformed state, however, the beam end angle being different from the undeformed configuration. A PRBM for such a compliant segment type was proposed by Lyon et al. [47], shown in Figure 2.19.

Figure 2.18. An Initially-Straight Fixed-Guided Compliant Beam with an Inflection Point in its Deformed State and a Non-Zero Beam End Angle

Figure 2.19. PRBM of an Initially-Straight Fixed-Guided Compliant Beam with an Inflection Point in its Deformed State and a Non-Zero Beam End Angle

This PRBM utilizes the well-known property of an inflection point to treat it as an instantaneous pin joint. The fixed-guided compliant beam is treated as a pair of fixed-pinned compliant segments, as shown in Figure 2.19. The PRBM, however, is valid for loads that cause an equal restoring torque at the torsional springs. The following set of equations has been proposed for the analysis of such a segment type:

$$\theta_E = \Theta_A + \beta - \Theta_B \tag{64}$$

$$\beta = C_A\Theta_A - C_B\Theta_B \tag{65}$$

$$F\gamma_A l_A \cos(\psi)\cos(\Theta_A) + F\gamma_A l_A \sin(\psi)\sin(\Theta_A) = k\Theta_A \tag{66}$$

$$F\gamma_B l_B \cos(\psi + \theta_E)\cos(\Theta_B) + F\gamma_B l_B \sin(\psi + \theta_E)\sin(\Theta_B) = k\Theta_B \tag{67}$$

$$k = \gamma K_\Theta \frac{EI}{l} \tag{68}$$

$$\frac{\Theta_A}{\Theta_B} = \frac{\gamma_B K_{\Theta B} l_A}{\gamma_A K_{\Theta A} l_B} \tag{69}$$

$$l_A + l_B = l \tag{70}$$

This dissertation provides a PRBM for an initially-straight fixed-guided compliant beam with an inflection point in its deformed state, with a non-zero beam end angle. The formulation developed applies the properties of inflection and the static equilibrium conditions to generate the set of governing equations. Section 3 discusses the PRBM for an initially-straight fixed-guided compliant beam with an inflection point.

2.3.5 PRBM for an Initially-Curved Pinned-Pinned Compliant Segment.

Figure 2.20 shows an initially-curved pinned-pinned compliant segment. PRBM for this segment type was presented by Edwards et al. [44], shown in Figure 2.21.

The PRBM considers this segment type as a pair of initially-curved fixed-pinned segments, fixed at the center of the initially-curved pinned-pinned segment, as shown in Figure 2.21.

Figure 2.20. An Initially-Curved Pinned-Pinned Compliant Segment

Figure 2.21. PRBM of an Initially-Curved Pinned-Pinned Compliant Segment

2.3.6 PRBM for a Fixed-Free Compliant Segment with an Initially-Straight or Initially-Curved SLFP. Figure 2.22 and Figure 2.23 show a fixed-free compliant segment subjected to beam end forces with an initially-straight and initially-curved SLFP, respectively. PRBM for these segment types is proposed by Howell and Midha [34], and later verified by Midha and Kuber [53], shown in Figure 2.24.

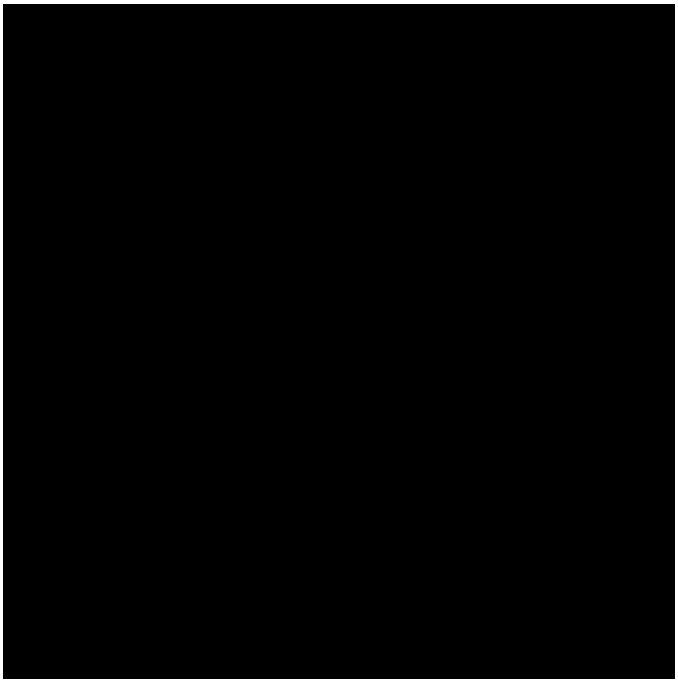

Figure 2.22. A Fixed-Free Compliant Beam with an Initially-Straight SLFP

Figure 2.23. A Fixed-Free Compliant Beam with an Initially-Curved SLFP

Figure 2.24. PRBM for a Fixed-Free Compliant Beam with a SLFP

The characteristic radius factor is given as

$$\gamma = \mathrm{L} + \frac{l}{2} \tag{71}$$

where, L is the length of the rigid-segment and *l* is the length of the compliant segment measured along the initial-curvature.

The spring constant of the torsional spring is given as

$$\mathrm{k} = \frac{\mathrm{EI}}{l} \tag{72}$$

The beam end angle and pseudo-rigid-body angle are equal for a fixed-free compliant segment with an initially-straight or initially-curved SLFP, that is

$$\theta_0 = \Theta \tag{73}$$

The beam end point coordinates for a fixed-free beam with an initially-straight SLFP can be calculated using the following equations [53].

$$a = \frac{l}{2} + \left(L + \frac{l}{2}\right)\cos(\Theta) \tag{74}$$

$$b = \left(L + \frac{l}{2}\right)\sin(\Theta) \tag{75}$$

$$k\Theta = F\left(L + \frac{l}{2}\right)\sin(\phi - \Theta) \tag{76}$$

The beam end point coordinates for a fixed-free beam with an initially-curved SLFP can be calculated using the following equations [53].

$$a = \frac{l}{2\kappa_0}\sin(\kappa_0) + \left(L + \frac{l}{2}\right)\cos(\Theta) \tag{77}$$

$$b = \frac{l}{2\kappa_0}(1 - \cos(\kappa_0)) + \left(L + \frac{l}{2}\right)\sin(\Theta) \tag{78}$$

$$k(\Theta - \Theta_i) = F\left(L + \frac{l}{2}\right)\sin(\phi - \Theta) \tag{79}$$

$$\Theta_i = \operatorname{atan}\left(\frac{b_i - \frac{l}{2\kappa_0}(1 - \cos(\kappa_0))}{a_i - \frac{l}{2\kappa_0}\sin(\kappa_0)}\right) \tag{80}$$

$$a_i = \frac{l}{\kappa_0}\sin(\kappa_0) + L\cos(\kappa_0) \tag{81}$$

$$b_i = \frac{l}{\kappa_0}(1 - \cos(\kappa_0)) + L\sin(\kappa_0) \tag{82}$$

where, a_i, and b_i are the initial beam end coordinates, and Θ_i the initial angle of the pseudo-rigid-body link.

2.4 PRBM CONCEPT TOWARDS COMPLIANT MECHANISM DESIGN AND ANALYSIS

The largest benefit of PRBM concept comes from its use in compliant mechanism design and analysis. The PRBM concept allows the transformation of compliant mechanisms into equivalent rigid-body mechanisms with characteristic compliance, represented by discrete springs, thus making available a wealth of the existing rigid-body mechanism synthesis and analysis knowledge to the treatment of compliant mechanisms.

Figure 2.25 shows a partially-compliant mechanism comprising of an initially-straight fixed-pinned segment, initially-curved SLFP, and an initially-straight SLFP. Figure 2.26 shows its PRBM constructed using the PRBM of constituent segment types.

Figure 2.25. A Partially-Compliant Mechanism

Figure 2.26. PRBM of the Partially-Compliant Mechanism shown in Figure 2.25

Such a transformation between rigid-body mechanisms and compliant mechanisms allows for the design of a wide-range of compliant mechanisms, resulting from a rigid-body mechanism design. Figure 2.27 shows all possible compliant mechanism designs for a pseudo-rigid-body four-bar mechanism [64].

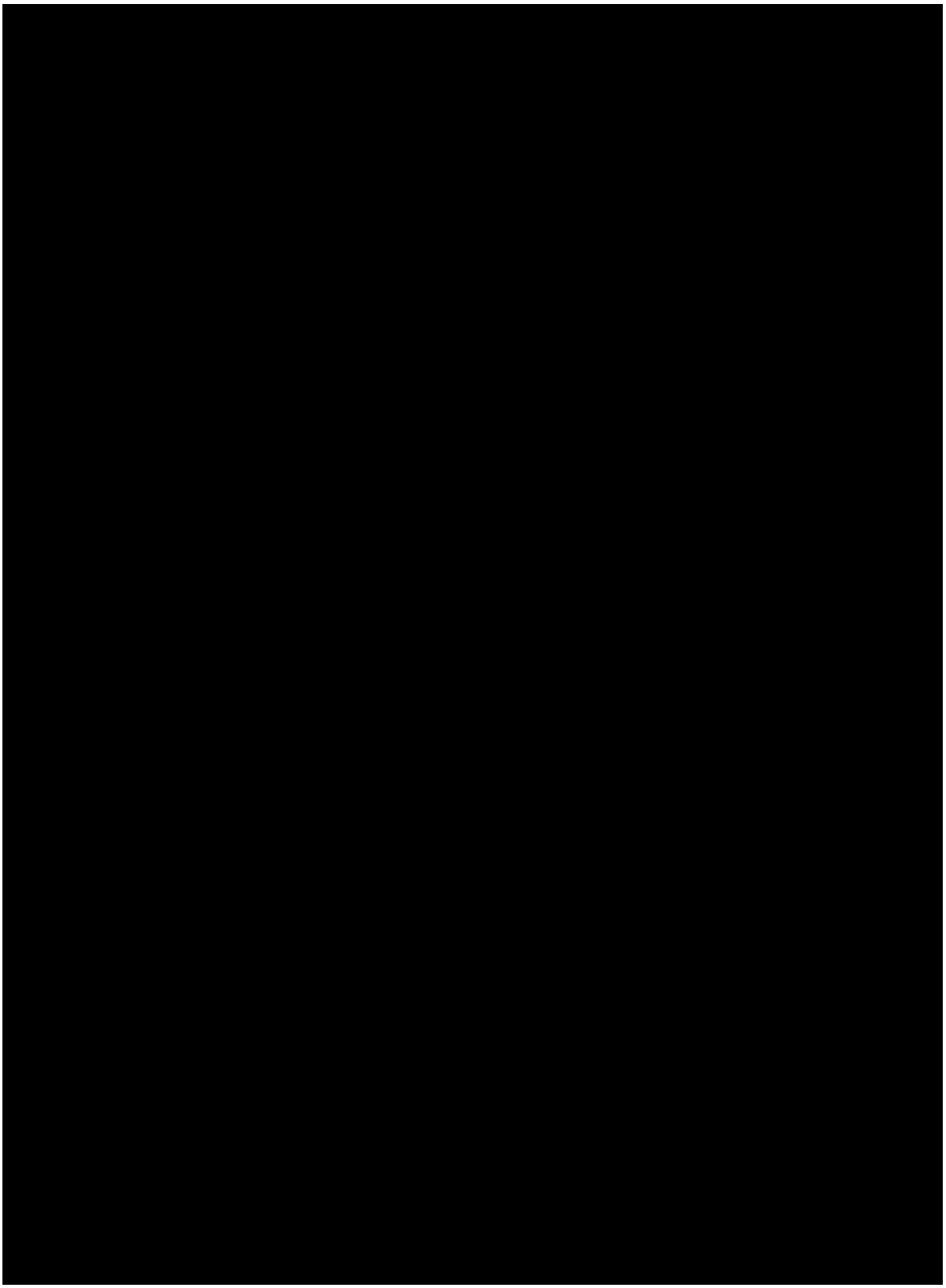

Figure 2.27. Possible Compliant Mechanism Designs for the pseudo-rigid-body four-bar mechanism

2.5 SUMMARY

This section presented three large-deflection analysis techniques. The closed-form solutions obtained using elliptic integral formulations provide accurate results. The complicated nature of the equations in the closed-form solutions limit its application to simple boundary conditions, and typically used for analysis purposes. The Chain Algorithm is a numerical technique that allows for an efficient and accurate analysis of compliant segments and compliant mechanisms. Even though the method is credible, it suffers from its unique limitations. The PRBM concept, in contrast, has been proved to be very simple and efficient method for the design and analysis of compliant segments and compliant mechanisms. The approach considers compliant segments and compliant mechanisms as an equivalent rigid-body kinematic chain and rigid-body mechanism, respectively. This dissertation applies the PRBM concept for providing synthesis, analysis and design methodologies for compliant segments and compliant mechanisms. The PRBM concept is also utilized in conjunction with the principle of minimum total potential energy to determine the expected mode shape of a given compliant mechanism.

3. PSEUDO-RIGID-BODY MODEL (PRBM) OF A FIXED-GUIDED COMPLIANT BEAM WITH AN INFLECTION POINT

This section provides an efficient method of analysis for a fixed-guided compliant beam with an inflection point, subjected to beam end load or displacement boundary conditions, or a combination thereof. To enable this, such a beam is modeled as a pair of well-established pseudo-rigid-body models (PRBMs) for fixed-free compliant beam segments. The analysis procedure relies on the properties of inflection in developing the necessary set of parametric, static equilibrium and compatibility equations for solution. The section further discusses the multiplicity of possible solutions, including displacement configurations, for any two specified beam end displacement boundary conditions, depending on the locations and types of the effecting loads on the beam to meet these boundary conditions. A unique solution may exist when a third beam end displacement boundary condition is specified; however, this selection is not unconditional. A concept of characteristic deflection domain is proposed to assist with the selection of the third boundary condition to yield a realistic solution. The analysis method is also used to synthesize a simple, fully-compliant mechanism utilizing the fixed-guided compliant segments.

3.1 BACKGROUND

This section focuses on the analysis of a fixed-guided compliant beam subjected to end load and/or displacement boundary conditions that give rise to an inflection point in the continuum of the beam, its location depending upon the displacements of the guided end. If the beam end of the initially-straight fixed-guided beam does not rotate as it is displaced, the point of inflection is located at mid-length of the compliant beam [36]. Initially-straight, fixed-guided beams with only one inflection point are considered in this work. The fixed-guided segments have largely manifested the occurrence of a single inflection point. The likelihood of multiple inflection points occurring naturally for a set of practical loads is very small. Such configurations are typically associated with higher potential energies and therefore structural instabilities, even though they may be theoretically achievable [55, 82]. The methodology presented herein may be similarly applied by discretizing beams containing more than one inflection point.

Mavanthoor [50] analyzed a fixed-guided compliant beam for end load boundary conditions using the pseudo-rigid-body model (PRBM) technique; however, the effort is limited to compressive axial loading. The present work may be regarded as a generalization of this effort. Lyon et al. [46, 47] presented a model for fixed-guided compliant beam with a final beam end angle different from the initial one, as in this section, using the principle of minimum total potential energy for its development. They also presented a simplified model in which the load and beam end deflection path are rendered uncoupled [48]. This simplified PRBM is similar to the model developed by Howell [36] for a constant beam end angle. Both models consider only a two degree-of-freedom problem (specified beam end angle and vertical deflection) with a predefined load factor (n). The assumptions therein introduce errors into the model, in the order of 10% with load boundary conditions, and higher for displacement boundary conditions; they suggest, therefore, that it is more of value for design and visualization than for the analysis of fixed-guided compliant beams. Kimball and Tsai [49] provided closed-form solutions using elliptic integral for the large-deflection analysis of initially-straight fixed-fixed compliant segments subjected to arbitrary end loads. The authors utilized this formation to generate the parametric relationships of a PRBM for a fixed-guided compliant beam. Holst et al. [83] demonstrated various buckling modes for a fixed-guided compliant beam, illustrating deflection domains with one, two and three points of inflection. Mettlach and Midha [41, 42] provided an analysis technique for a fixed-free compliant beam with specified load and/or displacement boundary conditions for forces and moments causing monotonically changing deflections. Saxena and Kramer [45] considered beam end forces with like moments, while Lyon et al. [46, 47] with opposing moments. More recently, Kim [84] proposed a method for the analysis of statically balanced compliant mechanisms. Beams with one and two points of inflection with a constant beam end angle are considered. A curve decomposition method using the theory of elastic stability is proposed; however, only vertical deflections are considered.

This section systematically develops a fundamental understanding of yet another commonly used segment/compliant mechanism type in compliant mechanisms, i.e. a fixed-guided compliant beam with an inflection point. An analysis method is presented taking into account predefined end load and/or displacement boundary conditions. The

model is successfully applied to both two degree-of-freedom (specified beam end vertical displacement and angle) and three degree-of-freedom (specified beam end horizontal and vertical displacements, and angle) analysis problems. The analysis method is implemented in the two-position synthesis of a fully-compliant mechanism, symmetrical about two-orthogonal planes, based on a fixed-guided compliant segment.

3.2 FIXED-GUIDED COMPLIANT BEAM

A fixed-guided compliant beam with end forces and moment is shown in Figure 3.1, where, P is the transverse force, nP the axial force, and M the moment. In Table 2.1, conditions on these loads are summarized that will yield an inflection point (P_i) [50].

Based on the boundary conditions, the beam may realize two possible deformed configurations. Figure 3.1shows one of these configurations with the beam end point having a positive slope, and Figure 3.2 the second configuration having a negative slope.

Figure 3.1. A Fixed-Guided Compliant Beam with End Forces and Opposing Moment in its Deformed and Undeformed State with a Positive Slope at the Beam End Point

Figure 3.2. A Fixed-Guided Compliant Beam with End Forces and Opposing Moment in its Deformed and Undeformed State with a Negative Slope at the Beam End Point

3.3 PRBM METHOD FOR ANALYSIS OF FIXED-GUIDED COMPLIANT BEAM WITH ONE INFLECTION POINT

Figure 3.3 shows a fixed-guided compliant beam in its deformed state with a positive beam end angle, where P, nP, and M are the transverse force, the axial force, and the moment, respectively; a, b, and θ_0 are the beam end horizontal location, the vertical location and the angle, measured relative to the undeformed position of the beam end. According to Table 2.1, an inflection point P_i will be generated. *The inflection point is characterized by zero curvature and, therefore, a zero moment*; this is a well-known fact that pervades the literature on the mechanics of beam deformation. This then allows the inflection point to be modeled as an instantaneous pin joint. Therefore, the fixed-guided compliant beam may be modeled as two fixed-free compliant segments, pinned at P_i. One of these segments is shown to be fixed at the origin O in the fixed reference frame O-X-Y, and the other fixed at the beam end E in the moving reference frame E-x-y, as shown in Figure 3.4, Figure 3.5, and Figure 3.6.

Considering the fixed-guided beam in Figure 3.4 as a pair of fixed-free segments, the internal forces at the inflection point will be in equilibrium, as shown in Figure 3.5,

where the subscripts 1 and 2 are associated with compliant segments 1 and 2, respectively. The PRBMs corresponding to the two compliant segments are shown in Figure 3.6. The resulting PRBM of the fixed-guided compliant beam with one inflection point is shown in Figure 3.7.

Figure 3.3. A Fixed-Guided Compliant Beam with One Inflection Point in its Deformed State with a Positive Slope at the Beam End Point

Figure 3.4. A Fixed-Guided Compliant Beam with One Inflection Point Considered as Two Compliant Segments

Figure 3.5. Segment 1 and Segment 2 of the Model Shown in Figure 3.4

Figure 3.6. PRBM of Segment 1 and Segment 2

Figure 3.7. PRBM of a Fixed-Guided Compliant Beam with One Inflection Point in its Deformed State

The 18 equations, Equations (83) through (104), summarized below are developed with the help of the free-body diagrams in Figure 3.5 and Figure 3.6, and comprise three distinct sets of equations in the analysis of the fixed-guided compliant beam, subjected to a variety of beam end load and/or displacement boundary conditions.

Based on the parametric expressions introduced by Pauly and Midha [38], Equations (83) through (94) are derived for segments 1 and 2, and are termed as *Parametric Equations*:

$$\gamma_1 = 0.855651 - 0.016438n_1 \qquad \text{for } -4 < n_1 \leq -1.5$$

$$\gamma_1 = 0.852138 - 0.018615n_1 \qquad \text{for } -1.5 < n_1 \leq -0.5 \quad (83)$$

$$\gamma_1 = 0.851892 - 0.020805n_1 + 0.005867n_1^2 - 0.000895n_1^3 + 0.000069n_1^4 - 0.000002n_1^5 \qquad \text{for } -0.5 < n_1 \leq 10$$

$$\gamma_2 = 0.855651 - 0.016438n_2 \quad \text{for } -4 < n_2 \leq -1.5$$

$$\gamma_2 = 0.852138 - 0.018615n_2 \quad \text{for } -1.5 < n_2 \leq -0.5 \tag{84}$$

$$\gamma_2 = 0.851892 - 0.020805n_2 + 0.005867n_2^2 - 0.000895n_2^3 + 0.000069n_2^4 - 0.000002n_2^5 \quad \text{for } -0.5 < n_2 \leq 10$$

$$c_{\theta_1} = 1.238945 + 0.012035n_1 + 0.00454n_1^2 \quad \text{for } -4 < n_1 \leq -0.5 \tag{85}$$

$$c_{\theta_1} = 1.238845 + 0.009113n_1 - 0.001929n_1^2 + 0.000191n_1^3 - 0.000007n_1^4 \quad \text{for } -0.5 < n_1 \leq 10 \tag{86}$$

$$c_{\theta_2} = 1.238945 + 0.012035n_2 + 0.00454n_2^2 \quad \text{for } -4 < n_2 \leq -0.5 \tag{87}$$

$$c_{\theta_2} = 1.238845 + 0.009113n_2 - 0.001929n_2^2 + 0.000191n_2^3 - 0.000007n_2^4 \quad \text{for } -0.5 < n_2 \leq 10 \tag{88}$$

$$K_{\Theta_1} = 2.66041 - 0.069005n_1 - 0.002268n_1^2 \quad \text{for } -4 < n_1 \leq -0.5 \tag{89}$$

$$K_{\Theta_1} = 2.648834 - 0.074727n_1 + 0.026328n_1^2 - 0.004609n_1^3 + 0.000390n_1^4 - 0.000013n_1^5 \quad \text{for } -0.5 < n_1 \leq 10 \tag{90}$$

$$K_{\Theta_2} = 2.66041 - 0.069005n_2 - 0.002268n_2^2 \quad \text{for } -4 < n_2 \leq -0.5 \tag{91}$$

$$K_{\Theta_2} = 2.648834 - 0.074727n_2 + 0.026328n_2^2 - 0.004609n_2^3 + 0.000390n_2^4 - 0.000013n_2^5 \quad \text{for } -0.5 < n_2 \leq 10 \tag{92}$$

where,

$$n_1 = \frac{-1}{\tan(\phi_1)} \tag{93}$$

$$n_2 = \frac{-1}{\tan(\phi_2)} \tag{94}$$

Equations (95) through (99) are derived from force and moment equilibrium using the free-body diagrams illustrated in Figure 3.5 and Figure 3.6, and are referred to as the *Static Equilibrium Equations*.

$$\frac{\mathrm{F}l_1^2}{\mathrm{EI}}\sin\left(\phi_1-\frac{\theta_{10}}{c_{\theta_1}}\right)-\mathrm{K}_{\Theta_1}\frac{\theta_{10}}{c_{\theta_1}}=0 \tag{95}$$

$$\frac{\mathrm{F}l_2^2}{\mathrm{EI}}\sin\left(\phi_2-\frac{\theta_{20}}{c_{\theta_2}}\right)-\mathrm{K}_{\Theta_2}\frac{\theta_{20}}{c_{\theta_2}}=0 \tag{96}$$

$$\mathrm{nP}+\mathrm{F}\left(\cos(\phi_2+\theta_0)\right)=0 \tag{97}$$

$$\mathrm{P}-\mathrm{F}\left(\sin(\phi_2+\theta_0)\right)=0 \tag{98}$$

$$\begin{aligned}\mathrm{M}-\left\{[\mathrm{nP}\cos(\theta_0)-\mathrm{P}\sin(\theta_0)]\gamma_2 l_2\sin\left(\frac{\theta_{20}}{c_{\theta_2}}\right)\right\}\\ -\left\{[\mathrm{P}\cos(\theta_0)+\mathrm{nP}\sin(\theta_0)]\left[(1-\gamma_2)l_2+\gamma_2 l_2\cos\left(\frac{\theta_{20}}{c_{\theta_2}}\right)\right]\right\}=0\end{aligned} \tag{99}$$

Equations (100) through (104) reflect constraints of length, slope, and displacements, and will be referred to as the *Compatibility Equations*.

$$l_1+l_2=l \tag{100}$$

$$\theta_{10}=\theta_{20}+\theta_0 \tag{101}$$

$$\phi_1=\phi_2+\theta_0 \tag{102}$$

$$\mathrm{b}=\gamma_1 l_1\sin\left(\frac{\theta_{10}}{c_{\theta_1}}\right)+\gamma_2 l_2\sin\left(\frac{\theta_{20}}{c_{\theta_2}}+\theta_0\right)+(1-\gamma_2)l_2\sin(\theta_0) \tag{103}$$

$$\mathrm{a}=(1-\gamma_1)l_1+\gamma_1 l_1\cos\left(\frac{\theta_{10}}{c_{\theta_1}}\right)+\gamma_2 l_2\cos\left(\frac{\theta_{20}}{c_{\theta_2}}+\theta_0\right)+(1-\gamma_2)l_2\cos(\theta_0) \tag{104}$$

Equations (83) through (104) summarize all the parametric, equilibrium and compatibility equations necessary to solve the fixed-guided compliant beam problem for a variety of displacement and load boundary condition types. These 18 equations contain 24 variables: $\mathrm{E}, \mathrm{I}, l, \gamma_1, \gamma_2, \mathrm{n}_1, \mathrm{n}_2, c_{\theta 1}, c_{\theta 2}, \mathrm{K}_{\Theta 1}, \mathrm{K}_{\Theta 2}, \phi_1, \phi_2, \mathrm{F}, \mathrm{L}_1, \mathrm{L}_2, \theta_{10}, \theta_{20}, \mathrm{P}, \mathrm{n}, \mathrm{M}, \mathrm{a}, \mathrm{b},$

and θ_0; the geometric and material properties, i.e. E, I and *l*, are typically specified, resulting in 21 variables. In order to solve the system of 18 equations deterministically, three additional variables would need to be specified. Typically, but not necessarily, these would be the boundary conditions.

3.4 ON THE UNIQUENESS OF SOLUTION FOR SPECIFIED BEAM END DISPLACEMENT BOUNDARY CONDITIONS

Infinite solutions (displacement configurations) exist for the planar, fixed-guided compliant beam for any two of three specified beam end displacement boundary conditions, depending on the locations and types of the effecting loads on the beam to satisfy these boundary conditions. A unique solution for the displacement configuration may exist when a third beam end displacement boundary condition is specified; however, this selection is not necessarily unconditional.

Two specified beam end displacement boundary conditions of, say, the vertical (transverse) deflection and angle may be met through various combinations of two effecting loads at different locations, with a direct impact on the location of the inflection point, as well as the horizontal (axial) displacement of the beam end. As examples, the following two combination of effecting load cases are considered: i) the transverse force and opposing moment at the beam end, and ii) two transverse forces, one applied at the beam end and the other at $0.8l$ from the fixed end. A combination case iii) considers the same two beam end displacement boundary conditions and, additionally, specifies a location of the inflection point, thus effectively comprising three specified displacement boundary conditions. To solve this problem, three effecting loads are selected at the beam end, i.e. a transverse force, an axial force and a moment, to enable a unique solution.

The Chain Algorithm [24], developed as a research tool for large-deflection beams of arbitrary geometry, calculates the effecting loads for specified boundary conditions, and is used satisfactorily for the combination of two loads in cases i) and ii). It is observed to have convergence difficulties for the combination of three loads in case iii), particularly when large compressive forces are experienced. For this case, the PRBM method discussed herein is used to determine the solution. A beam with the following

properties is chosen for the computations: The length of the fixed-guided compliant beam $l = 20$ inch; bending moment of inertia $I = 1.02 \times 10^{-5}$ in^4; the Modulus of Elasticity $E = 30 \times 10^6$ psi; the vertical deflection, $b = 5$ inch; and the beam end angle, $\theta_0 = -45$ deg.

The displacement configurations determined from all three cases are plotted in Figure 3.8, showing that while the two displacement boundary conditions, i.e. $b = 5$ in. and $\theta_0 = -45$ deg., have been met in each case, they are very different. It follows, as the displacement plots also show, that the location of the inflection point is different for each case. In case iii), an additional (third) axial displacement boundary condition specification yields a unique solution; however, it is generally difficult to achieve. This work considers this difficulty and proposes a method to arrive at a feasible set of axial (horizontal) displacement boundary conditions which would lead to a realistic solution for this case more readily.

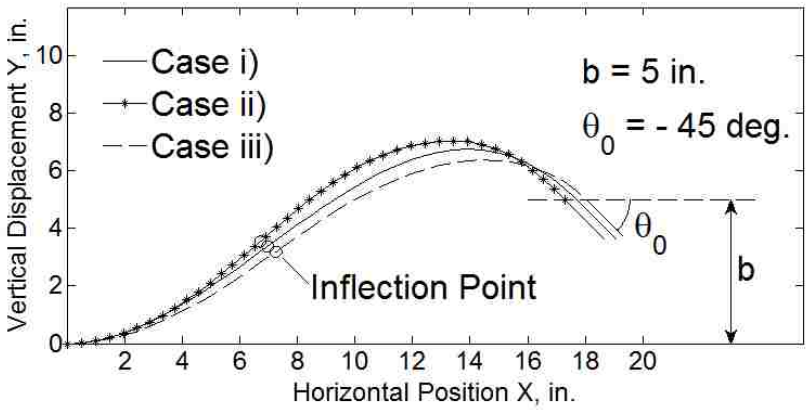

Figure 3.8. Displacement Plots for Effecting Load Combinations for a Fixed-Guided Compliant Beam

Using the case i) above, Table 3.1 summarizes the results from ANSYS®, Chain Algorithm [24] and the PRBM method. Note that loads are defined in their positive sense

in Figure 3.3. In the first row of Table 3.1, for given P and M values for a fixed-guided beam that create an inflection point, ANSYS® helps generate the beam end displacements. Two of these, i.e. the vertical deflection 'b' and beam end angle 'θ_0,' are then used as the specified boundary conditions for a fixed-guided beam, and the effecting loads at like locations are found using the Chain Algorithm and the PRBM method. The results obtained from ANSYS® and the Chain Algorithm are very similar due to the fact that both are finite element based approaches, and discretize the beam into 40 elements. On the other hand, the PRBM model gives a slightly different solution. Because the PRBM parameter values are generated w.r.t. comparisons with the closed-form elliptic integral solutions [33], the credibility of the results obtained using this approach cannot be underestimated. As mentioned earlier, infinite effecting load combinations (of load type and location) are possible to satisfy the given displacement boundary conditions. A unique displacement configuration will only be possible if a third displacement boundary condition is successfully applied. This will also be congruent with obtaining a unique inflection point location. Additionally, it is also reasoned that a set of displacement(s) and/or load boundary condition(s) at the beam end, for a total of three, will uniquely define the displacement configuration of the beam and, therefore, the location of the inflection point.

Theorem: i) For a planar fixed-guided beam, with two specified beam end displacement boundary conditions, an infinite set of displacement configurations are possible depending upon the type and location of the two effecting loads. A unique configuration with a uniquely located inflection point is only possible, whenever a solution can be determined, when a third beam end displacement boundary condition is specified. ii) For a planar fixed-guided beam, a set of three beam end displacement and/or load boundary condition(s) will uniquely define its displacement configuration, and hence the location of the inflection point.

Table 3.1. Impact of Method of Estimation of the Combination of Loads

Method	Input	Output	Verification with ANSYS® Input & Output
ANSYS®	P = 6.75	$a = 18.0163$	
	M = 72.5	$b = 5.2305$	
		$\theta_0 = -43.46$	
Chain Algorithm	b = 5.2305	a = *18.0238*	P = 6.75
	$\theta_0 = -43.46$	P = *6.75*	M = 72.54
		M = *72.54*	a = *18.0183*
			b = *5.2039*
			$\theta_0 = -43.62$
PRBM Method	b = 5.2305	a = *18.096*	P = 6.652
	$\theta_0 = -43.46$	P = *6.652*	M = 71.16
	$n_1 = 0$	M = *71.16*	a = *18.0345*
			b = *5.4165*
			$\theta_0 = -41.13$

Note 1: The units are: P lb; M in-lb; b in.; a in. and θ_0 deg.

Note 2: The italicized values represent output data

3.5 ANALYSIS OF A FIXED-GUIDED COMPLIANT BEAM WITH SPECIFIED BEAM END BOUNDARY CONDITIONS USING THE PRBM CONCEPT

3.5.1 Specified Load Boundary Conditions. As discussed in Section 3.4, a set of specified beam end load boundary conditions applied to a fixed-free compliant beam will result in a unique beam displacement configuration. Much is known about such a system and continuum mechanics, the PRBM concept, and nonlinear finite element analysis offer some approaches for determining the beam configuration.

Lyon et al. [46, 47] presented a simplified PRBM to analyze a fixed-guided compliant segment; however, the errors are reported to be in the order of 10% in

comparison to that obtained from the Chain Algorithm [24]. Mavanthoor and Midha [50, 51] extended the PRBM concept and developed the PRBM based approach for analyzing a fixed-guided compliant beam with significantly lower errors, in the order of 1.4% for the examples presented. Both of these works limited their efforts to compressive axial loads only. This section generalizes the work to include tensile loading as well.

Using the PRBM method, a fixed-guided compliant beam with specified load boundary conditions may be analyzed by solving the 18 nonlinear equations, Equations (83) through (104) for 18 unknowns, including the beam end characteristics $a, b, \text{and } \theta_0$.

3.5.2 Specified Displacement Boundary Conditions. The analysis of a compliant, large-deflection, fixed-guided beam with specified beam end displacement boundary conditions has traditionally been more complex and sparsely researched. In an early effort, Mettlach and Midha [42] developed a PRBM based analysis approach for a fixed-free compliant beam for displacement boundary conditions, however, with no inflection point occurring. Lyon et al. [46, 47] provided an approach for the analysis of a fixed-guided compliant beam with a specified end angle different from the initial value; however, the approach was limited to two displacement boundary conditions, with the reported error in the order of 15 %.

This work develops a PRBM based method for analyzing a fixed-guided compliant beam for varied combinations of beam end displacement boundary conditions, including a beam end angle that may be different from its initial value. This PRBM approach yields notably smaller errors. Each of the cases considered below is associated with a loading combination which helps satisfy the specified displacement boundary conditions.

Case 1: A three-degree-of-freedom analysis problem, wherein two beam end displacements and an end angle are specified. A fixed-guided compliant beam with three specified beam end displacement boundary conditions may be analyzed by solving the system of 18 nonlinear equations, i.e. Equations (83) through (104), for 18 unknowns that include the three beam end loads: the axial and transverse forces, and moment.

Case 2: A two-degree-of-freedom analysis problem, wherein a vertical beam end displacement and an end angle are specified. A fixed-guided compliant beam with two

specified beam end displacement boundary conditions may be analyzed for the following load combinations:

Case 2a: The transverse force and moment, while specifying a zero axial force, i.e. $n = 0$. A fixed-guided compliant beam with two specified displacement boundary conditions, and a specified zero axial force, may be analyzed by solving the 18 nonlinear equations, Equations (83) through (104), for 18 unknowns that include the two beam end loads: the transverse force and moment.

Case 2b: The axial and transverse forces, and moment, while specifying a non-zero load factor n. A fixed-guided compliant beam with two specified displacement boundary conditions, and a specified non-zero load factor n, may be analyzed by solving the 18 nonlinear equations, Equations (83) through (104), for 18 unknowns that include the three beam end loads: the axial and transverse forces, and moment.

Case 2c: The axial and transverse forces, and moment, while specifying the location of the inflection point (l_1). Specifying the third displacement boundary condition by means of the location of the inflection point, i.e. the length of the compliant segments, provides additional flexibility to the designer in achieving the same beam end vertical displacement and angle with unique, varying horizontal displacements. For instance, a fixed-guided compliant beam could be made to generate a straight-line motion with a specified stroke through controlling the end loads, while allowing the inflection point location to be varied.

A fixed-guided compliant beam with two specified displacement boundary conditions, and a specified location of the inflection point (l_1), may be analyzed by solving the 18 nonlinear equations, Equations (83) through (104), for 18 unknowns that include the three beam end loads: the axial and transverse forces, and moment. However, it should be noted that l_1 cannot be unconditionally selected over the entire length of the beam. The finite regions over which such solutions are feasible are related to the characteristic deflection domains [41, 42]. A numerical approach that assists in identifying such regions is described below.

3.6 CHARACTERISTIC DEFLECTION DOMAIN CONCEPT AND EVALUATION

The characteristic deflection domain is defined as a region or solution space wherein all possible beam end locations lie. A specific point in the deflection domain may be reached by the application of a set of effecting loads at the beam end. The development of the concept of the characteristic deflection domain for such geometrically nonlinear compliant beams has been an important development, hitherto relatively unknown, toward a clearer understanding of this physical nature of such systems. In introducing this concept, Mettlach and Midha [41, 42] made use of fixed-free compliant beam types for demonstration.

The characteristic deflection domain for a fixed-guided compliant beam is difficult to generate. In the work presented herein, the characteristic deflection domain of interest is generated numerically utilizing the location of the inflection point P_i, l_1, as shown in Figure 3.4. l_1 correlates with the horizontal location of the beam end point (the third displacement boundary condition) and, therefore, allows the development of the region comprising the beam end locations for a fixed-guided compliant beam with one inflection point as follows.

Consider a fixed-guided compliant beam with a positive beam end slope in its deformed state, Figure 3.9, where O represents the fixed end of the beam, E the guided end, OP_i the compliant segment 1, OP_1P_i its PRBM, P_1 its characteristic pivot, EP_i the compliant segment 2, EP_2P_i its PRBM, and P_2 its characteristic pivot.

A two-position (undeformed and deformed) vector-loop representation of the PRBM in Figure 3.9 is shown in Figure 3.10, where, $\bar{Z}_j$ represents the j^{th} vector, R_j its magnitude, and θ_j its orientation (angle). For an inflection point to exist, i) the orientation of vector $\bar{Z}_3$ should be greater than the beam end angle (Figure 3.10), and ii) for continuity, the resulting slopes of the compliant segments should be equal at the inflection point, P_i, as shown in Figure 3.4. In the spirit of providing the designer with reasonable estimates for possible locations of the inflection point, average PRBM parameters [33, 38 and 40] have been considered.

Figure 3.9. PRBM of a Fixed-Guided Compliant Beam with One Inflection Point in its Deformed State

Figure 3.10. A Vector-Loop Diagram for the PRBM shown in Figure 3.9

The loop-closure equations corresponding to Figure 3.10 may be solved for θ_3 and R_5 giving:

$$\theta_3 = \text{asin}\left[\frac{R_6 - R_2\sin(\theta_2) - R_4\sin(\theta_4)}{R_3}\right] \quad (105)$$

$$R_5 = R_7 - [R_1 + R_2\cos(\theta_2) + R_3\cos(\theta_3) + R_4\cos(\theta_4)] \quad (106)$$

where,

$$\theta_2 = \Theta_1;\ \theta_3 = \Theta_2 + \theta_0;\ \text{and}\ \theta_4 = \theta_0 \quad (107)$$

Using Equations (105) through (107), a computer code may be developed to determine feasible values for l_1 that are realistic and satisfy the abovementioned constraints, as outlined in the flowchart in Figure 3.11. It should be noted that the loop closure representation in Figure 3.10 will be very useful in a synthesis context as well.

The above methodology helps to develop the characteristic deflection domains, as outlined in the flowchart in Figure 3.12. Some representative characteristic deflection domains generated are presented in Figure 3.13. Such domains were invaluable in the specification of three realistic displacement boundary conditions, considered in the examples summarized in Table 3.3 through Table 3.6.

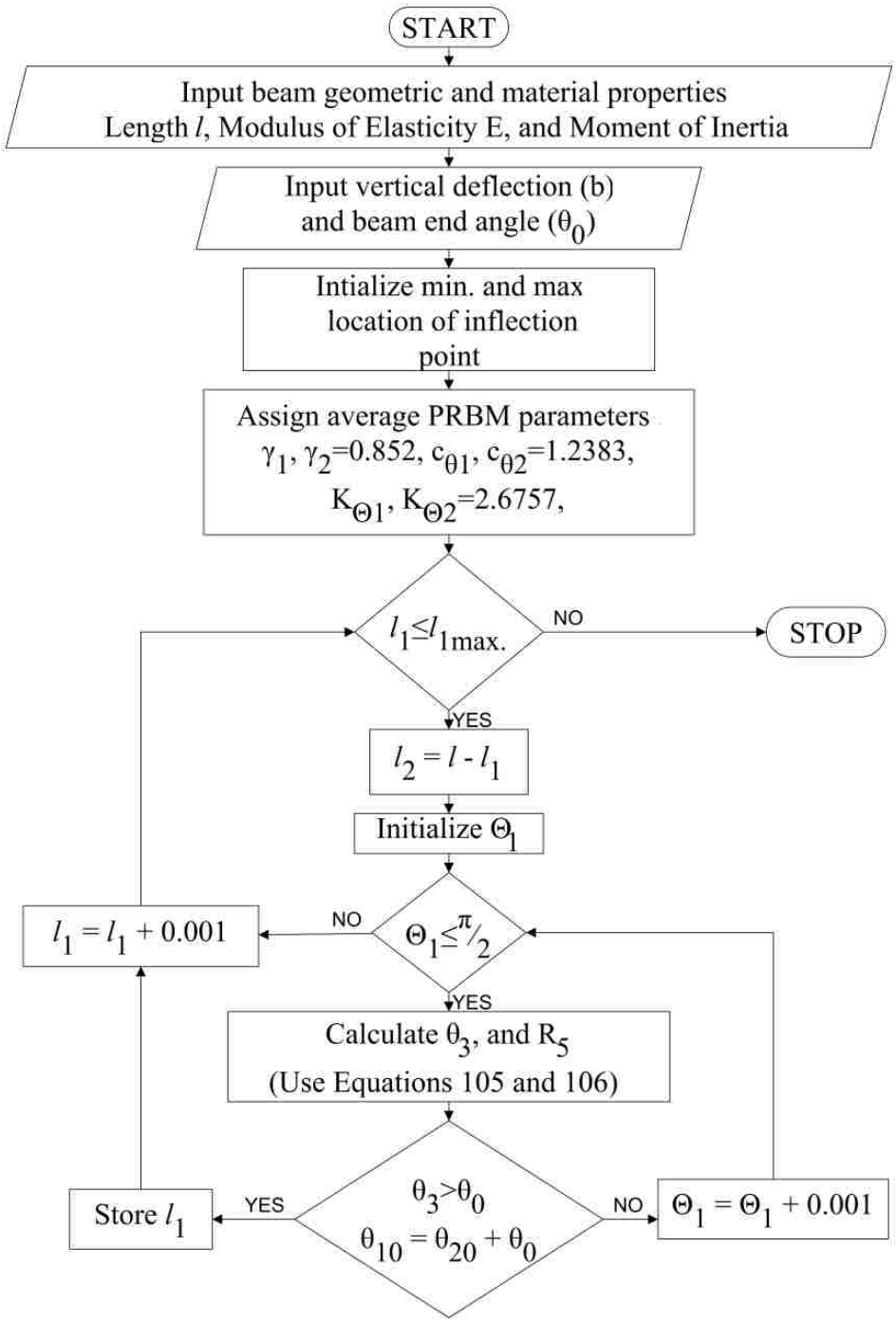

Figure 3.11. Flowchart for Estimating Feasible Values of l_1

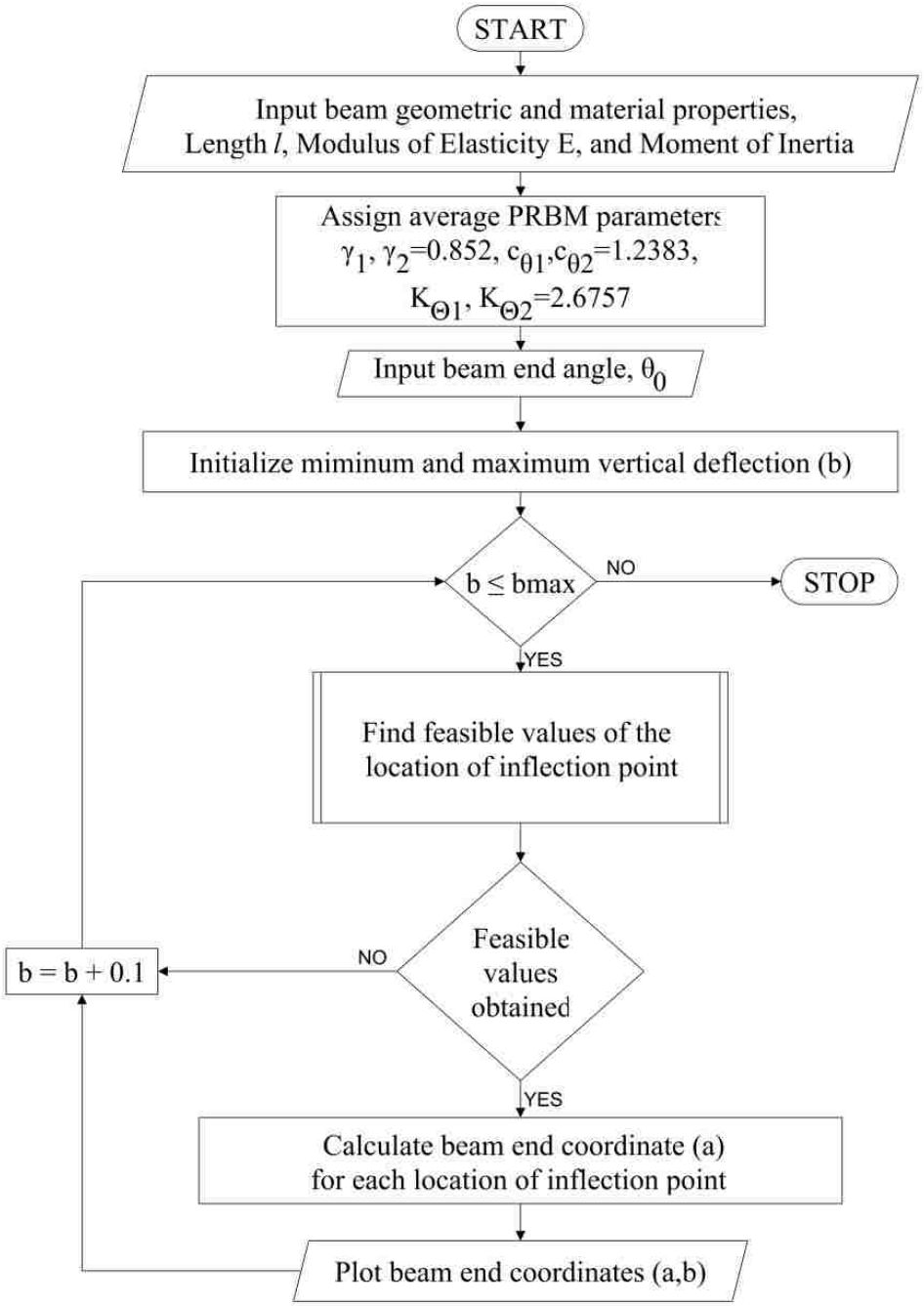

Figure 3.12. Flowchart for Determining Approximate Characteristic Deflection Domain

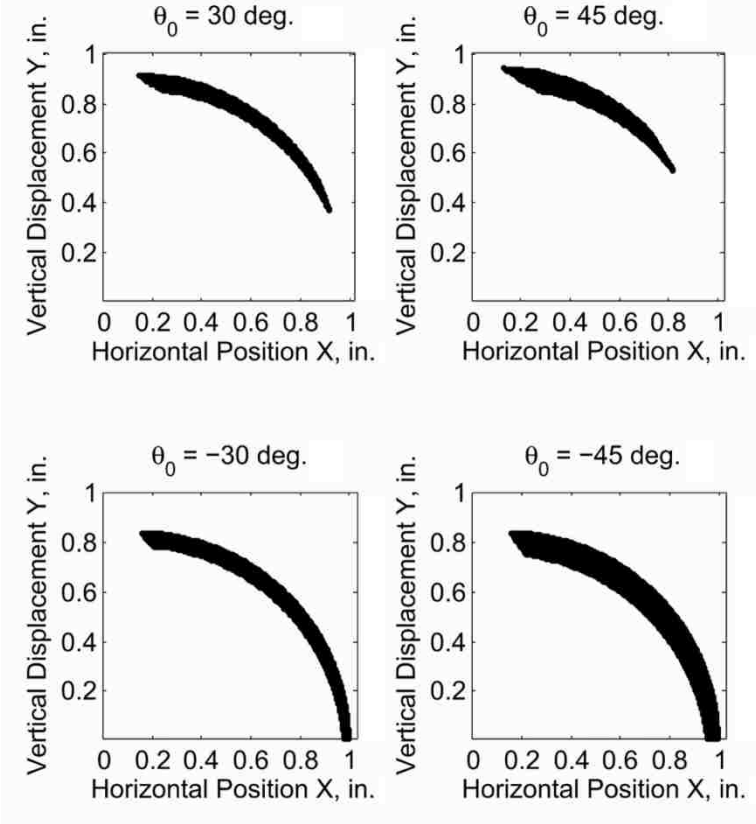

Figure 3.13. Approximate Characteristic Deflection Domain Plots for Various Beam End Angles

3.7 RESULTS AND DISCUSSIONS

The PRBM methodology outlined above yields results that are verified with those obtained from ANSYS® and the elliptic integral solution method provided by Kimball and Tsai [49], and followed by Zhang and Chen [55]. It should be noted that both the latter approaches present significant challenges when specifying displacement boundary conditions. Therefore, to alleviate this problem, the loads obtained from the PRBM method are utilized by these approaches to generate the beam end characteristics, i.e. a, b, and θ_0, for the purpose of comparing methods. Additionally, the elliptic integral method generally requires specification of precise initial estimates of beam end angle θ_0 for convergence, rendering the approach cumbersome.

A fixed-guided compliant beam of length $l = 20$ in.; width w $= 0.5$ in.; height h $= 0.0625$ in.; moment of inertia I $= 1.02 \times 10^{-5}$ in.^{4}; and modulus of elasticity E $= 30 \times 10^6$ psi is considered for the examples shown below. A variety of load and displacement boundary conditions have been considered. These results are tabulated in Table 3.2 to Table 3.6. The graphical beam displacement comparisons among the methods are shown to be indistinguishable, as exemplified in Figure 3.14. Note that the loads are defined in their positive sense in Figure 3.3.

A simple computational time comparison, for Example 2 in Table 3.2, shows that the PRBM method programmed on Maple® takes 0.09 s, only 2.5 % of the CPU time (3.51 s) taken by ANSYS®.

Table 3.2. Part (a): Analysis of a Fixed-Guided Compliant Beam with Specified Beam End Load Boundary Conditions

Load boundary conditions		**PRBM method**	**ANSYS®**	**Elliptic integral**
Ex. 1	nP $= 1.5$	a $= 12.287$	a $= 12.335$	a $= 12.336$
	P $= 3.5$	b $= 14.523$	b $= 14.423$	b $= 14.422$
	M $= 15$	$\theta_0 =$ *58.60*	$\theta_0 =$ *58.24*	$\theta_0 = 58.231$
Ex. 2	nP $= -15$	a $= 18.786$	a $= 18.783$	a $= 18.787$
	P $= 10$	b $= 6.082$	b $= 6.065$	b $= 6.053$
	M $= 55$	$\theta_0 =$ *−10.92*	$\theta_0 =$ *−10.39*	$\theta_0 =$ *−10.42*

Note 1: The units are: nP lb; P lb; M in-lb; b in.; a in. and θ_0 deg.

Note 2: The italicized values represent output data

Table 3.3. Part (b), Case 1: A Three-Degree-of-Freedom Analysis Problem

Displacement boundary conditions		**PRBM method**	**ANSYS®**	**Elliptic integral**
Ex. 1	a = 7	nP = *3.311*	a = 7.335	a = 7.333
	b = 17	P = 5.403	b = 16.85	b = 16.85
	θ_0 = 75	M = 23.58	θ_0 = *73.45*	θ_0 = *73.41*
Ex. 2	a = 16	nP = 1.559	a = 15.81	a = 15.786
	b = 11	P = 1.248	b = 11.172	b = 11.198
	θ_0 = 45	M = 7.128	θ_0 = *46.46*	θ_0 = *46.59*
Ex. 3	a = 18.5	nP = −35.635	a = 18.662	a = 18.705
	b = 5	P = 19.577	b = 5.06	b = 4.953
	θ_0 = −45	M = 130.23	θ_0 = *−42.70*	θ_0 = *−42.60*
Ex. 4	a = 18.5	nP = −19.235	a = 18.578	a = 18.58
	b = 5.5	P = 13.524	b = 5.532	b = 5.525
	θ_0 = −35	M = 94.683	θ_0 = *−33.08*	θ_0 = *− 33.20*

Note 1: The units are: nP lb; P lb; M in-lb; b in.; a in. and θ_0 deg.

Note 2: The italicized values represent output data

Table 3.4. Part (b), Case 2a: Specified Vertical Displacement, Beam End Angle, and Load Factor, n = 0

PRBM boundary conditions		PRBM method	ANSYS®	Elliptic integral
Ex. 1	b = 12	nP = *0*	b = 12.002	b = 11.996
	$\theta_0 = 40$	P = 3.897	$\theta_0 = 39.96$	$\theta_0 = 39.88$
	$n_1 = 0$	M = 17.052		
Ex. 2	b = 8	nP = *0*	b = 8.028	b = 8.023
	$\theta_0 = -25$	P = 7.094	$\theta_0 = -24.28$	$\theta_0 = -24.46$
	$n_1 = 0$	M = 68.76		

Note 1: The units are: nP lb; P lb; M in-lb; b in.; a in. and θ_0 deg.

Note 2: The italicized values represent output data

Table 3.5. Part (b), Case 2b: Specified Vertical Displacement, Beam End Angle, and Load Factor, n

PRBM boundary conditions		PRBM method	ANSYS®	Elliptic integral
Ex. 1	b = 12	nP = 0.803	b = 12.075	b = 12.033
	$\theta_0 = 40$	P = 3.212	$\theta_0 = 40.43$	$\theta_0 = 40.13$
	n = 0.25	M = 17.565		
Ex. 2	b = 12	nP = 2.352	b = 12.166	b = 12.178
	$\theta_0 = 40$	P = 1.882	$\theta_0 = 41.00$	$\theta_0 = 41.02$
	n = 1.25	M = 18.775		

Note 1: The units are: nP lb; P lb; M in-lb; b in.; a in. and θ_0 deg.

Note 2: The italicized values represent output data

Table 3.6. Part (b), Case 2c: Specified Vertical Displacement, Beam End Angle, and Location of Inflection Point, l_1

PRBM boundary conditions		**PRBM method**	**ANSYS®**	**Elliptic integral**
Ex. 1	$b = 12$	$nP = -1.972$	$b = 11.998$	$b = 11.949$
	$\theta_0 = 40$	$P = 5.565$	$\theta_0 = 39.83$	$\theta_0 = 39.58$
	$l_1 = 13.5$	$M = 15.905$		
Ex. 2	$b = 5$	$nP = -1.985$	$b = 5.043$	$b = 5.039$
	$\theta_0 = -30$	$P = 5.95$	$\theta_0 = -29.67$	$\theta_0 = -29.81$
	$l_1 = 8.5$	$M = 60.175$		
Ex. 3	$b = 5$	$nP = -11.995$	$b = 5.022$	$b = 5.017$
	$\theta_0 = -30$	$P = 5.41$	$\theta_0 = -28.71$	$\theta_0 = -28.71$
	$l_1 = 9$	$M = 74.098$		

Note 1: The units are: nP lb; P lb; M in-lb; b in.; a in. and θ_0 deg.

Note 2: The italicized values represent output data

As demonstrated in through Table 3.6, the PRBM method proves to be a simple yet efficient tool, yielding high accuracy while handling a variety of beam end boundary conditions. While observing the relatively favorable comparisons of the computed results, due to the characteristic approximations inherent in the development of each of these approaches, it would be very difficult to apportion the error contribution of these methods. The effectiveness of the PRBM method in generating large data sets readily lends itself for developing parametric relationships for the fixed-guided compliant beam with one point of inflection, in a vein to improve upon the existing analysis and synthesis methods [48, 49].

The PRBM approach is versatile in handling problems of analysis and synthesis, with displacement and force boundary conditions, lending itself well to visualization of the kinematics of deformation of compliant segment types. The concept of characteristic deflection domain graphically reveals an intrinsic limitation of compliant systems, and

provides a pathway to feasible analysis and synthesis with clear understanding. The other methods simply lack this capability, and efforts to employ them in such contexts frequently fail to converge, or converge to a realistic solution, leaving the designer guessing as to the reasons. This fundamental development should be extendible to more complex geometries. Although comparisons between the PRBM and other numerical approaches, e.g. the FEA, have not been a primary goal, several examples presented do speak to its efficacy.

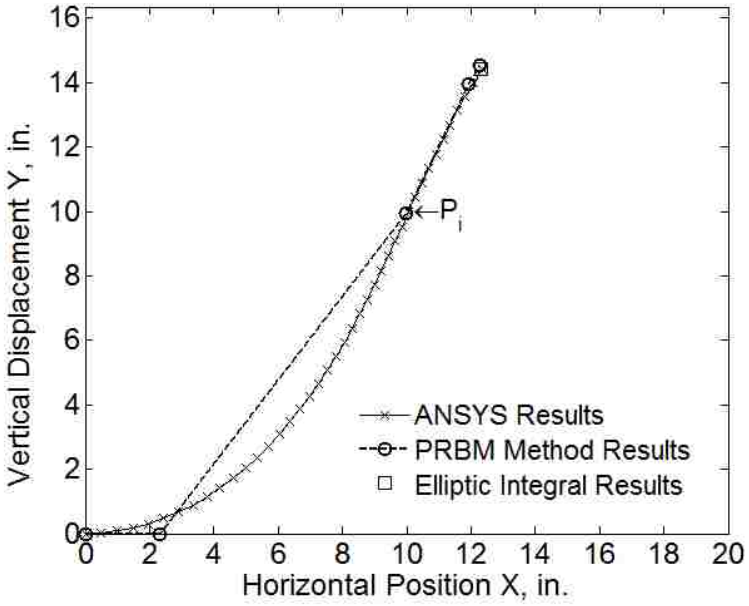

Figure 3.14. Graphical beam displacement comparisons among the methods for Ex. 1 of Table 3.2

3.8 SYNTHESIS USING COMPLIANT FIXED-GUIDED SEGMENTS WITH ONE INFLECTION POINT

The set of 18 *parametric, static equilibrium, and compatibility* equations, equations (83) to (104), containing 24 variables, may be utilized in the two-position (undeformed and deformed) synthesis of compliant mechanisms containing fixed-guided compliant segments with one inflection point in its deformed state. To solve the equations deterministically, six pragmatic 'free choices' will need to be specified from a list of seven possibilities: load and displacement boundary conditions ($\mathrm{P, n, M, dX, dY, and}\ \theta_0$), and the material property (E). Note that, depending on the synthesis need, any other set of variables may be specified as well. Of the 18 outcomes from the synthesis problem, for example, two typical ones may be the undeformed length (*l*) and area moment of inertia (I) of the segments. For convenience, equations (103) and (104) are restated in order that the displacement boundary conditions are readily specified:

$$\mathrm{dY} = \gamma_1 \mathrm{L}_1 \sin\left(\frac{\theta_{10}}{c_{\theta_1}}\right) + \gamma_2 \mathrm{L}_2 \sin\left(\frac{\theta_{20}}{c_{\theta_2}} + \theta_0\right) + (1-\gamma_2)\mathrm{L}_2 \sin(\theta_0) \tag{108}$$

$$\mathrm{dX} = \mathrm{L} - \left\{(1-\gamma_1)\mathrm{L}_1 + \gamma_1 \mathrm{L}_1 \cos\left(\frac{\theta_{10}}{c_{\theta_1}}\right) + \gamma_2 \mathrm{L}_2 \cos\left(\frac{\theta_{20}}{c_{\theta_2}} + \theta_0\right) + (1-\gamma_2)\mathrm{L}_2 \cos(\theta_0)\right\} \tag{109}$$

where, dY and dX are the transverse and longitudinal displacements (boundary conditions) of the beam end point w.r.t. the undeformed beam configuration.

Equations (108) and (109), in conjunction with equations (83) through (102), comprise the necessary set of equations for the synthesis of a fixed-guided compliant segment with one inflection point.

Example: This example, Figure 3.15, is inspired by the design of a compliant micro-restraining mechanism by a mechanical engineering senior design project [11] sponsored by Sandia National Laboratories at Missouri S&T. Due to its two-plane symmetry, only one of the eight segments need be synthesized, modeled as a fixed-

guided compliant segment with one inflection point in its deformed configuration. This can then be utilized to reconstruct the fully-compliant mechanism.

Consider the following specifications: the material chosen is Delrin®, an acetal based resin, with a modulus of elasticity, E = 450,000 psi. With choices of the actuation force at the handles of 4 lb and the undeformed orientation of the segments (in the first quadrant) of 45 deg., the following six summary specifications (6) are posed for the synthesis problem:

$E = 0.45 \text{ x } 10^6 \text{ psi}; P = 0.707 \text{ lb}; n = -1 \text{ (tensile)}; \ \theta_0 = 0 \text{ deg.}; dX' = 3/32 \ (0.09375) \text{ in.}; \text{and } dY' = 0.086 \text{ in.}$

where, dX' and dY' represent the horizontal and vertical displacement of the beam end point E in the fixed reference frame O-X'-Y'; and $P, n, \text{and } \theta_0$ represent the transverse load, load factor and change in the beam end angle, evaluated in the coordinate system O-X-Y affixed to the undeformed beam configuration, as shown in Figures 3(b), 6 and 10(b).

Equations (83) through (102), and (108) and (109), are then solved for the 18 unknowns. A subset of the synthesis outcomes lists the following important variables:

$l = 1.689 \text{ in.}; I = 4.323\text{x } 10^{-6} \text{ in}^4; \text{and } M = 0.55 \text{ in} - \text{lb (cw)}$

Assuming a rectangular beam cross section of width, $w = 3/16$ in., the thickness is obtained as $t = 0.065$ in. The resulting fully-compliant restraining mechanism is shown in Figure 3.16 and Figure 3.17. A finite element analysis validation using ANSYS®, of one-quarter mechanism substructure (one pair of fixed-guided segments) showed good correlations with dX' = 0.097 in. and dY' = 0.088 in. for specification of loads, and dX' = 0.09375 in. and dY' = 0.0854 in. for specification of displacements at the rigid-segment.

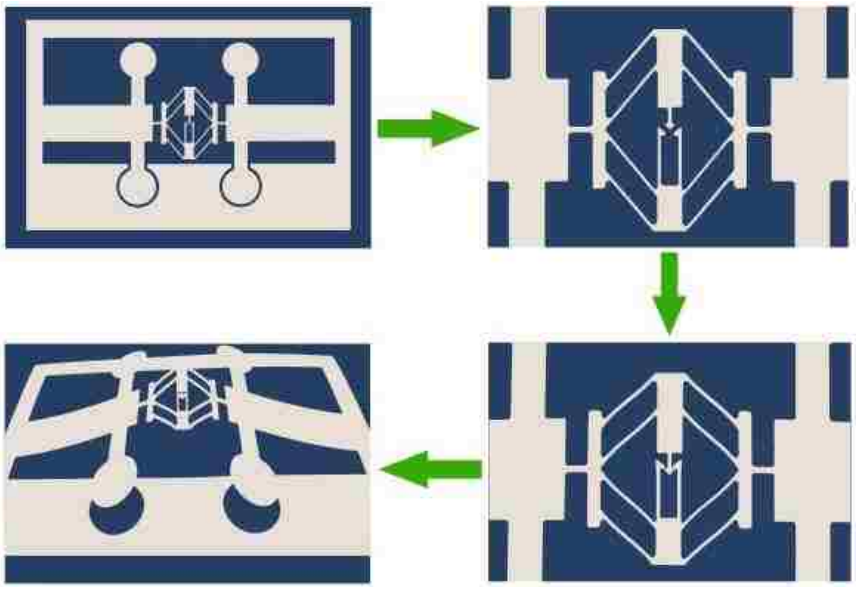

Figure 3.15. Configuration of the Fully-Compliant Micro-Restrainer Mechanism

Figure 3.16. Mechanism Configuration and Coordinates for Synthesis

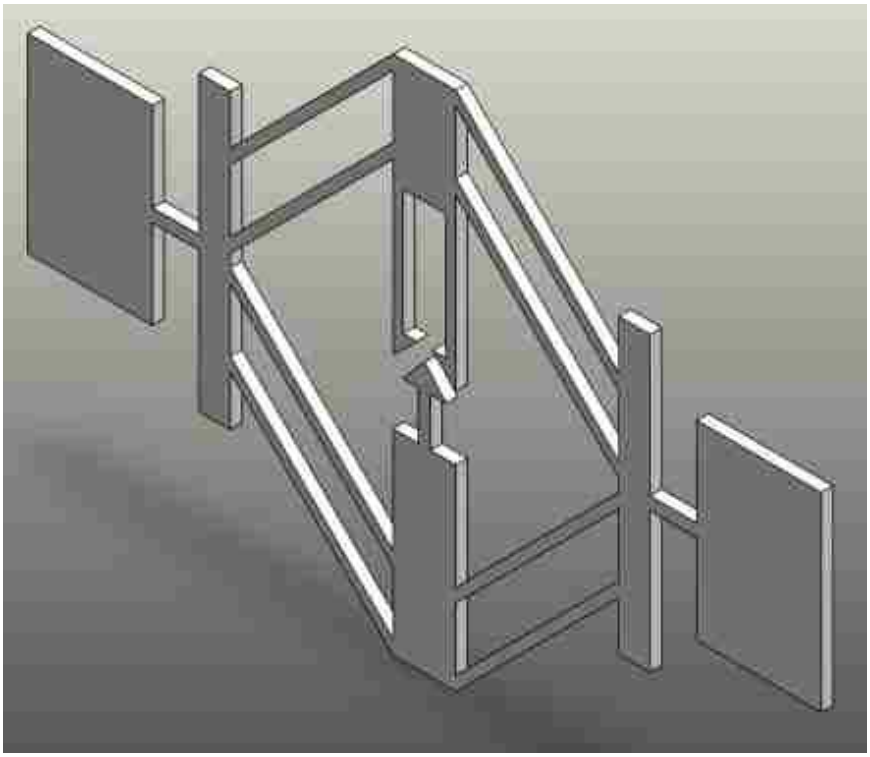

Figure 3.17. A Computer Aided Design (CAD) Rendering of the Synthesized Fully-Compliant Restraining Mechanism

3.9 SUMMARY

An accurate and simple method of analyzing a fixed-guided compliant beam has been presented. This method uses the well-known concept of the pseudo-rigid-body model (PRBM) to consider such a beam with more complex boundary conditions of load and displacement. The simplicity coupled with the efficiency of the methods makes it a practical tool for future investigations. The introduction of the concept of characteristic deflection domain renders the method more effective in its search for a feasible design for the more difficult problem types. A more detailed investigation into the concept of characteristic deflection domain is performed in Section 4.

The results obtained from the PRBM method are comparable to those from the finite element analysis software ANSYS®, and elliptic integral solutions. The vector loop representation of the kinematics of deformation of this system is offered to i) visually establish the relationships of various displacement terms, and ii) assist in the

development of a formal synthesis methodology. A two-position synthesis of a simple, fully-compliant mechanism exemplifies the analytical development of a basic fixed-guided compliant beam. The mechanics for multiple position synthesis quickly becomes formidable. Section 5 develops a promising, efficient approach for the synthesis of fully-compliant mechanisms contained fixed-guided compliant segment with one inflection point in its deformed state, including the synthesis of single-strip compliant mechanisms.

4. CHARACTERISTIC DEFLECTION DOMAIN OF COMPLIANT SEGMENT TYPES AND ITS IMPORTANCE IN COMPLIANT MECHANISM SYNTHESIS AND ANALYSIS

Compliant mechanism design inherently requires certain specified displacement boundary conditions to be satisfied. Obtaining realistic solutions for such problem types often becomes a challenge as the number of displacement boundary condition specifications increases. Typically, related failures are attributed to the numerical nature of the solution process. Little attention has been given to the fundamental understanding of the deformation behavior of flexible continuum with respect to its limits of mobility or reach. This section strives to provide an insight into this aspect of compliant mechanism design. This work systematically develops the characteristic deflection domain for a variety of compliant segment types. Pseudo-rigid-body model (PRBM) representation of the lower and upper boundaries of the characteristic deflection domain is calculated. The section also investigates the mobility characteristics of compliant mechanisms comprised of multiple segment types. Two case studies are presented that help exemplify the use of the characteristic deflection domain plots. Important insights and inferences are derived from the results obtained.

4.1 BACKGROUND

Specification of displacement boundary conditions is integral to compliant mechanism design. As the number of displacement boundary conditions increase, problems and challenges are frequently experienced in obtaining realistic solutions. Because of their nonlinear nature, such problems are erroneously attributed to the numerical nature of the solution process. Very little attention has been afforded to the mobility limits of the kinematics of deformation of various compliant segment types, subject to the specification of desired displacement boundary conditions.

Midha and Mettlach [41, 42] conducted foundational research towards the understanding of the kinematics of deformation, and presented the concept of domain of attraction. The authors utilized this concept to obtain initial estimates, and successfully implemented it in compliant mechanism design and analysis, using a numerical technique, i.e., the Chain Algorithm [24]. The convergence characteristics of the Chain

Algorithm showed significant improvements for the examples with initial estimates obtained using the concept of domain of attraction [42]. The results supported development of an understanding of the kinematics of deformation of compliant segments as being critical for a successful compliant mechanism design. In the absence of such understanding about the compliant segment types, the designer is often left with the challenging task of specifying achievable displacement boundary conditions. For random specifications, the process of obtaining solutions can become cumbersome.

Midha and Mettlach [41, 42] extended their initial work on the concept of domain of attraction and developed the concept of characteristic deflection domain. In this foundational work they utilized the pseudo-rigid-body model (PRBM) parametric expressions developed by Howell and Midha [33-36] to determine the bounding curves for the characteristic deflection domain. Investigations were conducted for an initially-straight fixed-pinned segment and fixed-fixed segment. The set of beam end loads considered by Midha and Mettlach [41, 42] resulted in deflected configurations with a monotonically increasing curvature. Recently, Holst et al. [83] and Midha et al. [80] investigated the deflection domain of fixed-guided compliant segments that have one inflection point. Midha et al. [80] utilized approximate PRBM parameters to develop the characteristic deflection domain for a specified beam end angle. The approximate domain can serve as a valuable tool in the analysis and synthesis of compliant mechanisms with fixed-guided compliant segments.

This section advances the concept of the characteristic deflection domain, and provides characteristic deflection domains for a variety of compliant segment types. Initially-straight and initially-curved compliant segments with constant cross-sectional properties along the length of the segment are considered. The work systematically develops their characteristic deflection domains and calculates the pseudo-rigid-body representation of the lower and upper boundary of the characteristic deflection domain. The section further provides a methodology for generating characteristic deflection domains of compliant mechanisms with multiple segment types, including single-strip mechanisms. Two case studies are presented to demonstrate the utility of the characteristic deflection domain of various segment types, and facilitate the design of compliant mechanisms.

4.2 CHARACTERISTIC DEFLECTION DOMAIN

A characteristic deflection domain comprises a region or solution space containing all possible beam end locations. The characteristic deflection domain of each segment type contains beam end locations for a wide range of possible beam end load combinations.

Characteristic deflection domain for compliant mechanisms with multiple segment types is a function of the deformation behavior of its constituent segments. Mobility in a compliant mechanism can only be achieved if the characteristic deflection domains of its constituent segments overlap either in part or in their entirety. In case they do not overlap, the antagonistic nature of the domains would render the compliant mechanism immobile. Therefore, the understanding of the characteristic deflection domain is very critical in the analysis and synthesis of compliant mechanisms that contain a variety of segment types.

The characteristic deflection domain concept facilitates an expedient estimation of the mobility characteristics of candidate compliant mechanisms. The pseudo-rigid-body representation of the characteristic deflection domain further assists in the process of estimation of mobility characteristics. Thus, the computationally intensive approaches, e.g. the finite element analysis, can be avoided initially to verify the suitability of candidate compliant mechanism solutions. The concept of characteristic deflection domain, in conjunction with the pseudo-rigid-body model concept, also assists a designer in the specification of realistic/achievable displacement boundary conditions. It provides a visual representation of the mobility characteristics, and guides a designer towards an improved candidate compliant mechanism design.

4.3 DEVELOPMENT OF CHARACTERISTIC DEFLECTION DOMAIN FOR VARIOUS COMPLIANT SEGMENT TYPES

The characteristic deflection domains for various compliant segment types are developed using the well-proven closed-form elliptic integral formulations. To develop the characteristic deflection domain for a fixed-guided compliant segment with one inflection point in its deformed state, a recently developed PRBM based method is utilized. The PRBM based method offers many advantages over the elliptic integral formulation for a fixed-guided compliant beam with one inflection point, as elaborated in Section 4.6.

A wide-range of practically possible beam end load combinations are applied to obtain a set of beam end point coordinates. A computer routine is developed to determine the lower and upper boundary of the solution space obtained. The routine also determines the characteristic radius factor to facilitate the pseudo-rigid-body representation of the characteristic deflection domain. Figure 4.1 shows the flowchart for the process used to develop characteristic deflection domain and its pseudo-rigid-body representation.

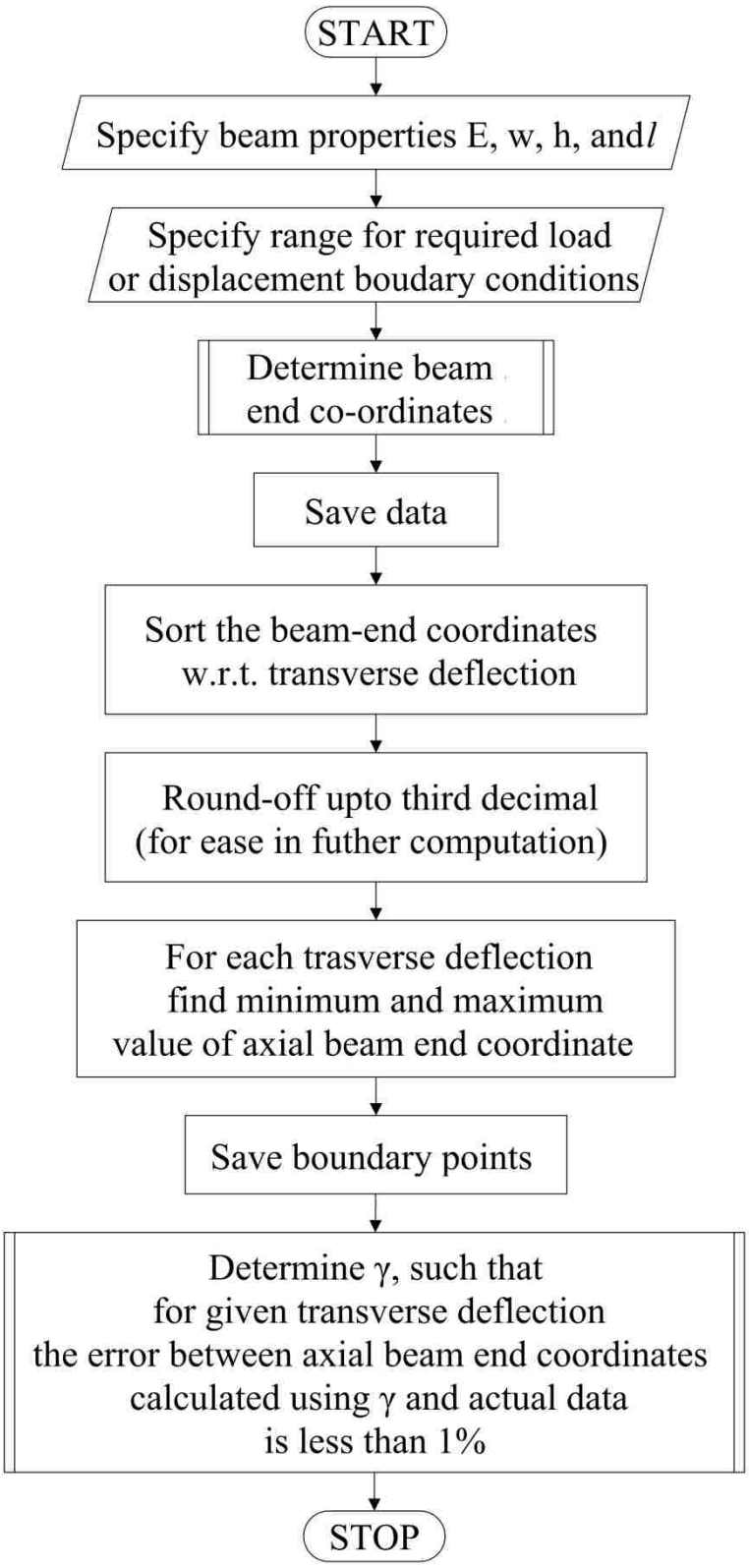

Figure 4.1. Procedure to Develop Characteristic Deflection Domain and its Pseudo-Rigid-Body Representation

4.4 CHARACTERISTIC DEFLECTION DOMAIN FOR AN INITIALLY-STRAIGHT FIXED-PINNED COMPLIANT SEGMENT

Figure 4.2 shows an initially-straight fixed-pinned compliant segment of length l, subjected to beam end forces nP and P. The beam end point coordinates for the compliant segment shown in Figure 4.2 are calculated using the closed-form elliptic integral formulation provided by Howell and Midha [33, 36], given in Equations (6) and (7).

Using a beam of length 20 in., width 0.5 in. and thickness 0.0625 in., with modulus of elasticity 30 x 10^6psi, and varying n from -4 to 10 in a step of 0.01 and θ_0 from 1 deg. to 90 deg. in step of 0.01 deg. the set of beam end point coordinates are obtained, shown in Figure 4.3.

The bounding curves and the resulting pseudo-rigid-body representations are obtained using the process presented in Figure 4.1. The calculated values for the characteristic radius factors are:

$$\gamma_l = 0.8053 \tag{110}$$

$$\gamma_u = 0.8829 \tag{111}$$

The resulting pseudo-rigid-body representation of the characteristic deflection domain is shown in Figure 4.4.

Figure 4.2. Initially-Straight Fixed-Pinned Compliant Segment

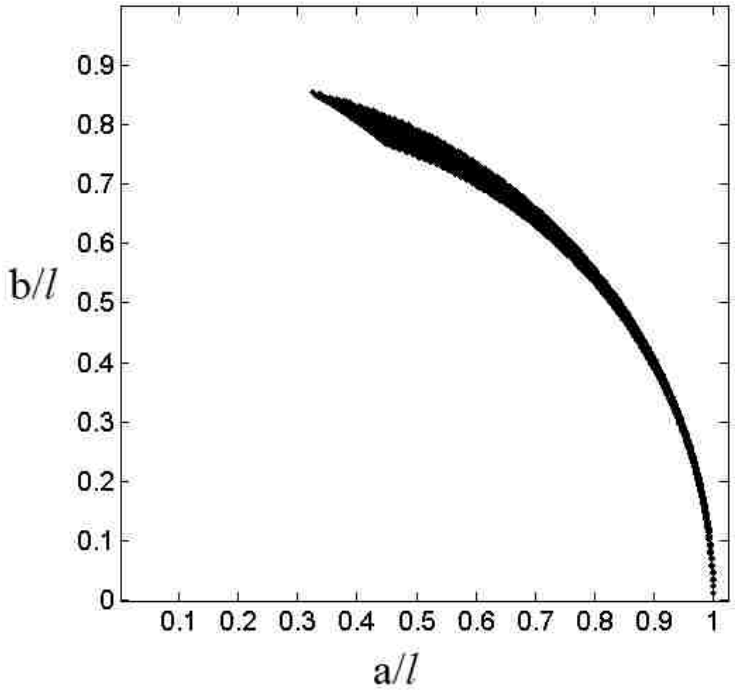

Figure 4.3. Beam End Point Locations for an Initially-Straight Fixed-Pinned Compliant Segment

Figure 4.4. Pseudo-Rigid-Body Representation of the Characteristic Deflection Domain for an Initially-Straight Fixed-Pinned Compliant Segment

4.5 CHARACTERISTIC DEFLECTION DOMAIN FOR AN INITIALLY-CURVED FIXED-PINNED COMPLIANT SEGMENT

Figure 4.5 shows an initially-curved fixed-pinned compliant segment of length *l*, subjected to beam end forces nP and P. The beam end point coordinates for this segment type are calculated using the closed-form elliptic integral formulation provided by Howell [36], given in Equations (8) and (9).

Su [52] provided a relation for determining the maximum beam end angle w.r.t. the nondimensional moment index, κ, such that

$$\theta_{0max} = \phi + \text{acos}(1-\kappa)\text{, for } \kappa \leq 2$$
$$\theta_{0max} = \infty\text{, for } \kappa > 2 \qquad (112)$$

where, $\phi = \text{atan}\left(\frac{1}{-n}\right)$

Using a beam of length 20 in., width 0.5 in. and thickness 0.0625 in, with modulus of elasticity 30 x 10^6psi, and varying n from -4 to 10 with a step size of 0.1, θ_0 from 1 deg. to 90 deg. with a step size of 1 deg., and κ from 0.1 to 5 with a step size of

0.1, the set of beam end point coordinates are obtained, shown in Figure 4.6. Su [52] showed that for load combinations with $\kappa > 5$ the effect of beam end force is negligible, leading the results towards a pure moment loading. The characteristic deflection domain for pure moment loading is an arc of radius equal to the lower bound of the characteristic deflection domain of an initially-curved fixed-pinned compliant segment.

The bounding curves and the resulting pseudo-rigid-body representations are obtained using the process presented in Figure 4.1. The calculated values for the characteristic radius factors are:

$$\gamma_l = 0.7431 \tag{113}$$

$$\gamma_u = 0.8148 \tag{114}$$

The resulting pseudo-rigid-body representation of the characteristic deflection domain is shown in Figure 4.7.

Figure 4.5. An Initially-Curved Fixed-Pinned Compliant Segment

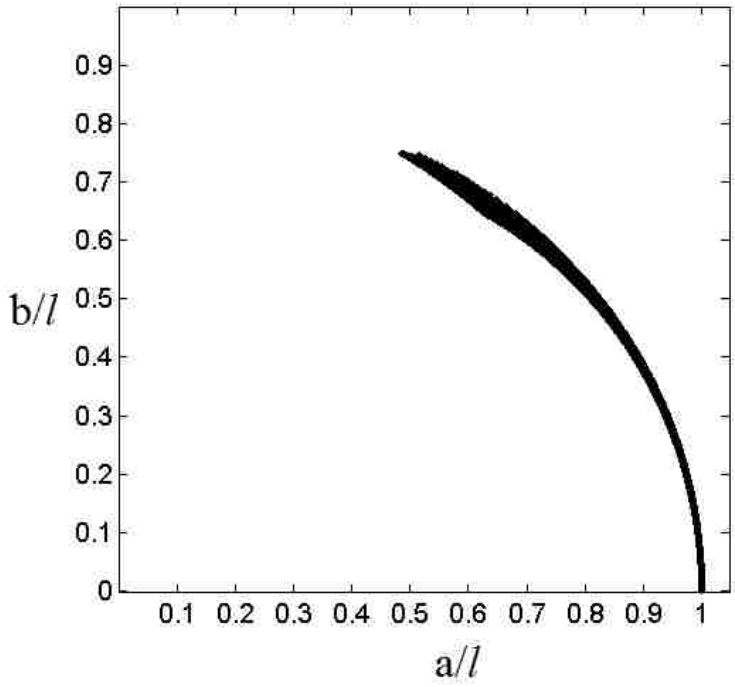

Figure 4.6. Beam End Point Locations for an Initially-Curved Fixed-Pinned Compliant Segment

Figure 4.7. Pseudo-Rigid-Body Representation of the Characteristic Deflection Domain for an Initially-Curved Fixed-Pinned Compliant Segment

4.6 CHARACTERISTIC DEFLECTION DOMAIN FOR AN INITIALLY-STRAIGHT FIXED-FIXED COMPLIANT SEGMENT

Figure 4.8, Figure 4.9, and Figure 4.10 shows an initially-straight fixed-fixed compliant segment in its three achievable deformation configurations. Depending upon the applied loading, an initially-straight fixed-fixed compliant segment can take any one of the configurations in its deformed state. If the transverse reaction force and moment at the beam end point of the fixed-guided segment are in the same sense, as shown in Figure 4.8, the fixed-fixed compliant segment will exhibit a deformation configuration with a monotonically increasing curvature. In case, the transverse force and moment are in the opposing sense, as shown in Figure 4.9 and Figure 4.10, the fixed-fixed compliant segment may show an inflection point in its deformed configuration. The necessary and sufficient conditions for the occurrence of inflection point in a fixed-guided compliant segment are discussed in Section 2.

Figure 4.8. An Initially-Straight Fixed-Fixed Compliant Segment with a Monotonically Increasing Curvature in its Deformed State

Figure 4.9. An Initially-Straight Fixed-Fixed Compliant Segment with an Inflection Point in its Deformed State with a Positive Slope at the Beam End

Figure 4.10. An Initially-Straight Fixed-Fixed Compliant Segment with an Inflection Point in its Deformed State with a Negative Slope at the Beam End

Howell [36] suggested that the closed-form elliptic integral formulation provided for an initially-curved compliant segment also applies for the large-deflection analysis of an initially-straight fixed-fixed compliant segment that has a monotonically increasing curvature in its deformed state. The beam end moment can be represented using κ_0, such that

$$\kappa_0 = \frac{\mathrm{M}l}{\mathrm{EI}} \tag{115}$$

Therefore, the characteristic deflection domain for the fixed-fixed compliant segment shown in Figure 4.8 can be represented by Figure 4.7.

The closed-form elliptic integral formulation for the large-deflection analysis of an initially-straight fixed-guided compliant segment with an inflection point, shown in Figure 4.9 and Figure 4.10, is provided by Kimball and Tsai [49], which is further developed for multiple inflection point situations by Zhang and Chen [55]. For ease of solutions, it is recommended that n, θ_0, and κ are specified [55]. Although these specifications provide accurate solutions for positive beam end angle specifications, experiences have demonstrated that the results do not correlate with finite element analysis results for negative beam end angle specifications. To overcome the difficulty with solutions, Kimball and Tsai [49] suggested an elliptic integral formulations with specified loads; P, nP, and M. In order to obtain solutions with load boundary condition specifications, appropriate initial estimates for α and θ_0 should be provided. Kimball and Tsai [49] provided an algorithm that can assist with the estimation of the initial estimates for α and θ_0.

Recently, Midha et al. [80] provided a PRBM based method that utilizes a well-known property of the inflection point to develop the set of algebraic equations for analysis of a fixed-guided segment with one inflection point. The method provides accurate results and is computationally more efficient to implement compared to the elliptic integral formulation. Therefore, this work develops the deflection domain for a fixed-guided compliant segment with one inflection point using the PRBM method presented by Midha et al. [80], shown in Figure 4.11.

Figure 4.11. PRBM for a Fixed-Guided Compliant Beam with One Inflection Point in its Deformed State

Using a beam of length 20 in., width 0.5 in. and thickness 0.0625 in., with modulus of elasticity 30 x 10^6psi, and varying n from -4 to 10 with a step size of 0.1, P from 1 to 10 with a step size of 0.1, and κ from 0.1 to 1.8 with a step size of 0.05, the set of beam end point coordinates are obtained, shown in Figure 4.12. The approach suggested by Su [52] is utilized to determine estimate the range of κ for a given n and θ_0, as explained in Section 4.6.1.

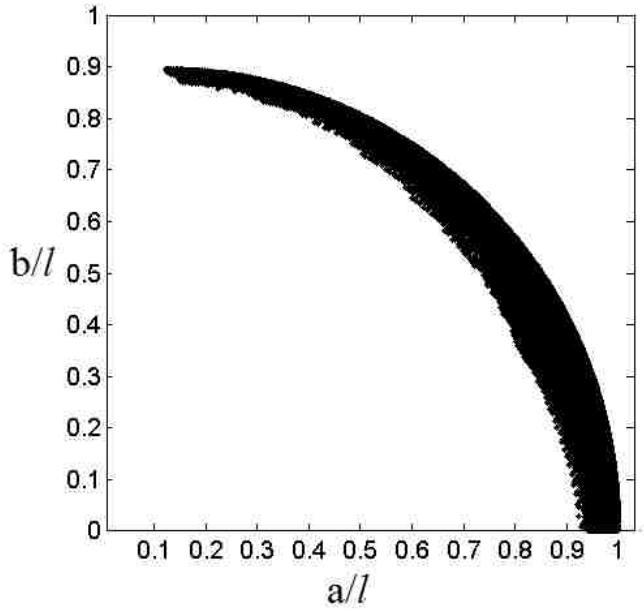

Figure 4.12. Beam End Point Locations for a Fixed-Guided Compliant Segment with one Inflection Point in its Deformed State

Using the approach presented in Figure 4.1, the boundary curves for the characteristic deflection domain are generated. The pseudo-rigid-body representation of the upper bound is calculated using the procedure presented in Figure 4.1. The same, however, cannot be estimated for the lower bound. Therefore, a curve-fit is performed using Microsoft Excel®, providing the following relation:

$$\hat{a} = 0.934 - 0.0591\hat{b} - 1.6211\hat{b}^2 + 4.9649\hat{b}^3 - 11.366\hat{b}^4 + 13.746\hat{b}^5 - 7.0759\hat{b}^6 \quad (116)$$

$$R^2 = 0.998$$

where, $\hat{a} = \frac{a}{l}$ and $\hat{b} = \frac{b}{l}$

Examination of the lower boundary of the characteristic deflection domain suggests that a piecewise pseudo-rigid-body representation may be generated. Using a slightly modified procedure, various values for $\bar{\gamma}_l$ are calculated, where $\bar{\gamma}_l l$ is the characteristic radius with its center at the fixed-end. The value of $\bar{\gamma}_l = 0.8945$ can

estimate the lower bound within an error of 1% for normalized transverse deflection between 0.4 and 0.85. The range for the other characteristic radii was observed to be very small. Therefore, the value of $\bar{\gamma}_l = 0.8945$ is used for further calculations. Figure 4.13 provides the percentage error in predicting the lower bound using this approximate characteristic radius factor.

Although the designer may use the curve fit equation for plotting the lower boundary, considering the convenience of the pseudo-rigid-body representation, the author recommends using the approximate characteristic radius factor for plotting the lower bound. The lower and upper bound of the characteristic deflection with its pseudo-rigid-body representation is shown in Figure 4.14. The resulting characteristic radius factor for the lower bound and upper bound are:

$$\bar{\gamma}_l = 0.8945 \tag{117}$$

$$\gamma_u = 0.9035 \tag{118}$$

Figure 4.15 shows the characteristic deflection domain plots using the approximate lower bound and the curve fit expression.

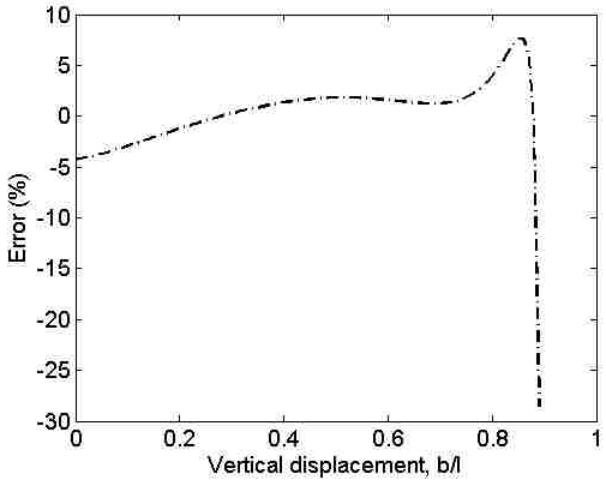

Figure 4.13. Error in Estimating the Lower Bound Curve with Approximate Pseudo-Rigid-Body Representation

Figure 4.14. Pseudo-Rigid-Body Representation of the Characteristic Deflection Domain of a Fixed-Guided Compliant Segment with One Inflection Point in its Deformed State

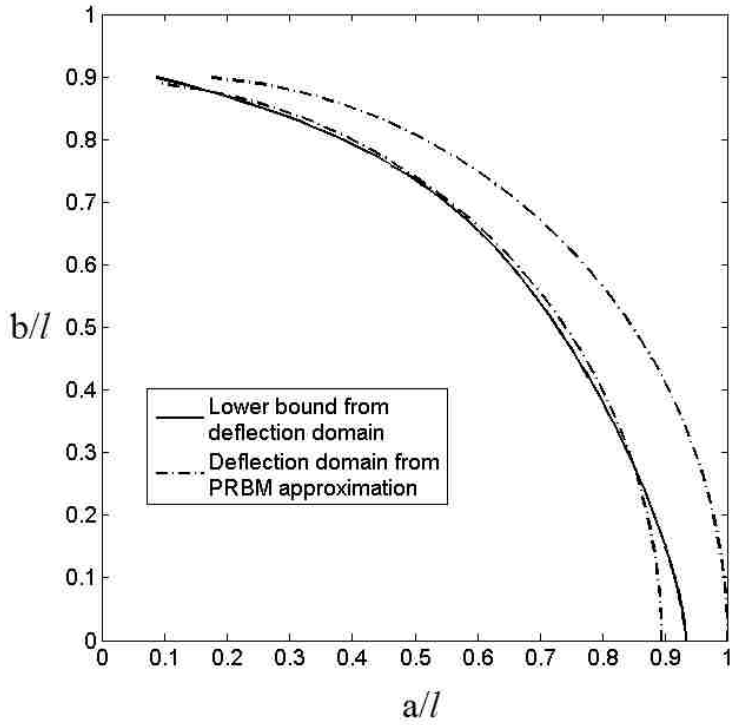

Figure 4.15. Characteristic Deflection Domain Plot using Curve Fit Expression and Pseudo-Rigid-Body Representation

Howell [36] showed that for an initially-curved fixed-fixed compliant segment, κ_0 can be written as,

$$\kappa_0 = \frac{Ml}{EI} + \frac{l}{R_i} \tag{119}$$

Such a representation allows the use of the characteristic deflection domain for initially-straight fixed-fixed compliant segments to the treatment of initially-curved fixed-fixed compliant segments.

4.6.1 Determining Bounds on Moment Load for Generating an Inflection Point.

A fixed-guided compliant segment subjected to a transverse force, axial force and opposing moment may or may not cause an inflection point in the beam continuum [47, 49]. The presence of an inflection point is guaranteed only when the following relation is satisfied [52].

$$\cos(\theta_0 - \phi) - \cos(\theta_i - \phi) + \kappa \geq 0 \tag{120}$$

where, $\phi = \operatorname{atan}\frac{-1}{n}$, θ_i the slope at the inflection point, and κ the nondimensional load ratio given by:

$$\kappa = \frac{M_0^2}{2PEI} \tag{121}$$

For a beam configuration with one inflection point,

$$\theta_i \geq \theta_0 \tag{122}$$

Utilizing equations (120) and (122), Su [52] presented a numerical technique to determine the minimum load ratio required to introduce an inflection point in the

deflected state of the fixed-guided compliant beam. The resulting equations for calculating κ_{min} are given by equations (123) and (124).

$$\kappa_{min} = \cos(\theta_i - \phi) - \cos(\theta_0 - \phi) \quad (123)$$

$$\theta_i = \theta_0 + \delta\theta_0 \quad (124)$$

In addition, excessive moment loads may results in a beam configuration with no inflection point. The beam will have a monotonically increasing curvature in the direction of the internal moment. For a wide range of practically applicable forces, Su [52] determined the following relation for the upper bound of the nondimensional load ratio.

$$\kappa > 2 \quad (125)$$

Using, the above presented equations a computer routine is generated that can determine the minimum and maximum nondimensional load ratio for a given load factor n, where $-4 \leq n \leq 10$. The computer routine is designed to calculate the κ values that can result in a beam end angle between -60 deg. and 60 deg., with the beam end in the deflected state located in the first quadrant. For the case with positive beam end angle, κ_{min} is calculated using $\delta\theta_0 = 5$ deg. and κ_{max} is calculated using $\theta_i = 85$ deg. For the case with negative beam end angle, κ_{min} is calculated using $\theta_i = 5$ deg. and κ_{max} is calculated using $\theta_i = 85$ deg. Figure 4.16 shows the flowchart of this computer routine.

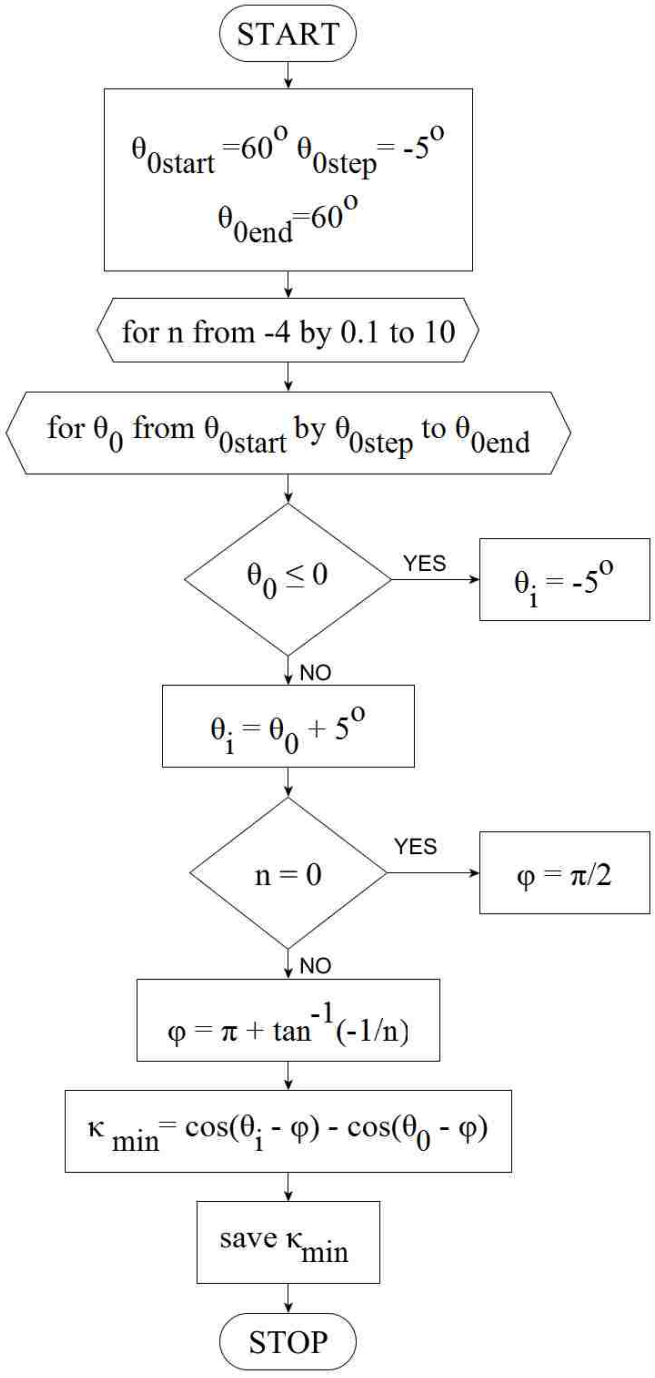

Figure 4.16. Flowchart for the Numerical Estimation of κ_{min}

Figure 4.17 thru Figure 4.22 show the variation of κ_{min} and κ_{max} for various load factor values. From these plots, this section generates the dataset for the following range of load ratio.

$$0.1 \leq \kappa \leq 1.8 \tag{126}$$

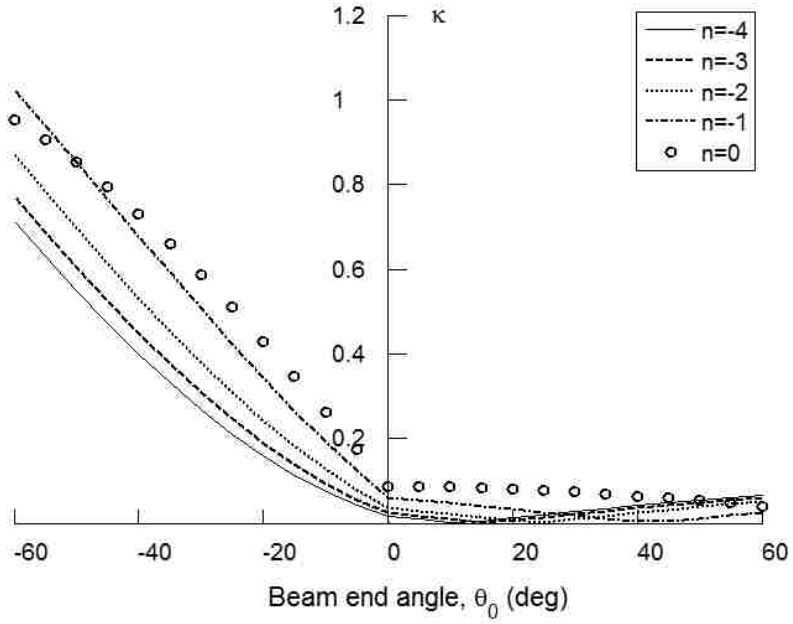

Figure 4.17. Variation of κ_{min} for load factor from $n = -4$ to $n = 0$

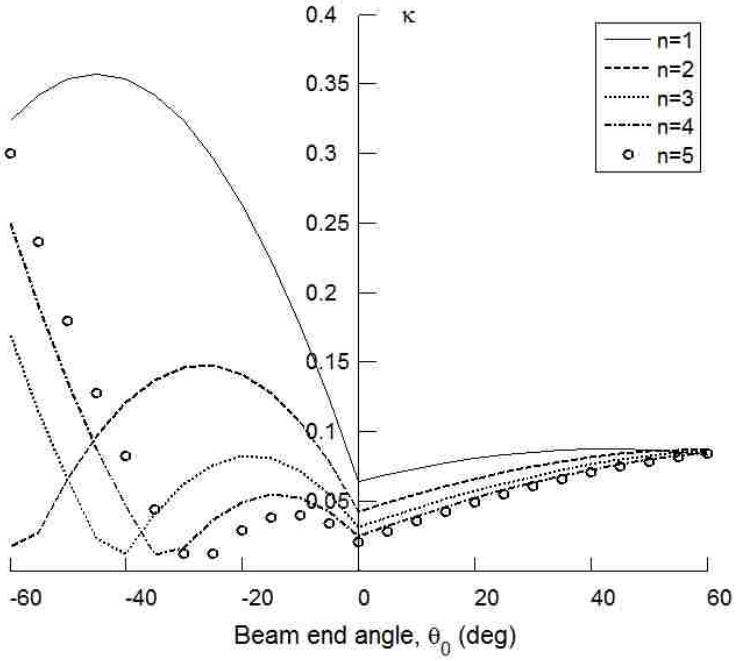

Figure 4.18. Variation of κ_{min} for load factor from n = 1 to n = 5

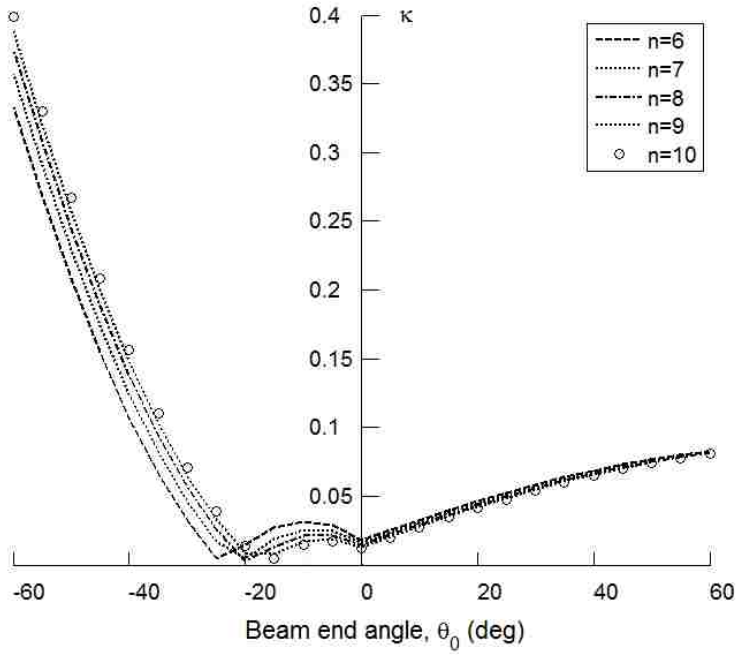

Figure 4.19. Variation of κ_{min} for load factor from n = 6 to n = 10

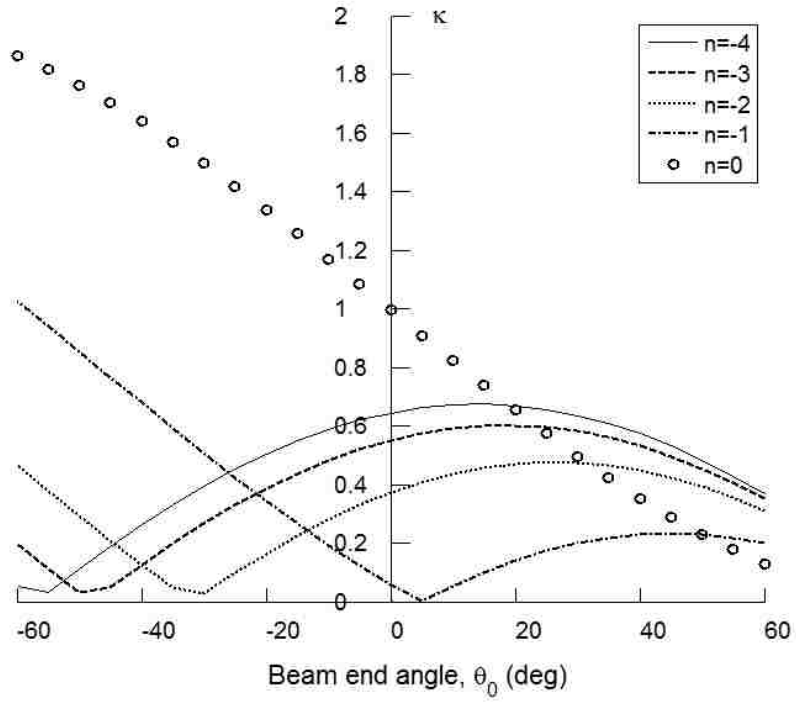

Figure 4.20. Variation of κ_{max} for load factor from $n = -4$ to $n = 0$

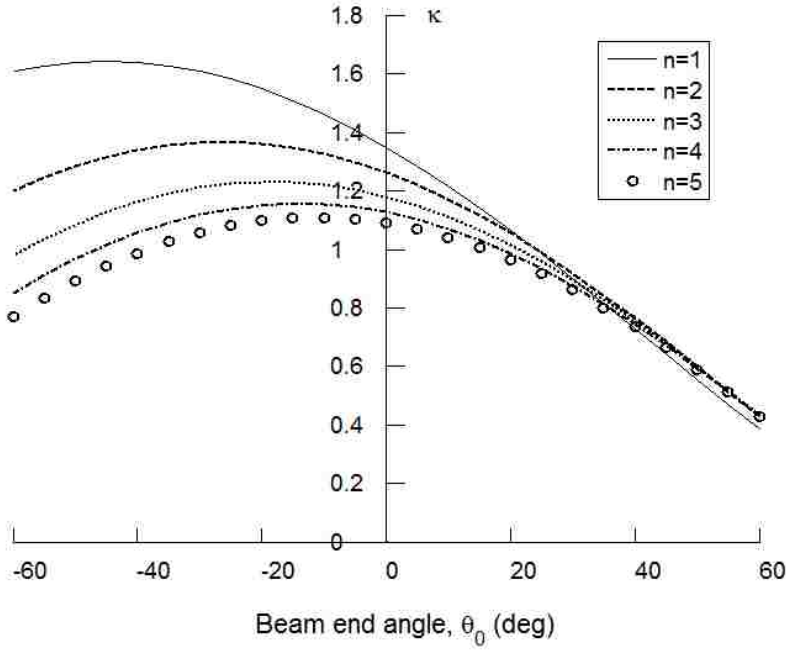

Figure 4.21. Variation of κ_{max} for load factor from $n = 1$ to $n = 5$

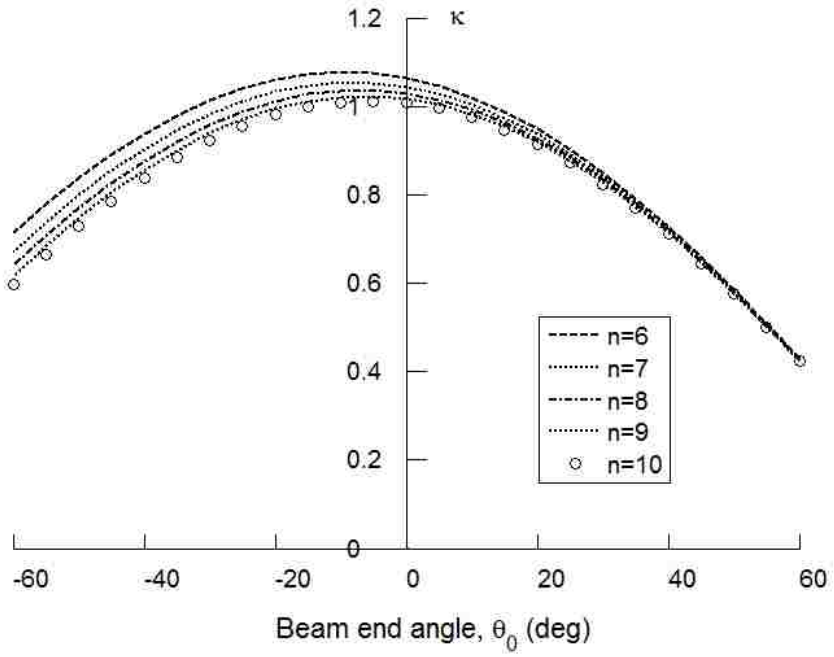

Figure 4.22. Variation of κ_{max} for load factor from n = 6 to n = 10

4.7 CHARACTERISTIC DEFLECTION DOMAIN FOR FIXED-FREE COMPLIANT SEGMENTS SUBJECTED TO BEAM END FORCES WITH INITIALLY-STRAIGHT AND INITIALLY-CURVED SMALL-LENGTH FLEXURAL PIVOT

Figure 4.23 and Figure 4.24 show a compliant segment of length $l + \mathrm{L}$, with an initially-straight and initially-curved small-length flexural pivot of length l, respectively. Midha and Kuber [53, 54] provided a closed-form elliptic integral formulation for such segment types. The authors demonstrate that the characteristic domain for such segment types is an arc. The radius of the arc is defined by the characteristic radius factor, given by:

$$\gamma_l = \gamma_{\mathrm{u}} = \frac{l}{2} + \mathrm{L} \tag{127}$$

where, l is measured along the undeformed configuration of the small-length flexural pivot.

Figure 4.23. A Fixed-Free Compliant Segment with an Initially-Straight SLFP

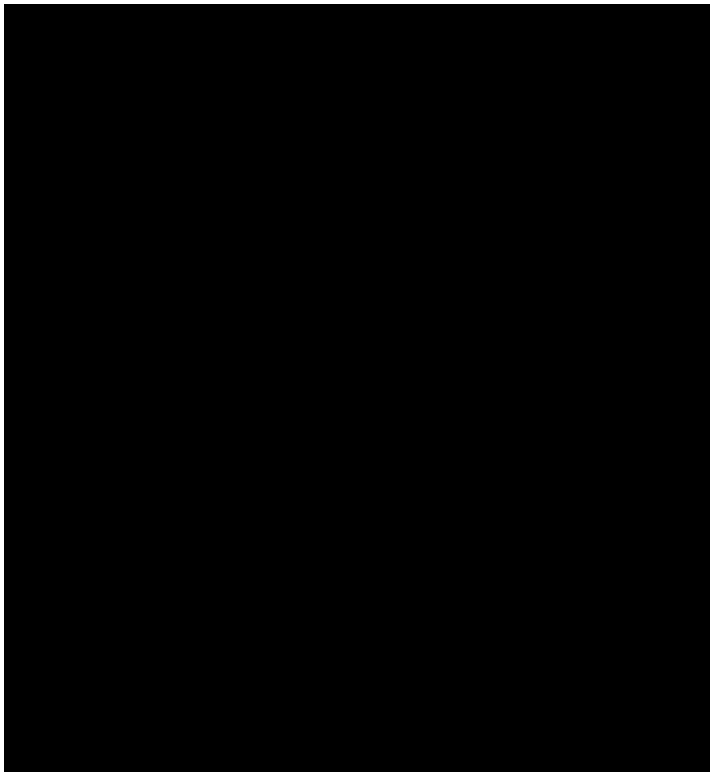

Figure 4.24. A Fixed-Free Compliant Segment with an Initially-Curved SLFP

4.8 CHARACTERISTIC DEFLECTION DOMAIN FOR COMPLIANT MECHANISMS CONTAINING A COMBINATION OF COMPLIANT SEGMENT TYPES

Characteristic deflection domains developed for various compliant segment types can be readily utilized to generate the characteristic deflection domain for compliant mechanisms containing a combination of segment types. The pseudo-rigid-body representation of the lower and upper bound of the characteristic deflection domain allows for a quick analysis of the mobility characteristics of a compliant mechanism containing multiple segment types. Figure 4.25 shows a compliant mechanism with one fixed-pinned compliant segment of length l. Its pseudo-rigid-body model is shown in Figure 4.26.

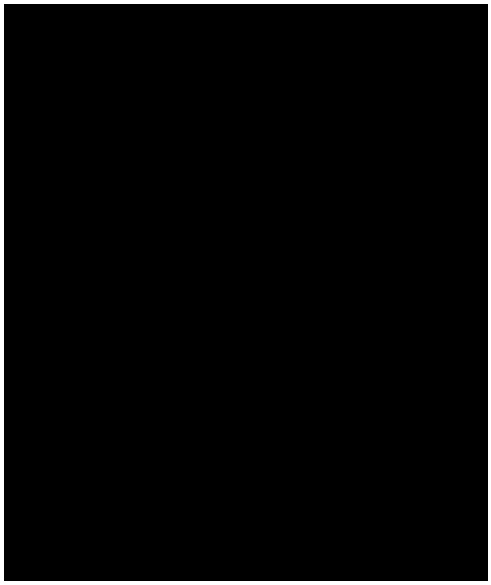

Figure 4.25. A Partially-Compliant Mechanism with one Fixed-Pinned Compliant Segment

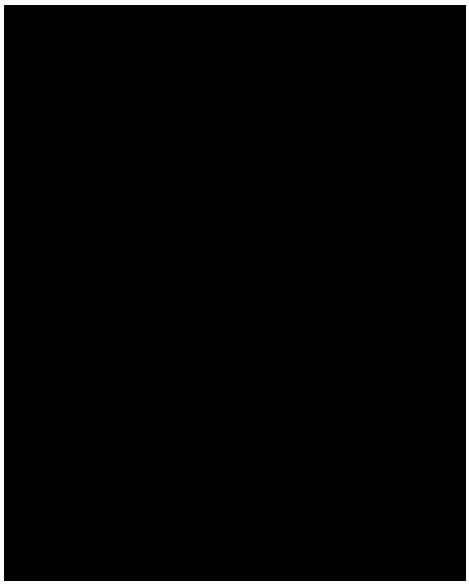

Figure 4.26. PRBM of the Partially-Compliant Mechanism shown in Figure 4.25

The deflection domain of the coupler point P can be estimated using the PRBM concept, in conjunction with the limit position synthesis provided by Midha et al. [63]. The PRBM properties are determined using the characteristic radius factor γ_l and γ_u to calculate the characteristic deflection domain for the coupler point. State-of-the-art rigid-body analysis techniques can be applied to the PRBM to obtain the characteristic deflection domain. Considering the length of compliant segment as 2 in., length of coupler link as 1.5 in., length of right side link as 2 in., extension on the coupler link of 0.5 in., initial angle of compliant segment and right side link as 90 deg., and the initial angle of coupler link as 0 deg., the deflection domain of the coupler point is obtained, shown plotted Figure 4.27.

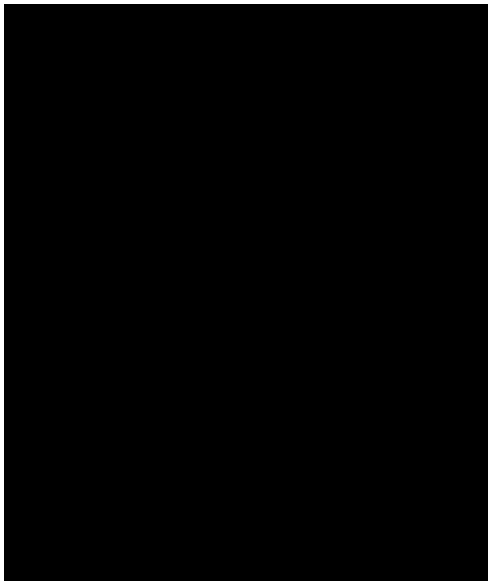

Figure 4.27. Characteristic Deflection Domain for the Coupler Point of the Partially-Compliant Mechanism shown in Figure 4.25

Figure 4.28 shows a compliant segment with non-uniform cross-section properties. Midha et al. [66] and Kolachalam [67] showed that compliant segments with non-uniform cross-section properties can be represented as a single-strip compliant mechanism. Such a representation allows for the application of rigid-body analysis and synthesis techniques to compound-compliant segments. Applying the same procedure as the stated above, the characteristic deflection domain of the beam end point for this segment is obtained. Considering the following for the compound compliant segment: $l_1 = 5$ in.; $L_1 = 3.5$ in.; $l_2 = 0.25$ in.; and $L_2 = 2.5$ in., the beam end point locations are obtained, shown plotted in Figure 4.29. Note that SLFP shown in Figure 4.28 will be subjected to a lesser moment, as compared to the fixed-guided compliant segment. Therefore, the angular rotation of the rigid-segment of length L_2 connected to the SLFP will be less than the angular rotation of the rigid-segment of length L_1 connected to the fixed-guided segment.

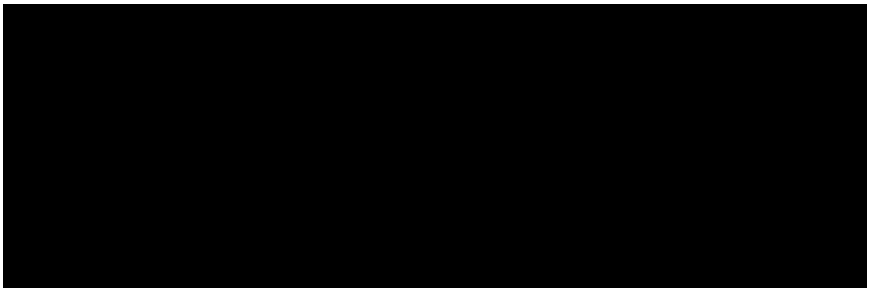

Figure 4.28. An Initially-Straight Compound Compliant Segment

Figure 4.29. Characteristic Deflection Domain for the Beam End Point for the Compound-Compliant Segment shown in Figure 4.28

4.9 IMPORTANCE OF CHARACTERISTIC DEFLECTION DOMAIN ON COMPLIANT MECHANISM ANALYSIS AND SYNTHESIS

The importance and the utility of the concept of characteristic deflection domain are demonstrated using two case studies. The first case study demonstrates that care should be exercised when analyzing compliant mechanisms. The second case study demonstrates that the type and properties of the constituent compliant segments affect the characteristic deflection domain of the compliant mechanisms, and therefore, its mobility characteristics.

Case Study 1: Figure 4.30 shows a fixed-guided compliant segment. Let us consider that the deformed configuration of the segment will contain one inflection point. The resulting characteristic deflection domain for such a configuration is shown plotted in Figure 4.30. Figure 4.31 shows a partially-compliant mechanism containing the segment shown in Figure 4.30 as one of its constituent segment. The characteristic deflection domain for the coupler point of the compliant mechanism shown in Figure 4.31 is estimated by the procedure presented in Section 4.8. The two compliant segments considered as 4 in. long, oriented at 90 deg. in its initial position, and connected with a 2.25 in. coupler segment. The coupler point P is located 0.75 in. from the top of the coupler segment, which is 0.25 in. thick.

Figure 4.30. An Initially-Straight Fixed-Guided Compliant Segment with its Characteristic Deflection Domain

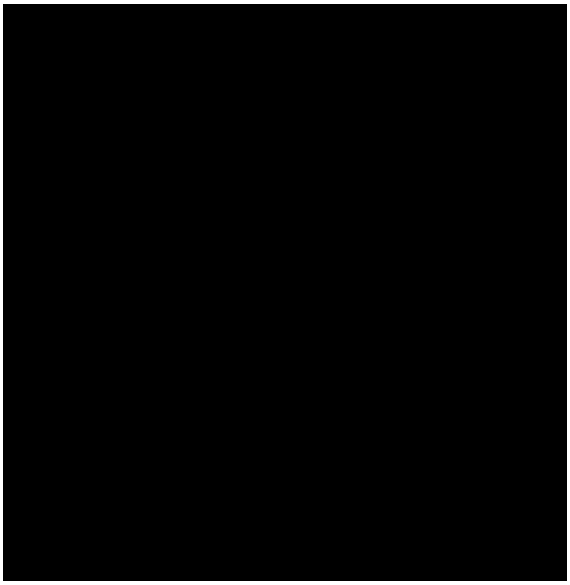

Figure 4.31. A Partially-Compliant Mechanism Utilizing the Segment shown in Figure 4.30

Figure 4.31 demonstrates that addition of different compliant segment types significantly affects the characteristic deflection domain of the coupler point located. Because of the combination of the different segment types, the knowledge of characteristic deflection domain of each segment type cannot be directly applied towards the analysis of compliant mechanisms. Greater care should be taken during the analysis of compliant segments and compliant mechanisms for specifications involving displacement boundary conditions.

Case Study 2: Figure 17 shows compliant mechanisms of the Type B presented in Figure 2.27. The deflection domain of the coupler point, calculated using the procedure presented in Section 4.8, is shown plotted in Figure 4.32. The fixed-fixed compliant segment is 4 in. long and initially-straight, and initially-curved SLFP is 0.25 in. long. The compliant segments are joined by two rigid-segments. The segment connecting the fixed-fixed compliant segment and the initially-curved SLFP is 2.5 in. long, and the segment connecting two SLFPs is 2.25 in. long. The coupler point is placed 1 in. from the top of the coupler segment, which is 0.25 in. thick on the left side and 0.3 in. on the right side. The initial orientation of the fixed-fixed segment shown in Figure 4.32 (a) is 90 deg., whereas the orientation in Figure 4.32 (b) is 100 deg.

The characteristic deflection domain plots for the coupler point, shown in Figure 4.33, demonstrate that the type and properties of compliant segments, e.g. orientation, affect the characteristic deflection domain of the resulting compliant mechanism. Thus, greater care should be taken by the designer during the synthesis of candidate compliant mechanisms. Specification of random free-choices may lead to solutions with limited mobility characteristics. Such mechanism solutions may demonstrate sensitivity towards the effecting loads and for a small error in the applied loading would render the mechanism immobile.

(a) (b)

Figure 4.32. Fully-Compliant Mechanisms of Type B with Different Initial Orientation of Fixed-Guided Compliant Segment

Figure 4.33. Deflection Domain Comparisons for the Coupler Point of Case Study 2

4.10 DISCUSSION

The concept of characteristic deflection domain provides valuable insights towards the better understanding of the mobility limits of the kinematics of deformation for various compliant segment types. The pseudo-rigid-body representation of the lower and upper bound of the characteristic deflection domain assists the designer in, both, analysis and synthesis of compliant segments and compliant mechanisms. The applications of this concept in multiple segment scenarios are multifold, and include the following:

The concept of characteristic deflection domain allows a designer to visualize and understand the mobility characteristics of a candidate compliant mechanism. The pseudo-rigid-body representation of the deflection domain allows for the application of the state-of-the-art rigid-body mechanism analysis techniques for understanding the nature and capabilities of candidate compliant mechanisms. Computationally intensive methods can be avoided initially to select candidate solutions. These methods can be efficiently utilized later to optimize the selected compliant mechanisms.

The design process may be accelerated because the designer can now better visualize the effect of free-choices and modify these appropriately. The effect of design variables can now be readily studied, enhancing the learning and insights to enable future design efforts expediently. Robustness of compliant mechanism solutions, e.g. sensitivity to the applied loadings, may be readily investigated. Such a study will help understand large discrepancies between the results obtained by various means, analytical or experimental.

4.11 SUMMARY

The characteristic deflection domains for a variety of compliant segment types have been presented in this section. Closed-form elliptic integral solutions are utilized to develop the characteristic deflection domain for fixed-pinned and fixed-free compliant segments. A recently developed PRBM based method is utilized to develop the characteristic deflection domain for a fixed-guided beam with one inflection point.

Pseudo-rigid-body representations of the lower and upper boundary curves of the characteristic deflection domain are obtained. The concept of characteristic deflection

domain is extended to multi-segment compliant mechanisms. Two case studies are presented that demonstrate that the number, type, and properties of compliant segments comprising the compliant mechanism significantly affect its mobility characteristics.

5. A METHODOLOGY FOR SYNTHESIS OF FULLY-COMPLIANT MECHANISMS WITH FIXED-GUIDED BEAMS WITH AN INFLECTION POINT USING THE PRBM CONCEPT

This section provides a methodology for the synthesis of fully-compliant mechanisms that contain fixed-guided segments with an inflection point in the deformed state. The synthesis methodology utilizes the vector loop representation of the pseudo-rigid-body model of the fixed-guided compliant beam, provided in section 3, to develop the necessary scalar equations. In addition to these, the synthesis framework contains equations to satisfy the length and slope compatibility conditions. The framework utilizes the pseudo-rigid-body model for a fixed-guided compliant beam with one inflection point, provided in section 3, to identify the free-choices, their selection criteria and associated constraints. The methodology is proposed for conventional tasks, such as, path generation and motion generation with energy storage characteristics or effecting loads specified at the precision positions. Design tables are developed to provide number of equations, number of unknowns, free-choices required and applicable constraints on free-choices. Considering that a fixed-guided compliant beam is a compliant mechanism in itself, in addition to being a fundamental building block for compliant mechanisms, the approach is built on one fixed-guided compliant segment. Consequently, the synthesis framework is not only applicable to a single-strip compliant mechanism, but also, towards the design of compliant mechanisms containing multiple fixed-guided compliant segments.

5.1 BACKGROUND

Howell and Midha [56] utilized the PRBMs of individual segment types as the building blocks and proposed a methodology for synthesis and analysis of compliant mechanisms, called as synthesis with compliance. The approach utilizes the state-of-the-art rigid-body synthesis techniques in conjunction with the energy and torque/force equations for compliant mechanism design. Midha et al. [64] later developed detailed design tables using synthesis with compliance for the design of compliant mechanisms towards conventional tasks, such as, function generation, path and motion generation, and path generation with prescribed timing with energy or torque/force values specified at the

precision positions. The approach considers average PRBM parameter values to transform a pseudo-rigid-body mechanism in a compliant mechanism. While the methodology has been proven to be versatile and does provide good results for a wide range of user specifications, the use of average PRBM parameter values leads to errors in the response of the compliant mechanism. The errors are significant in compliant mechanisms containing fixed-guided segments that have an inflection point in the deformed state [85]. The driving factor for the errors being the use of the PRBM that was developed by Howell [36] for a compliant parallel mechanism. In order to reduce this error, researchers have attempted to develop better PRBMs for a fixed-guided compliant beam. Some of the notable works are discussed below. This section utilizes one such recently developed efficient PRBM, proposed in section 3, to develop a new synthesis framework for the design of compliant mechanisms with fixed-guided segment(s) that exhibit an inflection point in the deformed state.

As stated before, researchers have been attempting to develop efficient and simpler PRBMs for the analysis and synthesis of fixed-guided segments with an inflection point. Lyon et al. [47] presented a PRBM for modeling a fixed-guided compliant beam with one inflection point. The PRBM was applicable to situations wherein the beam end angle value is different from its initial configuration. The model utilizes the principle of minimum total potential energy to develop the necessary set of equations for the analysis of this segment type. The PRBM can analyze the fixed-guided segment for two specified load or displacement boundary conditions. The model provides good results for a few cases, however, because of its unique schematic it could not be extended towards the synthesis of compliant mechanisms with fixed-guided segments [48]. Kimball and Tsai [49] provided a PRBM for the analysis of fixed-guided segments subjected to arbitrary end loads. The PRBM developed can be applied towards a configuration with a monotonically increasing curvature and a configuration with one inflection point in the deformed state. The schematic of the PRBM is similar to the one proposed by Howell [36], however, the parametric expressions result in an average error of 10.7% for the prediction of the beam end point displacements. Lyon and Howell [48] investigated the feasibility of the use of parametric expressions of the fixed-pinned segment towards the synthesis and analysis of fixed-guided segments with an inflection

point. This PRBM is also schematically similar to Howell [36]. The simplified model is expected to uncouple the load and deflection for a fixed-guided segment with an inflection point. The model, however, leads to large errors. The maximum error in the prediction of the beam end deflection is 10% and the maximum error in the prediction of beam end forces is 15%, when compared to the results obtained from the Chain Algorithm [24]. Su [52] provided a PRBM with three characteristic pivots, containing torsional springs at each characteristic pivot for analysis of a compliant segment subjected to arbitrary beam end loads. The PRBM can analyze fixed-pinned segments, fixed-guided segments with monotonically increasing curvature, and fixed-guided compliant segments with one inflection point in its deformed state. The PRBM parameter values are optimized such that a single set of values can be used for all of these beam types. The model performs well for predicting beam end point deflections with a fixed-pinned segment and a fixed-guided segment with monotonically increasing curvature. The model, however, results in errors while predicting the beam end point deflections for a fixed-guided segment with an inflection point, with an error of 3% for a positive slope at the beam end, and an error of 12% for a negative slope at the beam end, compared with the results obtained from the closed-form solutions. Awatar et al. [86] provided an analytical formulation for a fixed-guided compliant segment. The expressions presented are valid for small-displacements with the transverse deflections being an order of magnitude less than the compliant segment. The analytical formulation predicts the beam end point displacements within an error of 5% and the beam end forces with an error of 10% with the results obtained from the finite element analysis. The authors develop similar analytical formulations for a variety of compliant parallel modules.

Section 3 of this dissertation provided an efficient PRBM for the analysis of a fixed-guided compliant beam with one inflection point in its deformed state. The method utilizes the well-known property of inflection points to develop the set of governing equations for analysis and synthesis of a fixed-guided segment with an inflection point. The formulation requires solution of 18 nonlinear equations simultaneously, and therefore, is only feasible for a two-position synthesis and analysis task. This section simplifies the PRBM formulation presented in section 3 to provide a new synthesis

framework. The synthesis framework is built on one fixed-guided compliant segment, which allows it to be applicable to not only a single-strip compliant mechanism, but also, towards the design of compliant mechanisms containing multiple fixed-guided compliant segments. Design tables are provided for path generation synthesis, with energy storage characteristics or effecting loads specified at the precision positions. The applicability and effectiveness of the proposed framework is demonstrated with the help of three examples.

5.2 PRBM OF A FIXED-GUIDED COMPLIANT BEAM WITH ONE INFLECTION POINT IN ITS DEFORMED STATE

Figure 5.1, Figure 5.2 and Figure 5.3 show a fixed-guided compliant beam in its three possible configurations. A fixed-guided compliant beam will exhibit a deformed state with a monotonically increasing curvature when the reaction moment at the beam end point and the transverse force are in the same sense, as shown in Figure 5.1. When the reaction moment and transverse force are in the opposing sense, a fixed-guided compliant beam may show an inflection point in its deformed state, as shown in Figure 5.2 and Figure 5.3. If the magnitude of the moment load is such that equation (128) is satisfied, then the fixed-guided compliant beam will show an inflection point [49].

$$\cos(\theta_0 - \phi) - \cos(\theta_i - \phi) + \kappa \geq 0 \tag{128}$$

where, $\phi = \operatorname{atan}\left(\frac{-1}{n}\right)$, θ_i the slope at the inflection point, and κ the nondimensional load ratio.

$$\kappa = \frac{M^2}{2PEI} \tag{129}$$

For a configuration with one inflection point,

$$\theta_i > \theta_0 \tag{130}$$

The implementation of equations (128) through (130) is straight-forward for analysis of an individual segment, as shown by Su [52]. The same becomes cumbersome for a compliant mechanism containing multiple segment types. Section 8 of this dissertation provides [82] an approach that allows identifying the occurrence of inflection point(s) in a given compliant mechanism using the principle of minimum total potential energy in conjunction with the degrees of freedom analysis and the PRBM concept. The approach evaluates the expected deformed state qualitatively without any rigorous mathematical analysis.

Figure 5.4 shows the PRBM provided in section 3 for a fixed-guided compliant beam with one inflection point in its deformed state. The PRBM contains three revolute joints. Two of these function as characteristic pivots and the third functions as an instantaneous revolute joint that is located at the inflection point P_i. It is well-known that an inflection point is characterized by zero curvature. Application of Euler-Bernoulli beam equation therefore suggests no internal moment at P_i. Section 3 utilized this property and modeled a fixed-guided compliant beam with one inflection point as a pair of fixed-pinned compliant segments, pinned at the inflection point P_i, and derived the following 18 equations for the analysis and synthesis of a fixed-guided compliant beam with one inflection point. The governing equations, equations (131) through (152), constitute of *parametric equations*, *static equilibrium equations*, and *compatibility equations*. The subscripts 1 and 2 refer to the fixed-pinned compliant segment 1 and 2, respectively.

Figure 5.1 A Fixed-Guided Compliant Beam in its Undeformed and Deformed State with a Monotonically Increasing Curvature

Figure 5.2 A Fixed-Guided Compliant Beam in its Undeformed and Deformed State with one Inflection Point and a Positive Slope at the Beam End

Figure 5.3 A Fixed-Guided Compliant Beam in its Undeformed and Deformed State with one Inflection Point and a Negative Slope at the Beam End

Figure 5.4 PRBM of a Fixed-Guided Compliant Beam with one Inflection Point in its Deformed State

Parametric Equations:

$$\gamma_1 = 0.855651 - 0.016438n_1 \quad \text{for } -4 < n_1 \leq -1.5$$

$$\gamma_1 = 0.852138 - 0.018615n_1 \quad \text{for } -1.5 < n_1 \leq -0.5 \tag{131}$$

$$\gamma_1 = 0.851892 - 0.020805n_1 + 0.005867n_1^2 - 0.000895n_1^3 + 0.000069n_1^4 - 0.000002n_1^5 \quad \text{for } -0.5 < n_1 \leq 10$$

$$\gamma_2 = 0.855651 - 0.016438n_2 \quad \text{for } -4 < n_2 \leq -1.5$$

$$\gamma_2 = 0.852138 - 0.018615n_2 \quad \text{for } -1.5 < n_2 \leq -0.5 \tag{132}$$

$$\gamma_2 = 0.851892 - 0.020805n_2 + 0.005867n_2^2 - 0.000895n_2^3 + 0.000069n_2^4 - 0.000002n_2^5 \quad \text{for } -0.5 < n_2 \leq 10$$

$$c_{\theta_1} = 1.238945 + 0.012035n_1 + 0.00454n_1^2 \quad \text{for } -4 < n_1 \leq -0.5 \tag{133}$$

$$c_{\theta_1} = 1.238845 + 0.009113n_1 - 0.001929n_1^2 + 0.000191n_1^3 - 0.000007n_1^4 \quad \text{for } -0.5 < n_1 \leq 10 \tag{134}$$

$$c_{\theta_2} = 1.238945 + 0.012035n_2 + 0.00454n_2^2 \quad \text{for } -4 < n_2 \leq -0.5 \tag{135}$$

$$c_{\theta_2} = 1.238845 + 0.009113n_2 - 0.001929n_2^2 + 0.000191n_2^3 - 0.000007n_2^4 \quad \text{for } -0.5 < n_2 \leq 10 \tag{136}$$

$$K_{\Theta_1} = 2.66041 - 0.069005n_1 - 0.002268n_1^2 \quad \text{for } -4 < n_1 \leq -0.5 \tag{137}$$

$$K_{\Theta_1} = 2.648834 - 0.074727n_1 + 0.026328n_1^2 - 0.004609n_1^3 + 0.000390n_1^4 - 0.000013n_1^5 \quad \text{for } -0.5 < n_1 \leq 10 \tag{138}$$

$$K_{\Theta_2} = 2.66041 - 0.069005n_2 - 0.002268n_2^2 \quad \text{for } -4 < n_2 \leq -0.5 \tag{139}$$

$$K_{\Theta_2} = 2.648834 - 0.074727n_2 + 0.026328n_2^2 - 0.004609n_2^3 + 0.000390n_2^4 - 0.000013n_2^5 \quad (140)$$

$$\text{for } -0.5 < n_2 \leq 10$$

where,

$$n_1 = \frac{-1}{\tan(\phi_1)} \quad (141)$$

$$n_2 = \frac{-1}{\tan(\phi_2)} \quad (142)$$

Static Equilibrium Equations:

$$\frac{Fl_1^2}{EI}\sin\left(\phi_1 - \frac{\theta_{10}}{c_{\theta_1}}\right) - K_{\Theta_1}\frac{\theta_{10}}{c_{\theta_1}} = 0 \quad (143)$$

$$\frac{Fl_2^2}{EI}\sin\left(\phi_2 - \frac{\theta_{20}}{c_{\theta_2}}\right) - K_{\Theta_2}\frac{\theta_{20}}{c_{\theta_2}} = 0 \quad (144)$$

$$nP + F\left(\cos(\phi_2 + \theta_0)\right) = 0 \quad (145)$$

$$P - F\left(\sin(\phi_2 + \theta_0)\right) = 0 \quad (146)$$

$$M - \left\{[nP\cos(\theta_0) - P\sin(\theta_0)]\gamma_2 l_2 \sin\left(\frac{\theta_{20}}{c_{\theta_2}}\right)\right\} - \left\{[P\cos(\theta_0) + nP\sin(\theta_0)]\left[(1-\gamma_2)l_2 + \gamma_2 l_2\cos\left(\frac{\theta_{20}}{c_{\theta_2}}\right)\right]\right\} = 0 \quad (147)$$

Compatibility Equations:

$$l_1 + l_2 = l \quad (148)$$

$$\theta_{10} = \theta_{20} + \theta_0 \quad (149)$$

$$\phi_1 = \phi_2 + \theta_0 \quad (150)$$

$$b = \gamma_1 l_1 \sin\left(\frac{\theta_{10}}{c_{\theta_1}}\right) + \gamma_2 l_2 \sin\left(\frac{\theta_{20}}{c_{\theta_2}} + \theta_0\right) + (1-\gamma_2)l_2\sin(\theta_0) \quad (151)$$

$$a = (1-\gamma_1)l_1 + \gamma_1 l_1\cos\left(\frac{\theta_{10}}{c_{\theta_1}}\right) + \gamma_2 l_2\cos\left(\frac{\theta_{20}}{c_{\theta_2}} + \theta_0\right) + (1-\gamma_2)l_2\cos(\theta_0) \quad (152)$$

The above set of equations is comprised of 24 variables, six of these variables must be specified to solve for the remaining unknowns deterministically. Depending upon the specification of variables, the above set of equations can be used for two-position synthesis and analysis of a fixed-guided compliant beam with one inflection point. For a three-position synthesis the number of nonlinear equations required are 36. Solution of this set of equations typically becomes cumbersome, and therefore, the formulation could not be extended towards multi-position synthesis of a fixed-guided compliant segment with an inflection point [85].

In order to avoid the large number of equations, this section utilizes the vector loop representation of the PRBM, shown in Figure 5.5, to develop a new synthesis framework. The synthesis framework utilizes the governing equations to derive the necessary free-choices and initial estimates.

Figure 5.5 A Vector Loop Representation of the PRBM for a Fixed-Guided Compliant Beam with one Inflection Point

5.3 A FRAMEWORK FOR SYNTHESIS OF FIXED-GUIDED COMPLIANT BEAMS WITH AN INFLECTION POINT

Figure 5.6 and Figure 5.7 shows two fully-compliant mechanisms containing fixed-guided segments, in its 1^{st} and j^{th} precision position. The vector loop representation of the PRBM of the fixed-guided compliant segment, shown in Figure 5.5, can be readily applied towards the synthesis of fully-compliant mechanisms, as shown in Figure 5.8. Figure 5.9 shows a vector loop closure derived from Figure 5.8.

Figure 5.6 A Single-Strip Mechanism Containing a Fixed-Guided Compliant Segment with an Inflection Point

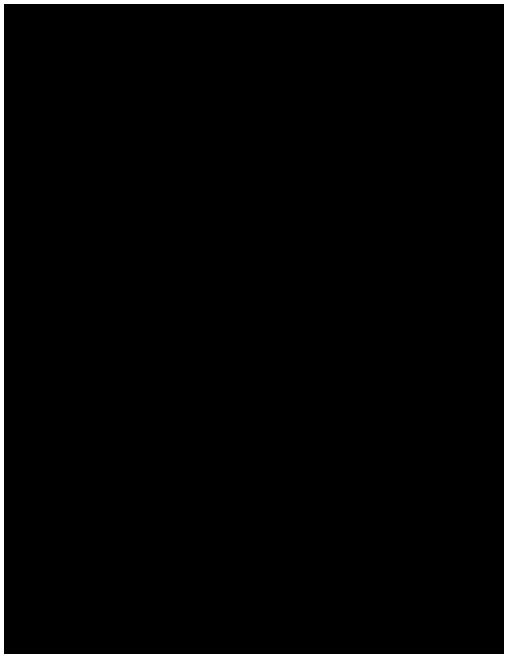

Figure 5.7 A Fully-Compliant Mechanism of Type A Containing a Fixed-Guided Segment with an Inflection Point

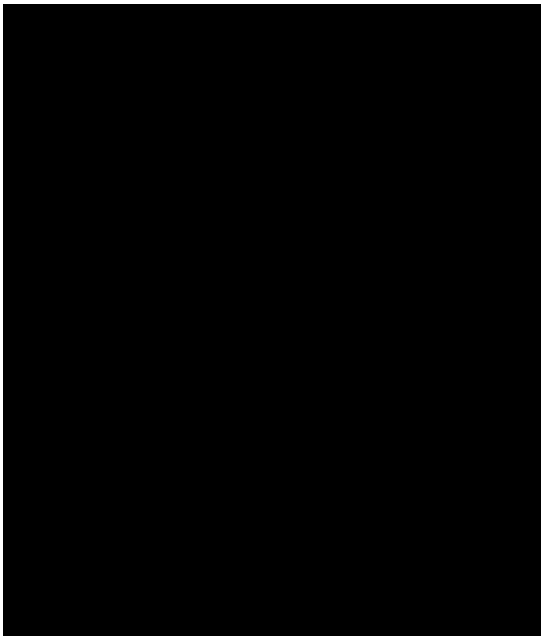

Figure 5.8 A Vectorial Representation of the Left Half of the Fully-Compliant Mechanism shown in Figure 5.7

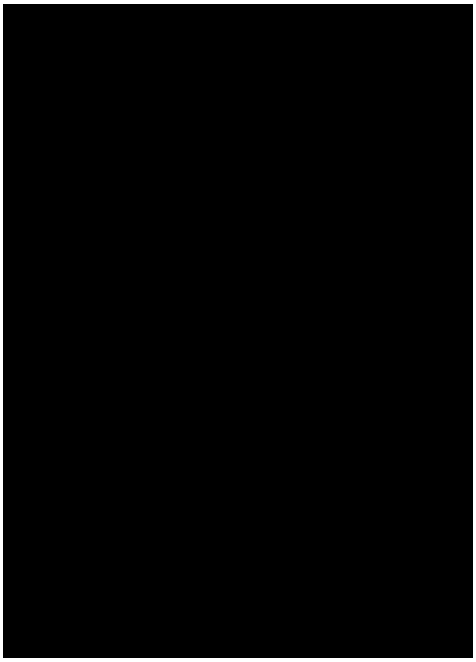

Figure 5.9 A Vector Loop Closure for the Synthesis of Fixed-Guided Compliant Segments with an Inflection Point

From Figure 5.9, we can write the vector loop as:

$$O \rightarrow E \rightarrow P_1 \rightarrow P_j \rightarrow E_j \rightarrow P_{2j} \rightarrow P_{ij} \rightarrow P_{1j} \rightarrow O \tag{153}$$

Using Figure 5.9, the vector loop can be written as:

$$\bar{Z}_6 + \bar{Z}_5 + \bar{\delta}_j - \bar{Z}_{5j} - \bar{Z}_{4j} - \bar{Z}_{3j} - \bar{Z}_{2j} - \bar{Z}_{1j} = 0 \tag{154}$$

The loop closure equation (154) can be written as:

$$\begin{aligned} R_6 e^{i\Theta_6} + R_5 e^{i\Theta_5} + \bar{\delta}_j \\ = R_5 e^{i(\Theta_5+\gamma_j)} + R_{4j} e^{i(\Theta_{4j}+\Theta_1)} + R_{3j} e^{i(\Theta_{3j}+\Theta_1)} + R_{2j} e^{i(\Theta_{2j}+\Theta_1)} \\ + R_{1j} e^{i\Theta_1} \end{aligned} \tag{155}$$

From geometry we have,

$$\Theta_6 = \Theta_1 \tag{156}$$

$$\Theta_4 = \gamma_j \tag{157}$$

$$R_{1j} = \frac{1-\gamma_{1j}}{\gamma_{1j}} R_{2j} \tag{158}$$

$$R_{4j} = \frac{1-\gamma_{2j}}{\gamma_{2j}} R_{3j} \tag{159}$$

Using equations (156) through (159), we have:

$$R_{2j}e^{i\Theta_1}\left[\frac{1-\gamma_{1j}}{\gamma_{1j}} + e^{i\Theta_{2j}}\right] + R_{3j}e^{i\Theta_1}\left[\frac{1-\gamma_{2j}}{\gamma_{2j}}e^{i\gamma_j} + e^{i\Theta_{3j}}\right] + R_5 e^{i\Theta_5}\left[e^{i\gamma_j} - 1\right] - R_6 e^{i\Theta_1} = \bar{\delta}_j \tag{160}$$

Using equation (160) we can develop two scalar equations for synthesis of fixed-guided compliant segments with an inflection point, given as

$$\begin{aligned} &R_{2j}\left[\frac{1-\gamma_{1j}}{\gamma_{1j}}\cos(\Theta_1) + \cos\left(\Theta_{2j} + \Theta_1\right)\right] \\ &\quad + R_{3j}\left[\frac{1-\gamma_{2j}}{\gamma_{2j}}\cos\left(\Theta_1 + \gamma_j\right) + \cos\left(\Theta_{3j} + \gamma_j\right)\right] \\ &\quad + R_5\left[\cos\left(\Theta_5 + \gamma_j\right) - \cos(\Theta_5)\right] - R_6\cos(\Theta_1) = \mathrm{Re}(\bar{\delta}_j) \end{aligned} \tag{161}$$

$$\begin{aligned} &R_{2j}\left[\frac{1-\gamma_{1j}}{\gamma_{1j}}\sin(\Theta_1) + \sin\left(\Theta_{2j} + \Theta_1\right)\right] \\ &\quad + R_{3j}\left[\frac{1-\gamma_{2j}}{\gamma_{2j}}\sin(\Theta_1 + \gamma_j) + \sin(\Theta_{3j} + \gamma_j)\right] \\ &\quad + R_5\left[\sin(\Theta_5 + \gamma_j) - \sin(\Theta_5)\right] - R_6\sin(\Theta_1) = \mathrm{Im}(\bar{\delta}_j) \end{aligned} \tag{162}$$

In addition to the scalar equations the following length and slope compatibility equations are also required, as shown in equations (148) and (149).

$$\frac{R_{2j}}{\gamma_{1j}} + \frac{R_{3j}}{\gamma_{2j}} = R_6 \tag{163}$$

$$\Theta_{2j} c_{\theta 1j} = \left(\Theta_{3j} - \gamma_j\right) c_{\theta_{2j}} + \gamma_j \tag{164}$$

Equations (161) through (164) comprise the set of equations required for the synthesis of a fixed-guided compliant segment with an inflection point. The PRBM parameter values can be readily calculated using equations (131) through (140) by specifying the load factor n as one of the free-choices, in conjunction with equations (142) and (150). Further details about the free-choice selection considerations are provided in the next section.

For synthesis of fixed-guided segments with energy specifications, the following equation should be also considered.

$$U_j = \frac{1}{2}\left[\gamma_{1j}^2 K_{\Theta_{1j}} \frac{EI}{R_{2j}} \Theta_{2j}^2 + \gamma_{2j}^2 K_{\Theta_{2j}} \frac{EI}{R_{3j}} \left(\Theta_{3j} - \gamma_j\right)^2\right] \tag{165}$$

For synthesis of fixed-guided segments with specification of effecting loads at the beam end point, the following equations should be added.

$$\frac{F_j R_{2j}^2}{EI\gamma_{1j}^2} \sin\left(\phi_{1j} - \Theta_{2j}\right) = K_{\Theta_{1j}} \Theta_{2j} \tag{166}$$

$$\frac{F_j R_{3j}^2}{EI\gamma_{2j}^2} \sin\left(\phi_{2j} - \Theta_{3j} + \gamma_j\right) = K_{\Theta_{2j}} \left(\Theta_{3j} - \gamma_j\right) \tag{167}$$

$$M_j = F_j R_{3j} \left\{\sin\left(\phi_{2j} - \Theta_{3j} + \gamma_j\right) + \frac{1 - \gamma_{2j}}{\gamma_{2j}} \sin\left(\phi_{2j}\right)\right\} \tag{168}$$

In order to apply these loads at a point on the rigid-coupler the following equations can be used.

$$P_j = F_j \sin\left(\phi_{2j} + \gamma_j\right) \tag{169}$$

$$nP_j = -F_j \cos(\phi_{2j} + \gamma_j) \quad (170)$$

$$F_x = -nP_j \cos(\Theta_1) - P_j \sin(\Theta_1) \quad (171)$$

$$F_y = -nP_j \sin(\Theta_1) + P_j \sin(\Theta_1) \quad (172)$$

$$M = M_j - F_x[d_2 \sin(\Theta_5) + d_1 \cos(\Theta_5)] + F_y[d_2 \sin(\Theta_5) - d_1 \cos(\Theta_5)] \quad (173)$$

5.4 DESIGN TABLES AND GOVERNING FREE-CHOICE SELECTION CONSIDERATIONS

Equations (161) through (168) can be utilized to synthesize a fully-compliant mechanism with a fixed-guided compliant segment for conventional tasks, such as, path generation and motion generation along with specified energy or load values at the precision positions.

Table 5.1, Table 5.2 and Table 5.3 provide a summary of the equations required for path generation synthesis problem specifications. Note that the tables are provided for the configuration shown in Figure 5.9. A compliant mechanism with multiple fixed-guided segments can be synthesized with the same set of equations, through the specification of a unique set of free-choices for each of the constituent segments.

It may be noted that the column listing the number of free-choices contain some numbers in the square brackets. The numbers in square brackets refer to the actual free-choice specifications. A majority of free-choices include the PRBM parameter values, each of these being function of the load factor. Specification of the load factor (n_1), in conjunction with equations (142) and (150), automatically specifies the remaining PRBM parameter values, using equations (131) through (142). Therefore, it is recommended to specify the load factors (n_{1j}) as free-choices.

Additionally, section 3 identified that for occurrence of an inflection point the angle of vector $\bar{Z}_3$ should be greater than the beam end angle, resulting in the following constraint equation for the specification of free-choices.

$$\Theta_{3j} > \gamma_j \quad (174)$$

Table 5.1 Design Table for Path Generation Synthesis of a Compliant Mechanism with Fixed-Guided Segment

Number of Precision Positions	Number of Equations	Number of Unknowns	Number of Free-Choices
2	4	$R_{22}, \Theta_{22}, \Theta_1, \gamma_{12}, R_{32}, \Theta_{32}, \gamma_{22}, \gamma_2, R_5, \Theta_5, R_6, c_{\theta_{12}}, c_{\theta_{22}}$ (13)	9 [6]
3	8	$R_{22}, \Theta_{22}, \Theta_1, \gamma_{12}, R_{32}, \Theta_{32}, \gamma_{22}, \gamma_2, R_5, \Theta_5, R_6, c_{\theta_{12}}, c_{\theta_{22}}, R_{23}, \Theta_{23}, \gamma_{13}, R_{33}, \Theta_{33}, \gamma_{23}, \gamma_3, c_{\theta_{13}}, c_{\theta_{23}}$ (22)	14 [8]
4	12	$R_{22}, \Theta_{22}, \Theta_1, \gamma_{12}, R_{32}, \Theta_{32}, \gamma_{22}, \gamma_2, R_5, \Theta_5, R_6, c_{\theta_{12}}, c_{\theta_{22}}, R_{23}, \Theta_{23}, \gamma_{13}, R_{33}, \Theta_{33}, \gamma_{23}, \gamma_3, c_{\theta_{13}}, c_{\theta_{23}}, R_{24}, \Theta_{24}, \gamma_{14}, R_{34}, \Theta_{34}, \gamma_{24}, \gamma_4, c_{\theta_{14}}, c_{\theta_{24}}$ (31)	19 [10]
5	16	$R_{22}, \Theta_{22}, \Theta_1, \gamma_{12}, R_{32}, \Theta_{32}, \gamma_{22}, \gamma_2, R_5, \Theta_5, R_6, c_{\theta_{12}}, c_{\theta_{22}}, R_{23}, \Theta_{23}, \gamma_{13}, R_{33}, \Theta_{33}, \gamma_{23}, \gamma_3, c_{\theta_{13}}, c_{\theta_{23}}, R_{24}, \Theta_{24}, \gamma_{14}, R_{34}, \Theta_{34}, \gamma_{24}, \gamma_4, c_{\theta_{14}}, c_{\theta_{24}}, R_{25}, \Theta_{25}, \gamma_{15}, R_{35}, \Theta_{35}, \gamma_{25}, \gamma_5, c_{\theta_{15}}, c_{\theta_{25}}$ (40)	24 [12]

Table 5.2 Design Table for Path Generation Synthesis of a Compliant Mechanism with Fixed-Guided Segment with Energy Specification

Number of Precision Positions	Number of Equations	Number of Unknowns	Number of Free-Choices
2	5	$R_{22}, \Theta_{22}, \Theta_1, \gamma_{12}, R_{32}, \Theta_{32}, \gamma_{22}, \gamma_2, R_5, \Theta_5, R_6, c_{\theta_{12}}, c_{\theta_{22}}, E, K_{\Theta_{12}}, K_{\Theta_{22}}, I$ (17)	12 [7]
3	10	$R_{22}, \Theta_{22}, \Theta_1, \gamma_{12}, R_{32}, \Theta_{32}, \gamma_{22}, \gamma_2, R_5, \Theta_5, R_6, c_{\theta_{12}}, c_{\theta_{22}}, R_{23}, \Theta_{23}, \gamma_{13}, R_{33}, \Theta_{33}, \gamma_{23}, \gamma_3, c_{\theta_{13}}, c_{\theta_{23}}, E, K_{\Theta_{12}}, K_{\Theta_{22}}, I, K_{\Theta_{13}}, K_{\Theta_{23}}$ (28)	18 [8]
4	15	$R_{22}, \Theta_{22}, \Theta_1, \gamma_{12}, R_{32}, \Theta_{32}, \gamma_{22}, \gamma_2, R_5, \Theta_5, R_6, c_{\theta_{12}}, c_{\theta_{22}}, R_{23}, \Theta_{23}, \gamma_{13}, R_{33}, \Theta_{33}, \gamma_{23}, \gamma_3, c_{\theta_{13}}, c_{\theta_{23}}, R_{24}, \Theta_{24}, \gamma_{14}, R_{34}, \Theta_{34}, \gamma_{24}, \gamma_4, c_{\theta_{14}}, c_{\theta_{24}}, E, K_{\Theta_{12}}, K_{\Theta_{22}}, I, K_{\Theta_{13}}, K_{\Theta_{23}}, K_{\Theta_{14}}, K_{\Theta_{24}}$ (39)	24 [9]
5	20	$R_{22}, \Theta_{22}, \Theta_1, \gamma_{12}, R_{32}, \Theta_{32}, \gamma_{22}, \gamma_2, R_5, \Theta_5, R_6, c_{\theta_{12}}, c_{\theta_{22}}, R_{23}, \Theta_{23}, \gamma_{13}, R_{33}, \Theta_{33}, \gamma_{23}, \gamma_3, c_{\theta_{13}}, c_{\theta_{23}}, R_{24}, \Theta_{24}, \gamma_{14}, R_{34}, \Theta_{34}, \gamma_{24}, \gamma_4, c_{\theta_{14}}, c_{\theta_{24}}, R_{25}, \Theta_{25}, \gamma_{15}, R_{35}, \Theta_{35}, \gamma_{25}, \gamma_5, c_{\theta_{15}}, c_{\theta_{25}}, E, K_{\Theta_{12}}, K_{\Theta_{22}}, I, K_{\Theta_{13}}, K_{\Theta_{23}}, K_{\Theta_{14}}, K_{\Theta_{24}}, K_{\Theta_{15}}, K_{\Theta_{25}}$ (50)	30 [10]

Table 5.3 Design Table for Path Generation Synthesis of a Compliant Mechanism with Fixed-Guided Segment with Effecting Force or Moment Specified

Number of Precision Positions	Number of Equations	Number of Unknowns	Number of Free-Choices
2	6	$R_{22}, \Theta_{22}, \Theta_1, \gamma_{12}, R_{32}, \Theta_{32}, \gamma_{22}, \gamma_2, R_5, \Theta_5, R_6, c_{\theta_{12}}, c_{\theta_{22}}, E, K_{\Theta_{12}}, K_{\Theta_{22}}, I, \phi_{12}, \phi_{22}$ (19)	13 [6]
3	12	$R_{22}, \Theta_{22}, \Theta_1, \gamma_{12}, R_{32}, \Theta_{32}, \gamma_{22}, \gamma_2, R_5, \Theta_5, R_6, c_{\theta_{12}}, c_{\theta_{22}}, R_{23}, \Theta_{23}, \gamma_{13}, R_{33}, \Theta_{33}, \gamma_{23}, \gamma_3, c_{\theta_{13}}, c_{\theta_{23}}, E, K_{\Theta_{12}}, K_{\Theta_{22}}, I, K_{\Theta_{13}}, K_{\Theta_{23}}, \phi_{12}, \phi_{22}, \phi_{13}, \phi_{23}$ (32)	20 [6]
4	18	$R_{22}, \Theta_{22}, \Theta_1, \gamma_{12}, R_{32}, \Theta_{32}, \gamma_{22}, \gamma_2, R_5, \Theta_5, R_6, c_{\theta_{12}}, c_{\theta_{22}}, R_{23}, \Theta_{23}, \gamma_{13}, R_{33}, \Theta_{33}, \gamma_{23}, \gamma_3, c_{\theta_{13}}, c_{\theta_{23}}, R_{24}, \Theta_{24}, \gamma_{14}, R_{34}, \Theta_{34}, \gamma_{24}, \gamma_4, c_{\theta_{14}}, c_{\theta_{24}}, E, K_{\Theta_{12}}, K_{\Theta_{22}}, I, K_{\Theta_{13}}, K_{\Theta_{23}}, K_{\Theta_{14}}, K_{\Theta_{24}}, \phi_{12}, \phi_{22}, \phi_{13}, \phi_{23}, \phi_{14}, \phi_{24}$ (45)	27 [6]
5	24	$R_{22}, \Theta_{22}, \Theta_1, \gamma_{12}, R_{32}, \Theta_{32}, \gamma_{22}, \gamma_2, R_5, \Theta_5, R_6, c_{\theta_{12}}, c_{\theta_{22}}, R_{23}, \Theta_{23}, \gamma_{13}, R_{33}, \Theta_{33}, \gamma_{23}, \gamma_3, c_{\theta_{13}}, c_{\theta_{23}}, R_{24}, \Theta_{24}, \gamma_{14}, R_{34}, \Theta_{34}, \gamma_{24}, \gamma_4, c_{\theta_{14}}, c_{\theta_{24}}, R_{25}, \Theta_{25}, \gamma_{15}, R_{35}, \Theta_{35}, \gamma_{25}, \gamma_5, c_{\theta_{15}}, c_{\theta_{25}}, E, K_{\Theta_{12}}, K_{\Theta_{22}}, I, K_{\Theta_{13}}, K_{\Theta_{23}}, K_{\Theta_{14}}, K_{\Theta_{24}}, K_{\Theta_{15}}, K_{\Theta_{25}}, \phi_{12}, \phi_{22}, \phi_{13}, \phi_{23}, \phi_{14}, \phi_{24}, \phi_{15}, \phi_{25}$ (58)	34 [6]

5.5 EXAMPLES

The applicability and effectiveness of the proposed synthesis framework is demonstrated using three examples. The solutions obtained using the synthesis approach are verified using the results obtained from closed-form elliptic integral solutions [49] and the finite element analysis software ANSYS®.

Example 1: A single-strip compliant mechanism is to be designed for three precision positon path generation with effecting force specified at the precision positions: $\bar{\delta}_2 = -1 - 0.75i; F_2 = 5 \text{ lb.}; \bar{\delta}_3 = -3 - 1.75i; \text{and } F_3 = 10 \text{ lb.}$

Using Table 5.3, we have 12 equations with 32 unknowns. 20 of these unknowns should be specified as free-choices in order to obtain a deterministic solution. However, because of the parametric relationships, only 6 of these 20 unknowns need to be specified. All other unknowns can be calculated using equations (131) through (142). The free-choices are specified to be: $\gamma_2 = -10 \text{ deg.}; \gamma_3 = -17 \text{ deg.}; \Theta_1 = 90 \text{ deg.}; n_{12} = 1; n_{13} = 1; \text{and } E = 450{,}000 \text{ psi.}$ A subset of the solutions obtained from the synthesis framework include the following:

$R_6 = 12.895 \text{ in.}; R_5 = 3.763 \text{ in.}; \Theta_5 = 15.192 \text{ deg.}; \text{ and } I = 6.735\text{x}10^{-5}\text{in}^4$

Considering a rectangular cross-section of width 1.5 inch, the thickness of the fixed-guided segment is 0.175 inch. Using equations (168) through (173) and $d_1 = 1 \text{ in.} \text{ and } d_2 = R_5/2$, the effecting forces are:

for position 2:

$F_x = -3.536 \text{ lb.}; F_y = -3.536 \text{ lb.}; M = 27.844 \text{ in.} - \text{lb.}$

for position 3:

$F_x = -7.071 \text{ lb.}; F_y = -7.071 \text{ lb.}; M = 58.678 \text{ in.} - \text{lb.}$

The synthesized single-strip mechanism is shown in Figure 5.10. The location of the coupler point is compared using ANSYS® and closed-form elliptic integral solutions [49], shown in

Table 5.4. In order to perform the verification using closed-form elliptic integral method, the effecting loads are applied at the beam end point, calculated using equations (168) through (172).

Figure 5.10 CAD Rendering of the Single-Strip Mechanism Synthesized in Example 1

Table 5.4 Coupler point location comparisons for specified loads at the beam end point

Coupler Point	**PRBM**		**ANSYS®**		**Elliptic Integral Solution**	
	X (in.)	Y (in.)	X (in.)	Y (in.)	X (in.)	Y (in.)
P_1	0	0	0	0	0	0
P_2	-1	-0.75	-0.972	-0.812	-1.298	-0.762
P_3	-3	-1.75	No Solution		-3.186	-1.764

Example 2: A fully-compliant mechanism of Type A is to be synthesized for four precision position motion generation:

$\bar{\delta}_2 = -3 - 0.75\text{i}; \gamma_2 = 10 \text{ deg.}; \ \bar{\delta}_3 = -3.5 - 1\text{i}; \ \gamma_3 = 12.5 \text{ deg.};$

$\bar{\delta}_4 = -4.5 - 1.75\text{i}; \ \gamma_3 = 20 \text{ deg.}$

For synthesis of this problem specification, we can use Table 5.1 with coupler rotations as designs specification, giving 12 equations with 28 unknowns. 16 of these unknowns should be specified as free-choices in order to obtain a deterministic solution. However, because of the parametric relationships, only 7 of these 16 unknowns need to be specified. All other unknowns can be calculated using equations (131) through (142). The free-choices are specified to be: $\Theta_1 = 90 \text{ deg.}; R_{22} = 1.5; \Theta_{33} = 29 \text{ deg.}; \ \Theta_{34} = 40 \text{ deg.}; \ n_{12} = -1; n_{13} = -1;$ and $n_{14} = -1$. A subset of the solutions obtained from the synthesis framework include the following:

$R_6 = 7.47 \text{ in.}; R_5 = 0.974 \text{ in.}; \text{ and } \Theta_5 = 133.082 \text{ deg.};$

Using the same set of equations, the other fixed-guided segment is synthesized. The free-choices specifications include: $\Theta_1 = 90 \text{ deg.}; R_{22} = 5; \ \Theta_{33} = 22.5 \text{ deg.};$

$\Theta_{34} = 30 \text{ deg.}; n_{12} = -1; n_{13} = -1;$ and $n_{14} = -1$. A subset of the solutions obtained from the synthesis framework include the following:

$R_6 = 8.33 \text{ in.}; R_5 = 4.894 \text{ in.}; \text{ and } \Theta_5 = 127.742 \text{ deg.};$

The synthesized mechanism is shown in Figure 5.11. The location of the coupler point is compared with ANSYS®, shown in Table 5.5. The verifications are performed by specifying the transverse deflection and rotation of the rigid coupler.

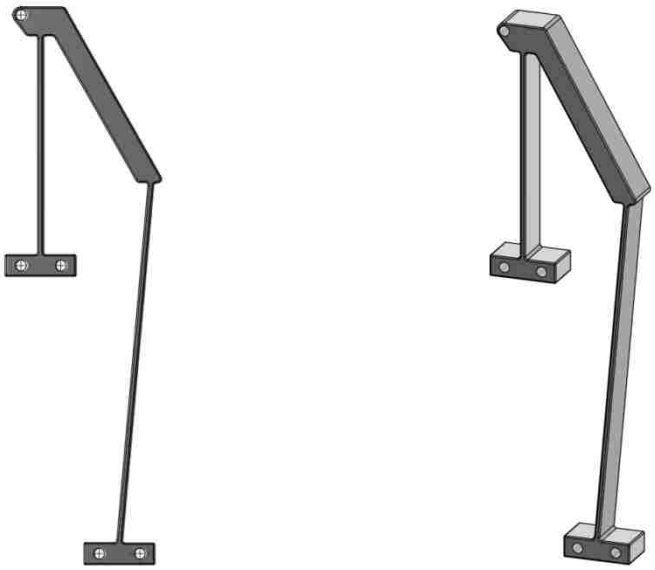

Figure 5.11 CAD Rendering of the Compliant Mechanism Synthesized in Example 2

Table 5.5 Coupler point location comparisons for Example 2

Coupler Point	**PRBM**			**ANSYS®**		
	X (in.)	Y (in.)	γ (deg.)	X (in.)	Y (in.)	γ (deg.)
P_1	0	0	0	0	0	0
P_2	-3	-0.75	10	-3	-0.778	10
P_3	-3.5	-1	12.5	-3.5	-1.05	12.5
P_4	-4.5	-1.75	20	-4.5	-1.8	20

Example 3: A fully-compliant mechanism of Type A is to be synthesized for three precision position motion generation with energy specified at the precision positions.
$\bar{\delta}_2 = -1.5 - 0.5\text{i}; \gamma_2 = -10 \text{ deg.}; \ \bar{\delta}_3 = -2 - 1\text{i}; \ \gamma_3 = -20 \text{ deg.};$
$U_2 = 20 \text{ in.} - \text{lb.}; \text{ and } U_3 = 40 \text{ in.} - \text{lb.}$

For synthesis of this problem specification, we can use Table 5.2 with coupler rotations as designs specification, giving 10 equations with 26 unknowns. 16 of these

unknowns should be specified as free-choices in order to obtain a deterministic solution. However, because of the parametric relationships, only 6 of these 16 unknowns need to be specified. All other unknowns can be calculated using equations (131) through (142). The free-choices are specified to be: $\Theta_1 = 85 \text{ deg.}; \Theta_{32} = 16 \text{ deg.}; \Theta_{33} = 18 \text{ deg.};$

$n_{12} = 1;$ and $n_{13} = 1.$ A subset of the solutions obtained from the synthesis framework, with a specified energy of half of the total energy storage, include the following:

$R_6 = 7.414 \text{ in.}; R_5 = 2.175 \text{ in.};$ and $\Theta_5 = 16.893 \text{ deg.};$

Using the same set of equations, the other fixed-guided segment is synthesized. The free-choices specifications include: $\Theta_1 = 110 \text{ deg.}; \Theta_{32} = 20 \text{ deg.}; \Theta_{33} = 35 \text{ deg.}; n_{12} = 1;$ and $n_{13} = 1$. A subset of the solutions obtained from the synthesis framework include the following:

$R_6 = 5.918 \text{ in.}; R_5 = 2.521 \text{ in.};$ and $\Theta_5 = 178.463 \text{ deg.};$

The synthesized mechanism is shown in Figure 5.12. The location of the coupler point is compared with ANSYS®, shown in Table 5.6. The verifications are performed by specifying the transverse deflection and rotation of the rigid-coupler. The strain energy stored in the compliant mechanism is also computed using ANSYS®. The values of 13.255 in.-lb. and 34.283 in.-lb. are obtained when the compliant mechanism is at second and third precision position, respectively.

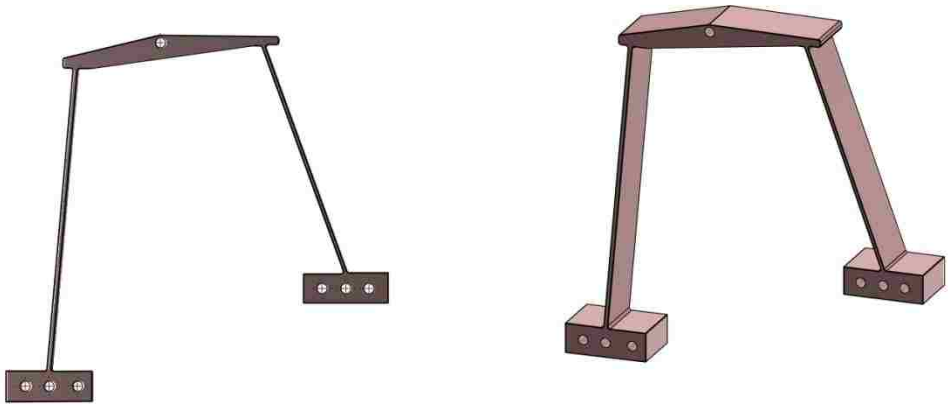

Figure 5.12 CAD Model of the Fully-Compliant Mechanism Synthesized in Example 3

Table 5.6 Coupler Point Location Comparisons for Example 3

Coupler Point	PRBM			ANSYS®		
	X (in.)	Y (in.)	γ (deg.)	X (in.)	Y (in.)	γ (deg.)
$\mathbf{P_1}$	0	0	0	0	0	0
$\mathbf{P_2}$	-1.5	-0.5	-10	-1.5	-0.496	-10
$\mathbf{P_3}$	-2	-1	-20	-2	-1.026	-20

5.6 SUMMARY

This section provided a new synthesis framework for the design of compliant mechanisms containing fixed-guided segments with an inflection point with energy/effecting loads specified at precision positions. The synthesis framework builds on the vector loop representation presented in section 3. The vector loop closure representation allows to reduce the number of equations from 18 to 4, required for a two-position synthesis of a fixed-guided compliant segment. The section provided design tables and guidelines for specification of free-choices for the synthesis of fixed-guided compliant segments with an inflection point for path and motion generation with energy/loads specified at the precision positions. The examples considered demonstrate the applicability of the synthesis approach, and the closed-form elliptic integral and finite element analysis results verify its effectiveness.

6. A GENERALIZED APPROACH FOR DESIGN OF COMPLIANT MECHANISMS USING THE PSEUDO-RIGID-BODY MODEL (PRBM) CONCEPT

This section provides a generalized approach for the design of compliant mechanisms. The approach utilizes the implicit uncoupling between the kinematic and energy/torque equations that is enabled by the pseudo-rigid-body model concept for designing a variety of compliant mechanism types for a wide-range of user specifications. Pseudo-rigid-body four-bar mechanisms, with one to four torsional springs located at the revolute joints, are considered to demonstrate the design methodology. Mechanisms are designed for conventional tasks, such as function, path and motion generation, and path generation with prescribed timing, with energy/torque specified at the precision-positions. State-of-the-art rigid-body synthesis techniques are applied to the pseudo-rigid-body model to satisfy the kinematic requirements. Energy/torque equations are then used to account for the necessary compliance, according to the user specifications. The approach utilizes a conventional, simple yet efficient optimization formulation to solve energy/torque equations that allows a designer to i) achieve realistic solutions, ii) specify appropriate energy/torque values, and iii) reduce the sensitivities associated with the 'synthesis with compliance' approach. A variety of examples are presented to demonstrate the applicability and effectiveness of the approach. All of the examples are verified with the finite element software ANSYS®.

6.1 BACKGROUND

A compliant mechanism gains some or all of its mobility from the deflection of its flexible members [1]. Because of its inherent advantages, e.g. reduced part count, cost, weight, wear, no lash or need for lubrication, and increased precision, ease of manufacturing and assembly, etc. compliant mechanism synthesis and design has continued to be an exciting area of research. Burns and Crossley [14, 15] performed early investigations towards the synthesis of flexible link mechanisms. They presented a graphical technique, known as kinetostatic synthesis, for the design of compliant mechanisms containing a flexible coupler segment and fixed-pinned side links. Midha et al. [23], Her et al. [24], and Sevak and McLarnan [16] developed numerical techniques,

such as the Chain Algorithm and finite element analysis, for analyzing and designing compliant mechanisms; however, these fell short of developing any insights into such systems.

Considering the challenges involved in these approaches, Midha and Her [32] embarked on preliminary discussions on the feasibility of a simple yet robust methodology, which would use equivalent rigid-body models with discrete springs at the revolute joints for compliant segment analysis, synthesis and design, now known as the pseudo-rigid-body model (PRBM) concept. Howell and Midha [33-36] and Howell et al. [37] successfully developed PRBMs for a variety of compliant segment types. Howell and Midha [33-37], Mettlach and Midha [42], Midha et al. [57], Midha et al. [64] and Annamalai and Midha [65], successfully extended the PRBM concept toward the design of fully-compliant and partially-compliant mechanisms that have a PRBM of a four-bar mechanism and developed a systematic design methodology referred to as *synthesis with compliance*. The method utilizes state-of-the-art rigid-body synthesis techniques, along with the energy/torque equations to generate a set of weakly and strongly-coupled equations. Even though the method is effective in its current form, it suffers from several limitations [68].

A number of researchers have recently presented methods that can overcome some of the limitations associated with the *synthesis with compliance* method. Su and McCarthy [69, 70] presented an approach for designing bi-stable compliant mechanisms using the polynomial homotopy technique. This approach transforms the energy/torque equations into approximate polynomial expressions that are solved using the homotopy solvers. The errors introduced as a result of the transformation render the solutions usable as initial estimates only. These estimates are then provided while solving the actual energy/torque equations. The approach is demonstrated for a partially-compliant mechanism with one fixed-fixed coupler segment and two fixed-pinned side links. Tari and Su [71] further modified this approach with a vectorial representation of links for the design of compliant mechanisms. This approach tends to be computationally intensive.

Ananthasuresh [72] implemented a structural optimization technique known as the homogenization method to design fully-compliant mechanisms. This approach formulates an optimization problem for a compliant mechanism design to minimize

weight, volume, error in deflection, and induced stress while maximizing compliance, energy storage, and so forth. Frecker et al. [73] provided a multi-criteria optimization formulation to design compliant mechanisms with the homogenization method. This formulation considered the ratio of strain energies, i.e. energy stored in the compliant mechanism while approaching the work piece to the energy stored while performing useful work. Saggere and Kota [74] provided an approach for synthesizing compliant mechanisms for compliant-segment motion generation. This approach is applicable to partially-compliant mechanisms with a flexible coupler segment that is attached to two fixed-pinned side links. The method requires specifications for both the initial and the final shape of the coupler, and considers small deflections only to facilitate the application of linearized beam theory. It utilizes equilibrium equations, along with a structural optimization routine, with the path vector of side links as the objective function to design a mechanism for compliant-segment motion generation.

Parkinson et al. [75] provided an optimization-based approach for designing fully-compliant mechanisms. This method considers a compliant mechanism to be a spline with various control points, parameterizes the design solution obtained from the optimization routine and creates a finite element model in ANSYS® to analyze the response of a candidate compliant mechanism. The response is compared to the desired outcome to determine the next step of optimization. Rai et al. [76] presented a structural optimization based approach for the synthesis of fully-compliant mechanisms for path generation using initially-curved frame elements. Their method designs a compliant mechanism for tracing the path, with the actuating forces serving as design variables.

Despite all the development to date, synthesis and design of compliant mechanisms remains a challenge. Most of these approaches were developed for a specific type of mechanism. In contrast, the *synthesis with compliance* approach is much more prolific in encapsulating a wide range of compliant mechanism design problems. Unfortunately, it also suffers from unique limitations that can be primarily attributed to the coupling of kinematic and energy/torque equations. This work attempts to overcome these limitations and provides a generalized approach to designing compliant mechanisms. The method utilizes an implicit uncoupling between the kinematic and compliance equations facilitated by the PRBM concept. This approach offers an

unconditional, significant improvement in the implementation of the *synthesis with compliance* framework.

6.2 IMPLICIT UNCOUPLING BETWEEN KINEMATICS AND COMPLIANCE AVAILABLE IN THE PRBM CONCEPT

The PRBM representation of a compliant mechanism facilitates in determining its mobility and energy storage or force/torque-deflection characteristics, henceforth referred to as kinematics and compliance, respectively. *Synthesis with compliance* provides a methodology for compliant mechanism design by considering these two properties as either weakly-coupled or strongly-coupled. To determine the nature of coupling Howell and Midha [56] proposed the following governing expression:

$$2m \geq n \tag{175}$$

where, m represents the number of springs, and n represents the number of energy/torque equations. If the above expression holds true, then the system can be considered as weakly-coupled. If it does not, the system is strongly-coupled. In case the kinematics and compliance equations are strongly-coupled, these have to be solved together. Experiences have shown that obtaining solutions for a strongly-coupled set of equations is cumbersome [68].

A closer examination of the *synthesis with compliance* framework presented by Howell and Midha [56] suggests that the coupling between the kinematics and compliance equations may also depend upon the problem specification, and its associated free-choices. In order to understand this, the kinematics and compliance equations are represented in terms of its constituent PRBM variables, shown in equation (176) and (177).

$$\text{Kinematics} = f(\gamma l, \Theta, \Theta_i, \kappa_i) \tag{176}$$

$$\text{Compliance} = f(k, \Theta, \Theta_i) \tag{177}$$

where, γl is the length of the pseudo-rigid-body link, Θ_i the undeformed orientation, κ_i the initial curvature, k the spring constant of the torsional spring, and Θ the angular deflection of the pseudo-rigid-body link. For a given rotation Θ, the kinematics and compliance of a compliant mechanism may be readily estimated if the pseudo-rigid-body link lengths, initial orientations and spring constants are known or specified.

Equations (176) and (177) show that if Θ and Θ_i are treated as problem specifications or free-choices then the kinematics and compliance equations can be treated as weakly-coupled set of equations, allowing the kinematics and compliance to be evaluated separately. Mathematically, such a consideration will provide a solution from a set of all possible solutions.

This section utilizes this implicit uncoupling property of the PRBM concept to design compliant mechanisms for a wide range of user specifications.

6.3 GENERALIZED APPROACH FOR COMPLIANT MECHANISM DESIGN

The generalized design process would begin with the synthesis of a rigid-body mechanism for specified tasks, such as, function, path and motion generation, and path generation with prescribed timing. Once the rigid-body synthesis is successfully achieved, the designer must determine the number and type of compliant segments that are needed to create the PRBM of the desired compliant mechanism. These segments (torsional springs) can be designed either for specified energy and/or specified force/torque.

Considering the nonlinear nature of energy and torque equations, a conventional optimization formulation is presented that will assist the designer in achieving realistic solutions for spring constants. The steps used for this generalized design approach are outlined below. The entire design process is presented in a flowchart in Figure 6.1.

*Step 1***:** Synthesize a rigid-body mechanism for specified tasks. These tasks may include function, path and motion generation, and path generation with prescribed timing.

*Step 2***:** (Optional) Determine the energy-free configuration of the mechanism.

*Step 3***:** Convert the rigid-body mechanism into the PRBM of a compliant mechanism by adding torsional springs at the revolute joints. Ensure that the degrees of freedom of the resulting compliant mechanism is at least zero.

*Step 4***:** Create an optimization formulation of energy and/or force/torque equations.

*Step 5***:** Provide necessary bounds to the design variables and input necessary constraints (optional). Solve the optimization problem for unknown torsional spring constant(s).

*Step 6***:** Determine the type of compliant segment, e.g. fixed-free, small-length flexural pivot, etc. to be used.

*Step 7***:** Determine the properties of compliant segment(s). Here, the material property (modulus of elasticity E) can be selected to determine the geometric property (moment of inertia I), and the details of the cross-section.

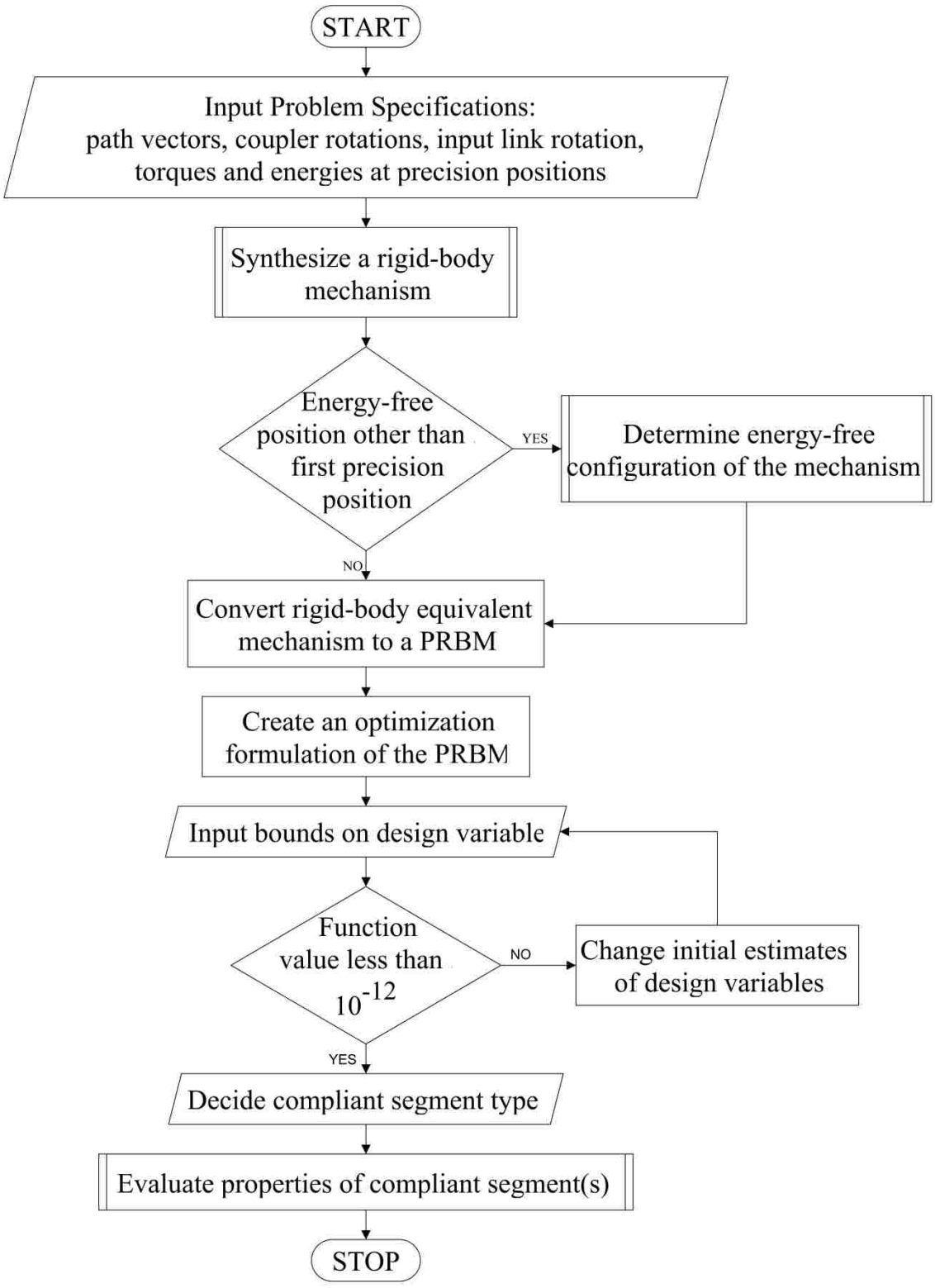

Figure 6.1 The Generalized Approach for Compliant Mechanism Design

6.3.1 Salient Features of the Generalized Synthesis Approach. The treatment of kinematics and energy/torque equations as a weakly-coupled set of equations facilitates in the development of a newer implementation scheme, within the framework of synthesis with compliance. The advantages of implementing these implicit properties of the PRBM are multifold.

The proposed generalized synthesis approach allows a straight-forward application of rigid-body synthesis techniques to design compliant mechanisms for either specified energy or specified force/torque. The approach utilizes the flexibility provided by the PRBM concept, and allows a PRBM to be transformed into multiple compliant mechanisms with same mobility, however, with unique energy storage and force/torque deflection characteristics. The optimization formulation utilized in the approach permits the application of a conventional optimization routine to obtain realistic solutions for spring constants. The application of an optimization routine may guide a designer toward meeting the energy/torque specifications.

The generalized synthesis approach permits the design of both partially-complaint and fully-compliant mechanisms using the same rigid-body mechanism design. Various synthesis cases that could not be solved by *synthesis with compliance* [87] may be readily solved. The approach can also be utilized to derive relationships between spring constants. Such an effort will provide the underlying relationships between the spring constants and readily allow generating a variety of energy or force/torque-deflection curves. The approach also facilitates in the design of functionally-similar and structurally-dissimilar compliant mechanisms.

6.4 REVIEW OF RIGID-BODY SYNTHESIS FOR FUNCTION, PATH AND MOTION GENERATION, AND PATH GENERATION WITH PRESCRIBED TIMING

Here a brief review of a rigid-body synthesis technique is presented, which may be used for function, path and motion generation, and path generation with prescribed timing. The dyadic approach reviewed here is for illustrative purposes only, and the user should not be limited towards it.

A vector schematic of a planar linkage, that is, using the complex number technique is proved to be the simplest, yet the most versatile method for synthesis of rigid-body mechanisms [88]. Most of the planar linkages may be thought of as a combination of vector pairs known as dyads [88]. In function generation, the vector loop closure $\bar{Z}_2 - \bar{Z}_3 - \bar{Z}_4 - \bar{Z}_{4j} - \bar{Z}_{3j} - \bar{Z}_{2j}$ that is shown in Figure 6.2 produces the following equation:

$$\bar{Z}_2\left(1 - e^{i\phi_j}\right) + \bar{Z}_3\left(1 - e^{i\gamma_j}\right) + \bar{Z}_4\left(e^{i\psi_j} - 1\right) = 0 \tag{178}$$

where, j is the precision-position.

Figure 6.2 Vector schematic of a four-bar function generation mechanism in both its 1^{st} and j^{th} position

For path generation, motion generation (rigid-body guidance), and path generation with prescribed timing, loops $\bar{Z}_2 - \bar{Z}_5 - \bar{\delta}_j - \bar{Z}_{5j} - \bar{Z}_{2j}$ and $\bar{Z}_4 - \bar{Z}_6 - \bar{\delta}_j - \bar{Z}_{4j} - \bar{Z}_{6j}$ that are shown in Figure 6.3 formed by dyads $\bar{Z}_2 - \bar{Z}_5$ and $\bar{Z}_4 - \bar{Z}_6$, respectively, produce the following equations:

$$\bar{Z}_2\left(e^{i\phi_j} - 1\right) + \bar{Z}_5\left(e^{i\gamma_j} - 1\right) = \bar{\delta}_j \tag{179}$$

$$\bar{Z}_4\left(e^{i\psi_j} - 1\right) + \bar{Z}_6\left(e^{i\gamma_j} - 1\right) = \bar{\delta}_j \tag{180}$$

where, j is the precision-position.

Equations (178) through (180) can be expanded for each precision-position to synthesize a rigid-body equivalent mechanism for function, path and motion generation, and path generation with prescribed timing.

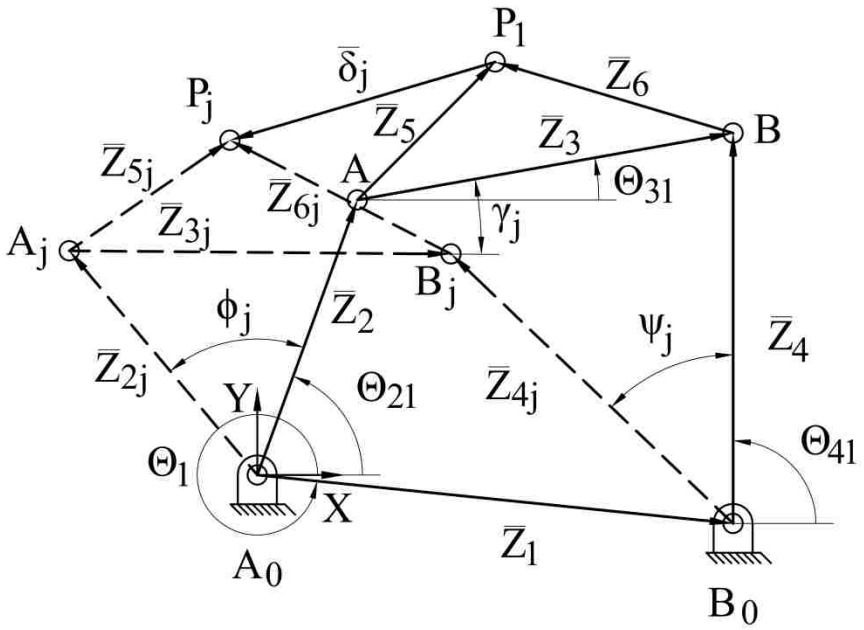

Figure 6.3 Vector schematic of four-bar mechanism showing vector dyads in both its 1st and jth position

6.5 OPTIMIZATION FORMULATION TO SOLVE ENERGY/TORQUE EQUATIONS

Energy Equations: Energy stored in a complaint mechanism during its structural deformation, in the precision-position, is estimated by the potential energy stored in the torsional springs of the PRBM [36, 42].

$$U_j = \frac{1}{2}\sum_{i=1}^{m} k_i(\beta_{ij} - \beta_{i0})^2; \text{ for } 1 \le m \le 4 \tag{181}$$

Torque Equations: The torque required to move a compliant mechanism through the precision-point is estimated by the restoring torque in the torsional springs of the PRBM [36, 42].

$$T_j = \sum_{i=1}^{m} k_i(\beta_{ij} - \beta_{i0})\frac{d\beta_{ij}}{dS}; \text{ for } 1 \le m \le 4 \tag{182}$$

where, m is the number of torsional springs in the PRBM, k the spring constant, β_{ij} the j^{th} angular position of the i^{th} torsional spring, β_{i0} the angular position of the spring in undeflected position, and S the input variable for the mechanism. If Θ_2 is the input, then $d\beta_{ij}/dS$ may be expressed as:

$$\frac{d\beta_{1j}}{d\Theta_2} = 1;\ \frac{d\beta_{2j}}{d\Theta_2} = h_{3j} - 1;\ \frac{d\beta_{3j}}{d\Theta_2} = h_{4j} - h_{3j}\ ;\ \frac{d\beta_{4j}}{d\Theta_2} = h_{4j}$$

where,

$$h_{3j} = \frac{R_2\sin(\Theta_{4j} - \Theta_{2j})}{R_3\sin(\Theta_{3j} - \Theta_{4j})}; \text{and } h_{4j} = \frac{R_2\sin(\Theta_{3j} - \Theta_{2j})}{R_4\sin(\Theta_{3j} - \Theta_{4j})}$$

The angle β_{ij} is related to the pseudo-rigid-body mechanism angles Θ as follows [56]:

$$\begin{aligned}
\beta_{1j} &= \Theta_{2j} \\
\beta_{2j} &= 180 - (\Theta_{2j} - \Theta_{3j}) \\
\beta_{3j} &= \Theta_{4j} - \Theta_{3j} \\
\beta_{4j} &= \Theta_{4j}
\end{aligned} \tag{183}$$

where, Θ_{nj} represents the angle of the n^{th} link at the j^{th} position measured counter-clockwise from the right horizontal.

Research has shown that solving both the energy and torque equations can be a challenging task [70]. Because the equations are nonlinear in nature, the solutions are dependent on the quality of the initial estimates. At some instances, very minor changes in the initial estimates have produced significantly different outcomes. These sensitivities prevent the designer from determining what is at fault: the initial estimates or the energy/torque specifications [68].

Realistic solutions can be difficult to obtain while solving nonlinear equations. Typically, accurate initial approximations are required to ensure convergence. As an alternative, an optimization technique has been proposed in the literature that helps a user the same way the Bisection method helps for a single equation, i.e. convergence is usually achieved even for poor initial approximation [89]. Considering the following mathematical equivalence, conventional optimization techniques may be readily implemented to solve the energy and torque equations:

If we consider a linear set of nonlinear equations,

$f_1(x_1, x_2, \dots, x_n) = 0;$

$f_2(x_1, x_2, \dots, x_n) = 0;$

$\dots;$

$f_n(x_1, x_2, \dots, x_n) = 0;$

then a solution $\mathbf{x} = (x_1, x_2, \dots, x_n)$ exists precisely when the function

$$q(x_1, x_2, \dots, x_n) = \sum_{i=1}^{n} [f_i(x_1, x_2, \dots, x_n)]^2 \quad (184)$$

has a minimal value of zero [89].

Using equation (184), the following optimization problem may be constructed to solve the compliance equations:

$$\begin{aligned}
&\underset{x}{\text{Minimize}}\ F = \sum_{j=1}^{n_p} f_j(x_1, x_2, \dots, x_n)^2 \\
&\text{subject to} \\
&g_i(x_1, x_2, \dots, x_n) \le 0; i = 1,2, \dots, n_i \\
&h_j(x_1, x_2, \dots, x_n) \le 0; j = 1,2, \dots, n_e \\
&x_k^l \le x_k \le x_k^u, k = 1,2, \dots, n
\end{aligned} \tag{185}$$

where $x = (x_1, x_2, \dots, x_n)$ is the vector of design variables that may include spring constants of torsional springs, F the design objective function that needs to be minimized, $f_j(x_1, x_2, \dots, x_n)$ the energy/torque expression for the j^{th} precision-position, $g_i(x_1, x_2, \dots, x_n)$ the inequality constraint function, $h_j(x_1, x_2, \dots, x_n)$ the equality constraint function, n_i the number of inequality constraint functions, n_e the number of equality constraint functions, n_p the number of precision positions (where a non-zero energy/torque is specified), n the number of design variables, x_k^l the lower bound, and x_k^u the upper bound.

This simple, yet efficient, optimization formulation not only helps in achieving realistic solutions with minimal effort but also guides a designer in specifying appropriate energies/torques at the precision positions. The designer may also choose to add constraints, e.g., the equality of spring constants, reliability based design constraints, limit stresses, and so forth.

6.6 SPECIFYING APPROPRIATE ENERGY/TORQUE AT PRECISION POSITIONS

Specifying appropriate energy/torque for a mechanism at various precision positions may be cumbersome. For simplicity, a heuristic judgment may be made between the energy/torque specifications and the rotation of the pseudo-rigid-body links of the compliant mechanism, to ensure the specifications are appropriate. On various occasions, however, a designer may still need assistance with providing appropriate

specifications. The above presented optimization formulation guides the designer with this.

The function value at the end of the optimization process is an excellent indicator of the energy or force/torque specifications. If the function value is not close to zero, then at first some iteration must be conducted by changing the initial estimates drastically. This will ensure a search for the global minimum. If the function value at these various starting positions is still not close to zero, then an unrealistic problem definition may exist. In this instance, the following steps should be utilized to better understand the change in direction:

1. Determine whether or not the energy/torque at various positions is in agreement with the rotation of the pseudo-rigid-body links.

2. If the result from Step 1 is deemed satisfactory, then the user should either increase or decrease the energy/torque specifications.

3. Examine the function value at the end of Step 2. If the function value is approaching zero, then continue in the same direction until the desired function value is achieved. In case the function value is diverging further, change the direction and repeat Step 3.

The above process is illustrated in examples presented in the following section.

6.7 EXAMPLES

The applicability of the generalized design methodology is presented with the help of the following examples, which encapsulate a wide-range of user specifications. Finite element verifications presented verify the effectiveness of the method.

Example 1: A fully-compliant mechanism is to be designed for three-precision-position motion generation synthesis, with torque specified at these precision positions:
$\overline{\delta_2} = -1.5 - 0.5\text{i};\ \overline{\delta_3} = -3.5 + 1.5\text{i};\ \gamma_2 = -10^{\text{o}};\ \gamma_3 = -15^{\text{o}};$
$T_1 = 8.75\ \text{in.}-\text{lb.};\ T_2 = 30\ \text{in.}-\text{lb.};\ \text{and}\ T_3 = 42.75\ \text{in.}-\text{lb.}$

Following the generalized design procedure, we synthesize a rigid-body mechanism for three-precision-position motion generation. Expanding equation (179) and (180) gives eight equations with 18 variables. Six of these are specified, thus giving a system of eight equations with 12 unknowns. In order to obtain a solution four free-choices are made: $\Theta_{21} = 80^o;\ \Theta_{41} = 100^o; \mathrm{R}_4 = 10$ and $\mathrm{R}_2 = 6$. The rigid-body mechanism is:

$$\bar{\mathrm{Z}}_1 = 5.063 - 1.855\mathrm{i}; \qquad \bar{\mathrm{Z}}_2 = 1.042 + 5.909\mathrm{i}$$
$$\bar{\mathrm{Z}}_3 = 2.284 + 2.084\mathrm{i}; \qquad \bar{\mathrm{Z}}_4 = -1.736 + 9.848\mathrm{i}$$
$$\bar{\mathrm{Z}}_5 = 2.906 + 2.206\mathrm{i}; \qquad \bar{\mathrm{Z}}_6 = 0.621 + 0.122\mathrm{i}$$
$$\phi_3 = 39.232^o; \qquad \psi_2 = 8.955^o$$
$$\psi_3 = 21.647^o$$

The problem definition suggests that the energy-free state of the mechanism is not at the first-precision-position. Using equation (179) and (180), and considering $\Theta_{20} = 75^o$, the following configuration is obtained:

$$\Theta_{30} = 46.745^o; \qquad \Theta_{40} = 97.995^o$$

Considering a fully-compliant mechanism with four SLFPs and using equation (185), a constrained optimization formulation is generated. The spring constants are obtained for specified torque values, subject to the following dimensional and stress constraints:

$$\mathrm{t}_1 = \mathrm{t}_2; \qquad \sigma_{\text{induced}} \leq \sigma_{\text{yield}}$$

The optimization formulation is generated using equation (182) and (186) to determine the thicknesses of the SLFPs.

$$
\begin{aligned}
&k_i = \frac{EI_i}{l_i}, \\
&\frac{l_1}{2} + L_2 + \frac{l_2}{2} = R_2, \\
&\frac{l_3}{2} + L_4 + \frac{l_4}{2} = R_4, \\
&l_1 = l_2 = 0.05L_2, \\
&l_3 = l_4 = 0.05L_4 \text{ and} \\
&\sigma_{induced} = \frac{M_i t_i}{2I_i}
\end{aligned}
\tag{186}
$$

The fully-compliant mechanism is constructed using unreinforced Nylon 46, with a flexural modulus of elasticity of 131 ksi and flexural strength of 15 ksi. Using equation (182) and (186), and considering a rectangular cross-section, the thicknesses are calculated to be:

$$
\begin{aligned}
t_1 &= 0.032802 \text{ in.}; \qquad & t_2 &= 0.032802 \text{ in.} \\
t_3 &= 0.11643 \text{ in.}; \qquad & t_4 &= 0.10855 \text{ in.}
\end{aligned}
$$

The lengths of the SLFPs and rigid-segments are: $l_1 = l_2 = 0.2857$ in.; $L_2 = 5.7143$ in.; $l_3 = l_4 = 0.4762$ in.; and $L_4 = 9.5234$in. The resulting fully-compliant mechanism is shown in Figure 6.4.

Figure 6.4 Solid Model of the Compliant Mechanism Designed in Example 1

The synthesis results obtained using the generalized approach are compared with the finite element software ANSYS®. The coupler curve obtained using the PRBM and the precision-position locations obtained from PRBM and ANSYS® are shown plotted in Figure 6.5. The input torque-deflection characteristic obtained using the PRBM is shown plotted in Figure 6.6. Input torques required to reach various precision-positions are summarized in Table 6.1. The maximum stress in the mechanism is experienced at P_3, calculated using ANSYS® as 12628.4 psi.

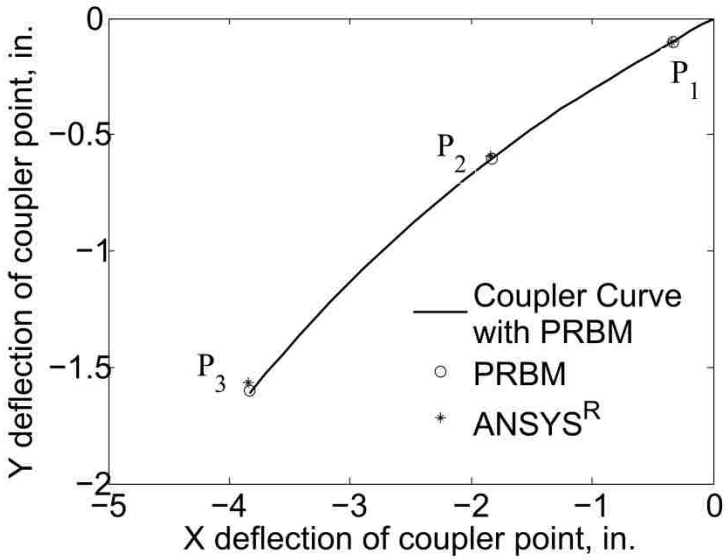

Figure 6.5 Coupler Curve of the Mechanism Designed in Example 1

Table 6.1 Input Torque Required to Reach Precision-Positions of Example 1

Precision Position	**Input Torque (T_2), in.-lb.**	
	PRBM	ANSYS®
P_1	8.75	8.75
P_2	30	29.5
P_3	42.75	41.35

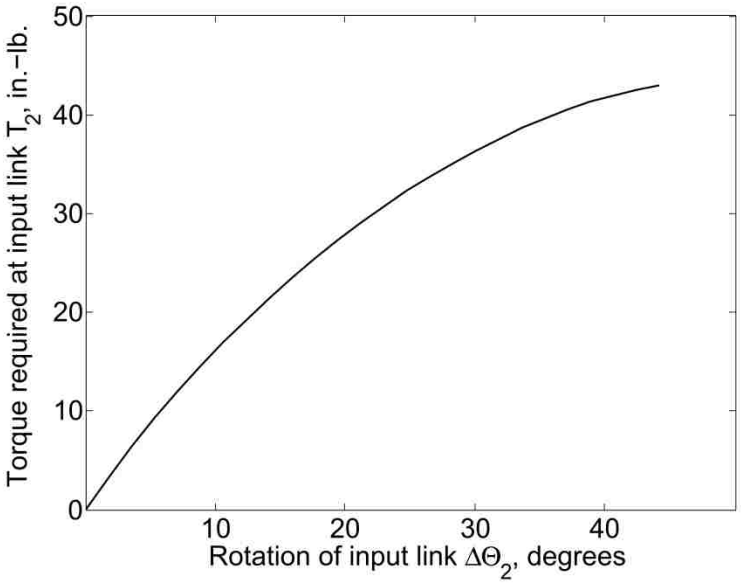

Figure 6.6 Torque-Deflection Characteristic of the Mechanism Designed in Example 2

*Example 2***:** It is desired to design a partially-compliant mechanism for three-precision-position function generation that shows bi-stable behavior, with energy specified at these precision-positions:

$\psi_j = g(\phi_j) = 2\phi_j - 20 \text{ deg.}; \ \phi_2 = 20 \text{ deg.}, \phi_3 = 40 \text{ deg.};$

$U_1 = 0, U_2 = 15 \text{ in.} - \text{lb. and } U_3 = 5 \text{ in.} - \text{lb.}$

Following the generalized design procedure, we synthesize a rigid-body mechanism for function generation. Expanding equation (178) gives four equations with 12 variables. Four of these are specified, thus giving a system of four equations with eight unknowns. In order to obtain a solution four free-choices are made; $\Theta_{21} = 130^o; \ \Theta_{31} = 200^o; R_4 = 7 \text{ and } \gamma_2 = 10^o$. The rigid-body mechanism is:

$$\bar{Z}_1 = -4.504 - 2.1i; \qquad \bar{Z}_2 = -2.094 + 2.496i$$

$$\bar{Z}_3 = -9.305 - 3.387i; \qquad \bar{Z}_4 = -6.895 + 1.209i$$

$$\gamma_3 = 34.212^o;$$

The problem definition suggests that the mechanism is in its energy-free state at this position. Let us design a partially-compliant mechanism that has a PRBM with one torsional spring. Using equation (185) an unconstrained optimization formulation is generated giving the following spring constants for the energy values of $U_2 = 14.925 \text{ in.} - \text{lb.}$ and $U_3 = 5 \text{ in.} - \text{lb.}$

$k_2 = 979.9148 \text{ in.} - \text{lb.} \text{ rad}$

The torsional spring designed above may be translated to either a SLFP or a fixed-pinned segment. Let us consider a compliant mechanism with a fixed-pinned segment. We know that for a fixed-pined segment:

$$k_i = \frac{\gamma K_\Theta E I_i}{l_i}, \text{ and}$$
$$\gamma l_n = R_n \qquad (187)$$

Considering rectangular cross-section of width $w = 0.5$ in., the thickness is $t_2 = 0.44409$ in. The resulting compliant mechanism is shown in Figure 6.7. The strain energy stored in the flexible members of the compliant mechanism is obtained from the PRBM and is compared with the results obtained from ANSYS®. The energy storage characteristic of the compliant mechanism designed is shown in Figure 6.8. The strain energy obtained from both PRBM and ANSYS® are also shown plotted on the energy curve.

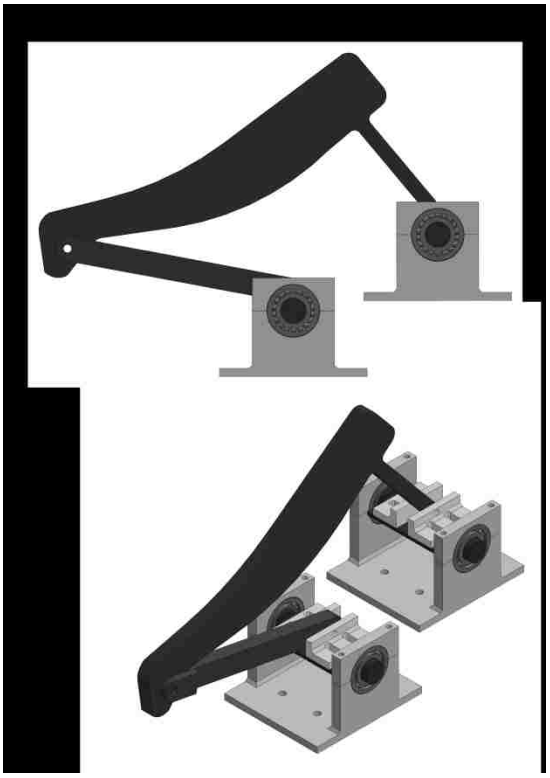

Figure 6.7 Solid Model of the Compliant Mechanism Designed in Example 2

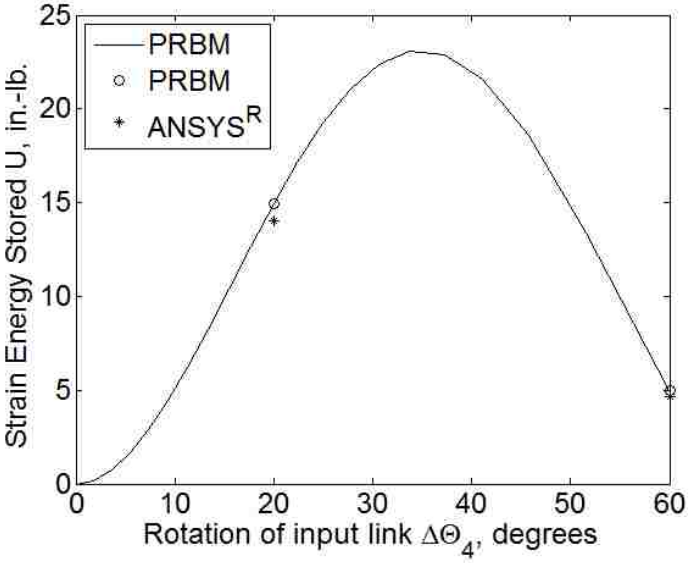

Figure 6.8 Energy Storage Characteristics of the Mechanism Designed in Example 2

Example 3: It is desired to design a compliant mechanism with fully-compliant segments for three-precision-position path generation with prescribed timing, with energy specified at these precision-positions:

$\overline{\delta_2} = -3 + 0.5\text{i};\ \overline{\delta_3} = -5 + 0.25\text{i};\ \phi_2 = 20^o;\ \phi_3 = 35^o;$

$U_1 = 0, U_2 = 15\ \text{in.} - \text{lb.}\ \text{and}\ U_3 = 45\ \text{in.} - \text{lb.}$

Following the generalized design procedure, we synthesize a rigid-body mechanism for three-precision-position path generation with prescribed timing. Expanding equations (179) and (180) gives eight equations with 18 variables. Six of these are specified, thus giving a system of eight equations with 12 unknowns. In order to obtain a solution four free-choices are made; $\Theta_{21} = 85^o;\ \Theta_{41} = 65^o; R_2 = 5.5\ \text{and}\ R_4 = 7$. The rigid-body mechanism is:

$$\bar{Z}_1 = 2.876 + 3.02\text{i}; \qquad \bar{Z}_2 = 0.479 + 5.479\text{i}$$
$$\bar{Z}_3 = 5.355 + 3.885\text{i}; \qquad \bar{Z}_4 = 2.958 + 6.344\text{i}$$
$$\bar{Z}_5 = 4.652 + 6.422\text{i}; \qquad \bar{Z}_6 = -0.703 + 2.537\text{i}$$
$$\gamma_2 = 9.286^o; \qquad \gamma_3 = 14.613^o$$
$$\psi_2 = 22.064^o; \qquad \psi_3 = 36.74^o$$

The problem definition suggests that the mechanism is in its energy-free state at this position. Considering a fully-compliant mechanism, that is, using a PRBM that contains four torsional springs placed at the revolute joints. Let $k_1 = k_2$ and $k_3 = k_4$. Using equation (185) a constrained optimization formulation is generated giving the following spring constants for the energy values of $U_2 = 15\ \text{in.} - \text{lb.}\ \text{and}\ U_3 = 45\ \text{in.} - \text{lb.}$

$$k_1 = 91.3141\ \text{in.} - \text{lb./rad}; \qquad k_2 = 91.3141\ \text{in.} - \text{lb./rad}$$
$$k_3 = 79.1763\ \text{in.} - \text{lb./rad}; \qquad k_4 = 79.1763\ \text{in.} - \text{lb./rad}$$

The torsional springs designed above may be translated to either four SLFPs or two fixed-guided segments. Let us consider a compliant mechanism with two fixed-guided segments. We know that for a fixed-guided segment:

$$\mathrm{k_i} = \frac{2\gamma \mathrm{K_\Theta EI_i}}{l_\mathrm{i}}, \text{ and}$$
$$\gamma l_\mathrm{n} = \mathrm{R_n} \tag{188}$$

Using equation (188), $\gamma = 0.851, \mathrm{K_\Theta} = 2.68$ and $\mathrm{E} = 450$ ksi, we have

$$l_2 = 6.458 \text{ in.}; \qquad \mathrm{I_2} = 2.87 \text{ x } 10^{-4} \text{ in}^4$$
$$l_4 = 8.219 \text{ in.}; \qquad \mathrm{I_4} = 3.168 \text{ x } 10^{-4} \text{ in}^4$$

Considering rectangular cross-section of width $\mathrm{w} = 0.5$ in., the thicknesses are $\mathrm{t_2} = 0.19028$ in. and $\mathrm{t_4} = 0.19663$ in. The resulting compliant mechanism is shown in Figure 6.9. Figure 6.10 shows the coupler curve obtained with the PRBM. The precision-position locations obtained from PRBM and ANSYS® are shown plotted in Figure 6.10. The strain energy stored in the mechanism at precision-position is summarized in Table 6.2.

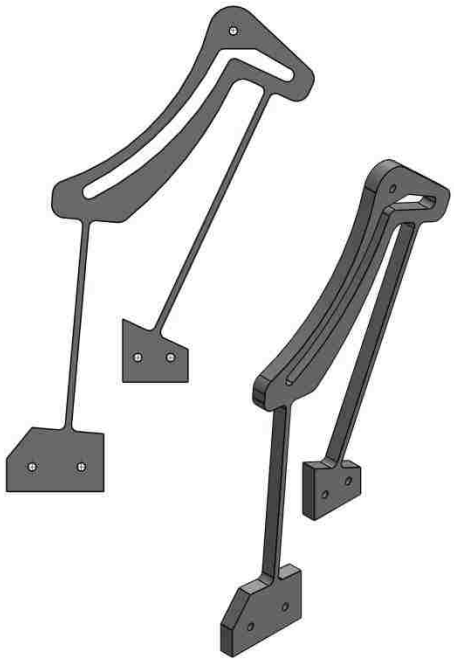

Figure 6.9 Solid Model of the Compliant Mechanism Designed in Example 3

Table 6.2 Strain Energy Stored in the Compliant Mechanism at Various Precision-Positions

Precision Position	**Strain energy stored (U) (in.-lb.)**	
	PRBM	ANSYS®
$\mathbf{P_1}$	0	0
$\mathbf{P_2}$	15	13.677
$\mathbf{P_3}$	45	41.215

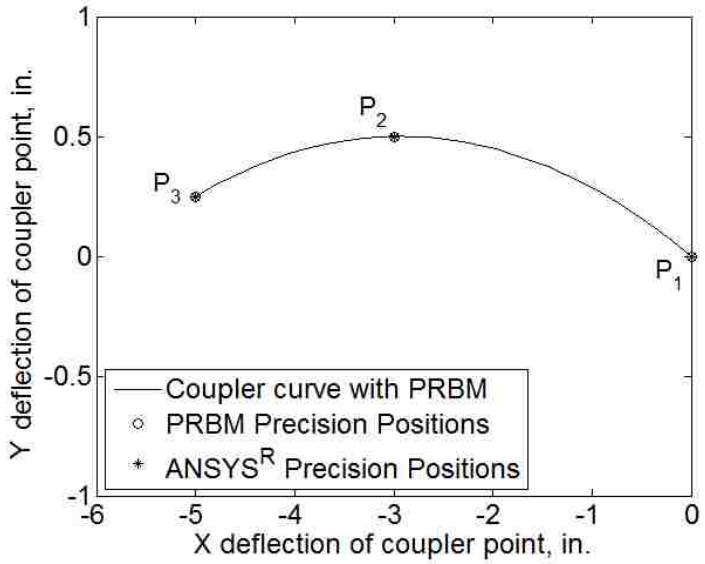

Figure 6.10 Coupler Curve of the Mechanism Designed in Example 3

6.8 SUMMARY

A generalized approach for the design of compliant mechanisms has been presented in this section. The design methodology utilizes an implicit uncoupling of kinematic and compliance equations, which is intrinsic to the PRBM concept, and solves a large variety of problem types using a weakly-coupled set of equations. Examples covering a wide range of user specifications are presented that demonstrate the applicability of the approach, while the finite element analysis comparisons validate its effectiveness. The method is effective for both partially- and fully-compliant mechanism designs. The simple and efficient optimization formulation presented not only allows for obtaining realistic solutions, but also guides a designer in specifying pragmatic energy/torque values.

7. MECHANICAL ADVANTAGE OF A COMPLIANT MECHANISM AND THE SIGNIFICANT FACTORS AFFECTING IT, USING THE PSEUDO-RIGID-BODY MODEL APPROACH

Although work related to mechanical advantage of compliant mechanisms has been presented almost two decades ago, unlike many rigid-body mechanism systems, this performance measure has seldom been used. In great part, the reasons are attributed to, one, the relatively recent development of and lack of familiarity with this technology and, two, the complexity of the understanding and evaluation of mechanical advantage of compliant systems. In an effort to simplify the evaluation, this section uses the pseudo-rigid-body model (PRBM) of a compliant mechanism, along with traditional notions of power conservation and angular velocity ratios using instant centers. As a first step, the inherent compliance in the mechanism is neglected in determining its mechanical advantage, followed by considerations to optimize its structural configuration for enhancing its mechanical advantage. The PRBM methodology, which offers us a way to estimate the characteristic compliance of the mechanism, now enables its inclusion in determining the mechanical advantage of the compliant mechanism. Two significant factors affecting it are i) the structural configuration of the PRBM, and ii) the energy stored in compliant elements of the mechanism. Several case studies are considered, which suggest that while minimizing the later relative to that of an optimized structural configuration may improve the mechanical advantage of a compliant mechanism, its effect on the mechanical advantage of the compliant mechanism cannot be neglected.

7.1 BACKGROUND

Compliant mechanisms are mechanical devices that gain some or all of its motion through the deflection of its flexible members, to transfer force, motion, and energy [1]. Because of the inherent advantages associated with compliant mechanisms, e.g. reduced part count, no lash or need for lubrication, increased precision, built-in compliance, ease of manufacturing and assembly, etc., compliant mechanisms have found their place in a wide range of applications including hand tools, automotive components, and micro-electromechanical systems (MEMS). While the rigid-body mechanisms are typically designed for providing force amplification between the output and input ports, the

mechanical advantage, compliant mechanism design has been focused towards transferring motion and/or energy storage characteristics. Even though work related to mechanical advantage of compliant mechanisms has been presented almost two decades ago [27, 28], unlike many rigid-body mechanism systems, this performance measure is seldom used. The recent development of the technology, and the complexities involved in the understanding and evaluation of mechanical advantage can be identified as the reasons for the lack of utilization of this performance measure. In an effort to simplify the evaluation of mechanical advantage, this section utilizes the well-proven compliant mechanism modeling technique called as the pseudo-rigid-body model (PRBM) concept, along with the traditional notions of power conservation and angular velocity ratios using instant centers.

Research efforts involving the mechanical advantage aspects of compliant mechanisms have been rather limited. In great part, the reasons are attributed to the complexity of the mechanical advantage analysis of compliant mechanisms, when compared to rigid-body mechanisms. Salamon and Midha [27, 28] performed initial investigations towards the understanding of mechanical advantage aspect in compliant mechanisms. Salamon and Midha [27, 28] presented a detailed investigation of this measure of performance. Mechanical advantage of a compliant mechanism was classified in three categories, associated with the dependent variable, say, location of work piece, input force, and stiffness of work piece. Salamon and Midha [27, 28] utilized the Chain Algorithm [23, 24] to perform their investigations, and identified the governing relations. Salamon and Midha [27, 28] also envisioned the use of rigid-body equivalent models and presented an expression for mechanical advantage of compliant mechanism using the relationship between strain energy and external work, the work-energy principle for elastic members; however, did not implement it in their investigations. Other works related to mechanical advantage analysis rely on the Newtonian mechanics and finite element methods. Howell [36] utilized the principle of virtual-work in conjunction with the PRBM concept and provided a systematic approach for deriving the expressions for mechanical advantage of compliant mechanisms. The method required only the forces and moments at the points of interest, avoiding carryover of the intermediate variables that are required in the free-body diagram (FBD) approach.

Although, the virtual-work approach is efficient, when compared to the FBD approach, a new expression needs to be derived when the location, quantity and type of input/output ports are changed. In addition, the approach does not guide the designer in the synthesis and design of compliant mechanisms with higher mechanical advantage. Alternatively, Wang [90], Parkinson et al. [91], and Hetrick [92] provided formulations for design of compliant mechanisms for a specified mechanical advantage. These formulations are typically utilized in an optimization routine as objective functions or constraint functions. As an intermediate step finite element methods are utilized to analyze the candidate mechanisms mechanical advantage.

This section provides a stepwise approach for the evaluation of mechanical advantage of compliant mechanisms. The formulation presented by Salamon and Midha [27, 28] is utilized in conjunction with the PRBM concept. Pseudo-rigid-body four-bar mechanisms with one to four torsional springs located at the revolute joints, to represent mechanism compliance, are considered to demonstrate the approach. The approach not only simplifies the evaluation of mechanical advantage, but also allows an understanding of the contribution of the constituent elements of the compliant mechanism, that is the structural configuration and the compliance. An understanding of the latter facilitates in the development of a methodology for the design of compliant mechanisms with higher mechanical advantage.

7.2 MECHANICAL ADVANTAGE OF COMPLIANT MECHANISMS

The mechanical advantage (MA) of a mechanism is defined as the instantaneous ratio of output force to input force.

$$\mathrm{MA} = \frac{\mathrm{F_o}}{\mathrm{F_i}} \tag{189}$$

where, F denotes force and the subscript o and i refer to the output and input, respectively. When the magnitudes of these forces are available, MA can be readily evaluated. However; this is usually not the case. Typically, the displacement or velocity

response of a mechanism is readily available, and therefore, is usually used to evaluate the mechanical advantage.

In rigid-body mechanisms, if all the links are assumed to be rigid, and friction and inertia forces are ignored, then MA can be evaluated by considering the conservation of power between input and output ports, such that

$$\begin{aligned} P_i &= P_o \\ T_i\omega_i &= T_o\omega_o \\ F_i d_i \omega_i &= F_o d_o \omega_o \\ MA &= \frac{F_o}{F_i} = \frac{d_i}{d_o}\frac{\omega_i}{\omega_o} \end{aligned} \tag{190}$$

where, P denotes power, T denotes torque, ω denotes angular velocity, d denotes the location of input and output forces w.r.t. the instant centers, and subscripts o and i refer to the output and input ports, respectively. Equation (190) represents the mechanical advantage of a single-input port and single-output port rigid-body mechanism. The angular velocity ratio contained in equation (190) can be evaluated using instant centers.

Mechanical advantage of a compliant mechanism; however, cannot be evaluated by a direct implementation of equation (190). Compliant mechanisms transfer motion and force by the deformation of its flexible members, consequently storing strain energy between the input and output ports. Salamon and Midha [27, 28], therefore, suggest that a single-input and single-output port compliant mechanism should be considered as a single-input port and multiple-output port mechanism. One of the output ports is the actual physical output port and the others are internal ports that perform work by elastically deforming the mechanism members.

Midha et al. [93] provided a formulation for the evaluation of mechanical advantage of single-input port and multiple-output port mechanisms. The effort,

however, only considered the case wherein the forces at the output ports are functionally related and functionally unrelated to each other. In compliant mechanisms, the output port forces and related to both the input ports force and location of work piece. In order to capture this relationship; Salamon and Midha [27, 28] utilized the work-energy principle, given by equation (191), and derived the expression for evaluation of mechanical advantage of compliant mechanisms, equation (192).

$$\delta U = \delta W \tag{191}$$

where, δU represents the change in the internal energy, and δW the change in the work done on the system.

$$MA = MA_R \left(1 - \frac{F_c}{F_i}\right) \tag{192}$$

where, MA_R is the mechanical advantage of the rigid-body mechanism, F_c the compliant component of the input force called as the compliance force, and F_i the input force.

This section provides an approach to apply equation (192) using the pseudo-rigid-body model concept, and develops a methodology for evaluation of mechanical advantage of compliant mechanisms.

7.3 EXPRESSIONS FOR COMPLIANCE TORQUE AND COMPLIANCE FORCE

The compliance force and compliance torque can be readily determined using the principle of virtual work [36]. Equations (193) through (198) comprise a comprehensive set of expressions of compliance torque and compliance force for the PRBMs shown in Figure 7.1 and Figure 7.2.

For pseudo-rigid-body mechanism shown in Figure 7.1 the compliance torque expressions are given by equations (193) through (195), with input at the left side link, coupler link, and right side link, respectively.

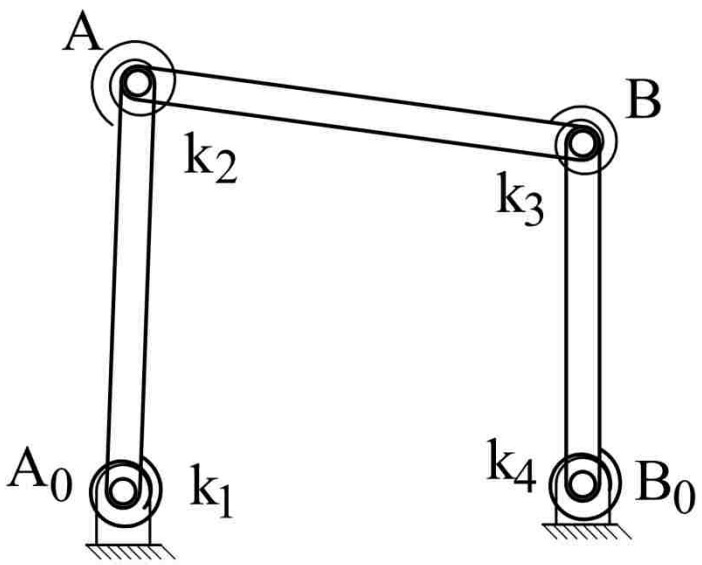

Figure 7.1 PRBM of a Pseudo-Rigid-Body Four-Bar Compliant Mechanism

$$T_c = k_1(\Theta_{2j} - \Theta_{20}) + k_2[(\Theta_{3j} - \Theta_{30}) - (\Theta_{2j} - \Theta_{20})](h_{3j} - 1) + k_3[(\Theta_{4j} - \Theta_{40}) - (\Theta_{3j} - \Theta_{30})](h_{4j} - h_{3j}) + k_4(\Theta_{4j} - \Theta_{40})h_{4j} \quad (193)$$

where, $h_{3j} = \frac{R_2 \sin(\Theta_{4j} - \Theta_{2j})}{R_3 \sin(\Theta_{3j} - \Theta_{4j})}$; and $h_{4j} = \frac{R_2 \sin(\Theta_{3j} - \Theta_{2j})}{R_4 \sin(\Theta_{3j} - \Theta_{4j})}$

$$T_c = k_1(\Theta_{2j} - \Theta_{20})h_{2j} + k_2[(\Theta_{3j} - \Theta_{30}) - (\Theta_{2j} - \Theta_{20})](1 - h_{2j}) + k_3[(\Theta_{4j} - \Theta_{40}) - (\Theta_{3j} - \Theta_{30})](h_{4j} - 1) + k_4(\Theta_{4j} - \Theta_{40})h_{4j} \quad (194)$$

where, $h_{2j} = \frac{R_3 \sin(\Theta_{3j} - \Theta_{4j})}{R_2 \sin(\Theta_{4j} - \Theta_{2j})}$; and $h_{4j} = \frac{R_3 \sin(\Theta_{3j} - \Theta_{2j})}{R_4 \sin(\Theta_{4j} - \Theta_{2j})}$

$$T_c = k_1(\Theta_{2j} - \Theta_{20})h_{2j} + k_2[(\Theta_{3j} - \Theta_{30}) - (\Theta_{2j} - \Theta_{20})](h_{3j} - 1) + k_3[(\Theta_{4j} - \Theta_{40}) - (\Theta_{3j} - \Theta_{30})](h_{4j} - h_{3j}) + k_4(\Theta_{4j} - \Theta_{40})h_{4j} \quad (195)$$

where, $h_{2j} = \frac{R_4 \sin(\Theta_{3j} - \Theta_{4j})}{R_2 \sin(\Theta_{3j} - \Theta_{2j})}$; and $h_{3j} = \frac{R_4 \sin(\Theta_{4j} - \Theta_{2j})}{R_3 \sin(\Theta_{3j} - \Theta_{2j})}$

Equations (196) through (198) provide the expressions for compliance torque and compliance force for the pseudo-rigid-body mechanism shown in Figure 7.2, with the input at the left side link, coupler link and slider, respectively.

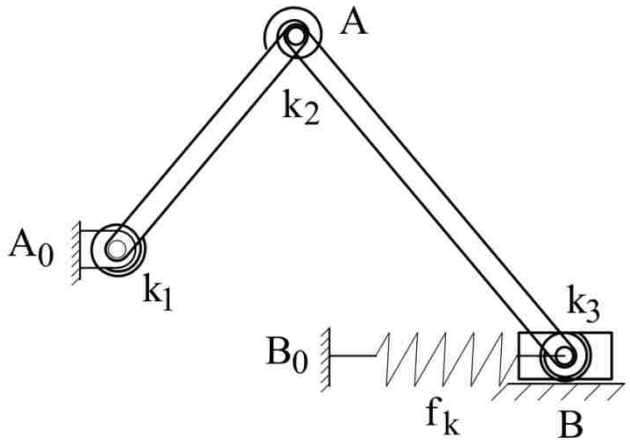

Figure 7.2 PRBM of a Pseudo-Rigid-Body Compliant Slider Mechanism

$$T_c = k_1(\Theta_{2j} - \Theta_{20}) + k_2[(\Theta_{3j} - \Theta_{30}) - (\Theta_{2j} - \Theta_{20})](g_{3j} - 1) + k_3(\Theta_{3j} - \Theta_{30})g_{3j} + f_k(R_{1j} - R_{10})R_2 \cos(\Theta_{2j})[\tan(\Theta_{3j}) - \tan(\Theta_{2j})] \quad (196)$$

where, $g_{3j} = \frac{-R_2 \cos(\Theta_{2j})}{R_3 \cos(\Theta_{3j})}$

$$T_c = k_1(\Theta_{2j} - \Theta_{20})g_{2j} + k_2[(\Theta_{3j} - \Theta_{30}) - (\Theta_{2j} - \Theta_{20})](1 - g_{2j}) + k_3(\Theta_{3j} - \Theta_{30}) + f_k(R_{1j} - R_{10})R_3\cos(\Theta_{3j})[\tan(\Theta_{2j}) - \tan(\Theta_{3j})] \quad (197)$$

where, $g_{2j} = \frac{-R_3\cos(\Theta_{3j})}{R_2\cos(\Theta_{2j})}$

$$F_c = k_1(\Theta_{2j} - \Theta_{20})g_{2j} + k_2[(\Theta_{3j} - \Theta_{30}) - (\Theta_{2j} - \Theta_{20})](g_{3j} - g_{2j}) + k_3(\Theta_{3j} - \Theta_{30})g_{3j} + f_k(R_{1j} - R_{10}) \quad (198)$$

where, $g_{2j} = \frac{-\cos(\Theta_{3j})}{R_2\sin(\Theta_{2j} - \Theta_{3j})}$; $g_{3j} = \frac{\cos(\Theta_{2j})}{R_3\sin(\Theta_{2j} - \Theta_{3j})}$

7.4 MECHANICAL ADVANTAGE EVALUATION OF COMPLIANT MECHANISMS USING THE PRBM CONCEPT

Mechanical advantage evaluation of a compliant mechanism using the PRBM concept is a two-stage process. First, the rigid-body mechanical advantage is evaluated by neglecting compliance in the PRBM and considering the notion of power conservation and angular velocity ratio using instant centers. Later, the effect of compliance is superimposed to evaluate mechanical advantage of the compliant mechanism. The approach helps in not only simplifying the mechanical advantage evaluation, but also is physically intuitive in nature. The latter hitherto lacking with the state-of-the-art. The formulation allows for a controlled study of the critical elements of a compliant mechanism: i) structural configuration and ii) energy storage or torque/force deflection characteristics, called as compliance. Steps of this process of evaluation are shown below:

Step 1: Construct a PRBM of the compliant mechanism.

Step 2: Neglect the compliance in the PRBM and derive the expression for rigid-body mechanical advantage. Consider the notion of power conservation, between input and output ports, and angular velocity ratio using instant centers.

Step 3: For the PRBM constructed in Step 1 determine the equation for compliance torque/force using equations (193) through (198).

Step 4: Calculate the mechanical advantage of rigid-body mechanism and the compliance torque at various locations of input and output ports, using the expressions derived in Step 2 and Step 3.

Step 5: Use equation (192) in conjunction with the results obtained in Step 4 to evaluate the mechanical advantage of a compliant mechanism.

This stepwise process of evaluation of mechanical advantage can be used to evaluate all three types of mechanical advantage of a compliant mechanism.

7.5 EXAMPLES

Initially, two examples are presented that illustrate the application of the process of evaluation of mechanical advantage. The results are compared with the mechanical advantage obtained using FBD approach, and the finite element analysis software ANSYS®. Following these initial examples, three mechanical devices are analyzed for their mechanical advantage performance.

Example 1: Evaluate the mechanical advantage of the partially-compliant slider mechanism shown in Figure 7.3.

Figure 7.3 PRBM of a Partially-Compliant Slider Mechanism

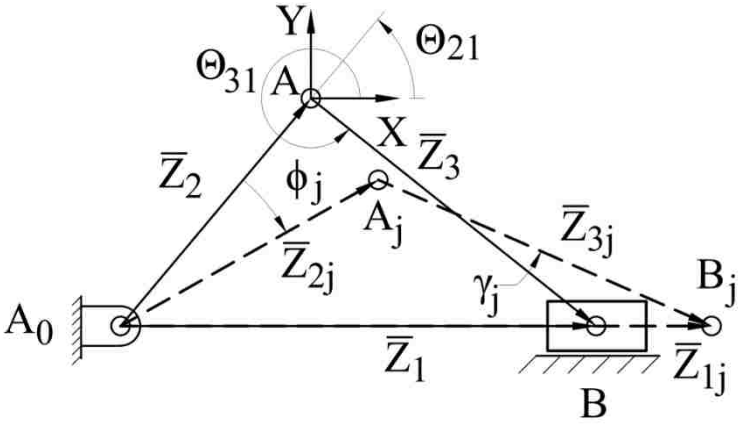

Figure 7.4 A Vector Schematic of the Mechanism Shown in Figure 7.3, in both its $1^{st}$and j^{th} Precision Position

The mechanism is designed for two-precision position path generation with prescribed timing, with input torque specified at the precision positions. Input torque is applied on link 2. The design specifications are:

$\Theta_1 = 0$ deg.; offset $= 0$ in.; $\delta_2 = 1.5 + 0\text{i}$; $\phi_2 = -30$ deg.

$T_1 = 0$; $T_2 = 12.75$ in.$-$lb.; and $T_{\delta=0.9+0\text{i}} = 6.5$ in.$-$lb.

Using the design approach presented in section 6 with two small-length flexural pivots, and considering $R_2 = 2.5$ in. and $\Theta_{31} = 320$ deg. as free-choices, we have:

$\bar{Z}_{11} = 3.779 + 0\text{i}$ $\quad$ $\bar{Z}_2 = 1.1083 + 2.2409\text{i}$

$\bar{Z}_3 = 2.6704 - 2.2408\text{i}$ $\quad$ $\gamma_2 = 16.565$ deg.

$k_2 = 8.4515$ (in.$-$lb.)/rad $\quad$ $k_3 = 7.5193$ (in.$-$lb.)/rad

Evaluating type 1 mechanical advantage of the mechanism shown in Figure 7.3.

Step 1: Figure 7.3 shows the PRBM of the partially-compliant slider mechanism.

Step 2: Neglecting the compliance in the PRBM, the rigid-body mechanism is considered. Applying the notion of power conservation and angular velocity ratio using instant centers mechanical advantage of the rigid-body mechanism shown in Figure 7.5 is derived as:

Figure 7.5 Rigid-Body Mechanism of the Partially-Compliant Mechanism Shown in Figure 7.3, with its Instant Centers Plotted on It

$$
\begin{aligned}
&P_i = P_o \\
&T_i\omega_i = F_o v_o \\
&F_i d_i \omega_i = F_o v_o \\
&MA_R = \frac{F_o}{F_i} = \frac{d_i\omega_i}{v_o} = \frac{d_i}{I_{12}I_{24}}
\end{aligned}
\tag{199}
$$

Step 3: Using equation (195), the expression for compliance torque is derived, shown in equation (200).

$$
\begin{aligned}
&T_c = k_2\left[\left(\Theta_{3j} - \Theta_{30}\right) - \left(\Theta_{2j} - \Theta_{20}\right)\right]\left(g_{3j} - 1\right) + k_3\left(\Theta_{3j} - \Theta_{30}\right)g_{3j} \\
&\text{where, } g_{3j} = \frac{-R_2\cos(\Theta_{2j})}{R_3\cos(\Theta_{3j})}
\end{aligned}
\tag{200}
$$

Step 4: Using equations (199) and (200) the rigid-body mechanical advantage, and the compliance torque is calculated, respectively, for various work piece locations, shown plotted in Figure 7.6.

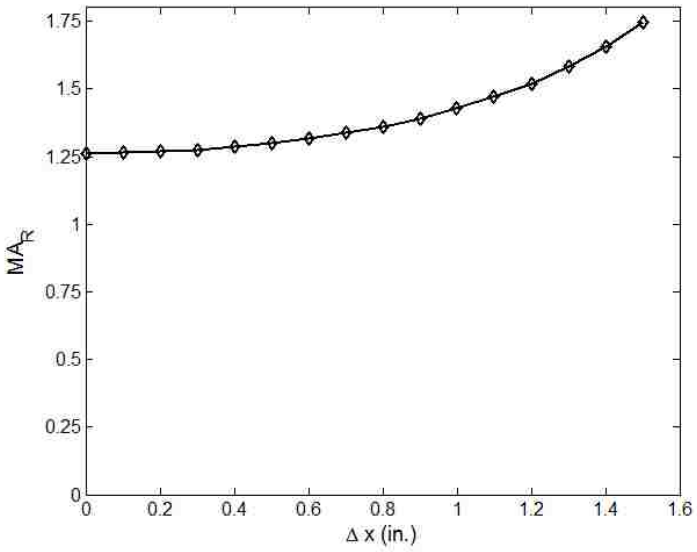

Figure 7.6 Rigid-Body Mechanical Advantage vs. Work Piece Location

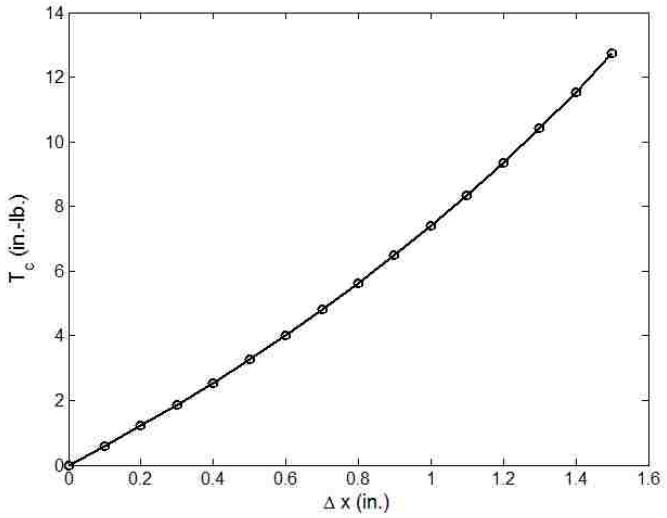

Figure 7.7 Compliance Torque vs. Work Piece Location

Step 5: Using equation (192) in conjunction with the results obtained in Step 4 the type 1 mechanical advantage of the partially-compliant mechanism shown in Figure 7.3 is evaluated, shown plotted in Figure 7.8, using $F_i = 10$ lb. and $d_i = 4$ in. Using the procedure provided by Salamon and Midha [27, 28] the mechanical advantage is also evaluated using ANSYS®, shown plotted in Figure 7.8. For the finite element analysis the modulus of elasticity of 450,000 psi is considered. Salamon [28] derived the mechanical advantage expression for a fully-compliant slider mechanism, shown in equation (201). The mechanical advantage evaluated using equation (201) is also shown plotted in Figure 7.8.

$$MA = \frac{1 - \frac{1}{T_i}\left\{T_1 + T_2 + \frac{R_2\cos(\Theta_2)}{R_3\cos(\Theta_3)}(T_2 + T_3)\right\}}{d_i R_2(\sin(\Theta_2) - \tan(\Theta_3)\cos(\Theta_2))} \tag{201}$$

where,

$T_1 = k_1(\Theta_{20} - \Theta_2)$;

$T_2 = k_2[(\Theta_3 - \Theta_{30}) + (\Theta_{20} - \Theta_2)]$;

$T_3 = k_3(\Theta_3 - \Theta_{30})$;

Figure 7.9 shows the mechanical advantage of the rigid-body mechanism and the compliant mechanism. Figure 7.8 shows that the mechanical advantage evaluated using the PRBM approach is in excellent agreement with that of the one evaluated using FBD approach.

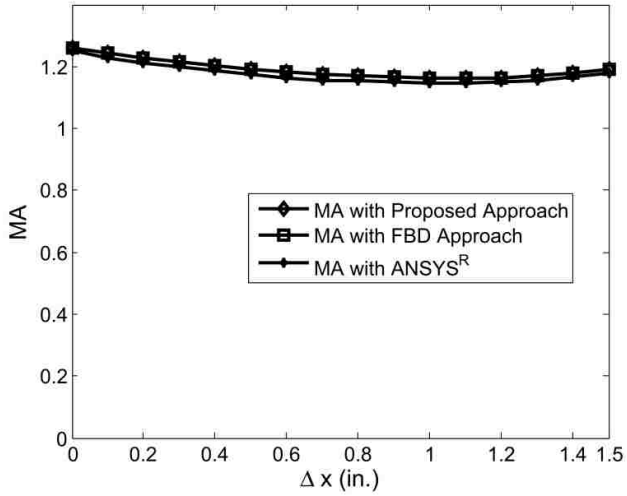

Figure 7.8 Mechanical Advantage for the Compliant Mechanism Shown in Figure 7.3 vs. Work Piece Location

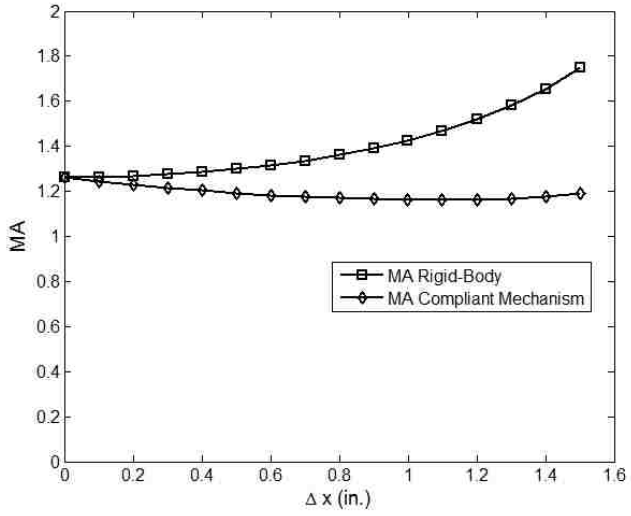

Figure 7.9 MA and MA_R vs. Work Piece Location

Example 2: Evaluate the mechanical advantage of the fully-compliant mechanism shown in Figure 7.10.

Figure 7.10 PRBM of a Fully-Compliant Mechanism

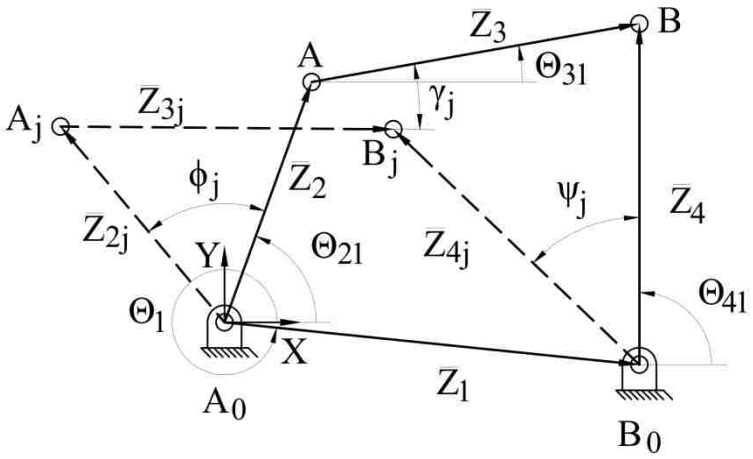

Figure 7.11 Vector Schematic of the Compliant Mechanism Shown in Figure 7.10 in its 1^{st} and j^{th} Precision Position

The mechanism is designed for three-precision position path generation with input torque specified at the precision positions. Input torque is applied on link 2. The design specifications are:

$\delta_2 = -3 + 0.5\text{i};\ \ \delta_3 = -5 + 0.25\text{i};$

$T_1 = 9\ \text{in.}-\text{lb.};\ T_2 = 13.75\ \text{in.}-\text{lb.};\ \text{and}\ T_3 = 17.5\ \text{in.}-\text{lb.}$

Using the design approach presented in section 6 with four small-length flexural pivots, and considering $R_2 = 5.5$ in., $\Theta_{21} = 65$ deg., $R_4 = 7$ in. and $\Theta_{41} = 35$ deg. as free-choices, we have:

$\bar{Z}_1 = 2.8759 + 3.0196\text{i}$ $\quad$ $\bar{Z}_2 = 2.3244 + 4.9847\text{i}$

$\bar{Z}_3 = 6.2946 + 2.0370\text{i}$ $\quad$ $\bar{Z}_4 = 5.7432 + 4.0020\text{i}$

$\bar{Z}_5 = 6.3122 + 4.6667\text{i}$ $\quad$ $\bar{Z}_6 = 0.1169 + 2.63\text{i}$

$\gamma_2 = 18.02\ \text{deg.};$ $\quad$ $\gamma_3 = 27.31\ \text{deg.}$

$\psi_2 = 30.12\ \text{deg.}$ $\quad$ $\psi_3 = 52.19\ \text{deg.}$

$k_1 = 1.1204\ (\text{in.}-\text{lb.})/\text{rad}$ $\quad$ $k_2 = 1.1204\ (\text{in.}-\text{lb.})/\text{rad}$

$k_3 = 9.7441\ (\text{in.}-\text{lb.})/\text{rad}$ $\quad$ $k_4 = 9.7441\ (\text{in.}-\text{lb.})/\text{rad}$

The problem definition suggests that the energy-free state of the mechanism is not at the first-precision-position. Considering $\Theta_{20} = 55$ deg., we have $\Theta_{30} = -2.16$ deg. and $\Theta_{40} = 10.17$ deg.

Evaluating type 1 mechanical advantage of the mechanism shown in Figure 7.10.

Step 1: Figure 7.10 shows the PRBM of the fully-compliant slider mechanism.

Step 2: Neglecting the compliance in the PRBM, the rigid-body mechanism is considered. Applying the notion of power conservation and angular velocity ratio using instant centers mechanical advantage of the rigid-body mechanism shown in Figure 7.12 is derived as:

$$
\begin{aligned}
&P_i = P_o \\
&T_i\omega_i = T_o\omega_o \\
&F_i d_i \omega_i = F_o d_o \omega_o \\
&MA_R = \frac{F_o}{F_i} = \frac{d_i\omega_i}{d_i\omega_o} = \frac{d_i}{d_o}\frac{I_{14}I_{24}}{I_{12}I_{24}}
\end{aligned}
\tag{202}
$$

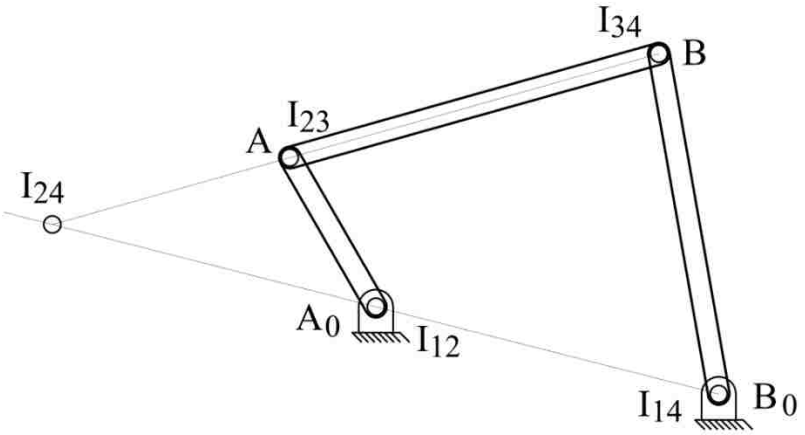

Figure 7.12 Rigid-Body Mechanism of the Fully-Compliant Mechanism Shown in Figure 7.10, with its Instant Centers Shown Plotted on it

Step 3: Using equation (8), the expression for compliance torque is given as:

$$
\begin{aligned}
T_c = {} & k_1(\Theta_{2j} - \Theta_{20}) + k_2\left[(\Theta_{3j} - \Theta_{30}) - (\Theta_{2j} - \Theta_{20})\right](h_{3j} - 1) \\
& + k_3\left[(\Theta_{4j} - \Theta_{40}) - (\Theta_{3j} - \Theta_{30})\right](h_{4j} - h_{3j}) \\
& + k_4(\Theta_{4j} - \Theta_{40})h_{4j}
\end{aligned}
\tag{203}
$$

where, $h_{3j} = \frac{R_2 \sin(\Theta_{4j} - \Theta_{2j})}{R_3 \sin(\Theta_{3j} - \Theta_{4j})}$; and $h_{4j} = \frac{R_2 \sin(\Theta_{3j} - \Theta_{2j})}{R_4 \sin(\Theta_{3j} - \Theta_{4j})}$

Step 4: Using equations (202) and (203) the rigid-body mechanical advantage, and the compliance torque is calculated, respectively, for various work piece locations, shown plotted in Figure 7.13.

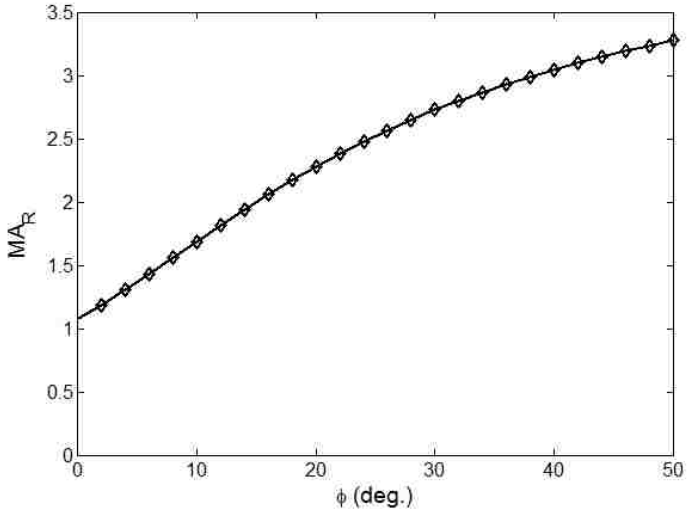

Figure 7.13 Rigid-Body Mechanical Advantage vs. Work Piece Location

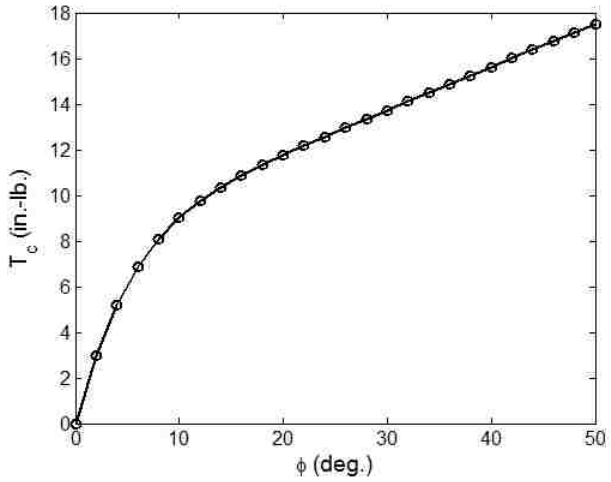

Figure 7.14 Compliance Torque vs. Work Piece Location

Step 5: Using equation (192) in conjunction with the results obtained in Step 4 the mechanical advantage of the fully-compliant mechanism shown in Figure 7.10 is evaluated, shown plotted in Figure 7.15, using $F_i = 10$ lb., $d_i = 5$ in., and $d_o = 1.5$ in. Using the procedure provided by Salamon and Midha [27, 28] the mechanical advantage is also evaluated using ANSYS®, shown plotted in Figure 7.15. For the finite element analysis the modulus of elasticity of 450,000 psi is considered. Using the principle of virtual-work along with the PRBM concept, the expression of mechanical advantage of the mechanism shown in Figure 7.10 is derived, shown in equation (204). The mechanical advantage evaluated using equation (204) is also shown plotted in Figure 7.15.

$$MA = \frac{d_i}{d_o}\{T_i h_2 - T_1 h_2 - T_2(h_3 - h_2) - T_3(1 - h_3) - T_4\}$$

where,

$$\begin{aligned} T_1 &= k_1(\Theta_2 - \Theta_{20}); \\ T_2 &= k_2[(\Theta_3 - \Theta_{30}) - (\Theta_2 - \Theta_{20})]; \\ T_3 &= k_3[\Theta_4 - \Theta_{40} - (\Theta_3 - \Theta_{30})]; \\ T_4 &= k_4(\Theta_4 - \Theta_{40}); \\ h_2 &= \frac{R_4 \sin(\Theta_3 - \Theta_4)}{R_2 \sin(\Theta_3 - \Theta_2)}; \text{ and } h_3 = \frac{R_4 \sin(\Theta_4 - \Theta_2)}{R_3 \sin(\Theta_3 - \Theta_2)} \end{aligned} \quad (204)$$

Figure 7.16 shows the mechanical advantage of the rigid-body mechanism and the compliant mechanism. Figure 7.15 shows that the mechanical advantage evaluated using the PRBM approach is in excellent agreement with that of the one evaluated using principle of virtual-work.

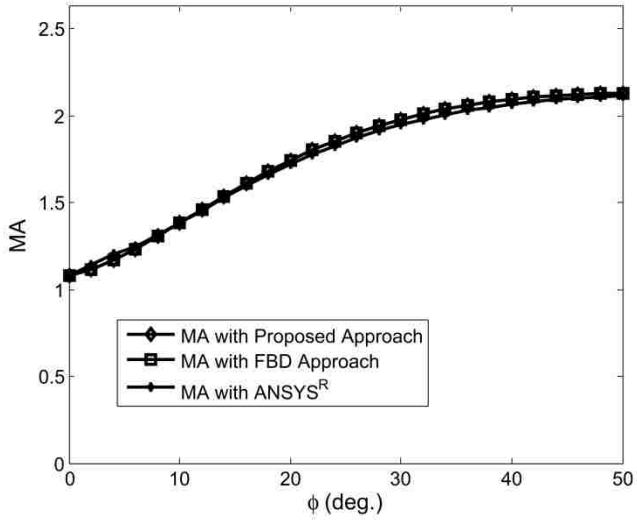

Figure 7.15 Mechanical Advantage of a Compliant Mechanism Shown in Figure 7.10 vs. Work Piece Location

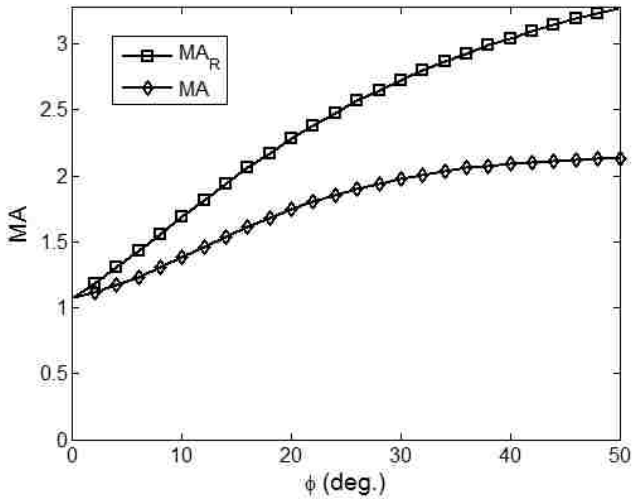

Figure 7.16 MA and MA_R vs. Work Piece Location

Considering the excellent agreement of the mechanical advantage evaluations between PRBM method and FBD/FEA methods, following examples investigate the

mechanical advantage characteristics using the PRBM method. Three hand-tools are considered for the evaluation of the Type 1 and Type 2 mechanical advantage.

Example 3: Figure 7.17 shows a CAD rendering of a popular fish-hook remover, Compliers®. Let us evaluate the mechanical advantage of this mechanical device. Considering the application of Compliers®, a fish-hook remover, only Type 2 mechanical advantage is evaluated.

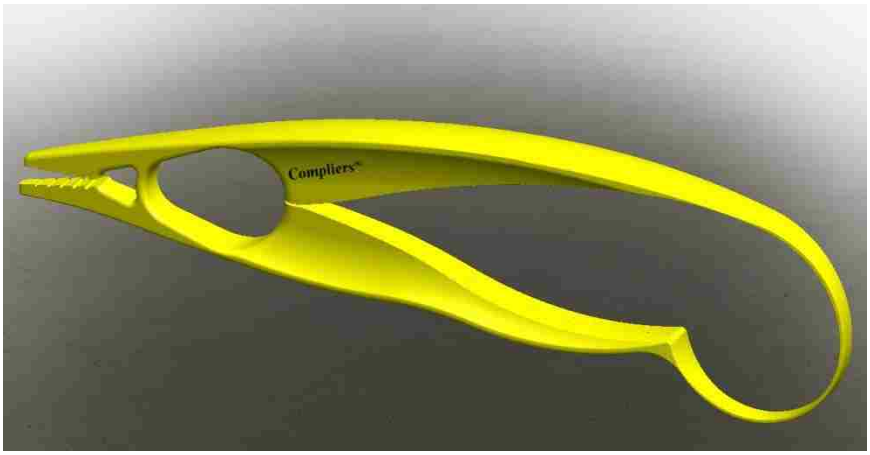

Figure 7.17 CAD Rendering of Compliers®

Compliers® can be modeled as a pseudo-rigid-body four-bar mechanism with three small-length flexural pivots and one rigid-body pin joint at the rolling contact. Compliers® exhibits a single-input port, and two-output ports, as shown in Figure 7.18. Let us fix link 1 that is the lower handle and evaluate the rigid-body mechanical advantage, shown in equation (205).

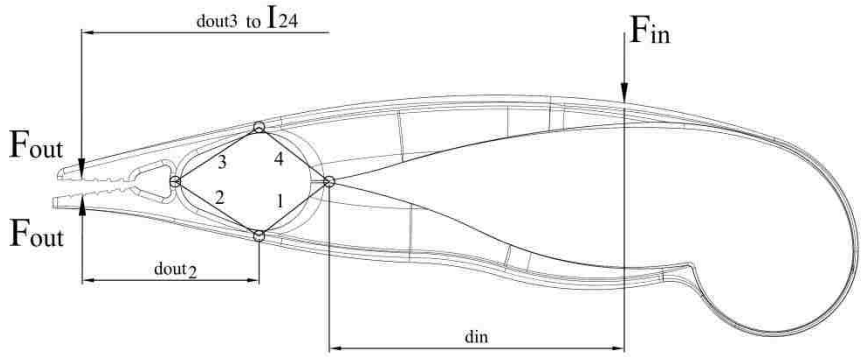

Figure 7.18 Rigid-Body Mechanism for Evaluating Mechanical Advantage of Compliers®

$$MA_R = \frac{F_o}{F_i} = \frac{d_i}{\frac{I_{14}I_{24}}{I_{12}I_{24}} d_{out2} + \frac{I_{14}I_{34}}{I_{13}I_{34}} d_{out3}} \tag{205}$$

Measurements taken from Compliers®, constructed with polypropylene of modulus of elasticity 200,000 psi provide the following properties for the PRBM:

$$\bar{Z}_1 = 0.7745 + 0.6004i \qquad \bar{Z}_2 = -0.9254 + 0.6004i$$
$$\bar{Z}_3 = 0.9254 + 0.6004i \qquad \bar{Z}_4 = -0.7745 + 0.6004i$$
$$k_1 = 143.55\ (\text{in.}-\text{lb.})/\text{rad} \qquad k_2 = 91.9385\ (\text{in.}-\text{lb.})/\text{rad}$$
$$k_3 = 143.55\ (\text{in.}-\text{lb.})/\text{rad} \qquad d_{in} = 3.25\ \text{in.};\ d_{out2} = 1.9513\ \text{in.}$$

Using the stepwise process of evaluation, the Type 2 mechanical advantage of Compliers® is determined, shown plotted in Figure 7.19.

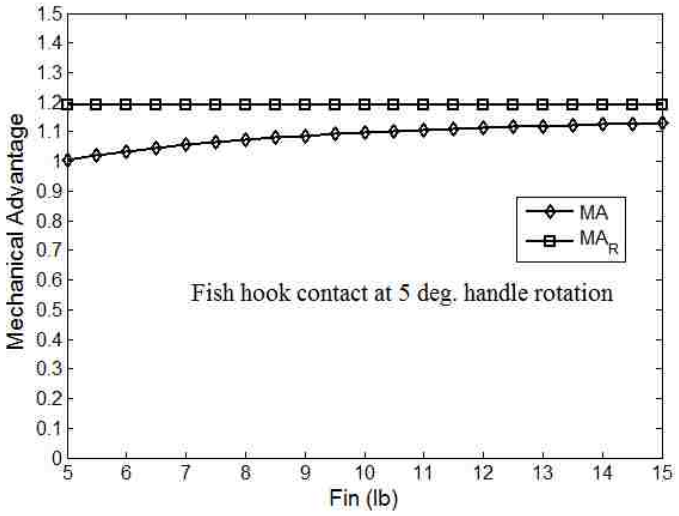

Figure 7.19 Type 2 Mechanical Advantage of Compliers®

Example 4: Figure 7.20 and Figure 7.21 shows CAD renderings of two alternative versions of fully-compliant crimping mechanisms designed by AMP, Inc. during the early 1980's. A third version of the fully-compliant mechanism constructed by AMP, Inc. is also investigated, which is schematically similar to the model shown in Figure 7.23 with a reduced thickness for its compliant segments. Let us investigate the mechanical advantage characteristics of these three fully-compliant crimping mechanisms.

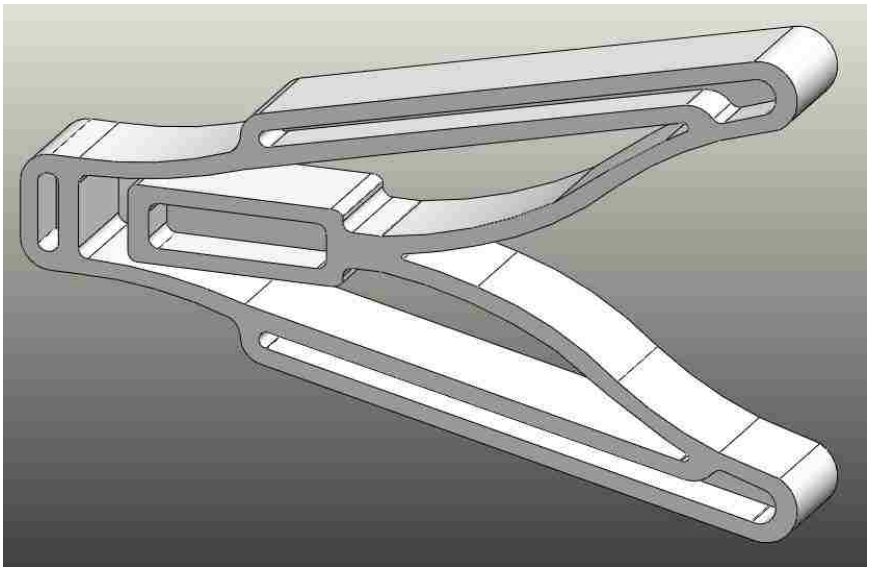

Figure 7.20 CAD Rendering of the Fully-Compliant Crimping Mechanism Designed by AMP, Inc.

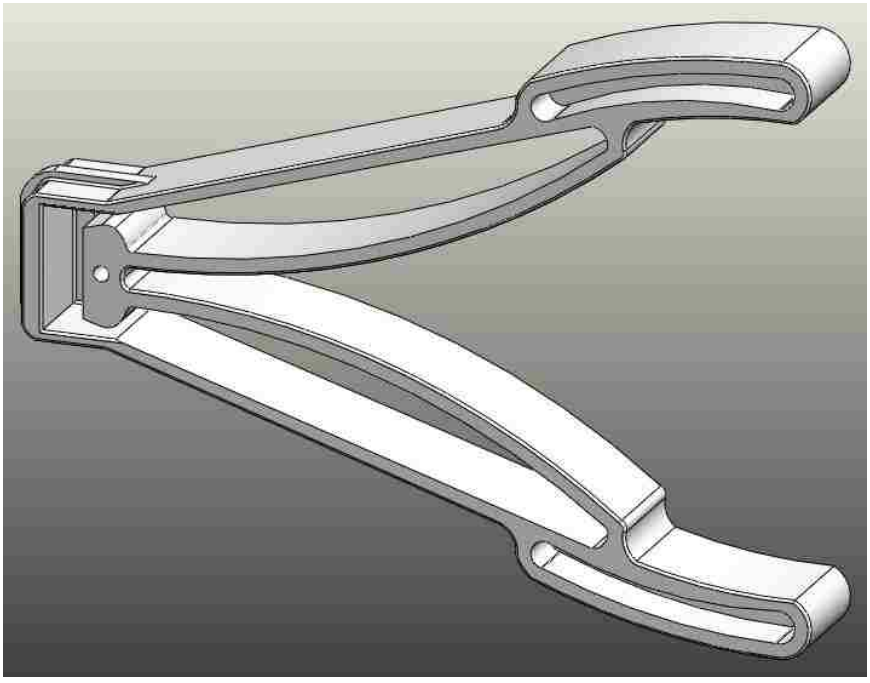

Figure 7.21 CAD Rendering of the Fully-Compliant Crimping Mechanism Designed by AMP, Inc.

Observations made during the testing of the crimping mechanisms allow it to be modelled as slider mechanisms, shown in Figure 7.22 and Figure 7.23. Because of the symmetry in its construction only one half of the model needs to be evaluated. Considering the notion of power conservation and angular velocity ratios using instant center, the mechanical advantage of the rigid-body mechanism is derived, equation (206).

$$MA_R = \frac{F_o}{F_i} = \frac{d_i \omega_i}{v_o} = \frac{d_i}{I_{12} I_{24}} \tag{206}$$

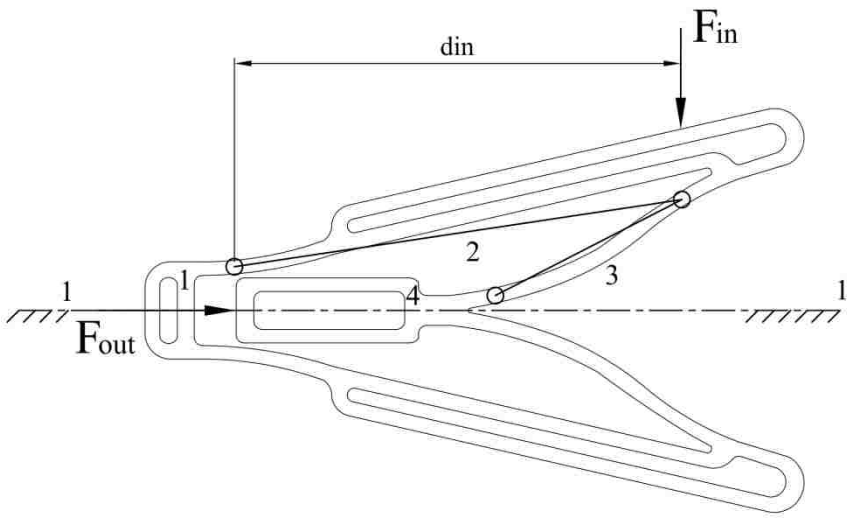

Figure 7.22 Rigid-Body Mechanism for Evaluating the Mechanical Advantage of the Crimping Mechanism Shown in Figure 7.20

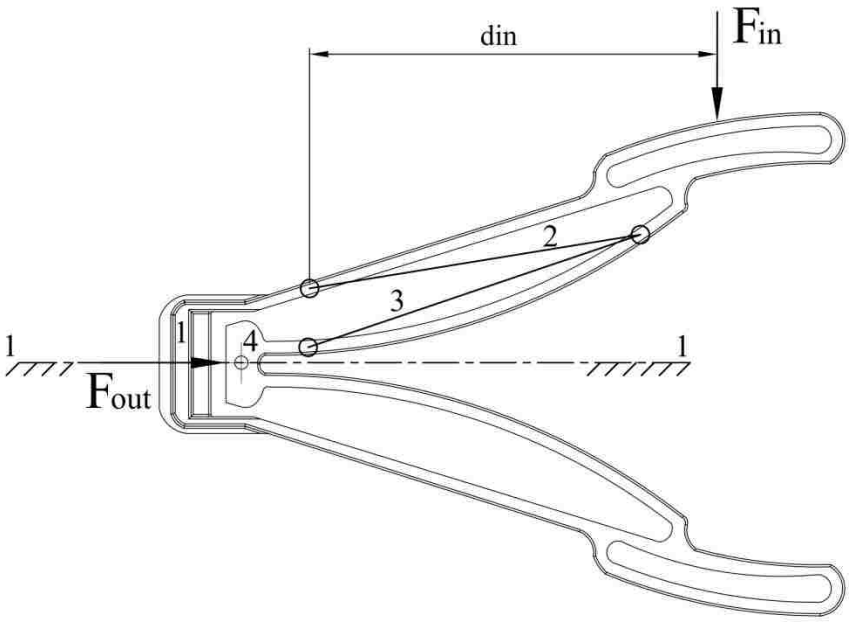

Figure 7.23 Rigid-Body Mechanism for Evaluating the Mechanical Advantage of the Crimping Mechanism Shown in Figure 7.21

Measurements obtained from the prototypes, constructed with Delrin® of modulus of elasticity 450,000 psi provide the following properties for the PRBMs:

Properties for the mechanism shown in Figure 7.22:

$\bar{Z}_{11} = 2.0585 + 0i$ $\bar{Z}_2 = 3.7043 + 0.8443i$

$\bar{Z}_3 = -1.6457 - 0.9924i$ $\bar{Z}_4 = 0 - 0.1481i$

$d_{in} = 3.85$ in. $k_1 = 75.0487$ (in.$-$lb.)/rad

$k_2 = 78.0735$ (in.$-$lb.)/rad $k_3 = 78.0735$ (in.$-$lb.)/rad

Properties for the mechanism shown in Figure 7.23:

$\bar{Z}_{11} = -0.1655 + 0i$ $\bar{Z}_2 = 2.0742 + 0.6571i$

$\bar{Z}_3 = -2.2397 - 1.0289i$ $\bar{Z}_4 = 0 - 3718i$

$d_{in} = 3$ in. $k_1 = 31.6082$ (in.$-$lb.)/rad

$k_2 = 49.2582$ (in.$-$lb.)/rad $k_3 = 49.2582$ (in.$-$lb.)/rad

A third fully-compliant crimping mechanism is also investigated. This version of the crimping mechanism has the same schematic as shown in Figure 7.21, however is

constructed with reduced thickness of compliant segments. The properties of this mechanism are determined to be:

$$\bar{Z}_{11} = -0.1655 + 0i \qquad \bar{Z}_2 = 2.0742 + 0.6571i$$

$$\bar{Z}_3 = -2.2397 - 1.0289i \qquad \bar{Z}_4 = 0 - 3718i$$

$$d_{in} = 3 \text{ in.} \qquad k_1 = 17.1246 \frac{\text{in.} - \text{lb.}}{\text{rad}}$$

$$k_2 = 26.2869 \text{ (in.} - \text{lb.)/rad} \qquad k_3 = 26.2869 \text{ (in.} - \text{lb.)/rad}$$

Using the stepwise process of evaluation, the mechanical advantage of the AMP crimpers is determined, shown plotted in Figure 7.24 through Figure 7.26.

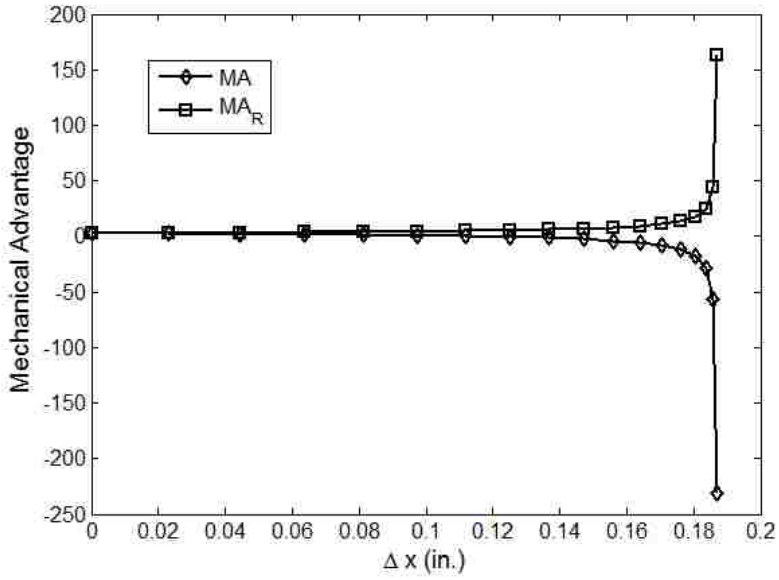

Figure 7.24 Type 1 Mechanical Advantage and MA_R of the Crimping Mechanism Shown in Figure 7.20

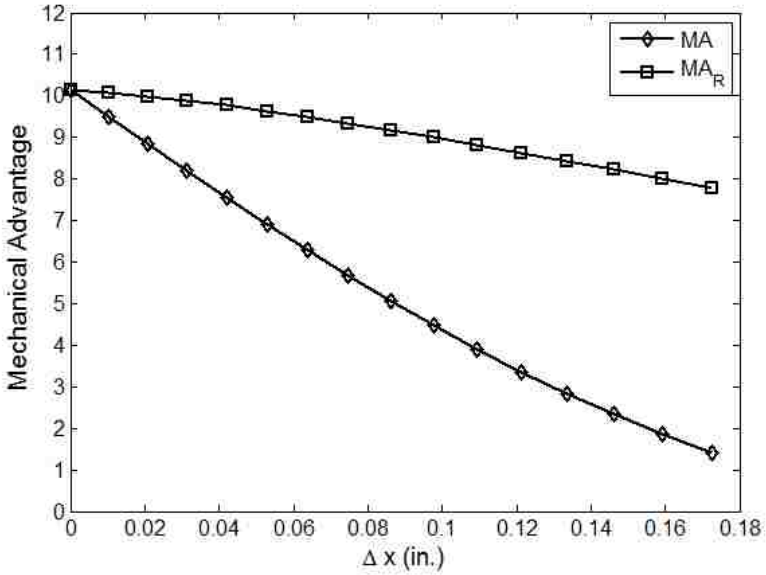

Figure 7.25 Type 1 Mechanical Advantage and MA_R of the Crimping Mechanism Shown in Figure 7.21

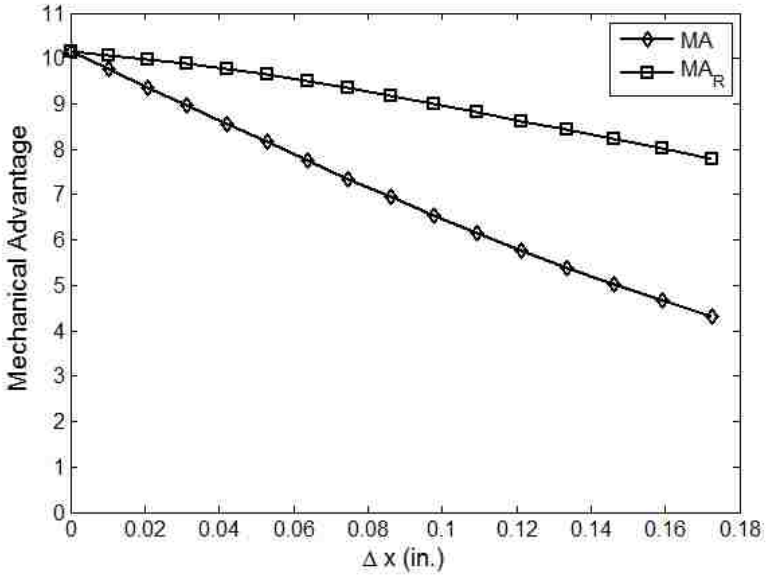

Figure 7.26 Type 1 Mechanical Advantage and MA_R of the Crimping Mechanism Shown in Figure 7.21, with a Reduced Thickness for Compliant Segments

7.6 DESIGNING COMPLIANT MECHANISMS WITH HIGHER MECHANICAL ADVANTAGE

The presented process of evaluation of mechanical advantage readily allows in the synthesis and design of compliant mechanisms with higher mechanical advantage. The PRBM method of analysis identifies two important areas for improving the mechanical advantage: i) the structural configuration and ii) energy storage characteristics in compliant members. While, the material properties and manufacturing processes do constrain the optimization of the latter; an improved structural configuration may readily allow for the design of improved compliance properties, as well. Though not very obvious, the effect of compliance may be detrimental, and should not be neglected. As demonstrated in the examples, the structural configuration and compliance have a coupled effect on the mechanical advantage characteristics of a compliant mechanism. Utilizing these findings an iterative design procedure is presented below that can assist in the design of compliant mechanisms with higher mechanical advantage.

Step 1: For a given compliant mechanism evaluate the mechanical advantage using the PRBM method.

Step 2: Using the rigid-body mechanism mechanical advantage expression, improve the rigid-body mechanical advantage. This may require redesign of the rigid-body mechanism, resulting in an optimized structural configuration.

Step 3: Using the torque/energy-deflection characteristics of compliant mechanism considered in Step 1, improve the compliance content.

Step 4: Evaluate the mechanical advantage of the compliant mechanism designed in Step 4.

Step 5: (optional) Redo steps 1 through 4 until the desired objectives are satisfied.

Following examples illustrate the application of the iterative design process.

7.7 EXAMPLES

Example 5: Improve the mechanical advantage properties of the compliant mechanism considered in Example 1, shown in Figure 7.3. Let us assume that the torque-deflection characteristics cannot be modified significantly, and design a partially-compliant slider mechanism with higher mechanical advantage.

Step 1: Figure 7.9 shows the mechanical advantage characteristics of the partially-compliant mechanism shown in Figure 7.3.

Step 2: Equation (199) suggests that the rigid-body mechanical advantage can be improved by: i) increasing d_i and ii) decreasing the distance between instant centers $I_{12}$and I_{24}. Considering that d_i can be increased only up to a certain extent, a new mechanism is synthesized, which has reduced distance between the instant centers. The properties of the new rigid-body mechanism are mentioned below:

$\bar{Z}_{11} = 7.97 + 0i$ $\quad$ $\bar{Z}_2 = 2.2854 + 2.6508i$

$\bar{Z}_3 = 5.6844 - 2.6507i$ $\quad$ $\phi_2 = -30$ deg.

$\gamma_2 = 14.408$ deg. $\quad$ offset $= 0$ in.

$\Delta x = 1.5$ in. $\quad$ $d_i = 4$ in.

Step 3: Let us maintain similar torque deflection characteristics Figure 7.27 shows the torque-deflection characteristics of the mechanism considered in Example 1 and the one designed in Step 2. The spring constants of the torsional springs of the new mechanism are:

$k_2 = 8.8117$ (in.$-$lb.)/rad $\quad$ $k_3 = 16.7631$ (in.$-$lb.)/rad

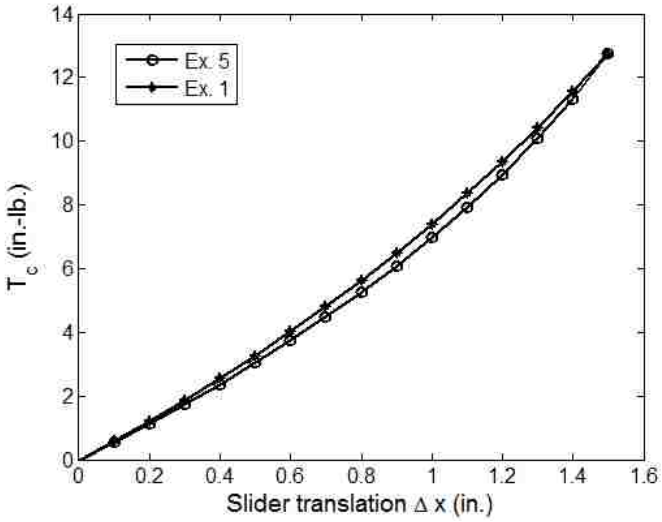

Figure 7.27 Torque-Deflection Characteristics for Example 1 and Example 5

Step 4: Figure 7.28 shows the mechanical advantage of the mechanism designed in Example 5. The mechanical advantage of Example 1 is also shown plotted on it.

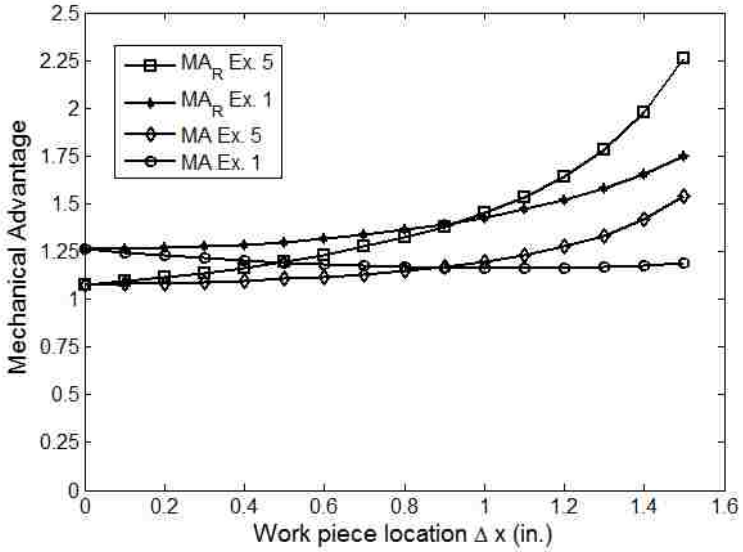

Figure 7.28 MA and MA_R for the Compliant Mechanism Designed in Example 1 and Example 5

Example 6: Improve the mechanical advantage properties of the compliant mechanism considered in Example 2, shown in Figure 7.10. Let us assume that the rigid-body mechanism cannot be modified, and design a fully-compliant mechanism with higher mechanical advantage.

Step 1: Figure 7.16 shows the mechanical advantage characteristics of the fully-compliant mechanism shown in Figure 7.10.

Step 2: Using the same rigid-body mechanism designed for Example 2.

Step 3: The torque-deflection characteristics of the mechanism considered in Example 2 exhibits a soft-spring behavior. Let us design a compliant mechanism that exhibits a hard-spring behavior, with the following specifications.
$T_1 = 5.5 \text{ in.} - \text{lb.}$; $T_2 = 9.75 \text{ in.} - \text{lb.}$; and $T_3 = 17.5 \text{ in.} - \text{lb.}$

The spring constants of torsional springs obtained using the procedure presented in section 6 are shown below:

$$k_1 = 16.6431 \text{ (in.} - \text{lb.)/rad} \quad k_2 = 16.6431 \text{ (in.} - \text{lb.)/rad}$$
$$k_3 = 1.1481 \text{ (in.} - \text{lb.)/rad} \quad k_4 = 1.1481 \text{ (in.} - \text{lb.)/rad}$$

The resulting torque deflection characteristic is shown in Figure 7.29.

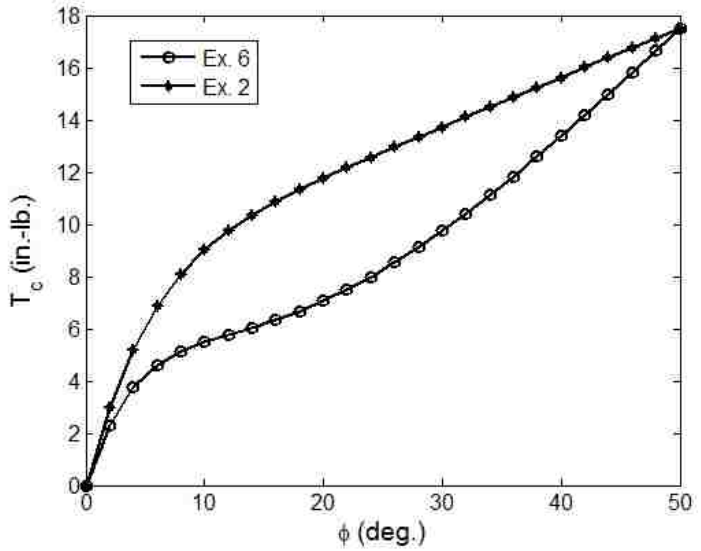

Figure 7.29 Torque-Deflection Characteristics for Example 2 and Example 6

Step 4: Figure 7.30 shows the mechanical advantage of the mechanism designed in Example 6. The mechanical advantage of Example 2 is also shown plotted on it.

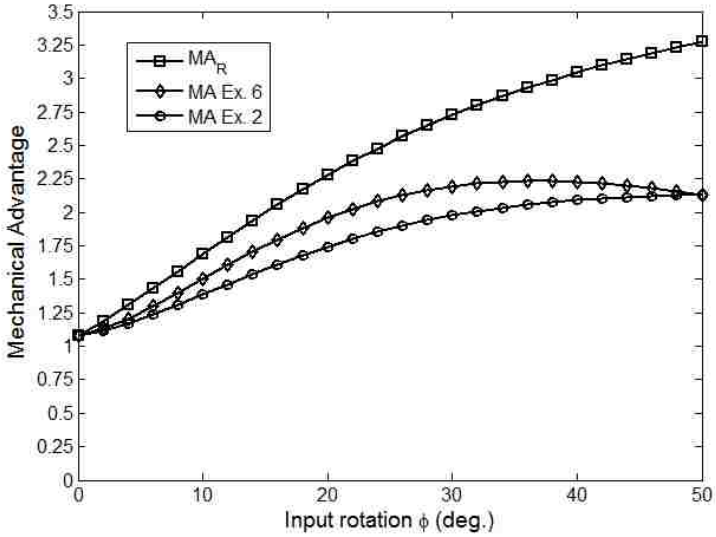

Figure 7.30 MA and MA_R for the Compliant Mechanism Designed in Example 2 and Example 6

7.8 DISCUSSION

The suggested PRBM method simplifies the evaluation of the mechanical advantage of compliant mechanisms, and provides a physically intuitive method for performing controlled studies of the critical elements of a compliant mechanism. All the types of mechanical advantage, Type 1, Type 2, and Type 3 can be readily evaluated using the PRBM method. Some important observations realized from the work presented in this section are listed below:

1. The mechanical advantage characteristics of a compliant mechanism should be evaluated by considering both, the structural configuration and the energy storage characteristics.
2. For a given torque-deflection characteristics, the mechanical advantage of the compliant mechanism can be improved by designing rigid-body mechanism with higher mechanical advantage.
3. For a given rigid-body mechanical advantage, the mechanical advantage of a compliant mechanism can be improved by modifying the torque-deflection characteristics of the compliant mechanism.
4. An optimized configuration can be obtained if both, the structural configuration and the torque-deflection characteristic can be optimized.

The structural configuration and the compliance content of a complaint mechanism are strongly-coupled, and therefore, should be considered together during the evaluation of the mechanical advantage of the compliant mechanism. Neglecting either of them may result in a mechanism with inferior mechanical advantage properties.

7.9 SUMMARY

This section investigated the mechanical advantage aspects of compliant mechanisms and provided a new approach for its evaluation using the PRBM method. The method considers a two-stage approach wherein, the compliance is ignored at first. Notions of power conservation and angular velocity ratios using instant centers are applied to obtain the rigid-body mechanical advantage. Later, the energy-storage characteristic of the compliant mechanism is superimposed to obtain the mechanical advantage of the compliant mechanism. Several examples are presented to demonstrate the approach. An iterative process of designing compliant mechanisms with higher mechanical advantage is also proposed. Summary observations presented should guide the designer towards better compliant mechanism designs. The PRBM method can be used for evaluating all types of mechanical advantage. The section lays out a formal methodology that can be used to investigate the effect of various factors on the mechanical advantage of compliant mechanisms.

8. A METHODOLOGY FOR DETERMINING STATIC MODE SHAPE(S) OF A COMPLIANT MECHANISM USING THE PSEUDO-RIGID-BODY MODEL CONCEPT AND THE DEGREES OF FREEDOM ANALYSIS

Traditionally, the deflected configuration of a compliant segment is determined through rigorous mathematical analysis using Newtonian mechanics. Application of the same principles towards evaluation of the deformed configuration of compliant mechanisms, containing a variety of segment types, becomes cumbersome. This section provides a new methodology to determine the expected deflected configuration(s) of a compliant mechanism, for a given set of load and/or displacement boundary conditions. The method utilizes the principle of minimum total potential energy in conjunction with the degrees of freedom analysis and the pseudo-rigid-body model concept. The static mode shape(s) of compliant segments are applied to identify the possible functional configuration(s) of a given compliant mechanism structural configuration. The methodology also facilitates in determining the deformed configuration of the constituent compliant segments, and thus assists in the identification of an appropriate pseudo-rigid-body model for design and analysis of compliant mechanisms.

8.1 BACKGROUND

The highly nonlinear geometrical nature of the deflections involved with compliant mechanisms complicates the design and analysis approaches. In response to these challenges, many researchers have been continually involved in the development of effective and efficient methods for the design and analysis of compliant mechanisms. All of the present day approaches utilize rigorous mathematical analysis with Newtonian mechanics to determine the expected deformed configuration for a given compliant segment subjected to load and/or displacement boundary conditions. Application of the same theory becomes cumbersome, if not impossible, for compliant mechanisms containing a variety of segment types. In the case of compliant mechanisms containing fixed-guided segments the structure may also become statically indeterminate, thus further increasing the complexity of determining the expected deformed shape. This section provides a straight-forward approach to determine the deformed configuration of a compliant mechanism. The proposed methodology provides this qualitative

information about a compliant mechanism subjected to a combination of load and/or displacement boundary conditions using the pseudo-rigid-body model (PRBM) approach, in conjunction with the principle of minimum total potential energy and the degrees of freedom analysis.

The continual development of the PRBMs over the years has rendered the methodology as a simple and accurate tool for design and analysis of compliant mechanisms. The largest benefit of the PRBM approach comes from its ability to transform a compliant mechanism into a rigid-body mechanism, and vice versa, thus making available a wealth of existing rigid-body mechanism synthesis and analysis knowledge to the treatment of compliant mechanisms. In order to extract the largest benefit of the PRBM concept, it is very important to transform a given compliant mechanism into an appropriate PRBM. The methodology proposed in this section will assist a designer in this task, as well.

8.2 STATIC MODE SHAPES OF COMPLIANT SEGMENTS AND THE CORRESPONDING PRBMS

Prasanna et al. [94] introduced the concept of static mode shape for a compliant segment. A static mode shape of a compliant segment is defined as

The specific kinematic deflected configuration acquired by a compliant segment on the application of a set of beam end load and/or displacement boundary conditions

Prasanna et al. [94] showed that a fixed-pinned segment and fixed-free segment with SLFP exhibits only one static mode shape, defined as their first static mode shape, shown in Figure 8.1 and Figure 8.2. The corresponding PRBMs are shown in Figure 8.3 and Figure 8.4. For a fixed-guided compliant segment Prasanna et al. [94] showed that theoretically infinite static mode shapes are possible, each of them are defined by the number of inflection points in the deformed state, achieved by application of a set of loads and/or displacements. The displaced configuration with a monotonically increasing curvature has zero inflection points, and is defined as the first static mode shape of a fixed-guided segment. The displaced configuration with one inflection point is defined as the second static mode shape of the fixed-guided compliant segment, as so on.

Figure 8.5 and Figure 8.6 shows the first two static mode shapes of a fixed-guided compliant segment. The corresponding PRBMs are shown in Figure 8.7 and Figure 8.8.

Figure 8.1 The First Static Mode Shape for a Fixed-Pinned Compliant Segment

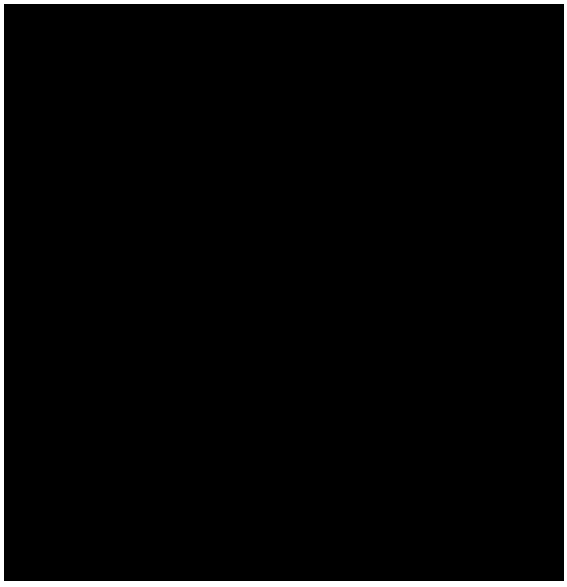

Figure 8.2 The First Static Mode Shape for a Fixed-Free Beam with a SLFP

Figure 8.3 PRBM for the First Static Mode Shape for a Fixed-Pinned Compliant Segment

Figure 8.4 PRBM for the First Static Mode Shape for a Fixed-Free Segment with a SLFP

Prasanna et al. [94] also showed that introduction of an inflection point increases the strain energy in the compliant members. Thus, the first static mode shape of a fixed-

guided segment is defined as the lowest potential energy configuration. The second static mode shape has higher potential energy associated with it, and so on.

Figure 8.5 First Static Mode Shape for a Fixed-Guided Compliant Segment

Figure 8.6 Second Static Mode Shape for a Fixed-Guided Compliant Segment

Figure 8.7 PRBM for the Fixed-Guided Compliant Segment in its First Static Mode Shape

Figure 8.8 PRBM for the Fixed-Guided Compliant Segment in its Second Static Mode Shape

8.3 PRINCIPLE OF MINIMUM TOTAL POTENTIAL ENERGY

The principle of minimum total potential energy states that [95]

Amongst all possible sets of deformations, that which ensures that all the equilibrium conditions are fulfilled will lead to minimization of the total potential

In other words, the principle of minimum total potential energy suggests that a structure under the influence of external disturbance will deform and result in a configuration that tends to minimize its total potential energy. This section utilizes this concept to determine the static mode shape(s) of a compliant mechanism subjected to load and/or displacement boundary conditions.

8.4 EVALUATION OF DEGREES OF FREEDOM OF A COMPLIANT MECHANISM

A compliant mechanism by definition is a structure, wherein the mobility is achieved through the deflection of its flexible members [1]. With this understanding, it can be said that the direct application of the degrees of freedom analysis using the Grubler's criteria [96], given by equation (207), will result in a value of freedom number $F \leq 0$.

$$F = 3(n-1) - 2j - h \tag{207}$$

where, F is the minimum inputs required to obtain a deterministic motion, j the number of lower pairs, and h the number of higher pairs.

Recently, Prasanna et al. [97, 98] presented a straight-forward approach to determine the degrees of freedom of active and passive compliant mechanisms (F_C), using the PRBM concept. In this approach, the authors generate a PRBM and apply Grubler's criteria to determine the *maximum* actuable degrees of freedom, using equation (208).

$$F_C = f_r + f_e \quad (208)$$

where, f_r represents the contribution of the closed-loop rigid-body mechanism and f_e the contribution of the flexible members to the total degrees of freedom F_C. Both f_r and f_e are calculated by the application of Grubler's criteria given by equation (207). Note that for active compliance systems $f_r = 0$.

8.5 A METHODOLOGY TO DETERMINE THE EXPECTED MODE SHAPE OF A COMPLIANT MECHNANISM AND ITS CORRESPONDING PRBM

The methodology to determine the static mode shape(s) of a given compliant mechanism utilizes the PRBM of the static mode shape(s) of individual segments and the degrees of freedom analysis. The methodology considers that the compliant mechanism will always tend to deform with a mode shape that has the lowest potential energy. This principle is coupled with the degrees of freedom analysis to obtain the expected deformed configuration of a given compliant mechanism. The methodology is explained in a stepwise manner below, and is represented in a flowchart in Figure 8.9.

Step 1: Identify the various segment types in the mechanism.

Step 2: Construct a PRBM of the mechanism by considering the lowest potential energy (first static mode shape) PRBM for the compliant segments identified in Step 1.

Step 3: Determine the degrees of freedom (F_C) for the PRBM constructed in Step 2, using equation (208).

Step 4: Review the results.

(a) If $F_C \leq 0$ then this static mode shape is not possible, and therefore, this PRBM is not a correct representation. If the constituent compliant segments can achieve higher order mode shape(s) then construct a new PRBM using the higher order mode shape of one of the constituent segments. Repeat Step 2 to 4(a) until a configuration with $F_C = 1$ is determined.

(b) If $F_C = 1$ then this mode shape represents the first static mode shape of the compliant mechanism. The corresponding PRBM should be utilized for the design and analysis

of the compliant mechanism subjected to one load or displacement boundary condition.

Step 5: If the constituent compliant segments can achieve higher order modes, then construct a new PRBM using the PRBM of the next higher order mode for one of the segments.

Step 6: Determine the degrees of freedom (F_C) for the PRBM constructed in Step 5, using the equation (208). Here F_C represents the number of load and/or displacement boundary conditions required to achieve this static mode shape.

Step 7: Repeat Steps 5 and 6 by constructing PRBMs for all possible combinations of segmental mode shapes to identify all possible static mode shape(s) of the compliant mechanism.

The methodology is illustrated using three examples in the following section.

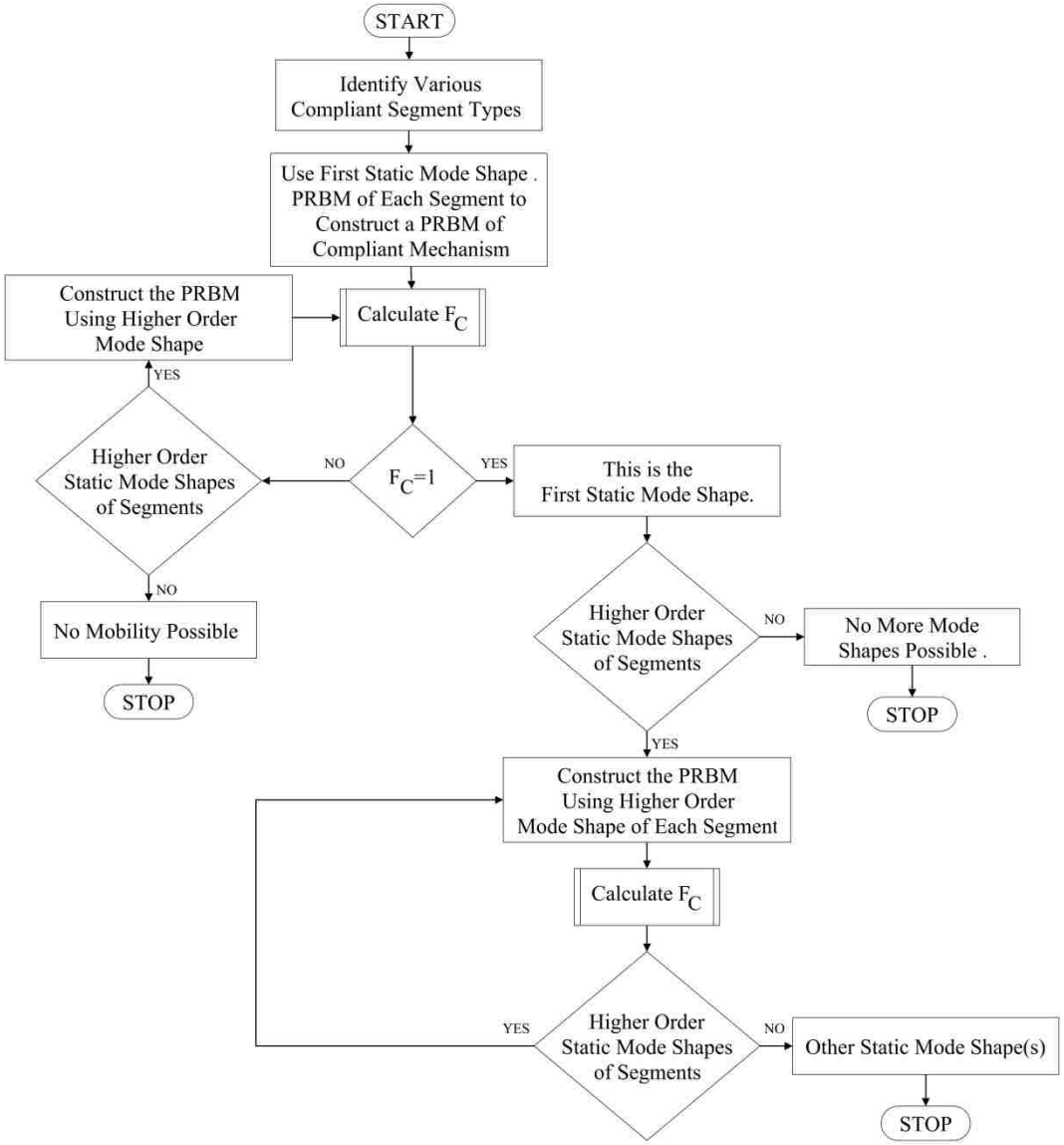

Figure 8.9 The Methodology to Determine the Static Mode Shape(s) and the Corresponding PRBM

8.6 EXAMPLES

Example 1: Determine the static mode shape(s) of the compliant mechanism shown in Figure 8.10, and its PRBM for compliant mechanism synthesis and analysis.

Figure 8.10 Schematic of a Fully-Compliant Mechanism

The stepwise procedure provided in Section 8.5 is utilized to determine the static mode shape(s) for the compliant mechanism shown in Figure 8.10.

Step 1: The constituent segments include two SLFPs and one fixed-guided segment.

Step 2: Figure 8.11 shows the PRBM that is constructed using the lowest potential energy PRBM of each segment type. The corresponding mode shape is shown in Figure 8.12.

Step 3: Using equation (208) and the procedure provided by Prasanna et al. [97, 98], we have:

$$F_C = f_r + f_e = 0 \tag{209}$$

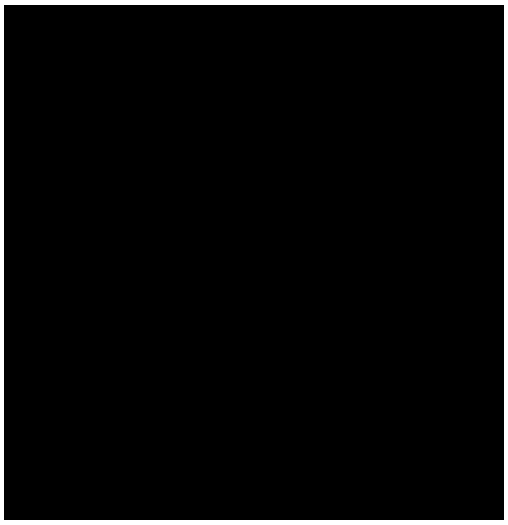

Figure 8.11 PRBM of a Static Mode Shape of the Compliant Mechanism Shown in Figure 8.10

Figure 8.12 A Static Mode Shape of the Mechanism Shown in Figure 8.10

Step 4: Equation (209) suggests that the PRBM constructed in Figure 8.11 is not feasible, and therefore, the corresponding static-mode shape is not possible. Using the second static mode shape of the fixed-guided segment, Steps 2 and 3 are repeated. The new PRBM is shown in Figure 8.13 and the corresponding static mode shape is shown in Figure 8.14. Using equation (208), we have:

$$F_C = f_r + f_e = 1 \quad (210)$$

Step 5: The fixed-guided compliant segment cannot be subjected to any more loads, and therefore it is not expected to generate the higher order static mode shape.

The above analysis suggests that the compliant mechanism shown in Figure 8.10 will have only one static mode shape, shown in Figure 8.14. Figure 8.15 shows the picture of the FEA verification performed using ANSYS® with a force applied at the coupler point, as shown in Figure 8.10. These results are in excellent agreement with the experimental observations performed by Prasanna et al. [97, 98].

Figure 8.13 PRBM of the Static Mode Shape Shown in Figure 8.10

Figure 8.14 A Static Mode Shape of the Compliant Mechanism Shown in Figure 8.10

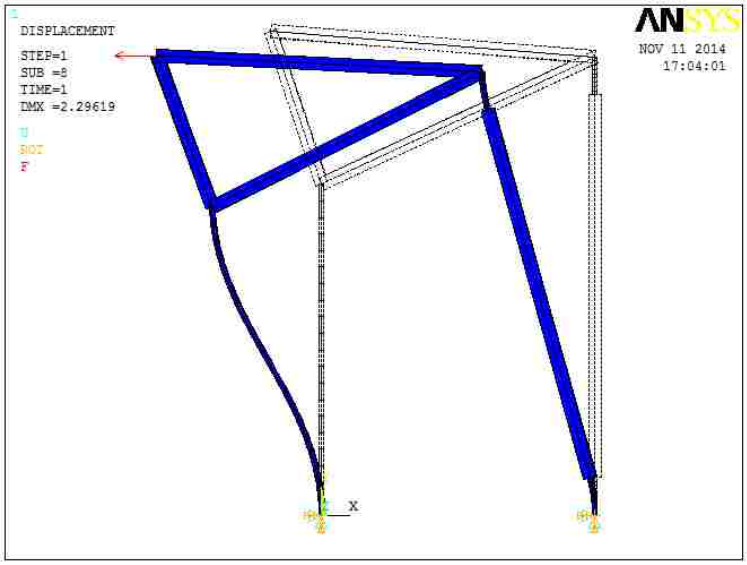

Figure 8.15 FEA Verification of the First Static Mode Shape of the Compliant Mechanism Shown in Figure 8.10, with one Load Boundary Condition

Example 2: Figure 8.16 shows the CAD rendering of the crimping mechanism designed by AMP, Inc. It is desired to determine the appropriate PRBM of this compliant mechanism to determine its mechanical advantage, when the tool is actuated with a force at the handle.

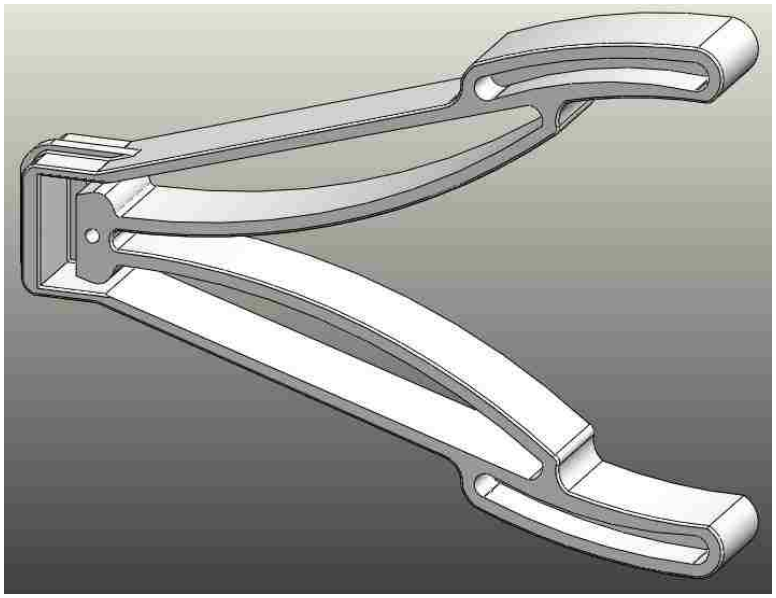

Figure 8.16 CAD Rendering of the Crimping Mechanism Designed by AMP, Inc.

The crimping tool shown in Figure 8.16 is symmetric, and each half contains two fixed-guided segments, a rigid coupler segment and a sliding pair.

The stepwise procedure presented in above is utilized to determine the first static mode shape. The resulting PRBM of the first static mode shape is shown in Figure 8.17. This PRBM is used to determine the mechanical advantage characteristics of the crimping mechanism, as shown in section 7. A finite element analysis is performed using SolidWorks®. The displacement plot of this analysis shows the first static mode shape, shown in Figure 8.18.

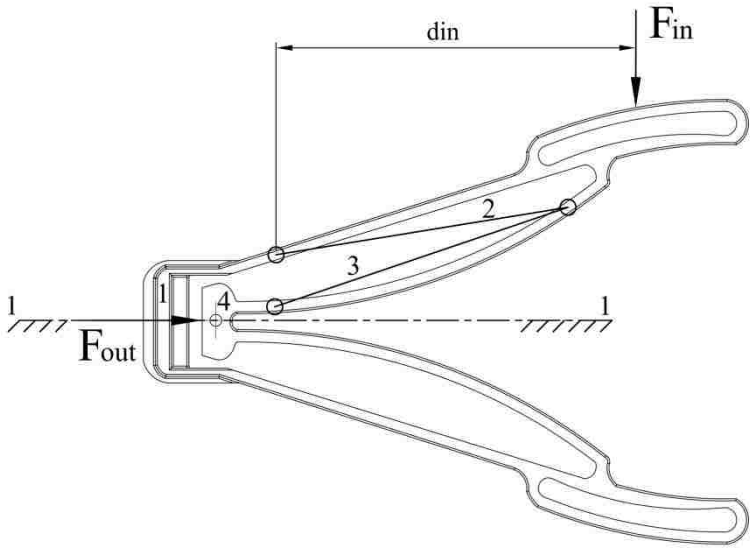

Figure 8.17 PRBM of the First Static Mode of the Crimping Mechanism Shown in Figure 8.16

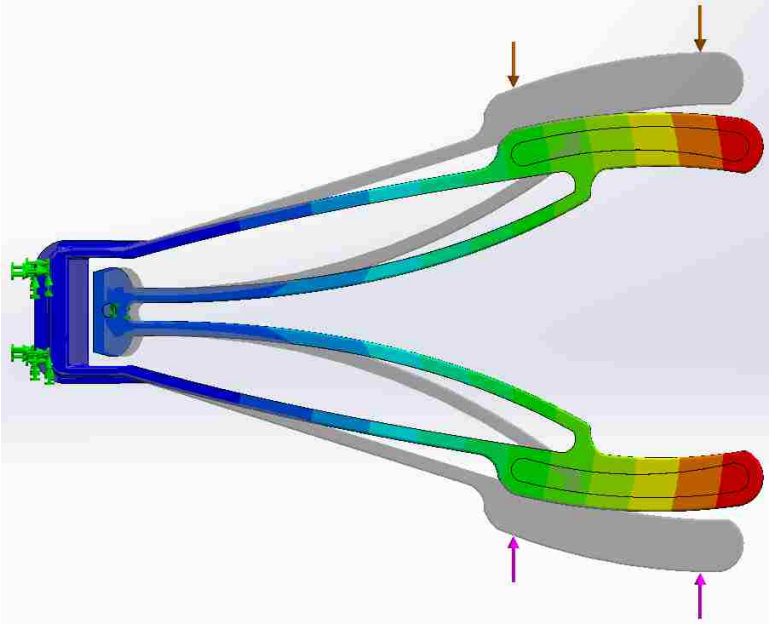

Figure 8.18 Displacement Plot Using FEA to Verify the Static Mode Shape with one Input

Example 3: Determine the functional configurations of the partially-compliant mechanism shown in Figure 8.19.

The partially-compliant mechanism shown in Figure 8.19 contains two compound fixed-pinned compliant segments, each composed of a fixed-fixed segment and a rigid fixed-pinned segment. Using the stepwise procedure provided above the static mode shapes are determined, shown in Figure 8.20 through Figure 8.22. The PRBMs constructed to determine the mode shapes are shown in Figure 8.23 and Figure 8.25.

Figure 8.19 Schematic of a Partially-Compliant Mechanism Containing Compound Compliant Segments

Figure 8.20 First Static Mode Shape of the Compliant Mechanism Shown in Figure 8.19

Figure 8.21 Second Static Mode Shape of the Compliant Mechanism Shown in Figure 8.19

Figure 8.22 Third Static Mode Shape of the Compliant Mechanism Shown in Figure 8.19

The partially-compliant mechanism shown in Figure 8.19 will exhibit a monotonically increasing curvature for its fixed-guided segments in its first static mode shape. Imparting additional displacement boundary condition(s) to the rigid-body revolute joints will transform the fixed-guided segment into its higher order mode, as shown in Figure 8.21 and Figure 8.22.

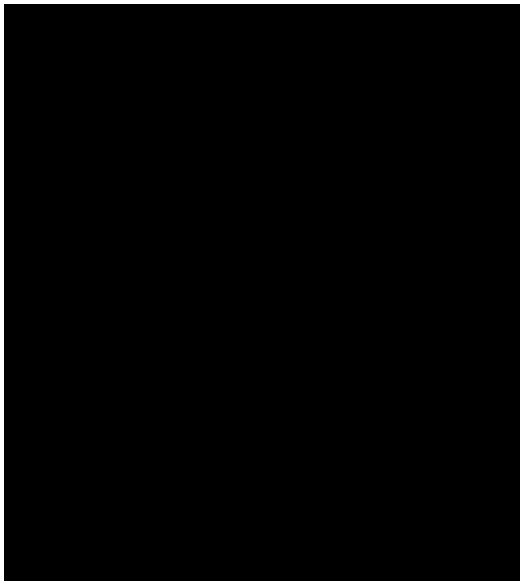

Figure 8.23 PRBM of the Static Mode Shape Shown in Figure 8.20

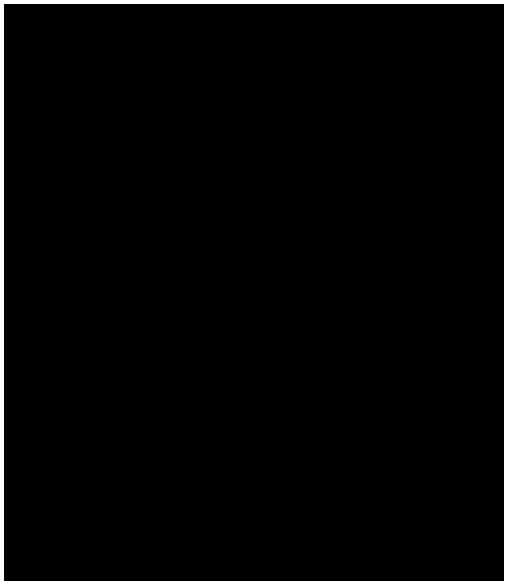

Figure 8.24 PRBM of the Static Mode Shape Shown in Figure 8.21

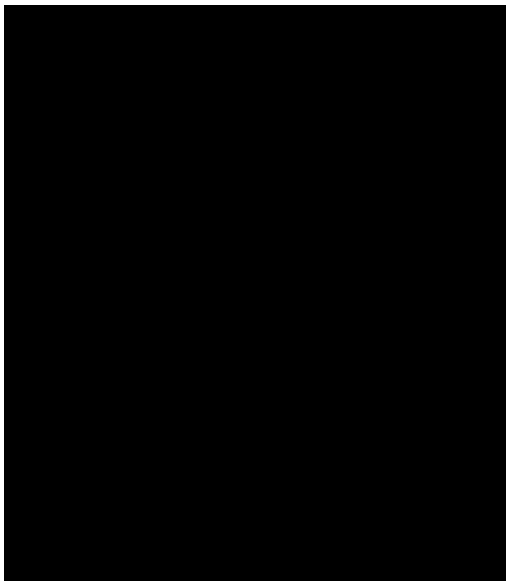

Figure 8.25 PRBM of the Static Mode Shape Shown in Figure 8.22

8.7 DISCUSSION

The proposed methodology provides an expedient approach to determine the expected deformed configuration of a compliant mechanism, subjected to a set of load and/or displacement boundary conditions. The method applies the principle of minimum total potential energy in conjunction with the degrees of freedom analysis using the PRBM concept. The approach eliminates the solution of static equilibrium equations, which become cumbersome for analysis of statically indeterminate beams.

The analysis approach helps to understand the underlying reasons for the occurrence of an inflection point. The results also show that the possibility of occurrence of two inflection points is abysmally small, unless the structural configuration of the compliant mechanism demands for it.

8.8 SUMMARY

This section provided a straight-forward and expedient approach for determining the mode shape(s) for a given compliant mechanism design. The methodology applies the principle of minimum total potential energy in conjunction with the degrees of

freedom analysis using the pseudo-rigid-body model (PRBM) concept to determine the expected mode shape(s) of a compliant mechanism, for a given set of load and/or displacement boundary conditions. The approach allows anticipating the deformed configuration of the constituent compliant segments, and thus facilitates in the identification of an appropriate PRBM for the design and analysis of compliant mechanisms. The methodology provides an expedient qualitative assessment of a compliant mechanism design while avoiding rigorous mathematical analysis for the same.

9. EXPERIMENTAL VALIDATION OF THE PSEUDO-RIGID-BODY MODEL CONCEPT FOR COMPLIANT MECHANISM DESIGN

The pseudo-rigid-body model concept has been proved to be very simple and efficient method for compliant mechanism design and analysis. This section summarizes the experimental investigations performed to validate the effectiveness of this method for compliant mechanism design and analysis. Investigations are performed on compliant segments, partially-compliant mechanisms, and fully-compliant mechanisms. The tests verify the accuracy of the pseudo-rigid-body model approach in compliant mechanism synthesis and analysis. The experimental investigations reveal that the pseudo-rigid-body model concept successfully captures the maximum possible actuable degrees of freedom of a compliant mechanism. To facilitate the wide range of tests a new test setup is designed.

9.1 BACKGROUND

The pseudo-rigid-body model (PRBM) concept has been proven to be a simple, efficient, and accurate method for compliant mechanism design and analysis. The largest benefit of the PRBM concept comes from its ability to utilize a wealth of existing rigid-body mechanism analysis and synthesis knowledge to the treatment of compliant mechanisms. PRBM results have always demonstrated to be in excellent agreement with analytical methods like elliptic integral formulations and finite element analysis. This section verifies the feasibility of the PRBM concept experimentally. The experimental investigations allow verification of the degree of freedom evaluated using the PRBM concept. Attempts to verify the concept of the maximum possible degree of freedom through analytical methods have been usually unsuccessful. The results obtained in this section validate the heuristic notions of the application of segmental PRBMs to the synthesis and analysis of fully-compliant and partially-compliant mechanisms. The tests capture the large-deflections possible in a compliant segment and demonstrate the accuracy, efficiency, and the ease of the application of the PRBM concept towards its synthesis and analysis. A new test setup is designed to facilitate the wide-range of experimental investigations performed in this work. Tests are performed to validate the PRBM analysis and synthesis techniques. Test samples include: i) a fixed-pinned

compliant beam with a metallic insert, ii) a partially-compliant mechanism, and iii) a combination of fully-compliant and partially-compliant mechanisms. The test results show excellent correlation with the PRBM estimations.

9.2 DESIGN OF THE TEST SETUP

A new test setup is designed to facilitate the wide-range of the experimental investigations. Figure 9.1 shows the CAD rendering of the setup, and Figure 9.2 shows the manufactured setup. The setup consists of two mounting regions; the top-half is utilized for testing beam deflection and the bottom-half for analyzing partially-compliant and fully-compliant mechanisms. The test setup is designed to operate on a table top. The setup is 2.5 ft. high, 1 ft. deep and 2 ft. long.

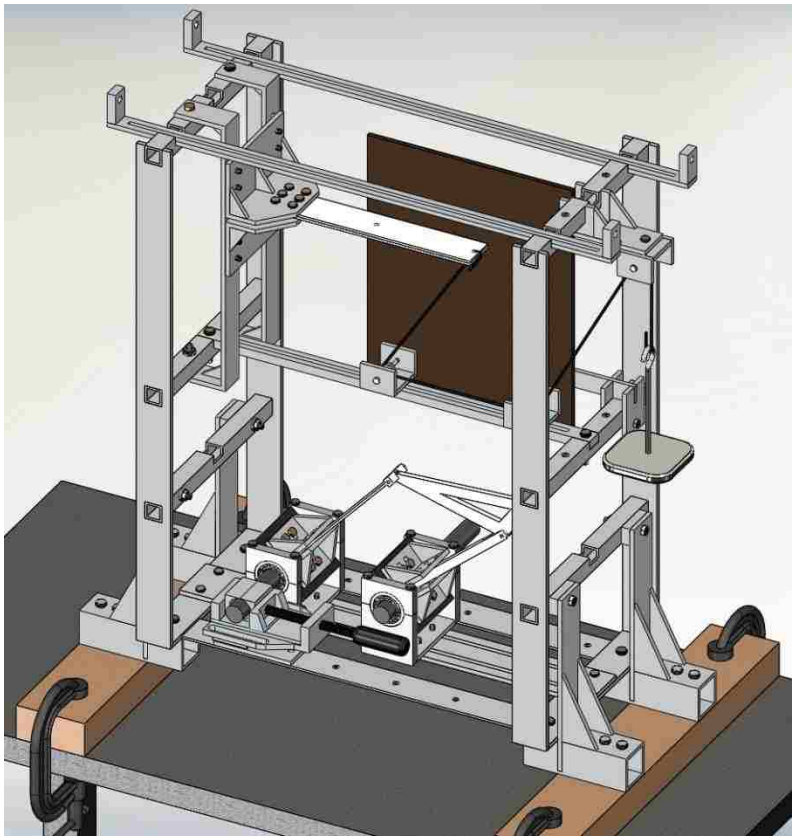

Figure 9.1 CAD Rendering of the Test Setup Design

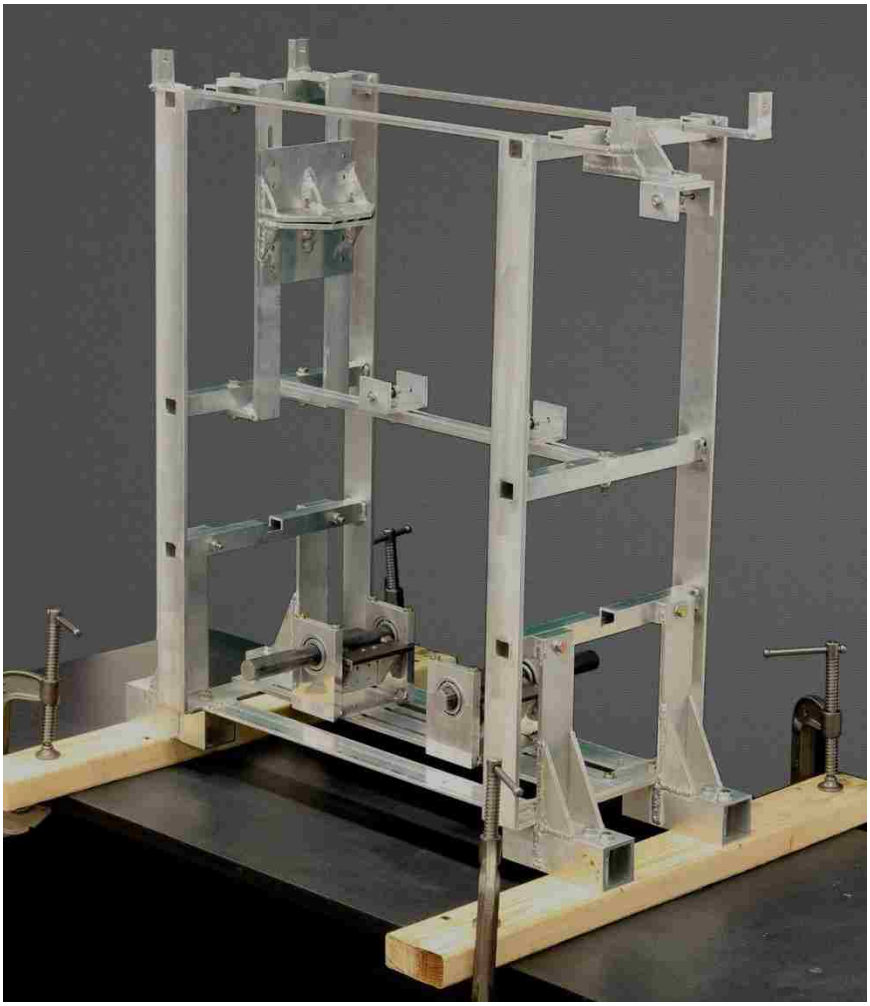

Figure 9.2 A Photograph of the Manufactured Test Setup

The top-half of the test setup is designed to test a compliant beam subjected to beam end forces. It consists of a clamping region, measuring region and loading region. The clamps can accommodate beams of widths ranging from 0.5 inch to 6 inch. A sliding pair provided at the clamping region allows for accommodating test specimens of thicknesses up to 1 inch. The cantilevered boundary condition is obtained by the set of screws provided in the clamping region. The clamps, screws, and the mounting structure is designed and analyzed for an applied load of 100 lb. The compliant beam can be readily subjected to a variety of beam end loads, which include: i) purely vertical load, ii) a transverse load and an axial load that is tensile, and iii) a transverse load and an axial

load that is compressive. The latter loading cases are obtained with a pair of sliders, loading rope and pulley arrangement. The loads are applied with a weight hanger, installed on the top right corner of the setup. The pulleys comprise of u-groove antifriction bearings. The pulley surface is well-lubricated to prevent any friction between the loading rope and pulley. The relative locations of the sliders determine the load applied on the beam end point. Figure 9.3 shows the top-half of the test setup design; Figure 9.4 through Figure 9.6 shows the various regions of the top-half of the test setup.

The beam end point coordinates are plotted on a graph paper, mounted on a bracket directly behind the compliant beam. Vernier Calipers® are used to measure the beam end point deflections.

Some preliminary tests showed that irrespective of the amount of lubrication between the loading rope and pulley, some friction is always observed between them. In order to account for this friction loss the Capstan friction equation is applied [99], shown in equation (211).

$$T_2 = T_1 e^{\mu\beta} \tag{211}$$

where, T_1 is the amount of tension required to balance the applied tension T_2, β the total angle of contact between the rope and pulley, and μ the coefficient of friction between the loading rope and pulley, as shown in Figure 9.7. Experiments are performed on one loading rope and pulley combination to obtain the coefficient of friction, evaluated to be 0.01. Considering that the test setup may contain three such pulleys, the friction losses are incorporated in the PRBM calculations, as shown in Figure 9.8. The effects due to the follower type of loading conditions are also taken into account in the PRBM analysis.

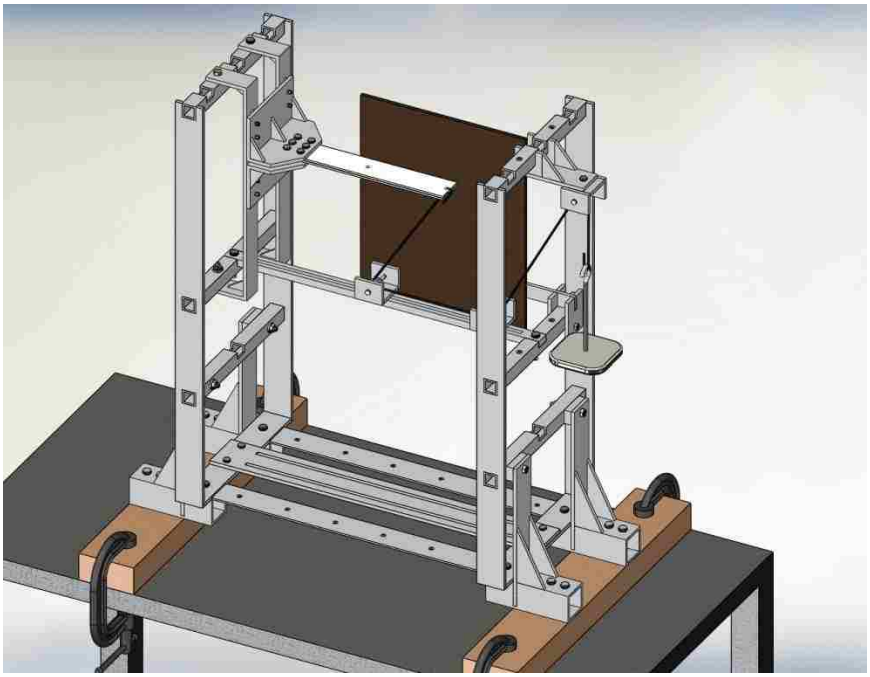

Figure 9.3 CAD Rendering Showing the Top-Half of the Test Setup

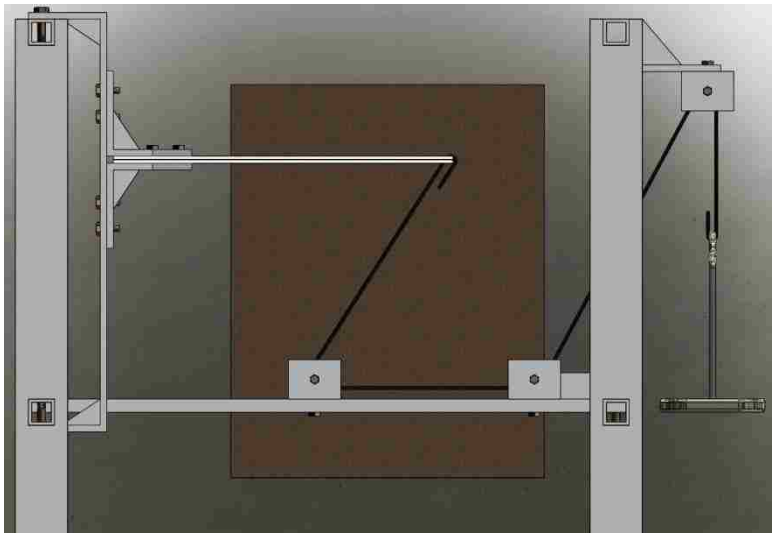

Figure 9.4 A CAD Image Showing the Loading of Beams

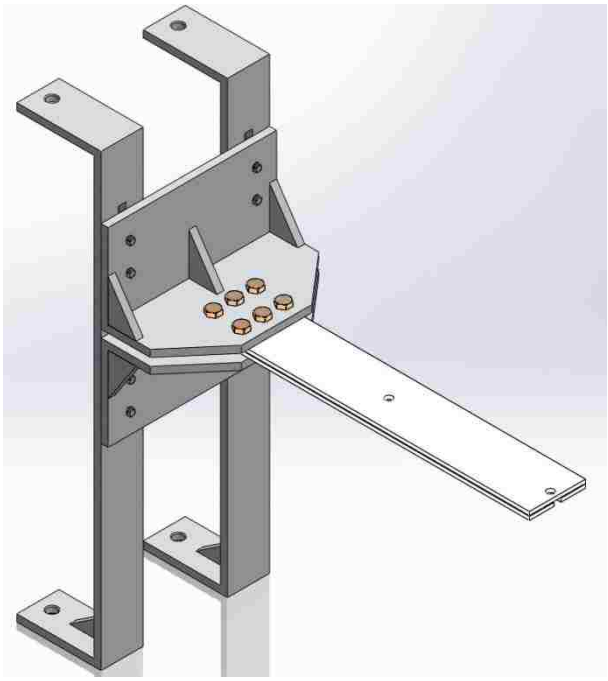

Figure 9.5 CAD Rendering of the Beam Clamping Zone

Figure 9.6 A CAD Image Showing the Slider Pair at the Clamping Zone

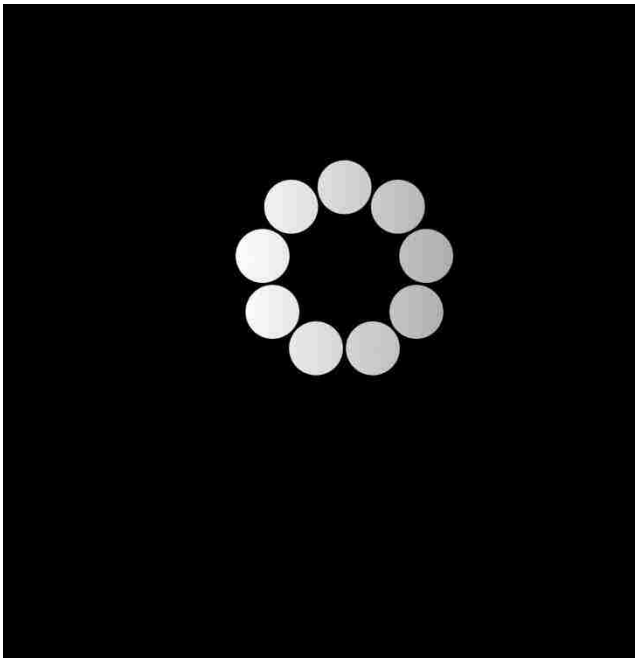

Figure 9.7 Experimental Setup for Calculating Coefficient of Friction

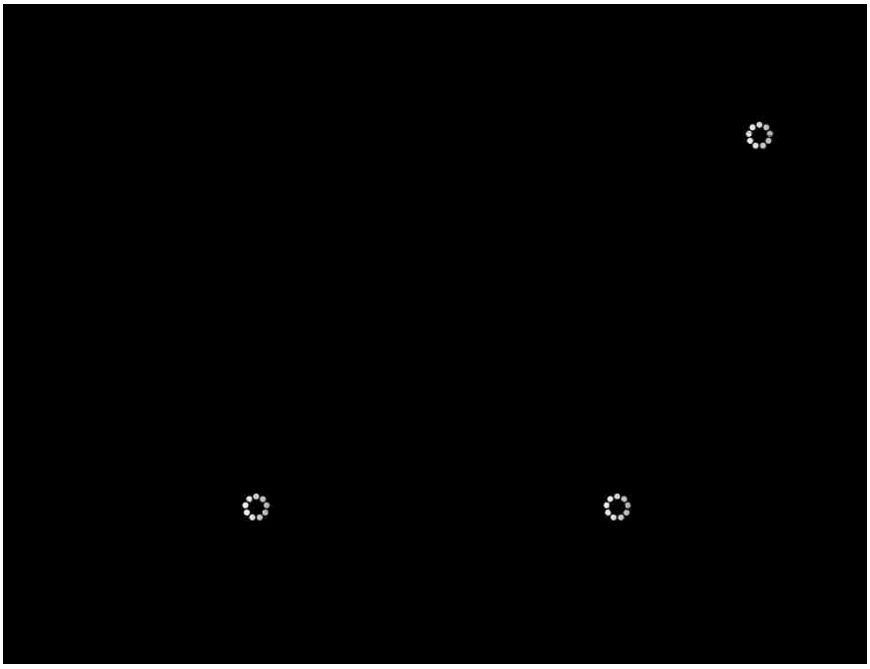

Figure 9.8 A CAD Image Showing the Procedure for Calculating Force Applied at the Beam End Point

The bottom-half of the test setup is used to analyze partially-compliant and fully-compliant mechanisms. The mechanisms may be actuated by either load or displacement boundary conditions. This half of the test setup also constitutes of three regions; clamping/mounting region, loading region, and measuring region. The loading and measuring regions are similar to the top-half of the test setup. The clamping region for the bottom-half, however, has some unique features. The clamps can be utilized to act as a fixture or to act as a rigid-body revolute joint. The clamps contain two brackets that hold the compliant mechanism. The brackets can accommodate compliant segments of widths ranging from 0.5 inch to 4 inch. The slider pair provided at the brackets assists in mounting compliant segments of thicknesses up to 0.75 inch. The brackets are mounted on a swivel plate that is held by a pair of antifriction bearings. Such an arrangement allows for the testing of mechanisms with variable initial orientations. The swivel plate contains an overhang that can be utilized to restrict the mobility, essentially providing a fixture, by a combination of a miniature vice and blocks with high coefficient of friction lining pads. These unique features in the clamping region allow it to be utilized as a fixture or as a rigid-body revolute joint. Two such clamps are utilized in the test setup with a slider pair between the clamp and the supporting structure. The slider pair allows the setup to accommodate compliant mechanisms of variable overall length. All components in the bottom-half of the test setup are designed and analyzed for an applied load of 100 lb. Figure 9.9 shows the bottom-half of the test setup, and Figure 9.10 through Figure 9.11 shows its various regions.

Similar to the analysis of compliant beams, the friction between the loading rope and pulley is incorporated. The corrections are made on the loading hanger, because of the necessity of meeting the coupler point precision-positions.

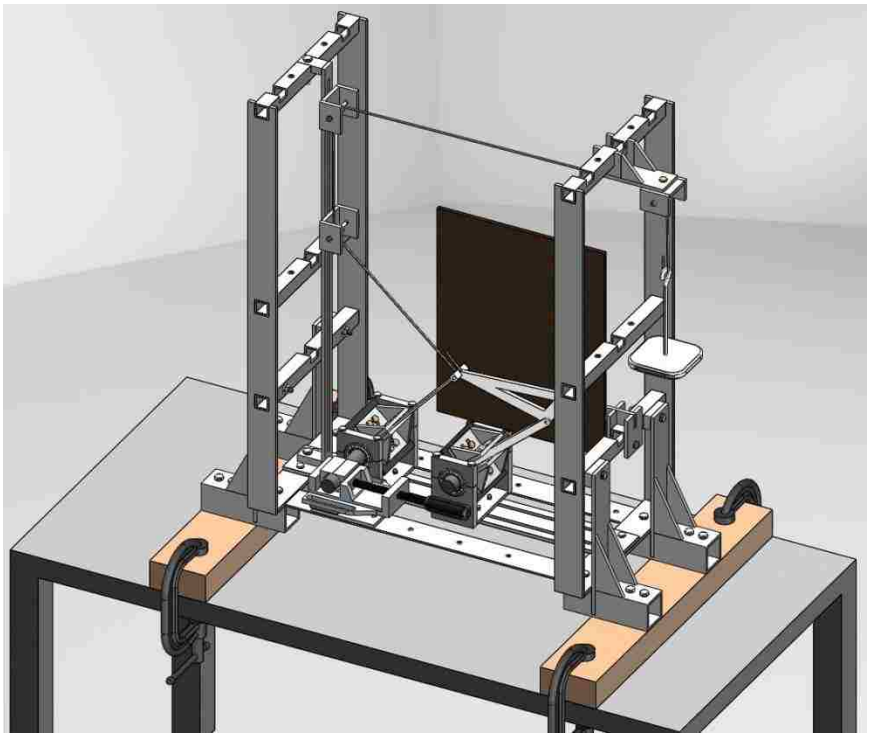

Figure 9.9 CAD Rendering Showing the Bottom-Half of the Test Setup

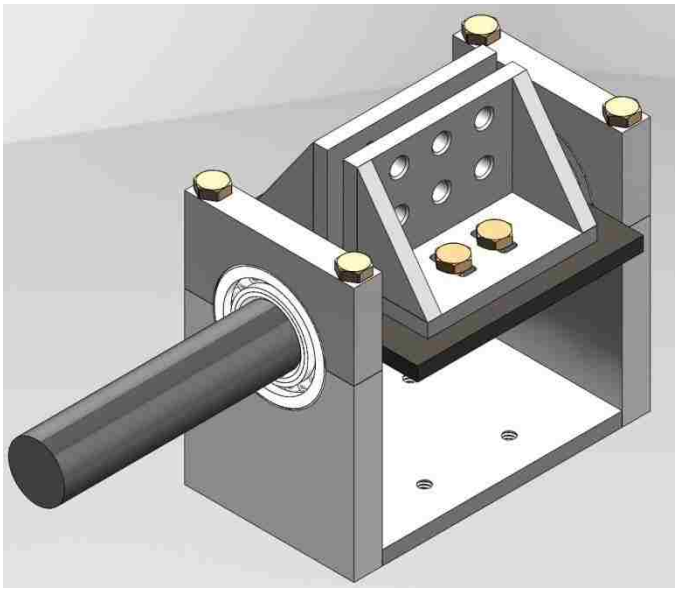

Figure 9.10 A CAD Image for the Clamp in the Bottom-Half of the Test Setup

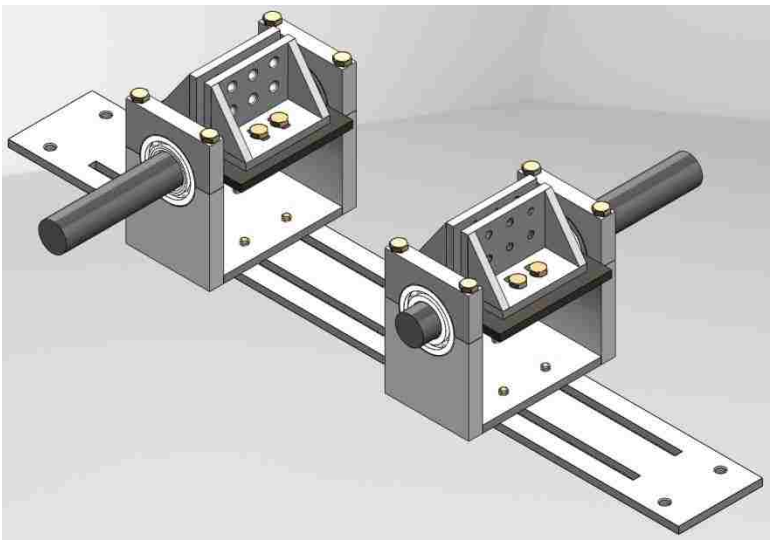

Figure 9.11 A CAD Image Showing the Slider Pair at the Clamping Zone in the Bottom-Half of the Test Setup

9.3 EXPERIMENTAL INVESTIGATIONS FOR THE VALIDATION OF THE PRBM CONCEPT

The PRBM concept is validated for the design and analysis of compliant beams, and partially-compliant and fully-compliant mechanisms.

9.3.1 Compliant Beam Deflections. A composite-compliant beam, containing a metallic segment sandwiched between two plastic segments is considered to verify the PRBM concept for analysis and synthesis of compliant segments. Figure 9.12 shows the test specimen designed by Kuber [54]. The specimen constitutes of three beam segments. The outer segments are made from Delrin® of modulus of elasticity of 550,000 psi. These segments are 0.125 inch thick, 2.5 inch wide and 10 inch long. The middle segment is made from spring steel of modulus of elasticity $\mathbf{30 \times 10^6}$ psi. This segment is 0.025 inch thick, 1 inch wide and 10 inch long.

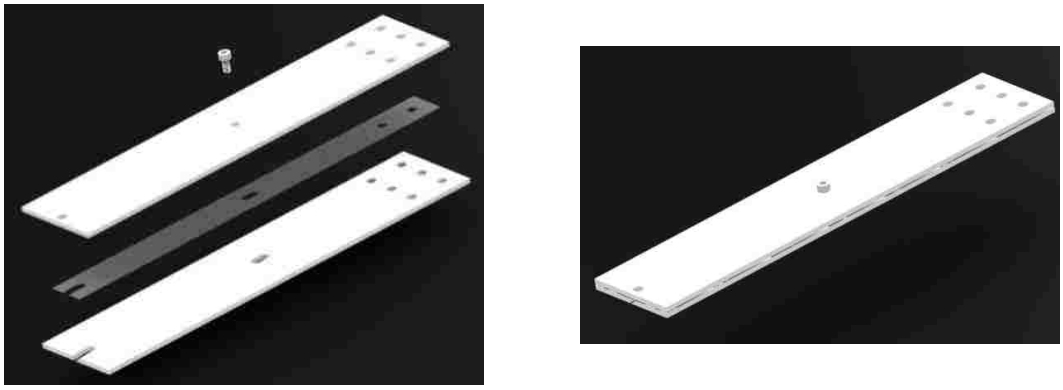

Figure 9.12 Assembly View and Exploded View for the Test Specimen Designed for Test 1 [54]

The outer segments are held together with plastic binding posts. The test specimen is well lubricated, and slots are provides in the middle segment and the bottom segment, such that the experimental setup is in line with the assumptions made in PRBMs [54, 100], which include: i) no bonding between layers, and ii) negligible friction that allows sliding between layers.

The PRBM for a fixed-pinned composite-compliant segment provided by Midha et al. [100] is utilized to determine the beam end point coordinates.

9.3.2 Test 1(a): Fixed-pinned composite-compliant beam subjected to a purely vertical force.

Figure 9.13 shows the experimental setup for test 1(a), photographed at an intermediate loading step. Table 9.1 shows the beam end coordinate values obtained using the PRBM method and the values recorded during the test. These are also shown plotted in Figure 9.14.

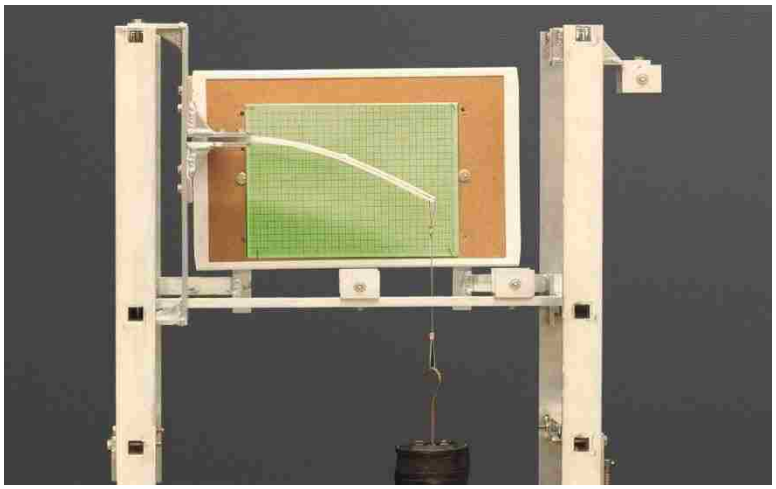

Figure 9.13 Experimental Setup for Test 1(a)

Table 9.1 Beam End Point Location Comparisons for Test 1(a)

Applied Force (lb.)	PRBM Results		Test Results		Relative Error (%)
	a (in.)	b (in.)	a (in.)	b (in.)	
0	10	0	10	0	0.0
4	9.549	2.732	9.56	2.735	0.2173
5	9.355	3.25	9.341	3.243	0.2728
6	9.146	3.717	9.148	3.677	0.6505
7	8.929	4.134	8.962	4.088	0.8685
8	8.711	4.505	8.731	4.467	0.6283
8.5	8.602	4.676	8.624	4.626	0.7826

Figure 9.14 Graphical Comparison for Beam End Point Location for Test 1(a)

9.3.3 Test 1(b): Fixed-pinned composite-compliant beam subjected to a transverse force and a compressive axial force; $\mathbf{n = 0.896}$. Figure 9.15 shows the experimental setup for test 1(b), photographed at an intermediate loading step. Table 9.2 shows the beam end coordinate values obtained using the PRBM method and the values recorded during the test. These are also shown plotted in Figure 9.16.

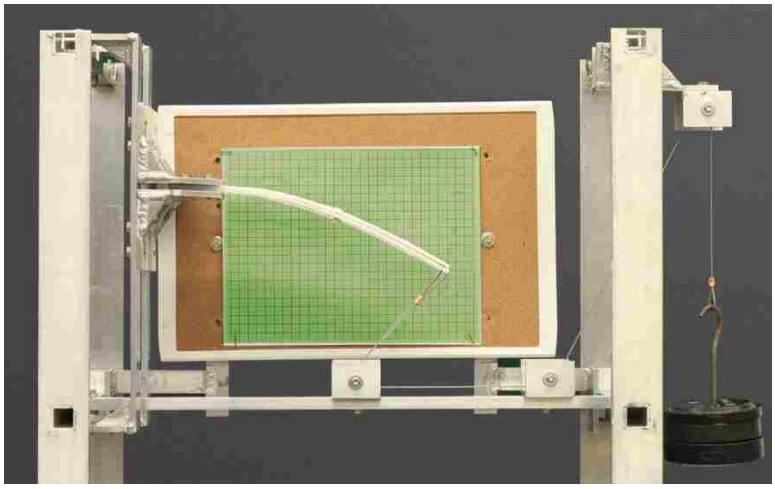

Figure 9.15 Experimental Setup for Test 1(b)

Table 9.2 Beam End Point Location Comparisons for Test 1(b)

Applied Force (lb.)	PRBM Results		Test Results		Relative Error (%)
	a (in.)	b (in.)	a (in.)	b (in.)	
0	10	0	10	0	0.0
4	9.621	2.489	9.629	2.481	0.2261
5	9.408	3.089	9.422	3.09	0.2511
6	9.162	3.644	9.182	3.592	0.9141
7	8.882	4.168	8.911	4.127	0.7664
8	8.562	4.675	8.588	4.614	0.9490
8.5	8.392	4.912	8.423	4.873	0.6928

Figure 9.16 Graphical Comparison for Beam End Point Location for Test 1(b)

9.3.4 Test 1(c): Fixed-pinned composite-compliant beam subjected to a transverse force and a tensile axial force; $\mathbf{n = -0.673}$. Figure 9.17 shows the experimental setup for test 1(c), photographed at an intermediate loading step. Table 9.3 shows the beam end coordinate values obtained using the PRBM method and the values recorded during the test. These are also shown plotted in Figure 9.18.

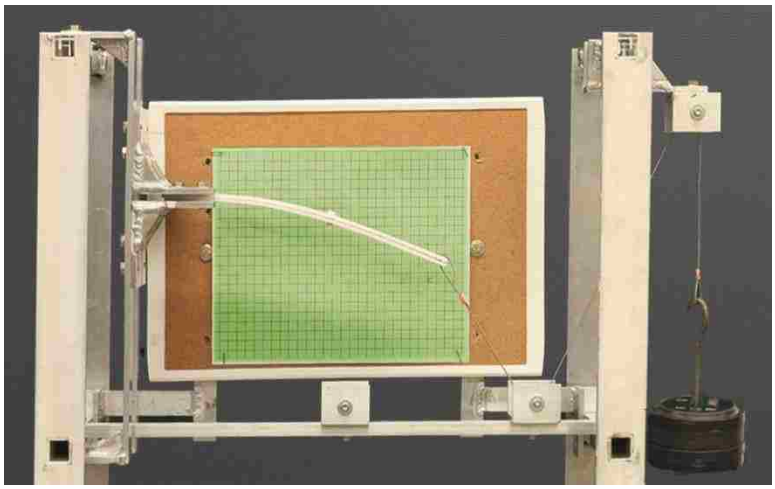

Figure 9.17 Experimental Setup for Test 1(c)

Table 9.3 Beam End Point Location Comparisons for Test 1(c)

Applied Force (lb.)	PRBM Results		Test Results		Relative Error (%)
	a (in.)	b (in.)	a (in.)	b (in.)	
0	10	0	10	0	0.0
4	9.781	1.933	9.791	1.902	0.7399
5	9.712	2.213	9.734	2.197	0.5772
6	9.647	2.45	9.652	2.421	0.5930
7	9.582	2.664	9.596	2.621	0.8733
8	9.515	2.859	9.539	2.819	0.8688
8.5	9.488	2.938	9.488	2.938	0.8214

Figure 9.18 Graphical Comparison for Beam End Point Location for Test 1(c)

9.3.5 Compliant Mechanism Synthesis and Analysis. A partially-compliant mechanism that can be represented as a pseudo-rigid-body four-bar mechanism, shown in Figure 9.19, is considered for the verification of the PRBM concept for compliant mechanism synthesis and analysis. The mechanism constitutes of one torsional spring. According to the design tables presented by Midha et al. [64], such a configuration should be solved as a strongly-coupled set of equations. Instead of this consideration, the PRBM is designed using the weakly-coupled set of equations by following the design procedure presented in section 6. A partially-compliant mechanism is designed for three precision-position path generation with torque specified at the precision positions, such that:

$\bar{\delta}_2 = -0.646 + 1.58\text{i};\ \bar{\delta}_3 = -1.227 + 2.54\text{i}\ ;$

$T_1 = 9.75\ \text{in.} - \text{lb.};\ T_2 = 17.20\ \text{in.} - \text{lb.};\ T_3 = 22.875\ \text{in.} - \text{lb.}$

The resulting compliant mechanism has the following properties [87]:

$\bar{Z}_1 = 3.902 - 0.8802\text{i}$ $\bar{Z}_2 = 4.754 + 2.767\text{i}$

$\bar{Z}_3 = 6.249 - 2.176\text{i}$ $\bar{Z}_4 = 7.099 + 1.471\text{i}$

$\bar{Z}_5 = 7.929 - 0.148\text{i}$ $\bar{Z}_6 = 1.68 + 2.027\text{i}$

$\psi_2 = 11.95$ deg. $\psi_3 = 19.83$ deg.;

$\Theta_{20} = 15.86$ deg.; $\Theta_{30} = -28.36$ deg.; $\Theta_{20} = -6$ deg.

Spring constant $k_1 = 38.356$ in. $-$lb./rad

Figure 9.19 PRBM for the Partially-Compliant Mechanism for Test 2

Considering that the partially-compliant mechanism contains one fixed-pinned segment made of Delrin® of modulus of elasticity 550,000 psi, the length of the compliant segment is calculated to be 6.4706 inch. For a rectangular cross-section of width 1.5 inch, the thickness of the compliant segment is 0.121 inch. The resulting compliant mechanism is shown in Figure 9.20.

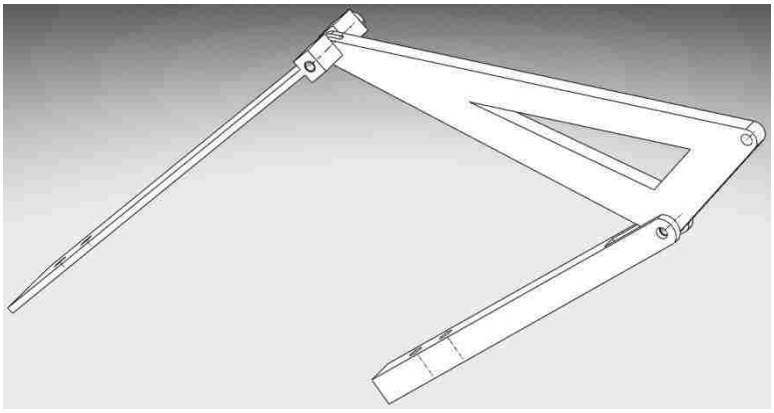

Figure 9.20 CAD Rendering of the Partially-Compliant Mechanism for Test 2

9.3.6 Test 2: A partially-compliant mechanism subjected to a specified input torque. Figure 9.21 shows the experimental setup for test 2, photographed at an intermediate loading step. The coupler point locations obtained using the PRBM method and the values recorded during the test are shown in Table 9.4 and plotted in Figure 9.22. The data is obtained when the design torque is applied at the fixed-pinned compliant segment, as shown in Figure 9.21.

Table 9.4 Coupler Point Location Comparisons for Test 2

Coupler Point	PRBM Results		Test Results		Relative Error (%)
	X (in.)	Y (in.)	X (in.)	Y (in.)	
$\mathbf{P_0}$	0	0	0	0	0
$\mathbf{P_1}$	-0.412	2.523	-0.414	2.52	0.1315
$\mathbf{P_2}$	-1.059	4.103	-1.1	4.07	1.2446
$\mathbf{P_3}$	-1.64	5.063	-1.685	4.992	1.5831

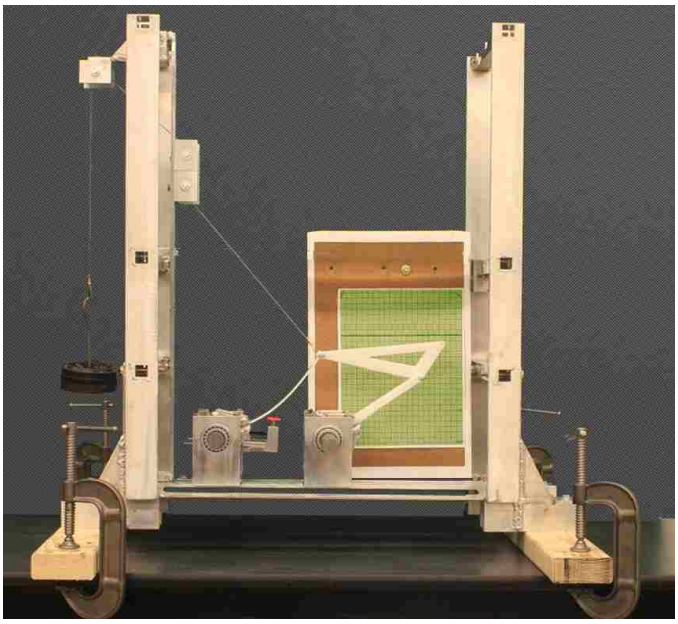

Figure 9.21 Experimental Setup for Test 2

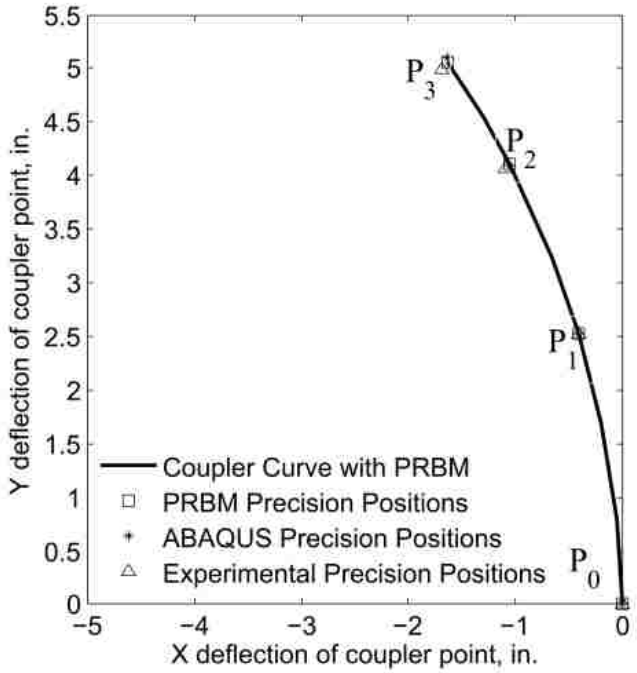

Figure 9.22 Coupler Point Location Comparisons for Test 2

9.3.7 Degrees of Freedom of a Compliant Mechanism. Three compliant mechanisms, including partially-compliant and fully-compliant mechanisms, are designed and analyzed for verifying the maximum possible degrees of freedom. The test specimens constitute of fixed-pinned segments, fixed-guided segments, and compliant segments with small-length flexural pivots. PRBM based design approaches presented by Howell and Midha [33], Howell et al. [37] Pauly and Midha [38], Midha et al. [80], and Howell [36] are used to design the test specimens. All specimens are designed to allow for a pseudo-rigid-body angle of 30 deg., and are manufactured from Delrin® of modulus of elasticity 500,000 psi. Detailed descriptions of the test specimen designs can be found in Prasanna et al. [97, 98]. Figure 9.23 shows the schematics of the test specimens considered for the degrees of freedom verification.

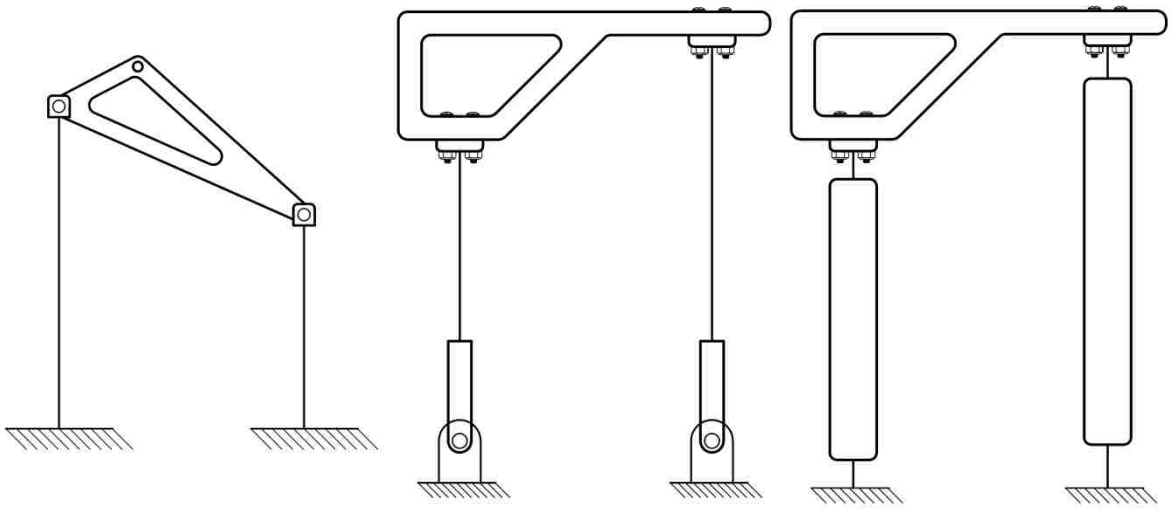

Specimen 1 Specimen 2 Specimen 3

Figure 9.23 Test Specimens for Degrees of Freedom Verification

The PRBM based approach provided by Prasanna et al. [97, 98] is used to analytically determine the maximum possible degrees of freedom. The bottom-half of the test setup is utilized to experimentally verify the degrees of freedom calculated using the PRBM method. Figure 9.24 shows the experimental setup for one of the test specimens and Table 9.5 shows the comparisons between the test results and the PRBM for the test 3. The description of the test procedure and the PRBM method of evaluating the degrees of freedom of a compliant mechanism can be found in Prasanna et al. [97, 98].

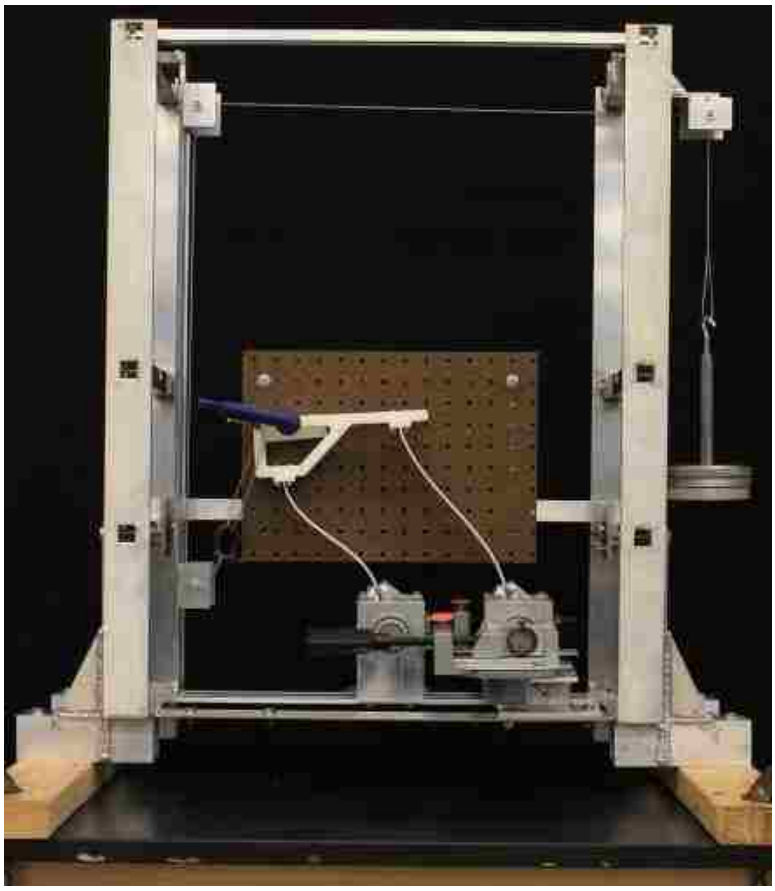

Figure 9.24 Experimental Setup for the Degrees of Freedom Test of Test Specimen 2

Table 9.5 Comparison of the Experimental and Analytical Results for Evaluating Degrees of Freedom of a Compliant Mechanism

Test Specimen	Experimental results		Maximum DOF by PRBM approach
	Minimum DOF	Maximum DOF	
Specimen 1	1	1	1
Specimen 2	1	3	3
Specimen 3	1	1	1

9.4 DISCUSSION OF RESULTS

The PRBM concept for modeling, design and analysis of compliant mechanisms was verified with the use of a test setup. Test specimens included a compliant segment with metallic insert, partially-compliant mechanisms and fully-compliant mechanisms. A wide range of tests were conducted to validate the PRBM concept for compliant mechanism design and analysis.

The test results are in excellent agreement with the PRBM estimations. The small errors in the PRBM results, compared to the measured values, may be due to the assumed material properties and human errors occurring during the marking of beam end point or coupler point locations. The estimated coefficient of friction between the loading rope and the pulley, and the unaccounted friction between the metallic insert and plastic beams may have added to the observed errors between PRBM and test results. Even with these errors, the comparison plots provided for tests 1 and 2 allows to infer that the PRBM concept is an efficient method for compliant mechanism design and analysis.

Test 3 successfully demonstrated PRBM concept's ability to capture the intrinsic behavior of a given compliant mechanism. PRBM concept in conjunction with the rigid-body analysis techniques provides a straight-forward approach to determine the maximum possible degrees of freedom. A similar approach can be applied to determine the expected deformed configuration of a compliant mechanism. Such a simple analysis may eliminate the numerical simulations required during the early design stages.

9.5 SUMMARY

This section summarized the experimental tests performed to validate the effectiveness of the pseudo-rigid-body model concept for compliant mechanism design and analysis. Tests were conducted on a compliant segment and partially and fully-compliant mechanisms. The results suggested that PRBM method is simple and efficient in its application, while also provided accurate results. The PRBM concept also successfully captures the number and type of deformation configurations possible for a given compliant mechanism.

10. CONCLUSIONS AND FUTURE RECOMMENDATIONS

The pseudo-rigid-body model (PRBM) concept proposed for the analysis and design of large-deflection flexible members in compliant mechanisms has proven to be a simple, efficient and accurate tool for the synthesis, analysis and design of compliant mechanisms. This dissertation investigated a variety of analysis and design problems related to compliant mechanisms using the PRBM concept.

Section 3 of this dissertation provided a PRBM and the associated governing equations for the analysis and synthesis of a fixed-guided compliant beam with one inflection point in its deformed state. This section also investigated the conditions for a unique deformed configuration, summarized by statements presented as two theorems. The section utilized the concept of characteristic deflection domain to specify realistic beam end point displacements. The results obtained from the PRBM method are in excellent agreement with the solution obtained from closed-form elliptic integral solutions and finite element analysis software ANSYS®. However, because of the assumptions associated with each of the methods, experimental testing is recommended to validate the theoretical developments. If appropriate, a robustness/sensitivity analysis could accompany this effort to account for errors in the measured beam end displacement boundary conditions. Such information would be useful in the development of high-precision sensors, or characterizing the existing ones. Also, future work may encompass extending this methodology to study beams with more than one point of inflection, if needed.

Section 4 provided characteristic deflection domains for a variety of compliant segment types. The work also provides pseudo-rigid-body representations for the lower and upper boundary curves of the characteristic deflection domain. The case studies presented therein demonstrate that the number, type and the properties of compliant segments comprising the compliant mechanism significantly affect its mobility characteristics. A future effort may be to extend the study to determine the combination of segment types that would provide a robust compliant mechanism design. Such a mechanism will have very small errors in the coupler point path when subjected to larger errors in the input force/displacement.

Section 5 provided a new framework for the synthesis of fully-compliant mechanisms containing fixed-guided segments with an inflection point in their deformed state. The approach builds on the vector-loop representation of the PRBM model of a fixed-guided compliant segment with an inflection point, as presented in Section 3. The coupler point displacements for the mechanisms synthesized are compared with the closed-form elliptic integral solutions and ANSYS®. As future work, the coupler point displacements may be compared experimentally as well.

Section 6 of this dissertation revisited the 'synthesis with compliance method' for the synthesis of compliant mechanisms. The work determines the conditions for treating the kinematic and compliance equations as weakly-coupled, and presents a generalized approach for the synthesis and design of compliant mechanisms using the PRBM concept. The compliant mechanism designs obtained from this approach are compared for the coupler point displacements with results obtained from ANSYS®. The rather favorable comparisons demonstrate the effectiveness of the approach, and the wide range of examples reinforce its applicability.

Section 7 provided a new approach for determining the mechanical advantage of a compliant mechanism using the PRBM concept. The approach consists of a two-stage process wherein the compliance is ignored at first. Notions of power conservation and angular velocity ratios using instant centers are applied to obtain the rigid-body mechanical advantage. Later, the energy storage characteristics of the compliant mechanism is superimposed to obtain the mechanical advantage of the compliant mechanism. The section further utilizes the generalized approach provided in Section 6 to develop a methodology for the synthesis and design of compliant mechanisms with higher mechanical advantage. As future work, this approach may be used to determine the effect of the characteristic deflection domain on the mechanical advantage of a given compliant mechanism. Experimental validation may be undertaken to corroborate the predicted mechanical advantage values.

Section 8 provided a new approach for determining the static mode shapes of a given compliant mechanism structural configuration. The methodology applies the principle of minimum total potential energy in conjunction with the degrees of freedom analysis using the PRBM concept. The approach allows anticipating the deformed

configuration of the constituent compliant segments, and thus facilitating the identification of an appropriate PRBM for the design and analysis of compliant mechanisms. A future scope of this research would be to extend this methodology in the design of compliant mechanisms for a given set of load and/or displacement boundary conditions.

Finally, the dissertation summarizes the experimental investigations performed to validate the effectiveness of the PRBM concept in the synthesis, design and analysis of compliant segments and compliant mechanisms. To facilitate the tests, an experimental test setup is designed. Experiments are performed on a compliant segment with a metallic insert, a partially compliant mechanism, and a combination of fully- and partially-compliant mechanisms. The tests satisfactorily validate the PRBM in the analysis of compliant segments, and the synthesis and analysis of compliant mechanisms.

The range of the problems investigated in this dissertation, coupled with favorable comparisons with results obtained from other methods, demonstrate and highlight the accuracy, simplicity, efficacy and applicability of the PRBM concept for synthesis, analysis and design of compliant segments and compliant mechanisms.

REFERENCES

[1] Midha, A., Norton, T. W., and Howell, L. L., "On the Nomenclature, Classification, and Abstractions of Compliant Mechanisms," *Journal of Mechanical Design*, Trans. ASME, Vol. 116, No. 1, March 1994, pp. 270-279

[2] Norton, T. W., "On the Nomenclature, Classification, and Mobility of Compliant Mechanisms," M.S. Thesis, Purdue University, 1991

[3] Mettlach, G. A., Khanuja, S. S., and Midha, A., "Design of an Ergonomic Compliant Modular Chair," *Proceedings of 4th National Applied Mechanisms and Robotics Conference*, December, 1995, pp. AMR95-009-1-10

[4] McCarthy, J. M., "21st Century Kinematics: Synthesis, Compliance and Tensigrity," *ASME Journal of Mechanisms and Robotics*, Vol. 3, No. 2, May 2011, pp. 020201-1-3

[5] Grabianowski, Ed. "How the Tweel Airless Tire Works" 10 May 2007. HowStuffWorks.com. <http://auto.howstuffworks.com/tweel-airless-tire.htm> 25 September 2014

[6] Nice Kicks, "adidas Springblade Blue/Silver" 21 October 2013. nicekicks.com <www.nicekicks.com/2013/10/21/adidas-springblade-bluesilver.htm> 25 September 2014

[7] Brigham Young University, "BYU engineers conceive disc replacement to treat chronic low back pain" 12 June 2012. byu.edu <news.byu.edu/archive12-jun-spine.aspx> 25 September 2014

[8] Adams, R., Doherty, B., Lamarr, J., and Rasch, D., "Force Sensing Clamp," Senior Design Project Report, Advisor: A. Midha, ME 4761: Engineering Design, Missouri University of Science and Technology, project sponsored by Compliers Inc., May 2010

[9] Byers, F. K., "Design of a Compliant Gripper Mechanism," B.S. Honors Thesis, Purdue University, 1990

[10] Byers, F. K., and Midha, A., "Design of a Compliant Gripper Mechanism," Proceedings of the 2nd National Applied Mechanism and Robotics Conference, Cincinnati, Ohio, 1991, pp. XC-1-1 – XC-1-12

[11] Finch, N., Griner, J., Lange, S., and Rieker, G., "Complaint Micro-Restrainer," Senior Design Project Report, Advisor: A. Midha, ME 4761: Engineering Design, Missouri University of Science and Technology, project sponsored by Sandia National Laboratories, December 2002

[12] Howell, L. L., Magleby, S. P., and Olsen, B. M., Elements of Mechanisms, Mechanisms and Example Applications, In L. L. Howell, S. P. Magleby, and B. M. Olsen (Eds.), *Handbook of Compliant Mechanisms*, John Wiley & Sons Inc., 2013

[13] NASA Jet Propulsion Laboratory, California Institute of Technology, "In-situ Exploration and Sample Return: Autonomous Planetary Mobility" www.nasa.gov <mars.jpl.nasa.gov/mer/technology/is_autonomous_mobility-01.html> 25 September 2014

[14] Burns, R. H., and Crossley, F. R. E., "Kinetostatic Synthesis of Flexible Link Mechanisms," ASME Paper 68-MECH-36, 1968

[15] Burns, R. H., "The Kinetostatic Synthesis of Flexible Link Mechanisms," Ph.D. Dissertation, Yale University, 1964

[16] Sevak, N. M., and McLarnan, C. W., "Optimal Synthesis of Flexible Link Mechanisms with Large Static Deflections," *Journal of Engineering for Industry*, Trans. ASME, May 1975, pp. 520-526

[17] Bisshopp, K. E., and Drucker, D. C., "Large Deflection of Cantilever Beams," *Quarterly of Applied Mathematics*, Vol. 3, No. 3, 1945, pp. 272-275

[18] Frisch-Ray, R., *Flexible Bars*, Butterworth, Washington, DC, 1962

[19] Shoup, T. E., "On Analytical Investigations of the Large-Deflections of Flexible Beam Spring," Ph.D. Dissertation, The Ohio State University, 1969

[20] Midha, A., Class Notes for ME 597: Special Topics in Compliant Mechanisms, The Pennsylvania State University, May 1983

[21] Holl, J., Koffler, W., and Midha, A., "Compliant Mechanism Synthesis in Prosthetic Design," *AMD Symposia Series*, ASME, New York, Vol. 56, 1983, pp. 63–66

[22] Midha, A., "Compliant Mechanisms," Section 9.10, *Modern Kinematics: Development in the last forty years*, (Eds.: A. G. Erdman), John Wiley & Sons Inc., New York, NY, 1993, pp. 369-449

[23] Midha, A., Her, I., and Salamon, B. A., "A Methodology for Compliant Mechanisms Design: Part I – Introduction and Large Deflection Analysis," *Advances in Design Automation*, 18th ASME Design Automation Conference, DE-Vol. 44, No. 2, 1992, pp. 29-38

[24] Her, I., Midha, A., and Salamon, B. A., "A Methodology for Compliant Mechanisms Design: Part II – Shooting Method and Application," *Advances in Design Automation*, 18th ASME Design Automation Conference, DE-Vol. 44, No. 2, 1992, pp. 39-45

[25] Her, I., "Methodology for Compliant Mechanisms Design," Ph.D. Dissertation, Purdue University, December 1986

[26] Her, I., and Midha, A., "A Compliance Number Concept for Compliant Mechanisms, and Type Synthesis," *Journal of Mechanisms, Transmissions, and Automation in Design*, Trans. ASME, Vol. 109, No. 3, 1987, pp. 348-355

[27] Salamon, B. A., and Midha, A., "An Introduction to Mechanical Advantage in Compliant Mechanisms," *Journal of Mechanical Design*, Trans. ASME, Vol. 120, No. 1, June 1998, pp. 311-315

[28] Salamon, B. A., "Mechanical Advantage Aspects in Compliant Mechanism Design," M.S. Thesis, Purdue University, 1989

[29] Nahvi, H., "Static and Dynamic Analysis of Compliant Mechanisms Containing Highly Flexible Members," Ph.D. Dissertation, Purdue University, 1991

[30] Hill, T. C., and Midha, A., "A Graphical User-Driven Newton-Raphson Technique for the Use in the Analysis and Design of Compliant Mechanisms," *Journal of Mechanical Design*, Trans. ASME, Vol. 112, No. 1, 1990, pp. 123-130

[31] Hill, T. C., "Applications in the Design and Analysis of Compliant Mechanisms," M.S. Thesis, Purdue University, 1987

[32] Midha, A., and Her, I., "Research Notes," Purdue University, 1985

[33] Howell, L. L., and Midha, A., "Parametric Deflection Approximations for End-Loaded, Large-Deflection Beams in Compliant Mechanisms," *Journal of Mechanical Design*, Trans. ASME, Vol. 117, No. 1, March 1995, pp. 156-165

[34] Howell, L. L., and Midha, A., "A Method for the Design of Compliant Mechanisms with Small-Length Flexural Pivots," *Journal of Mechanical Design*, Trans. ASME, Vol. 116, No. 1, March 1994, pp. 280-290

[35] Howell, L. L., "The Design and Analysis of Large-Deflection Members in Compliant Mechanisms," M.S. Thesis, Purdue University, 1991

[36] Howell, L. L., "A Generalized Loop Closure Theory for the Analysis and Synthesis of Compliant Mechanisms," Ph.D. Dissertation, Purdue University, 1993

[37] Howell, L. L., Midha, A., and Norton, T. W., "Evaluation of Equivalent Spring Stiffness for use in a Pseudo-Rigid-Body Model of Large-Deflection Compliant Mechanisms," *Journal of Mechanical Design,* Trans. ASME, Vol. 118, No. 1, March 1986, pp. 126-131

[38] Pauly, J., and Midha, A., "Improved Pseudo-Rigid-Body Model Parameter Values for End-Force-Loaded Compliant Beams," *Proceedings of the 28th Biennial ASME Mechanisms and Robotics Conference*, Salt Lake City, Utah, September 2004, pp. DETC57580-1-5

[39] Pauly, J., "Analysis of Compliant Mechanisms with Complex-Shaped Segments," M.S. Thesis, University of Missouri-Rolla, 2002

[40] Howell, L. L., *Compliant Mechanisms*, John Wiley & Sons Inc., New York, NY, 2001

[41] Mettlach, G. A., and Midha, A., "Characteristic Deflection Domain Concept in Compliant Mechanism Design and Analysis," *Proceedings of the 6th National Applied Mechanisms & Robotics Conference*, Cincinnati, Ohio, December, 1999, pp. 27-01 – 27-06

[42] Mettlach, G. A., "Analysis and Synthesis of Compliant Mechanisms using Analytical and Graphical Techniques," Ph.D. Dissertation, Purdue University, 1996

[43] Edwards, B. T., "Functionally Binary Pinned-Pinned Segments," M.S. Thesis, Brigham Young University, 1996

[44] Edwards, B. T., Jensen, B. D., and Howell, L. L., "A Pseudo-Rigid-Body Model for Initially-Curved Pinned-Pinned Segments used in Compliant Mechanisms," *Journal of Mechanical Design,* Trans. ASME, Vol. 123, No. 3, September 2001, pp. 464-472

[45] Saxena, A., and Kramer, S. N., "A Simple and Accurate Method for Determining Large Deflections in Compliant Mechanisms Subjected to End Forces and Moments," *Journal of Mechanical Design,* Trans. ASME, Vol. 120, No. 3, September 1998, pp. 392-400, erratum, Vol. 121, No. 2, 1999, pp. 194

[46] Lyon, S. M., "The Pseudo-Rigid-Body Model for Dynamic Predictions of Macro and Micro Compliant Mechanisms," Ph.D. Dissertation, Brigham Young University, August 2003

[47] Lyon, S. M., Howell, L. L., and Roach, G. M., "Modeling Flexible Segments with Force and Moment End Loads via the Pseudo-Rigid-Body Model," *Proceedings of the ASME Dynamic Systems and Controls Division,* at the 2000 ASME International Mechanical Engineering Congress and Exposition, Orlando, FL, November 5-10, 2000, Vol. 69, No. 2, pp. 883-890

[48] Lyon, S. M., and Howell, L. L., "A Simplified Pseudo-Rigid-Body Model for Fixed-Fixed Flexible Segments," *Proceedings of the ASME Design Engineering Technical Conferences & Computers and Information in Engineering Conference*, Montreal, Canada, September 29 – October 2, 2002, pp. DETC34203-23-33

[49] Kimball, C., and Tsai, W., "Modeling of Flexural Beams Subjected to Arbitrary End Loads," *Journal of Mechanical Design*, Trans. ASME, Vol. 124, No. 2, June 2002, pp. 223-235

[50] Mavanthoor, A., "Design and Stability Analysis of Compliant Mechanisms," M.S. Thesis, University of Missouri-Rolla, December 2003

[51] Mavanthoor, A., and Midha, A., "Bistable Compliant Four-Bar Mechanisms with a Single Torsional Spring," *Proceedings of the 30th ASME Mechanisms and Robotics Conference*, Philadelphia, Pennsylvania, September 2006, pp. DETC99453-1-7

[52] Su, H.-J., "A Pseudo-Rigid-Body 3R Model for Determining Large Deflection of Cantilever Beams Subject to Tip Loads," *Journal of Mechanisms and Robotics*, Trans. ASME, Vol. 1, No. 2, May 2009, pp. 021008-1-9

[53] Midha, A., and Kuber, R., "Closed-Form Elliptic Integral Solution for Initially-Straight and Initially-Curved Small-Length Flexural Pivots," *Proceedings of the ASME 2014 International Design Engineering Technical Conferences & Computers and Information in Engineering Conference*, Buffalo, NY, August, 2014, pp. DETC35268-1-7

[54] Kuber, R. S., "Development of a Methodology for Pseudo-Rigid-Body Models of Compliant Segments with Inserts, and Experimental Validations," M.S. Thesis, Missouri University of Science and Technology, 2013

[55] Zhang, A., and Chen, G., "A Comprehensive Elliptic Integral Solution to the Large Deflection Problems of Thin Beams in Compliant Mechanisms," *Journal of Mechanisms and Robotics*, Trans. ASME, Vol. 5, No. 1, May 2013, pp. 021006-1-10

[56] Howell, L. L., and Midha, A., "A Loop-Closure Theory for the Analysis and Synthesis of Compliant Mechanisms," *Journal of Mechanical Design*, Trans. ASME, Vol. 118, No. 1, March 1996, pp. 121-125

[57] Midha, A., Christensen, M. N., and Erickson, M. J., "On the Enumeration of Synthesis of Compliant Mechanisms using Pseudo-Rigid-Body Four-Bar Mechanisms," *Proceedings of the 5th National Applied Mechanisms & Robotics Conference*, Vol. 2, Cincinnati, Ohio, October, 1997, pp. 93-01 – 93-08

[58] Murphy, M. D., "A Generalized Theory for the Type Synthesis and Design of Compliant Mechanisms," Ph.D. Dissertation, Purdue University, December 1993

[59] Murphy, M. D., Midha, A., and Howell, L. L., "The Topological Synthesis of Compliant Mechanisms," *Mechanism and Machine Theory*, Vol. 31, No. 2, February 1996, pp. 185-199

[60] Murphy, M. D., Midha, A., and Howell, L. L., "Type Synthesis of Compliant Mechanisms Employing a Simplified Approach to Segment Type," *Mechanism Synthesis and Analysis: Proceedings of the 1994 ASME Mechanisms Conference*, DE-Vol. 70, 1994, pp. 51-60

[61] Murphy, M. D., Midha, A., and Howell, L. L., "On the Mobility of Compliant Mechanisms," *Machine elements and Machine Dynamics: Proceedings of the 1994 ASME Mechanisms Conference*, DE-Vol. 71, 1994, pp. 475-479

[62] Howell, L. L., and Midha, A., "The Effects of a Compliant Work Piece on the Input/Output Characteristics of Rigid-Link Toggle Mechanisms," *Mechanisms and Machine Theory*, Elsevier Science Ltd., Vol. 30, No. 6, February, 1995, pp. 801-810

[63] Midha, A., Howell, L. L., and Norton, T. W., "Limit Positions of Compliant Mechanisms using the Pseudo-Rigid-Body Model Concept," *Mechanisms and Machine Theory*, Vol. 35, No. 1, 2000, pp. 99-115

[64] Midha, A., Annamalai, Y., and Kolachalam, S. K., "A Compliant Mechanism Design Methodology for Coupled and Uncoupled Systems, and Governing Free-Choice Selection Considerations," *Proceedings of the ASME 2004 Design Engineering Technical Conferences & Computers and Information in Engineering Conference*, Salt Lake, Utah, September, 2004, pp. DETC57579-1-9

[65] Annamalai, Y., "Compliant Mechanism Synthesis for Energy and Torque Specifications," M.S. Thesis, University of Missouri-Rolla, 2003

[66] Midha, A., Kolachalam, S. K., and Annamalai, Y., "On the Classification of Compliant Mechanisms and Synthesis of Compliant Single-Strip Mechanisms," *Proceedings of the ASME 2011 International Design Engineering Technical Conferences & Computers and Information in Engineering Conference*, Washington, DC, August, 2011, pp. DETC48845-1-13

[67] Kolachalam, S. K., "Synthesis of Compliant Single-Strip Mechanisms that may be Represented by a Dyad," M.S. Thesis, University of Missouri-Rolla, 2003

[68] Midha, A., Annamalai, Y., Kolachalam, S. K., Bapat, S. G., and Koli, A. B., "On a Compliant Mechanism Design Methodology using the Synthesis with Compliance Approach for Coupled and Uncoupled Systems," *Advances in Mechanisms, Robotics, and Design Education and Research*, Mechanisms and Machine Science, Vol. 14, Kumar, V., Schmiedeler, J., Sreenivasan, S. V., and Su, H.-J., Eds., Springer International Publishing, Switzerland, pp. 95-116

[69] Su, H.-J., and McCarthy, J. M., "Synthesis of Bistable Compliant Four-Bar Mechanisms using Polynomial Homotopy," *Journal of Mechanical Design*, Trans. ASME, Vol. 129, No. 1, 2007, pp. 1094-1098

[70] Su, H.-J., and McCarthy, J. M., "A Polynomial Homotopy Formulation of the Inverse Static Analysis of Planar Compliant Mechanisms," *Journal of Mechanical Design*, Trans. ASME, Vol. 128, July, 2006, pp. 776-786

[71] Tari, H., and Su, H.-J., "A Complex Solution Framework for the Kinematic Synthesis of a Compliant Four-Bar Mechanism," *Mechanism and Machine Theory*, Vol. 46, 2011, pp. 1137-1152

[72] Ananthasuresh, G. K., "A New Design Paradigm for Micro-Electro-Mechanical Systems and Investigations on the Compliant Mechanism Synthesis," Ph.D. Dissertation, University of Michigan, Ann-Arbor, 1994

[73] Frecker, M. I., Ananthasuresh, G. K., Nishiwaki, S., Kikuchi, N., and Kota, S., "Topological Synthesis of Compliant Mechanisms using Multi-Criteria Optimization," *Journal of Mechanical Design*, Trans. ASME, Vol. 119, 1997, pp. 238-245

[74] Saggere, L., and Kota, S., "Synthesis of Planar, Compliant Four-Bar Mechanisms for Compliant-Segment Motion Generation," *Journal of Mechanical Design*, Trans. ASME, Vol. 123, No. 1, 2001, pp. 535-541

[75] Parkinson, M. B., Howell, L. L., and Cox, J. J., "A Parametric Approach to the Optimization-Based Design of Compliant Mechanisms," *Proceedings of the ASME Design Engineering Technical Conferences*, Sacramento, California, September, 1997, DAC3763-1-8

[76] Rai, A. K., Saxena, A., and Mankame, N. D., "Synthesis of Path Generating Compliant Mechanisms using Initially-Curved Frame Elements," *Journal of Mechanical Design*, Trans. ASME, October, 2007, Vol. 129, pp. 1056-1063

[77] Harrison, H. B., "Post-Buckling Analysis of Non-Uniform Elastic Columns," *International Journal of Numerical Methods in Engineering*, Vol. 7, 1973, pp. 196-210

[78] Miller, R. E., "Numerical Analysis of a Generalized Plane Elastica," *International Journal for Numerical Methods in Engineering*, Vol. 15, 1980, pp.325-332

[79] Coutler, B. A., and Miller, R. E., "Numerical Analysis of a Generalized Plane Elastica with Non-Linear Material Behavior," *International Journal for Numerical Methods in Engineering*, Vol. 26, 1988, pp. 617-630

[80] Midha, A., Bapat, S. G., Mavanthoor, A., and Chinta, V., "Analysis of a Fixed-Guided Compliant Beam with an Inflection Point using the Pseudo-Rigid-Body Model Concept," *Journal of Mechanisms and Robotics*, Trans. ASME, Vol. 7, Aug. 2015, pp. 031007-1-10

[81] Midha, A., Kuber, R. S., Chinta, V., and Bapat, S. G., "A Method for a More Accurate Calculation of the Stiffness Coefficient in a Pseudo-Rigid-Body Model (PRBM) of a Fixed-Free Beam Subjected to End Forces," *Proceedings of the ASME 2014 International Design Engineering Technical Conferences & Computers and Information in Engineering Conference*, Buffalo, NY, August, 2014, pp. DETC35366-1-10

[82] Bapat, S. G., Prasanna, P., and Midha, A., "A Methodology for Determining Static Mode Shape(s) of a Compliant Mechanism Using the Pseudo-Rigid-Body Model and the Degrees of Freedom Analysis," *Proceedings of the ASME 2015 International Design Engineering Technical Conferences & Computers and Information in Engineering Conference*, Boston, MA, August 2-5, 2015, manuscript under preparation

[83] Holst, G. L., Teichert, G. H., and Jensen, B. D., "Modeling and Experiments of Buckling Modes and Deflection of Fixed-Guided Beams in Compliant Mechanisms," *Journal of Mechanical Design*, Trans. ASME, Vol. 133, May 2011, pp. 051002-1-10

[84] Kim, C., "Curve Decomposition Analysis for Fixed-Guided Beams with Applications to Statically Balanced Compliant Mechanisms," *Proceedings of the ASME 2011 International Design Engineering Technical Conferences & Computers and Information in Engineering Conference*, Washington, DC, August, 2011, pp. DETC47829-1-10

[85] Chinta, V. R., "Analysis and Synthesis of Mechanisms with Fixed-Guided Compliant Segments," M.S. Thesis, Missouri University of Science and Technology, Rolla, 2013

[86] Awatar, S., Slocum, A. H., and Sevincer, E., "Characteristics of Beam-Based Flexural Modules," *Journal of Mechanical Design*, Trans. ASME, Vol. 129, June 2007, pp. 625-639

[87] Koli, A. B., "A Generalized Approach for Compliant Mechanism Design using the Synthesis with Compliance Method, with Experimental Validations," M.S. Thesis, Missouri University of Science and Technology, Rolla, 2013

[88] Erdman, A. G., Sandor, G. N., and Kota, S., *Mechanism Design – Analysis and Synthesis*, Volume 1, Prentice Hall, New Jersey, 2001

[89] Burden R. L., and Faires, D. J., *Numerical Analysis*, Thomas & Brooks/Cole, 8th Edition, Section 10

[90] Wang, M. Y., "Mechanical and Geometric Advantages in Compliant Mechanism Optimization," *Frontiers of Mechanical Engineering in China*, Vol. 4, No. 3, 2009, pp. 229-241

[91] Parkinson, M. B., Jensen, B. D., and Kurabayashi, K., "Design of Compliant Force and Displacement Amplification Micro-Mechanisms," *Proceedings of the ASME 2001 Design Engineering Technical Conferences & Computers and Information in Engineering Conference*, Pittsburgh, Pennsylvania, September 9-12, 2001, pp. DAC21809-1-8

[92] Hetrick, J. A., "An Energy Efficiency Approach for Unified Topological and Dimensional Synthesis of Compliant Mechanisms," Ph.D. Dissertation, University of Michigan – Ann Arbor, 1999

[93] Midha, A., Hall, A. S., Her, I., and Bubel, G. M., "Mechanical Advantage of Single-Input and Multiple-Output Ports Mechanical Device," *Journal of Mechanisms, Transmissions, and Automation in Design*, Trans. ASME, Vol. 106, No. 4, 1984, pp. 462-469

[94] Midha, A., and Prasanna, P., "Mode Shapes in Compliant Mechanisms, and a Procedure to Identify Appropriate Pseudo-Rigid-Body Model Type," *Proceedings of the ASME 2015 International Design Engineering Technical Conferences & Computers and Information in Engineering Conference*, Boston, MA, August 2-5, 2015, pp. DETC-47694 – 1-9, under review

[95] Roy, S., and Chakrabarty, S., *Fundamentals of Structural Analysis*, S. Chand and Company Ltd., New Delhi, India, 2003

[96] Waldron, K. J., and Kinzel, G. L., *Kinematics, Dynamics, and Design of Machinery*, John Wiley & Sons, Inc., 2nd Edition, Hoboken, NJ, 2004

[97] Prasanna, P., "On an Interpretation of the Compliance Number Concept and its use in Concurrence with Static Mode Shapes for Compliant Mechanism Design and Analysis," M.S. Thesis, Missouri University of Science and Technology, Rolla, 2015

[98] Prasanna, P., Midha, A., and Bapat, S. G., "Classification of Compliant Mechanisms and Evaluation of its Degrees of Freedom using the Compliance Number and Pseudo-Rigid-Body Model Concept," to be the *Journal of Mechanical Design*

[99] Merian, J. L., *Engineering Mechanics Volume 1 STATICS*, John Wiley & Sons, New York, NY, 1978, pp. 301-302

[100] Midha, A., Kuber, R. S., and Bapat, S. G., "Development of a Methodology for Pseudo-Rigid-Body Models of Compliant Beams with Inserts, and Experimental Validations," *Proceedings of the ASME 2015 International Design Engineering Technical Conferences & Computers and Information in Engineering Conference*, Boston, MA, August 2-5, 2015, pp. DETC-47943 – 1-10, under review

[101] Midha, A., and Bapat, S. G., "Characteristic Deflection Domain for Various Compliant Segment Types, and its Importance in Compliant Mechanism Synthesis and Analysis," *Proceedings of the ASME 2014 International Mechanical Engineering Congress & Exposition*, Montreal, Canada, November, 2014, pp. IMECE38795-1-10

[102] Bapat, S. G., Midha, A., and Koli, A. B., "On a Generalized Approach for Design of Compliant Mechanisms using the Pseudo-Rigid-Body Model Concept," *Proceedings of the ASME 2014 International Mechanical Engineering Congress & Exposition*, Montrel, Canada, November, 2014, pp. IMECE38788-1-10

[103] Midha, A., Bapat, S. G., and Midha, P., "Mechanical Advantage of a Compliant Mechanism and the Significant Factors Affecting it, using the Pseudo-Rigid-Body Model Approach," *Proceedings of the ASME 2015 International Design Engineering Technical Conferences & Computers and Information in Engineering Conference*, Boston, MA, August 2-5, 2015, pp. DETC-47930 – 1-13, under review

[104] Bapat, S. G., Prasanna, P., Kuber, R. S., Koli, A. B., and Midha, A., "Experimental Validations of the Pseudo-Rigid-Body Model (PRBM) Concept for Compliant Mechanism Design," to be submitted to the *Journal of Mechanical Design*

[105] Bapat, S. G., and Midha, A., "Synthesis Approach for Fully-Compliant Mechanisms Containing Fixed-Guided Segments with an Inflection Point," to be submitted to the *Journal of Mechanisms and Robotics*

VITA

Sushrut G. Bapat was born in Pune, India on August 21, 1986 to Gangadhar P. Bapat and Bhagyashree G. Bapat. He was raised in Ahmedabad, India and later moved to Mumbai, India. He received his Bachelor of Engineering in Mechanical Engineering degree from University of Mumbai in February 2008. After completion of his undergraduate course work in June 2007 he worked in Engineering and Design Tecnimont ICB Pvt. Ltd. (EDTICB) as an Engineer in Equipment Design department, responsible for machinery and process package unit design activities at Mumbai, India and Milano, Italy. He was admitted to the Master of Science graduate degree program in Mechanical Engineering at Missouri University of Science and Technology, Rolla, MO in spring semester, 2010. Later, he changed his degree program to a Direct PhD in Mechanical Engineering and received his degree in May 2015.